

Signal modeling and foundations of
Near-field Naval MIMO radar
for small targets discrimination

by

HAMET Bastien
OBRIOT Nicolas

MASTER THESIS

in

Mobile Communication systems



*Department of Electronic Systems
Aalborg University*

February - May 2012

Supervised by:
Patrick C. Eggers

Thesis informations

Title:

Signal modeling and foundations of Near-field Naval MIMO radar

for small targets discrimination.

Report:

Total pages number: 200.

Number of copy: 2.

Period:

February - May 2012.

Group:

Mobile Communication Systems.
Group 1010.

Supervisor:

Patrick C. Eggers.

Wednesday 30th May, 2012,
Frederik Bajers Vej 7, 9220 Aalborg Ø

Members:

HAMET Bastien.

OBRIOT Nicolas.

Abstract

Nowadays, piracy is a major issue and represents an important human and economic cost. Pirates commonly use small dinghies which can be hidden by sea-waves. These boats are therefore hardly visible for shipping vessels radars. Surprise effect is an important factor in attack successfulness.

Radar technology can help to detect such threats. In order to improve actual radar systems, we investigate the impact of using a large antenna array on big vessel to build a MIMO radar.

This master thesis deals with foundations and signal modeling for near-field MIMO radar. The report focuses mainly on sea-clutter, signal modeling, polarization and the near-field MIMO possibilities. A complete naval radar model is implemented and allows to simulate small target detection.

Sea-clutter models results show that Tsallis-distribution models more accurately the sea-response amplitude than the commonly used K-distribution.

Polarization results show that onboard weapons have a well defined polarimetric signature. However, unstable sea-clutter and boat responses hide this signature and makes it harder to detect.

Results show that MIMO radar provides a large SCR gain compared to SIMO radar. MIMO radar outperforms SIMO radar small targets detection capacity on a rough sea.

Table of contents

Abstract	1
List of Symbols	11
List of Acronyms	14
Preface	16
1 Introduction	17
1.1 Context presentation	17
1.2 Related works	20
1.3 Motivation	20
1.4 Problem definition	21
1.5 Project delimitations	22
1.5.1 Boats dimension	22
1.5.2 Simulation parameters	22
1.5.3 Project study	23
2 Radar main features	24
2.1 Basics of radar	24
2.2 Overview of the main types of radar	25
2.3 Frequency bands regulation	27
2.4 Emitted signal	28
2.5 Radar detection	29
2.5.1 Directivity and gain of antennas	30
2.5.2 Radar range resolution	31
2.6 Doppler shift	31
2.7 Radar equation	32
2.8 Polarization	34
2.8.1 General polarization	34
2.8.2 Linear polarization	34
2.8.3 Polarization loss factor	35
2.8.4 Co-polarization and Cross-polarization	36
2.8.5 Cross polarization discrimination	36
2.8.6 Linear polarization modulation	37
3 Model	39
3.1 General overview	39

3.2	Radiating near-field	41
3.3	Earth curvature	43
3.3.1	Maximum range	43
3.3.2	Flat earth model	44
3.4	System Grid	45
3.4.1	Symmetry axis	45
3.4.2	Resolution	45
3.4.3	Radar pulses	46
4	Radar Cross Section	47
4.1	Sea-clutter radar cross section	47
4.1.1	Models	47
4.1.2	GIT model	48
4.2	Target fast fading : Swerling models	49
4.2.1	Swerling I	49
4.2.2	Swerling II	51
4.2.3	Swerling III	51
4.2.4	Swerling IV	51
4.2.5	Swerling V or Swerling 0	51
4.3	Target radar cross section	52
4.3.1	Boat composition	52
4.3.2	Hull RCS	53
4.3.3	Rifles RCS	53
4.3.4	Environment polarimetric sensitivity	56
4.4	Objects orientation	56
4.4.1	Studied planes	56
4.4.2	Weapons orientation in the dinghy plane	57
4.4.3	Boat orientation	57
4.4.4	Weapons orientation in the antenna plane	58
4.5	AK-47 polarimetric detector	60
5	Sea-clutter	61
5.1	Physical sea clutter	61
5.1.1	Physical description	61
5.1.2	Sea state	61
5.1.3	Pierson-Moskowitz model	62
5.1.4	Flat see range attenuation	63
5.1.5	Shadowing	65
5.2	Electromagnetic sea responses	68
5.2.1	K-distribution	68
5.2.2	Tsallis distribution	68
5.2.3	Distribution comparison	70
6	MIMO Radar	71
6.1	Usual MIMO radars	71
6.1.1	Basics	71
6.1.2	Target detection and quality indicators	72

6.2	Antenna placement	73
6.2.1	Antenna spacing	73
6.2.2	Single antennas or Cluster	74
6.3	Target detection techniques	75
6.3.1	Space diversity	76
6.3.2	Beam-less radar technique	78
6.3.3	Space focusing	78
6.3.4	MIMO added-value for detection	82
6.4	Target Localization techniques	83
6.4.1	Near-field localization	83
6.4.2	MIMO value-added for NF localization	86
6.4.3	Far-field localization	88
6.5	Target classification technique	92
6.5.1	Polarization discrimination	92
6.6	MIMO radar scenario	93
6.6.1	Choice discussion	93
6.6.2	Radar illumination	95
6.6.3	Target tracking	95
7	Radar signal simulation	97
7.1	Sea surface generation	98
7.2	Pre-processing	100
7.2.1	Signals properties	100
7.2.2	Illuminated path	101
7.3	Downlink	101
7.3.1	DL attenuation	103
7.3.2	DL shadowing	104
7.4	Backscattered coefficient	104
7.4.1	RCS	105
7.4.2	Tsallis amplitude	107
7.4.3	Operation on signals	107
7.5	Uplink	108
7.5.1	UL attenuation	108
7.5.2	UL shadowing	108
7.6	Signal processing: MIMO reception	109
7.7	Signal processing: Detection	111
7.8	Signal processing: Localization	114
8	Radar operation results	115
8.1	Metrics and simulation parameters	115
8.1.1	Metrics	115
8.1.2	Antenna placement	116
8.1.3	Scenario	116
8.2	Simulations results	117
8.2.1	Detailed results	119
8.2.2	Performance ranking	124
8.3	Discussions	124

8.3.1	Calm sea	124
8.3.2	Strong sea	125
8.3.3	Shadowing	125
8.3.4	MIMO/SIMO comparison	125
Conclusion		127
References		128
Appendix A Weapons length impact on RCS		132
Appendix B 3-planes study of weapon RCS		136
Appendix C Signal correlation		140
C.1	Correlation definition	140
C.2	Shadowing coefficients correlation (UL and DL)	141
C.3	Tsallis distribution : Neighbors cells amplitude correlation (DL)	146
C.4	Tsallis : Backscattered signal and pixel mismatch	148
C.5	Overall signal amplitude correlation along the vessel (UL)	158
C.6	Correlation conclusion and discussions	163
Appendix D Singular Value Decomposition technique		164
D.1	Definition	164
D.2	SVD interpretation	165
D.3	2×2 MIMO system	166
D.4	Weapon orientation estimation and polarization ellipticity	166
D.5	Polarimetric discrimination	168
D.5.1	Principle	168
D.5.2	Application	170
Appendix E Weapon polarimetric signature		176
Appendix F Tsallis and K-distributions		179
F.1	Parameters estimation	179
F.2	Simulation results	180
F.3	Metrics	183
F.4	K-distribution cross-fit : $A_R \rightarrow \Delta A_R$	184
F.5	Tsallis-distribution cross-fit : $\Delta A_R \rightarrow A_R$	186
F.6	Overall Cross- D_{KL} comparison	188
F.7	Distribution correlation	190
F.8	Conclusions	191
Appendix G Matlab scripts		192
G.1	Main scripts	192
G.2	Polarization	197
G.3	Tsallis/K-distribution comparisons	198
G.3.1	estimate_k_and_tsallis_parameters.m	199
G.3.2	compute_mre_results.m	199

G.4	figures	199
G.4.1	piracy_plot.m	199
G.4.2	sea_roughness.m	199
G.4.3	tsallis_sketch.m	200
G.4.4	plot_illuminated_range.m	200
G.4.5	detection_probability.m	200
G.4.6	swerling_pdf.m	200
G.4.7	plot_mrc_results.m	200

List of Figures

1.1	Piracy acts over the world [2,3]	18
1.2	Suspected Somalian pirates in their small dinghy [4]	18
1.3	Maximum gain pattern of a broadside array on the boat	19
1.4	Blind zones covered by another boat	19
2.1	Radar simplified architecture	25
2.2	Time representation during the radar operating period	29
2.3	2D azimuthal plane pattern in linear scale	31
2.4	2D elevation plane pattern in linear scale	31
2.5	Radar resolution illustration	32
2.6	Target motion influence on the EM wave phase	32
2.7	Elliptically polarized wave illustration as a function of time [11].	35
2.8	x, y and z polarizations	35
2.9	Polarization unit vectors	36
2.10	Co and cross polarization example	37
2.11	2 components antenna polarization affected by a change in the feeding signals	38
3.1	General process in the model	39
3.2	Calculation of the downlink signal	40
3.3	Calculation of the global EM response	40
3.4	Uplink part in the model	41
3.5	Bad MIMO performances region	42
3.6	Earth curvature error representation	44
3.7	Region of interest for the analysis	46
4.1	Target RCS fast fading [19]	50
4.2	Target RCS probability at each scan for a $RCS_{average} = 0.25 m^2$ target following Swerling I model.	50
4.3	Target RCS probability at each scan for a $RCS_{average} = 0.25 m^2$ target following Swerling I model.	52

4.4	Target components geometry	53
4.5	AK-47 shape and composition	54
4.6	orientation of the weapons compared to polarization in [18].	54
4.7	Co and Cross-polarization RCS signature of the AK-47.	55
	(a) Co-polarized AK-47 RCS [18]	55
	(b) Cross-polarized AK-47 RCS [18]	55
4.8	Comparison between co and cross-polarization looking at the AK-47 RCS [18].	55
4.9	Antenna plane illustration	57
4.10	Dinghy plane illustration	57
4.11	Possible ways for a weapon to be carried and the corresponding angles in the Dinghy plane.	58
4.12	Possible configurations for pirates attack	59
5.1	Beaufort scale examples	62
	(a) Beaufort 4 - Moderate breeze [26]	62
	(b) Beaufort 8 - Gale [26]	62
5.2	RMS roughness depending on the wind power with double-path model threshold for different candidate frequencies.	64
5.3	Shadowing created by waves	66
5.4	Tsallis probability distribution function	70
6.1	Illustration of the configuration for the linear perturbation model. . . .	73
6.2	Possible antenna configuration : Phased clusters in sparse antenna array.	75
6.3	Detection probability for a $N \times N$ MIMO radar with equation (6.6) versus a single antenna probability of detection.	77
6.4	Probability of false alarm for a $N \times N$ MIMO radar with equation (7.24) versus a single antenna probability of false alarm.	77
6.5	Beam-less multi-static radar illustration	79
6.6	Post detection focus scan with knowledge of the ranges.	79
6.7	Expected value of the interference [33].	81
6.8	(a),(a') Baseband representation [$m_I(t)$ and $m_Q(t)$] of the signal trans- mitted by antenna A. (b),(b') Baseband representation [i.e., $m'_I(t)$ and $m'_Q(t)$] of the signal reverberated inside the cavity and received by an- tenna B [34].	81
6.9	Near field delay and attenuation between antennas.	83
6.10	Example of near-field induced delay and amplitude loss between two receiving antennas.	84
6.11	Define configuration for ranges estimation	85
6.12	Possible received signals delays for 11 receivers on the boat with possi- ble offsets depending on the transmitter position. Sea state 6 and the dinghy placed at (230,200).	87
6.13	Illustration of the possible jitter induced by the environment, thermal noise and the wave propagation.	88
6.14	Antenna organization for ESPRIT algorithm	90
6.15	Wave possible path for same Tx/Rx	91
6.16	Wave possible path for different Tx/Rx	91

6.17	Different MIMO possibilities concerning space implementation.	94
6.18	MIMO radar scenario	94
7.1	Overall implementation block diagram	97
7.2	Pierson-Moskovitz sea-surface model block	98
7.3	Sea-surface height model in meter with the Pierson-Moskovitz algorithm for sea-state 6 and wind direction $7\pi/8$ taking into consideration the earth curvature with 2km range	98
7.4	Sea-surface model with the Pierson-Moskovitz algorithm for sea-state 9 and wind direction $\pi/4$ taking into consideration the earth curvature with 2km range	99
7.5	Sea-surface model with the Pierson-Moskovitz algorithm for sea-state 9 and wind direction $\pi/4$ taking into consideration the earth curvature with 6km range	99
7.6	Total illuminated area for a maximum range of 4km and 3 transmitters.	102
7.7	Total illuminated area for a maximum range of 10km and 3 transmitters.	102
7.8	Downlink attenuation block	103
7.9	Backscattered coefficient block.	104
7.10	Sea RCS versus the distance in $dB[m^2]$ for a 1° beamwidth.	106
7.11	Uplink attenuation block	108
7.12	Received signal from antenna #1 to antenna #1 before MRC.	110
7.14	MRC of signals from fig. 7.12 and 7.13.	110
7.13	Received signal from antenna #1 to antenna #2 before MRC.	111
7.15	Signal processing block for target detection	111
7.16	Received signal and the estimated mean and detection threshold	113
7.17	Signal processing block for target localization	114
8.1	Hull and bridge antenna configurations.	116
8.2	SCR for MIMO and SIMO systems.	118
8.3	P_D for MIMO and SIMO systems.	118
8.4	SCR for MIMO and SIMO systems - sea state: 6 - wind direction: $\pi/4$.	119
8.5	SCR for MIMO and SIMO systems - sea state: 6 - wind direction: $7\pi/8$.	120
8.6	SCR for MIMO and SIMO systems - sea state: 9 - wind direction: $\pi/4$.	120
8.7	SCR for MIMO and SIMO systems - sea state: 9 - wind direction: $7\pi/8$.	121
8.8	SCR results for the 240 scans with 1×4 SIMO and 2×2 MIMO systems.	122
8.9	SCR results for the 240 scans with 1×9 SIMO and 3×3 MIMO systems.	123
A.1	Comparison between co (Y pol) and cross-polarization (X pol) AK-47 RCS [18].	134
A.2	I-plates co-polarisation RCS [18].	134
A.3	T-plates co-polarisation RCS [18].	135
B.1	3-plans looking to find gun RCS	137
B.2	Normalized backscattering patterns of the weapon RCS for a co and cross polarizations in the three possible illumination.	139
C.1	Representation of angular correlation.	142

C.2	Angular shadowing correlation. Sea state 6 - antenna/wind angle 15° - Beam-width : 20°	143
C.5	Angular shadowing correlation. Sea state 6 - antenna/wind angle 127.5° - Beam-width : 2°	143
C.3	Angular shadowing correlation. Sea state 9 - antenna/wind angle 127.5° - Beam-width : 5°	144
C.4	Angular shadowing correlation. Sea state 6 - antenna/wind angle 15° - Beam-width : 5°	145
C.6	Shadowing correlation for downlink and uplink case	145
C.7	Correlation response from adjacent cells.	147
C.8	Tsallis amplitude correlation coefficient of adjacent cells, with sea state 6 and antenna/wind angle 15°	148
C.9	Doppler shift for 7.5° , 15° , 60° and 180° angular spread from [40] . . .	149
C.10	Signal power correlation for 7.5° , 15° , 60° and 180° angular spread from [40]	150
C.11	Illuminated areas by transmitters 1 (brown) and 2 (yellow) (300 m apart) for ranges 4000 m and 6000 m - Beam-width : 2°	152
C.12	Illuminated areas by transmitters 1 (brown) and 2 (yellow) (300 m apart) for ranges 200 m, 400 m, 1000 m, 4000 m and 6000 m - Beam-width : 45°	152
C.13	Pixel mismatch illustration between receivers 1 and 2 for 3 pixels illuminated (short range and narrow beam-width case)	153
C.14	Tsallis correlation in uplink. Sea state 6 - antenna/wind angle 15° - Beam-width : 20°	155
C.15	Tsallis correlation in uplink. Sea state 9 - antenna/wind angle 127.5° - Beam-width : 5°	156
C.16	Tsallis correlation in uplink. Sea state 6 - antenna/wind angle 15° - Beam-width : 5°	156
C.17	Tsallis correlation in uplink. Sea state 6 - antenna/wind angle 127.5° - Beam-width : 2°	157
C.18	Signal power correlation of a single source (MS) versus the place on the antenna array from mobile communication system. [41]	159
C.19	Signal correlation along the vessel for short and long range echo. Sea state 6 - antenna/wind angle 15° - Beam-width : 20°	161
C.21	Signal correlation along the vessel for short and long range echo. Sea state 6 - antenna/wind angle 15° - Beam-width : 5°	161
C.20	Signal correlation along the vessel for short and long range echo. Sea state 9 - antenna/wind angle 127.5° - Beam-width : 5°	162
C.22	Signal correlation along the vessel for short and long range echo. Sea state 6 - antenna/wind angle 127.5° - Beam-width : 2°	162
D.1	Transmission using SVD of the channel	165
D.2	SVD operator illustration on a simple circle	165
D.3	Dominant mode transmission and reception polarizations corresponding to SVD example.	168

D.4	Study of the dominant mode polarization in transmission and reception after the SVD weighting, the estimated weapon position (threshold) and the real weapon position in three basics MIMO cases.	172
D.5	Study of the transmission polarization of the dominant and second mode after the SVD weighting, the estimated weapon position (threshold) and the real weapon position in three basics MIMO cases.	173
D.6	Obtained normalized polarization for sea only, boat only and sea plus boat as backscatterer.	174
F.1	K and Tsallis distributions fit compared to a given dataset	181
	(a) K-distribution fit - MRE = 0.0077	181
	(b) Tsallis-distribution fit - MRE = 0.0007	181
F.2	K and Tsallis distributions fit compared to a given dataset	182
	(a) K-distribution fit - MRE = 0.0400	182
	(b) Tsallis-distribution fit - MRE = 0.0062	182
F.3	D_{KL} comparison for K and Tsallis distributions over 245 radar measurements.	183
F.4	Cross- D_{KL} of K-distribution over differentiated data (ΔA_R).	185
F.5	Cross- D_{KL} of K-distribution over differentiated data (ΔA_R).	185
F.6	Cross- D_{KL} of Tsallis-distribution over non-differentiated data (A_R). . .	187
F.7	Cross- D_{KL} of Tsallis-distribution over non-differentiated data (A_R). . .	187
F.8	D_{KL} comparison for K and Tsallis distributions over 245 radar measurements.	189
F.9	Cross- D_{KL} of K-distributions over differentiated data (ΔA_R).	189
F.10	Tsallis realization computed cell after cell	190
G.1	Matlab console - <i>help get_transmitter_data</i> output	196
G.2	Matlab console - <i>main.m</i> output	197

List of Tables

1.1	Assumed boat dimensions.	22
1.2	Different set of parameters that will be used for simulation.	23
2.1	Radar features with respect to the International Telecommunication Union (ITU) operating bands. [10].	28
4.1	Sea-clutter radar cross section models [18] [6].	48
4.2	All possible angles of the weapon from the antenna point of view	59
5.1	Different sea-states associated with the wind speed. [26].	62
5.2	Thresholds for two ray model application	65

6.1	DOA Estimation by MUSIC & ESPRIT for varying SNR. (Input $\theta = 25$ deg, $M=4$, $k=100$). [37]	89
7.1	Possible RCS of the weapon depending on φ and θ .	106
8.1	Compared MIMO and SIMO systems.	116
8.2	Results table for SIMO and MIMO radars SCR improvement for dinghy range 4000 m.	117
8.3	Ranking for the MIMO and SIMO systems.	124
A.1	Cylinders size corresponding to [18] experiment.	132
A.2	Cylinders theoretical and observed reasoning wavelength corresponding to [18] experiment.	132
A.3	Γ -plates size corresponding to [18] experiment.	133
B.1	3-plans RCS values for a handgun at 700 MHz [18].	137
B.2	3-plans RCS values for a handgun at 2.7 GHz [18].	137
B.3	3-plans RCS estimation for the AK-47 at 245 MHz [18].	138
B.4	3-plans RCS estimation for the AK-47 at 2.7 GHz [18].	138
C.1	Surface of 5×5 m ² pixels illuminated depending on the range and beam-width.	151
D.1	Simple cases for 2x2 MIMO system study.	170
E.1	Expected values of the defined variables for target classification in dB with a sea-state 6.	176
E.2	Simulated average values over 30 realizations	177
E.3	SCR, WDR and WCR study for HH polarization in dB.	177
E.4	SCR, WDR and WCR study for VV polarization in dB.	177
E.5	Simulations of the XPD , the <i>leakage</i> and the PD in dB for sea-state 6 and default polarization VV .	178
F.1	Tsallis and K distributions efficiency comparison	180
F.2	Tsallis and K distributions D_{KL} comparison	183
F.3	Tsallis and K distributions Cross- D_{KL} comparison	188

List of Symbols

Symbol	Description
α	Angle of arrival of the EM wave [rad]
α_{LIMIT}	Limit angle with the axis of the boat to be in the near-field [rad]
a_e	Semi-major axis of an ellipse. [m]
A	steering matrix.

A_0	Amplitude of the signal emitted by the radar [V]
A_{cell}	Sea grid cell area [m^2]
A_e	Antenna effective aperture [m^2]
A_g	Geometric antenna area [m^2]
A_p	Projected object surface [m^2]
A_R	Amplitude of the signal depending on the range [V]
b_e	Semi-minor axis of an ellipse. [m]
C_{XY}	Covariance coefficient between X and Y distributions.
c	Speed of light [$m \cdot s^{-1}$]
c_0	Speed of an electromagnetic wave in the air [$m \cdot s^{-1}$]
c_{earth}	Shadowing coefficient due to the earth curvature
c_{shadow}	Shadowing coefficient applied to the RCS of the dinghy
c_{shadow}^{UL}	Shadowing coefficient for uplink path
c_{shadow}^{DL}	Shadowing coefficient for downlink path
c_{wave}	Shadowing coefficient due to sea-waves
d	Distance between the dinghy and a wave [m]
d_{curv}	distance along the earth [m]
d_{flat}	distance along the earth tangent [m]
D	Antenna directivity.
D_a	Length of the vessel [m]
D_d	Length of the dinghy [m]
D_{dinghy}	Horizon distance which is seen by the dinghy [m]
$D_{far-field}$	Boundary between the radiating near-field and far-field regions
$D_{horizon}$	Maximum theoretical detection range by the radar [m]
D_{KL}	Kullback-Leibler divergence.
$D_{near-field}$	Boundary between the reactive and radiating near-field regions
D_r	Antena directivity
D_{vessel}	Horizon distance which is seen by the vessel [m]
DOA	Signal direction of arrival [rad]
ΔR	Radar range resolution [m]
$\Delta R_{n+1 \rightarrow n}$	Range difference between the $n + 1^{th}$ and n^{th} antenna [m]
Δ_{IES}	Inter-elements spacing [m]
$E - field$	Electric field [$V \cdot m^{-1}$]
E_s	Energy of the sent signal [J]
E_{xx}	Antenna polarization.
$e_{d-flatness}$	Error percentage between d_{curv} and d_{flat}
f_c	Carrier frequency [Hz]
f_d	Doppler frequency shift [Hz]
f_{dr}	is the resonant frequency of a dipole [Hz]
f_{mr}	is the resonant frequency of a monopole [Hz]
Γ	Gamma function
G	Antenna gain [dB]
G_{Tx}	Transmitting antenna gain [dB]
h_{avg}	average Sea waves height m

h_{sea}	Sea height including earth curvature m
h_{PM-sea}	Sea height from Pierson-Moskovitz m
h_{vessel}	Height of the vessel, waves understood $[m]$
h_{dinghy}	Height of the dinghy, waves understood $[m]$
$h_{wave-dinghy}$	Height of the waves under the dinghy $[m]$
I_{ft}	Power density at the target $[W/m^2]$
K_a	Antenna efficiency.
Λ	diagonal unitary matrix with phase shifts
λ	Wavelength $[m]$
λ_{bias}	Biased wavelength coefficient.
L_a	Antenna length $[m]$
M	Number of transmitting antennas
μ_R	Mean of a given realization.
μ_T	Mean non biased estimator.
n_p	Number of pulses for the radar signal.
N	Number of receiving antennas
N_0	Power of noise received by the antenna. $[W]$
N_a	Number of element of the each radar antenna array (transmitter or receiver)
$P_{clutter}$	Received power of the clutter in the echo $[W]$
P_D	Probability of detection.
P_e	Ratio between semi-minor and semi-major axis of the polarization ellipse.
P_{echo}	Received power of the target in the echo $[W]$
P_{fa}	Probability of false alarm.
P_r	Power of a signal received by the antenna. $[W]$
P_s	is the received power of the useful signal. $[W]$
P_{Tx}	Transmitted power an antenna. $[W]$
P_{re}	Power re-radiated by the target. $[W]$
p_K	K-distribution probability density function
R	Range: distance between the radar and the target $[m]$
R_a	Radar illumination angle $[rad]$
R_e	Earth radius $[m]$
R_{max}	Maximal range for detection $[m]$
R_r	Antena reflectivity.
$R_{Tsallis}$	Correlation between adjacent cells for the Tsallis amplitude.
R_{Uplink}	Correlation between adjacent cells for the uplink process.
$RCS_{average}$	Radar cross section excluding swerling fading $[m^2]$
RCS_{dinghy}	Radar cross section of the pirates boats $[m^2]$
RCS_{real}	Radar cross section including swerling fading $[m^2]$
$RCS_{shadowed}$	Radar cross section of the pirates boats after applying shadow coefficient $[m^2]$
r_{XY}	Correlation coefficient between X and Y random variables.
r_e	Pirate engine radius $[m]$

$\hat{\rho}_\omega$	Incident wave unit polarization vector.
$\hat{\rho}_a$	Antenna wave unit polarization vector.
ϕ_{boat}	azimuthal angle of the dinghy <i>rad</i>
ϕ'	azimuthal angle of the weapon in the dinghy plane <i>rad</i>
ϕ_{weapon}	azimuthal angle of the weapon in the antenna plane <i>rad</i>
ψ_p	Angle between the two polarization vectors.
σ	Radar Cross Section [m^2]
σ_{engine}	RCS of the pirate engine [m^2]
σ_N	Noise standard deviation [V].
σ_T	Non biased Tsallis realization standard deviation estimator.
σ_R	Realization standard deviation.
σ_{sea}	RCS of the sea [m^2]
$S_{m,n}$	Signal send by the m^{th} transmitter and received by the n^{th} receiver.
S_{PM}	Pierson-Moskowitz sea-surface frequency spectrum [Hz]
$S_{resolution}$	Spatial resolution for an antenna [m]
T_{ns}	unique nonsingular transformation matrix
T_p	Threshold for PDF integration
T_{pulse}	Pulse duration for the radar [s]
τ	Time delay [s]
θ	elevation angle of the dinghy <i>rad</i>
θ'	elevation angle of the weapon in the dinghy plane <i>rad</i>
θ_{weapon}	elevation angle of the weapon in the antenna plane <i>rad</i>
v_r	Target relative velocity from the radar point of view [$m \cdot s^{-1}$]
v_t	Target velocity [$m \cdot s^{-1}$]
W_a	Antenna bandwidth [Hz]
W_θ	weapon orientation in the x-z plane [<i>rad</i>]

List of Acronyms

Acronym	Description
2D-MUSIC	2-Dimensional Multiple Signal Classification
CRLB	Cramer-Rao Lower Bound
EM	Electromagnetic
ESPRIT	Estimation of Signal Parameters via Rotational Invariance Techniques
hp	Horse power
nmi	Nautical miles
DOA	Direction of Arrival
DCR	Dinghy-to-Clutter Ratio
DL	Downlink
FF	Far-Field

GIT	Georgia Institute of Technology
GDOP	Geometric Dilution of Precision
HPBW	Half Power Beamwidth
IEEE	Institute of Electrical and Electronics Engineers
IFFT	Inverse Fast Fourier Transform
IMB	International Maritime Bureau
ITU	International Telecommunication Union
KPI	Key Point Indicators
MIMO	Multiple Input Multiple Output
MRC	Maximal Ratio Combining
MRE	Mimimum Relative Entropy
MTI	Moving Target Indicator
NF	Near-Field
PD	polarimetric discrimination
PDF	Probability Density Function
PFA	Probability of False Alarm
PLF	Polarization loss factor
PM	Pierson-Moskovitz
PRF	Pulse Repetition Frequency
PRT	Pulse Repetition Time
RADAR	Radio Detection And Ranging
RCS	Radar Cross Section
RE	Relative Entropy
RMS	Root Mean Squared
RPG	rocket-propelled grenade
SIMO	Single Input Multiple Output
SISO	Single Input Single Output
SCR	Signal-to-Clutter Ratio
SCNR	Signal-to-Clutter plus Noise Ratio
SNR	Signal-to-Noise Ratio
SVD	Singular Value Decomposition
TR	Time Reversal
TSC	Technology Service Corporation
TWS	Track-While-Scan
UL	Uplink
US	United States
WCR	Weapons-to-Clutter Ratio
WDR	Weapons-to-Dinghy Ratio
XPD	Cross Polarization Discrimination

Preface

This report has been written for a 10th semester Master Thesis in Mobile Communication Systems in Aalborg University in February-May 2012. The goal of this report is to show the efficiency of a MIMO radar use to improve the detection of small targets in a sea-clutter, investigating several candidates techniques. This work is built on the same scenario as a previous Aalborg University 8th semester Report about *Near Field Macro Array Reception for Small Radar Targets in Sea-clutter* made in February-May 2010. This previous work is a starting point for us.

In this report, notations will follow the IEEE recommendations. All equations will be denoted with number in parentheses (). The numbers into brackets [] will refer to references. To refer to a figure, Figure x.y or Fig. x.y notation will be used. x being the chapter number and y being the figure number in that chapter. Three levels of chapter will be used, therefore sections could be numbered with 3 numbers being respectively the chapter, section and subsection.

This project deals mostly with signal modeling and the foundations of naval near-field MIMO radar. The report will have the following structure. Chapter 1 is an introduction of the project which describe the context, the problem definition, motivations and project delimitations. Chapter 2 is a theoretical background about radars and their applications. Chapter 3 introduces the defined model and assumptions. Chapters 4 and 5 deal respectively with the radar cross section and the sea-clutter modeling. Chapter 6 introduces and explains the MIMO candidates techniques and possibilities. Chapter 7 describes the model implementation. Chapter 8 presents the results of MIMO radar SCR improvement compared to a SIMO radar. All annex work is presented in Appendices, from A to G.

We would like to acknowledge the devoted efforts and support of Patrick C. F. Eggers.

Chapter 1

Introduction

1.1 Context presentation

Piracy is an old practice, which had decreased in the 18th and 19th century [1]. After the world war II, frequency of pirates attacks has increased because of two main factors [1]:

- Improved technology on board
Big vessels need smaller crews to navigate thanks to the technology advancements and pirates increased their speed and weapons. Pirates are getting more dangerous while vessels more vulnerable.
- Lack of regulation
There are no specific laws in international waters and a certain lack in the willing of punishment of these piracy acts. No one really controls the international waters, and countries do not know what to do with foreigner pirates.

In the 2000s, piracy acts have dramatically increased. Figure 1.1 shows the number of piracy acts per year according to the IMB (International Maritime Bureau). Since 2000, 360 vessels and their crews are attacked by pirates every year in average. Human and economic costs are both major.

To try to combat this increasing number of piracy acts, vessels use detection technology to be able to detect small pirate dinghies. A better detection of these threats could help to prevent such a number of successful pirates attacks. Surprise is an important factor in the successfulness of an attack.

A dinghy example is shown in Figure 1.2. These dinghies have a particularity: a small Radar Cross Section (RCS, defined in section 4.3), which makes the detection difficult, especially when the sea state (defined in section 5.1.2) is high. We can also consider that if the dinghy is moving toward the vessel, the RCS will be reduced since the boat will be presented from prow, and therefore have a reduced RCS. Moreover their little size makes them be easily hidden by the sea waves.

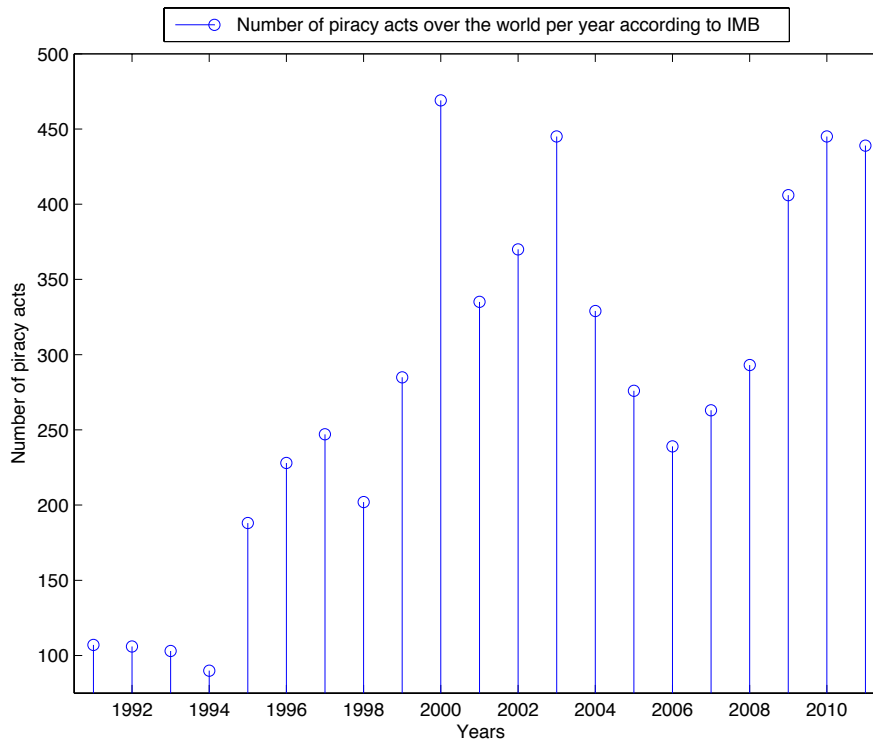


Figure 1.1: Piracy acts over the world [2,3]



Figure 1.2: Suspected Somali pirates in their small dinghy [4]

Radar technology improved significantly in term of technical achievement since its first use during the first world war [5]. Now, it facilitates the handing of a large amount of information depending on the type of radar used. However it is not efficient enough yet to prevent the piracy acts.

The use of large array MIMO radar on a vessel could potentially improve the detection of threats in the sea-clutter. In that situation, the received signal is different at each point and the system brings new information, thanks to space diversity. Two antennas could detect the target using two different paths. The path diversity would

permit to confirm or to infirm all the detections made by one path.

Another issue of that radar application is the presence of regions called *blind zones*. These areas are invisible to the radar due to different factors (See Figure 1.4):

- **Radar switching time and space resolution**

The radar needs time to switch between the transmitting and receiving mode. Plus, all backscattered signals during the transmitting time are lost. In that little amount of time, the received sea-clutter echo cannot be processed, and therefore any detection is impossible.

- **Vessel shadowing**

Depending on the architecture of the vessel, there could be objects that shadows the EM-waves transmission or reception, especially if transmitting and receiving antennas are not placed on the bridge (higher on the vessel).

Large linear arrays have a disadvantage which is that their directivity does not permit to be the same efficient in the array axis as in a perpendicular axis. To fight against blind zones, vessels could navigate in side by side convoy to cover each other blind spots as illustrated in Figures 1.4 and 1.3.

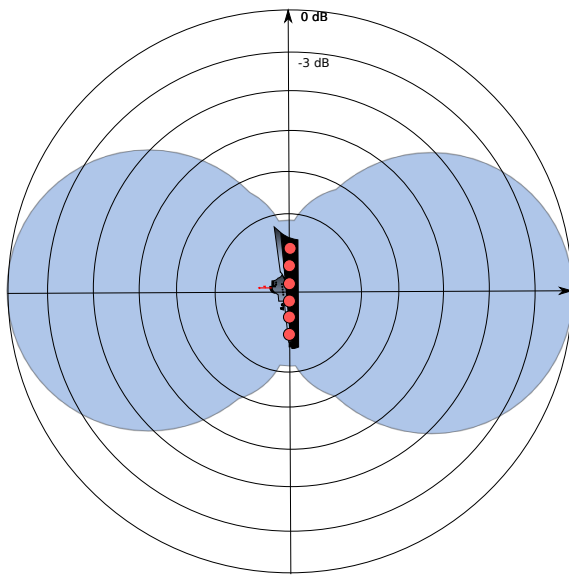


Figure 1.3: Maximum gain pattern of a broadside array on the boat

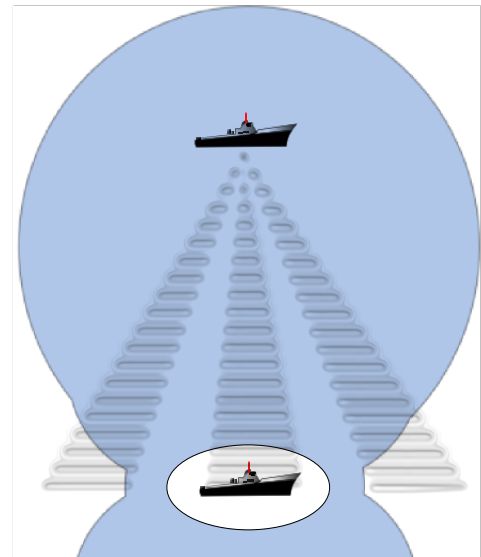


Figure 1.4: Blind zones covered by another boat

This project will therefore investigate fundamentals techniques and MIMO possibilities for near-field (definition given in section 3.2) small targets detection. The possibility to use different modeling distributions, the correlation between antennas, the benefit of polarization diversity and space diversity will be investigated in order to improve small targets detection in sea-clutter.

1.2 Related works

Investigations on naval radars have already been done in a project on SIMO radar study [6] made in 2010 in Aalborg University. The main idea was to use the huge dimension of a vessel to build an antenna array for the reception antenna. The large antenna array provides space diversity and therefore a better discrimination of targets, especially when they are close compared with the size of the antenna, i.e. when the radar operates in the near-field. Space diversity helps to build a more robust detection thanks to several copies of the same process. That space diversity is lost if the target and the antenna array are aligned.

According to [6], there is an improvement in the chance to detect a small boat in a sea-clutter using the huge antenna array. The detection is enhanced, but there is still a quite high Probability of False Alarm (P_{fa}) and the performance is not satisfactory enough. The goal of our project is to investigate whether it is possible to further enhance the detection thanks to fundamental aspects of MIMO radar systems.

1.3 Motivation

This project is mostly motivated by the piracy cost at two different levels:

- **Human cost**

The human cost of those attacks is high. 4185 seafarers were attacked in 2010 and only 342 survived in their vessels. The others were taken hostage (1090), used as human shields (516) or killed. [7]

- **Economic cost**

The economic cost is also important. If we take the case of Somalian pirates we will note that in 2011 they attacked 237 vessels. Even if they only successfully hijacked 28 of them, the economic cost estimation is near to 7 billion dollars. [7]

Another motivation for that problem is to enhance the detection of small objects, especially in the maritime environment.

- **Floating objects**

We could use that technology to improve the detection of floating objects such as sinking ships. Depending on the results achieved it would even be possible to detect smaller objects.

- **Sea surface**

The analysis could help to improve to detect dangers in the sea such as rocks or icebergs using only the MIMO diversity. Ships could potentially avoid isolated dangers if the radar is able to detect them.

1.4 Problem definition

Studies have been done to find the most efficient way to detect small targets in sea clutter using monostatic radars or multistatic radars with one transmitter and an array of antennas for the reception. The new technologies discovered to increase the efficiency of wireless communications could permit to discretize the small targets compared with the sea clutter. Our project will investigate the fundamentals and combination of new techniques and signal modeling operating on a near-field MIMO radar.

The purpose of this project is to investigate the possibilities given by the combination of near-field and MIMO system techniques. This project mainly tries to explore the array and signal possibilities. Several solutions will be investigated:

- Sea-clutter/signal model:
Usual radar systems usually model the sea-clutter with the K-distribution, which represents the electromagnetic amplitude response of the sea. Recent tracks suggest that the Tsallis distribution would model the electromagnetic differentiated amplitude of the sea [8]. Comparisons and performance of each-distribution will be evaluated.
- Polarization diversity:
Most of the radar systems operating over sea-clutters use vertical polarization [9] because it provides an overall better target discrimination (*SCR*). The use of a multiple polarizations in transmission and reception could provide a bigger benefit out of the MIMO system. This possibility will be investigated.
- Weapon detection:
Instead of trying to increase the *SCR* only, the polarization diversity brings more information on the target. We will study the polarimetric properties of weapons to see if it can be associated to a specific signature. If a specific signature comes out of this study, we will investigate the possibility to use it in order to classify the nature of a detection.
- Near-field MIMO space diversity:
Near-field properties allow the use of a complete set of possible techniques in order to enhance the *SCR* but also to locate targets easily. Sets of techniques will be looked up to see whether it enhances the localization accuracy, detection probability or *SCR*. Finally, the MIMO system will be compared to a SIMO system studied in [6].

1.5 Project delimitations

1.5.1 Boats dimension

In that project, we will assume the vessel and dinghy dimensions being the ones given by Table 1.1.

Vessel			Dinghy		
Length [m]	Width [m]	Height [m]	Length [m]	Width [m]	Height [m]
300	30	30	7	2	1

Table 1.1: Assumed boat dimensions.

The height of the vessel is taken for the hull height, i.e. any radar on the vessel would be placed at this height. Usually, on big boats, radars are placed higher on the bridge, because the illumination angle is more important and therefore the target discrimination can be better. The benefit of placing the radar on the bridge rather than at the same height on the boat will not be investigated in this project.

The sizes can be changed for the simulations, but they have to be scaled relatively to that dimension in order to keep all assumptions valid.

This report will not deal with multiple targets and possible ambiguities due to the multiple echos of several targets. The number of targets will always be included in the system limits.

The system will perform detection over a 2D azimuthal plane. The total range of the radar does not exceed *10 km*.

1.5.2 Simulation parameters

One of the main concerns about the small pirates dinghies is that they have a small RCS but they could also be shadowed by sea-waves, which makes them hard to detect.

In this project, we cannot really investigate all possible sea/wind scenarios. We are going to limit our simulation with some given set of parameters. For instance, we will choose 2 possibles sea-states (details in section 5.1.2), one average with easier detection (weak shadowing) and another sea state which is more rough (dinghy often shadowed). The wind direction will be also considered for 2 values, one with a perpendicular sea-wavefront which is likely to shadow targets and another more parallel where the target are less likely to be hidden by the sea-waves.

The total set of possible values for the sea and wind parameters are summed up in table 1.2. This set of parameters is illustrated with figures 7.4, 7.3 and 7.5.

Sea state		Wind direction	
6	9	$\pi/4$	$7\pi/8$

Table 1.2: Different set of parameters that will be used for simulation.

1.5.3 Project study

This project will cover the radar signal modeling, sea-wave shadowing, the sea-clutter and target responses, the uplink process and finally the target detection and localization.

The focus will be on the signal modeling and foundations of naval MIMO radar. The main goal of the project is to investigate fundamentals about arrays and signal modeling on this near-field MIMO system. Conclusions will decide whether techniques, models or combinations are possible and if their benefit is significant. The gain compared to a SIMO system will also be analyzed.

In the case of night traveling, the sun is no longer keeping the air at the sea surface warm. Therefore, the use of thermal detection could be a more appropriated solution. Indeed, the temperature difference between human bodies and the air becomes much higher during the night than in the day time.

Another idea could be to use the engine noise to find pirates. The process would be to separate the vessel engine noise from the total surrounding noise, to look for little boats. Such solutions are out of the scope of the project but could be considered as alternative solutions.

Chapter 2

Radar main features

To understand the following parts of the project it is important to have a theoretical background on radar main features such as what signal to send, how to obtain the range of a target, what is the accuracy and resolution of the radar and how to find the doppler shift. Then we will see the radar equation and the importance of the Radar Cross Section of the target.

2.1 Basics of radar

Principle. RADAR is the acronym for Radio Detection And Ranging and it is based on waves propagation. The radar principle is that a transmitter sends a wave which will propagate across an environment. Every object encountered will impact the wave and some of its energy will be scattered back to a receiver. This is called *backscattering* and the backscattering over a target produces its *echo*. The received signals are then processed to be amplified and to extract the target's echo from the total environment response. The clutter will then be considered as noise and the echo as the wanted signal. The signal extraction could be done using the environment clutter knowledge and it could be possible to detect objects, their positions, and even their shapes. [5]

Application. The first use of radar has been done for military applications. The radar technology first definition was made by the US Navy in 1940 [5]. Radars permit to detect, track and guide things such as military forces in the ground, the air, the sea or even the space. However it has been adapted to civil utilization. We can find radar technology in the ground-based level for the control of air traffic, sea traffic, weather forecasting... It is also used in sea-based level for collision avoidance and navigation or in air-based level for altimeters or navigation. Radar resolution could go from few centimeters to kilometers, therefore its usage is spread in all kind of domains and applications. [5]

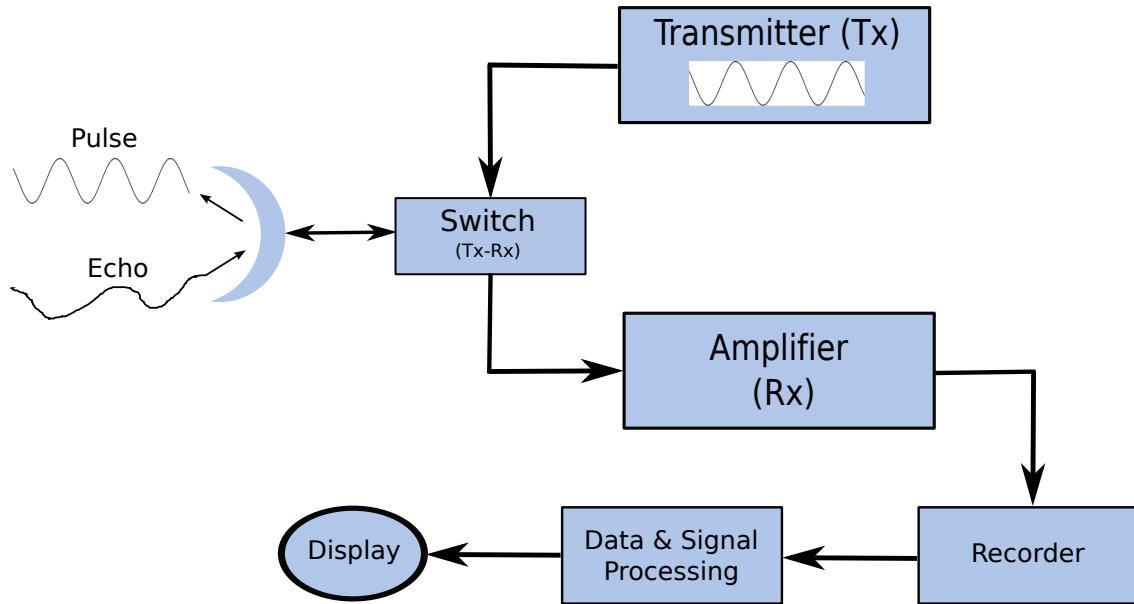


Figure 2.1: Radar simplified architecture

How does it work? The radar functionality could be divided in several main tasks as shown by Figure 2.1. If we use only one antenna we need to switch its state from a transmitting state to a receiving state. For the case of a pulse radar, the first step is to send a wave at a certain carrier frequency and to pulse it on and off. The signal is then sent by the antenna which will be turned into a receiver mode by the switch immediately after. In the receiving mode, the antenna is listening to responses. The backscattering due to a non-free space environment will be detected by the antenna, amplified and then processed to obtain an image of the environment. The radar has an internal clock which permits to compute the time delay between the signal sent and the response. This delay can be used to know how far a target is from the antenna using the speed of the wave in the air (2.1) . [5]

$$R = \frac{c_0 \cdot \tau}{2} \quad (2.1)$$

Where:

- τ is the time delay between sent signal and response [s]
- R is the range: distance between the radar and the target [m]
- c_0 is the speed of the electromagnetic wave in vacuum $3 \cdot 10^8$ [m · s⁻¹]

2.2 Overview of the main types of radar

The radar technology is in reality way more complex and particularly in a processing point of view. It depends on the application we want the radar to work

with and as mentioned, radar is used in many domains. Consequently different types of radars were designed and there are many parameters to characterize them. From a physical point of view we can distinguish two types:

- **Monostatic radars** are radars that use only one antenna. The transmitting antenna and the receiving antenna are then the same. The mode of the antenna is managed by a switch as shown by Figure 2.1.
- **Multistatic radars** are radars using several antennas. The most known of the multistatic radars is the bistatic radar which has transmitter and receiver separated. An advantage of using the multistatic radars is to profit of the decorrelation between antennas signals to obtain better quality. [6]

The second main parameter that defines a radar is the radiated signal. According to [10] four main types of radar emission exist:

- **Pulse radar** produces a rectangular signal pulse which is radiated periodically. Skolnik considers it as the *default* radar and can characterize radars with no special features.
- **Pulse compression radar** uses frequency or phase modulation in a long pulse to obtain the energy of a long pulse with the resolution of a short one.
- **Moving target Indicator (MTI)**. Pulse radar that is able to detect moving target in a special clutter using low Pulse Repetition Frequency (PRF). The range has no ambiguities but the Doppler domain does not permit to obtain the speed of a target.
- **Continuous wave radar** radiates a continuous sine wave and uses Doppler frequency shift to detect moving targets.

The last parameter which permits to differentiate the radars is their application and according to [10] four radar applications are dominant:

- **Surveillance radar** is used to detect objects in range and angle. Concentrating on object it could permit to obtain its track over the time.
- **Tracking radar** is used to obtain the target trajectories. There are four different tracking radars used depending on several parameters such as the number of targets for example.
- **Imaging radar**. Usually these radars are moving and they provide images of a environment in two dimensions. The most known application of these are to map the earth surface.
- **Guidance radars**. The main application of these radar is the self guidance. For example the radar is on a missile and it detects the target so the missile just goes in the target direction.

It is possible to extract many information from the use of radar. The more important ones are: [10]

- **The range** is the distance between the receiving antenna and the target. It is computed using (2.1) for a monostatic radar. It could go from centimeters to kilometers depending on the radar parameters and especially the radar bandwidth.
- **Radial velocity** represents the velocity of the target looking at the rate of change of its range over the time. The second way to obtain the radial velocity is to use the Doppler frequency shift.
- **Angular direction** depends on the directivity of the receiving antenna. The angular direction is the angle where the magnitude of the echo is the highest.

If the environment permits to have a good echo from the target in a low profile clutter then we can use these data to obtain more detailed information about the target such as its size and shape. Obviously, it depends also on the radar resolution and the waveform of its emitted signal. The Signal-to-Clutter Ratio (SCR) between the power of the signal backscattered by the target and the clutter in the received echo is analogous to the Signal-to-Noise Ratio (SNR) usually used in communication transmissions as showed by (2.2) and (2.3)

$$SNR = \frac{P_s}{N_0} \quad (2.2)$$

Where:

P_s is the received power of the useful signal [W]
 N_0 is the received power of the noise [W]

$$SCR = \frac{P_{echo}}{P_{clutter}} \quad (2.3)$$

Where:

SCR is the Signal-to-Clutter Ratio
 P_{echo} is the received power of the target in the echo [W]
 $P_{clutter}$ is the received power of the clutter in the echo [W]

2.3 Frequency bands regulation

The radar technology can use specific frequencies bands. The allowed frequencies could go from 5 MHz for the lowest and can go above 95 GHz. As the higher

frequencies provide wider bandwidths with narrow beamwidths, they permit to reach higher range resolution and accuracy. According to [10], the radar frequency band could be divided in several bands used for different applications. Due to cohabitation problems leading to interference with other wireless technologies the entire 5MHz to 95GHz band is not usable by radar technology. This is the reason why the International Telecommunication Union (ITU) allocates parts of the frequency bands to specific usage. The specific frequencies allocated to the radar technology can be found in Table 2.1.

Frequency band	Radar usage	Specific radar band defined by ITU
HF (3-30 MHz)	Very long range (more than 200 nmi)	-
VHF (30-300 MHz)	Long range air surveillance and ballistic missiles	138-144 MHz 216-225 MHz
UHF (300-1000 MHz)	Airborne moving targets, tracking of satellites and missiles or wind profiling	420-450 MHz 890-942 MHz
L Band (1-2 GHz)	Long range air surveillance radar and intercontinental ballistic missiles	1215-1400 MHz
S Band (2-4 GHz)	Airport surveillance, 3D images and weather estimation	2.3-2.5 GHz 2.7-3.7 GHz
C Band (4-8 GHz)	Boundary between S and X bands	4.2-4.4 GHz 5.25-5.925 GHz
X Band (8-12 GHz)	Imaging, missile guidance, high-resolution and military ground-based applications	8.5-10.68 GHz
K Bands (12-40 GHz)	Physically small radars	13.5-14 GHz 15.7-17.7 GHz 24.05-24.25 GHz 24.65-24.75 GHz 33.4-36 GHz
Millimeter Wave radar (12-94 GHz)	Scientific applications	59-64 GHz 76-81 GHz 92-100 GHz

Table 2.1: Radar features with respect to the International Telecommunication Union (ITU) operating bands. [10]

2.4 Emitted signal

The range of a target is found using (2.1). In this equation the time delay τ of the target echo is the time for the emitted pulse to go from the radar emitter to the target and to come back to the radar receiver. The pulse period is the length of the pulse and it represents the transmitting period of the radar (see Figure 2.2). The

entire time period composed by the radar is the pulse repetition time (PRT) and it is repeated periodically.

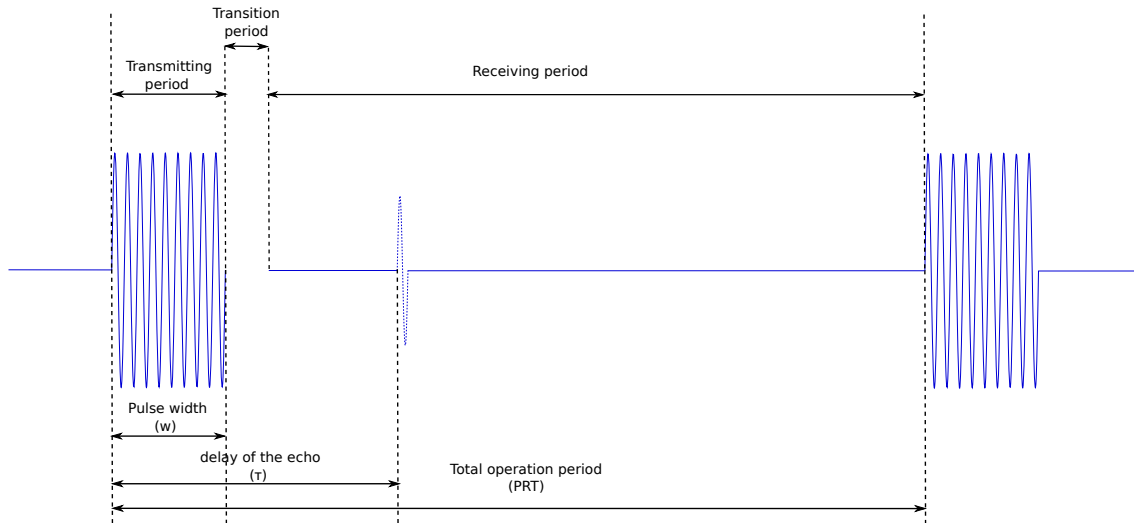


Figure 2.2: Time representation during the radar operating period

The pulses are transmitted at a certain carrier frequency to profit of the waves propagation properties. An major point in radar system is to pay attention at the length of the pulse repetition period in comparison to the maximum range we want to be able to detect a target. As the range is computed depending on the time delay of the target echo it is necessary to have enough time to detect the target before to retransmit the pulse. The PRT gives the maximum range it is possible to detect by (2.4). If the delay is not respected or if two targets are too close one to the other their echos will give an *ambiguous* result and if the echo arrives alone or in time compared to the PRT then the range will be *unambiguous*.

$$R_{max} = \frac{c_0 \cdot PRT}{2} \quad [m] \quad (2.4)$$

2.5 Radar detection

The detection of a target by the antenna is made if the antenna orients its beam in the good direction. Depending on the antenna characteristics, the echo will arrive with enough power to be detected or not. That is the reason why we are going to see these main parameters that define antennas and the reception quality.

2.5.1 Directivity and gain of antennas

The way an antenna radiates is defined by its radiation pattern. The more simple antenna in term of pattern is the omnidirectional antenna which radiates exactly the same way in all directions. The radiation pattern represents the distribution of the power which is radiated by the antenna depending on the direction. As it is possible for an antenna to radiate differently around itself, a notion of directivity appeared.

The directivity is defined by the *IEEE Standard Definitions Terms for Antennas* as “the ratio of the radiation intensity in a given direction from the antenna to the radiation intensity average over all directions” [11]. Its notation is $D(\theta, \phi)$. As part of the total power given to the antenna is affected by dielectric and conduction losses, the total radiated power is not the same. These two attenuation coefficients e_c and e_d and the directivity of the antenna permit to compute the gain of the antenna $G(\theta, \phi)$. The gain represents the radiated pattern of an antenna taking into account the antenna efficiency and follows (2.5) [11].

$$G(\theta, \phi) = e_c \cdot e_d \cdot D(\theta, \phi) \quad (2.5)$$

To characterize the antenna beam we will consider that the directivity is taken from the place where the radiation intensity is the higher. Two planes are defined for this project:

- **Azimuthal plane:** it represents the ground plane, the horizontal plane. We will define it by the x and y axis.
- **Elevation plane:** it represents the altitude plane, the vertical plane. We will define it by the y and z axis.

The beam is characterized by the Half Power Beamwidth (HPBW) which is the illuminated zone where the power radiated is more than $-3dB$ in the azimuthal plane and in the elevation plane. The HPBW for the azimuthal and elevation plane are respectively shown in Figure 2.3 and 2.4. According to [12] radar applications use small beams in azimuthal plane but large ones in the elevation plane. For a Fan-beam antenna $HPBW_\theta$ is between 20° and 30° and $HPBW_\phi$ is equal to 1° .

In our situation the antenna is placed on a large vessel and to reach the target the beam has to touch it. It means that the boat has to be inside the $HPBW_\phi$ of the antenna. As we want the target to be detected from any position in the maximal range, the beam is directed in all directions in order to scan the landscape and all the positions will then be illuminated by the beam. Thanks to the very small $HPBW_\phi$, we can sweep the azimuthal plan with a high definition.

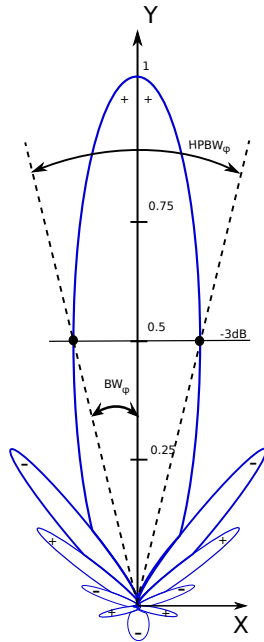


Figure 2.3: 2D azimuthal plane pattern in linear scale

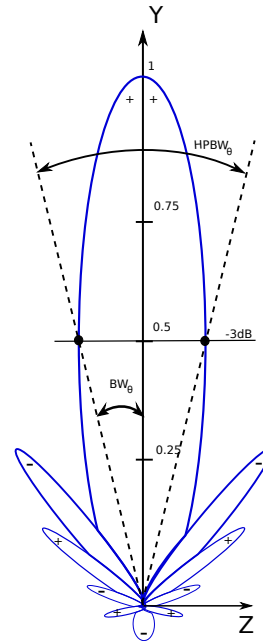


Figure 2.4: 2D elevation plane pattern in linear scale

2.5.2 Radar range resolution

The radar range resolution (ΔR) permits to define if the emitted signal will permit to detect the targets in an unambiguous way or not. When two objects are very close, the radar is then not able to detect the two of them. This space is defined by the pulse width. If the delay between two targets echo is bigger than the pulse width (W) then the two targets will be detected. If it is not the case then the detection will be ambiguous (see Figure 2.5). The radar range resolution is defined by (2.5).

$$\Delta R = \frac{c_0 \cdot W}{2} \quad [m] \quad (2.6)$$

2.6 Doppler shift

When a target is in motion the reflected waves are impacted. A change in frequency appears. It is called the Doppler effect. If the target goes directly to the radar, the frequency will be increased because the path is shortened for the EM wave (Figure 2.6). Obviously, if the target moves in the opposite side of the incoming EM wave then the frequency will be lowered. The doppler shift characterizes this change in frequency following equation (2.7). [5]

$$f_d = \frac{2 \cdot v_r}{\lambda} = \frac{2 \cdot v_t \cdot \cos(\theta)}{\lambda} \quad (2.7)$$

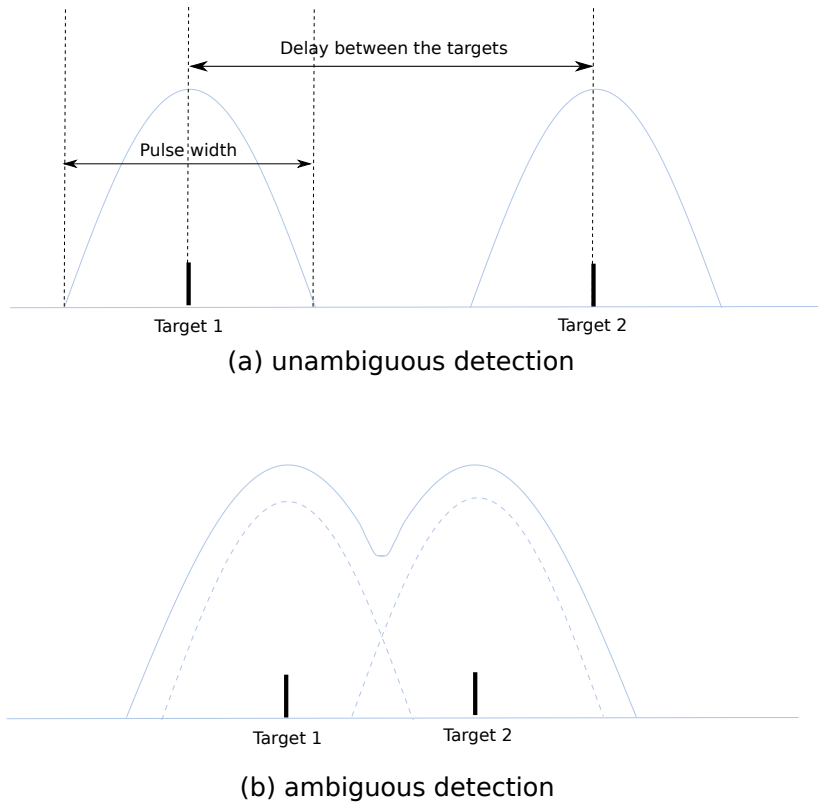


Figure 2.5: Radar resolution illustration



Figure 2.6: Target motion influence on the EM wave phase

In equation (2.7), the presence of the factor 2 is due to the radar system. If the target goes in the radar direction it will shorten the path for the EM wave to go from the radar to the target but also from the target to the radar. The frequency shift will create a continuous change of speed in the phase evolution of the EM wave. For a $\frac{\lambda}{2}$ movement of the target in the radar direction the total path shortened for the EM wave will be λ and the phase shift will be 2π and not only π .

2.7 Radar equation

The radar equation is the equation which permits to calculate power of the received echo from a target from the input power. First, we have to calculate the power density at the target is given by (2.8) [13].

$$I_{ft} = \frac{P_{Tx}G_{Tx}}{4\pi R^2} \quad [W/m^2] \quad (2.8)$$

Where:

P_{Tx}	Total radiated power by the transmitter.
G_{Tx}	Transmitter gain.
R	The range between the radar and the target.

Then, a certain amount of that power density is reflected/scattered back to the transmitter. This energy amount is proportional to the reflecting surface of the target. Then, it is straightforward that the bigger is the target, the more energy will be sent back to the radar. The Radar Cross section, that will be denoted by σ , represents the equivalent reflection surface for the radar. The re-radiated power is given by (2.9).

$$P_{re} = \frac{P_{Tx}G_{Tx}\sigma}{4\pi R^2} \quad [W] \quad (2.9)$$

This applies in the isotropic propagation case. Finally, the power is re-radiated towards the radar. Once again, there is a range attenuation due to the travelled distance. The power flux density at the reception side is given by (2.10) [13].

$$I_{fr} = \frac{P_{Tx}G_{Tx}\sigma}{(4\pi R^2)^2} \quad [W/m^2] \quad (2.10)$$

To calculate the amount of received power, we need to know the geometric area of the receiving antenna. If we know the efficiency of the antenna, we can write the effective antenna aperture with (2.11) [13].

$$A_e = A_g K_a \quad [m^2] \quad (2.11)$$

Where:

A_e	Effective antenna aperture.
A_g	Geometric antenna area.
K_a	Antenna efficiency.

The mean power received by the radar is given in (2.12).

$$P_r = \frac{P_{Tx}G_{Tx}\sigma A_e}{(4\pi R^2)^2} \quad [W] \quad (2.12)$$

2.8 Polarization

One of the most important factor that defines the good reception of a polarized signal is the polarization factor. The polarization of an antenna can filter signals at the receiving point. In radar system, target echo could be polarized depending on the target electro-magnetic properties. The polarization is defined by the direction of the electric field (E-field) vector. There are three possible polarizations: linear, circular and ellipsoid [11].

2.8.1 General polarization

In the general case, the polarization of waves is elliptical. It means that the E-field direction varies following an ellipse as shown by Figure 2.7. The requirements to have an elliptical polarization are the following ones:

- “The field must have two orthogonal linear components, and
- The two components can be of the same or different amplitude.
- (1) If the two components are not of the same magnitude, the time-phase difference between the two components must not be 0° or multiples of 180° (because it will then be linear). (2) If the two components are of the same magnitude, the time-phase difference between the two components must not be odd multiples of 90° (because it will then be circular)” [11].

The time phase difference between the two components implies that there will be a phase-leading component and a phase-lagging one. The sense of rotation of the E-field is determined by going from the phase-leading component toward the phase-lagging one. If the sense of rotation goes clockwise then it is called right-hand (or clockwise) elliptically polarization. If the sense of rotation goes counterclockwise then it is called left-hand (or counterclockwise) elliptically polarization.

2.8.2 Linear polarization

In our project we are going to focus on the linear polarization which implies then a time-phase difference between the two components of 0° or multiples of 180° . This choice is based on the low sensitive properties of the boat and the sea to the type of polarization in front of the high sensitivity of the weapons (detailed in section 4.3.4). For example, a dipole or a straight wire antenna has a linear polarization. If the antenna is placed along the elevation z-axis it will be z-polarized (also called vertically polarized) and if the antenna is placed along the x-axis it will be x-polarized and if placed along the y-axis: y-polarized. The x-polarization and y-polarization are also called horizontal polarization. Figure 2.8 illustrates these three different linear polarizations.

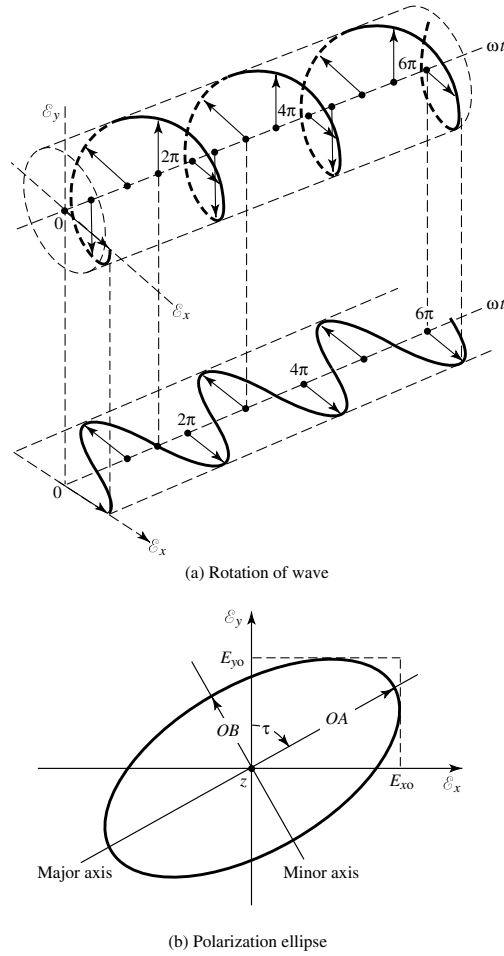


Figure 2.7: Elliptically polarized wave illustration as a function of time [11].

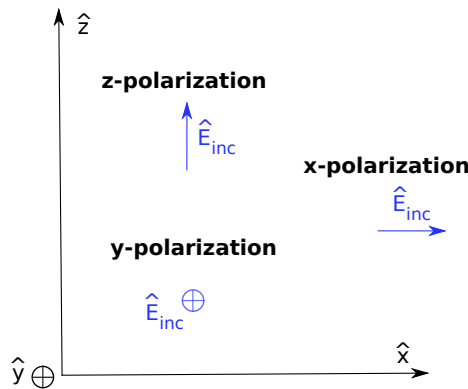


Figure 2.8: x, y and z polarizations

2.8.3 Polarization loss factor

The polarization loss factor (PLF) permits to qualify the matching between an incident wave polarization and the antenna one. It could go from 0 to 1 and is defined

by (2.13) [11]. Figure 2.9 illustrates the polarization vectors.

$$PLF = |\hat{\rho}_\omega \cdot \hat{\rho}_a|^2 = |\cos \psi_p|^2 \quad (2.13)$$

Where:

PLF	Polarization loss factor.
$\hat{\rho}_\omega$	Incident wave unit polarization vector.
$\hat{\rho}_a$	Antenna wave unit polarization vector.
ψ_p	Angle between the two polarization vectors.

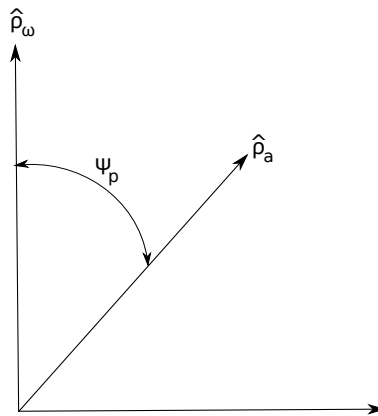


Figure 2.9: Polarization unit vectors

2.8.4 Co-polarization and Cross-polarization

In the polarization domain we often need to qualify the polarization depending on another one. To optimize the reception of an antenna, it must be polarized the same direction as the arriving signal. For example, two antennas communicating together could have two different polarizations. If their polarizations have identical E-field direction over time, then the polarization of the receiving antenna is said co-polarized. If E-field directions are orthogonal over the time, then the receiving antenna is said to be cross-polarized. In figure 2.10, the antenna polarized following the $\rho_{antenna}$ vector would be co-polarized to a z-polarized antenna but cross-polarized to a x-polarized or y-polarized antenna. For radar applications using one linearly polarized antenna as transmitter and receiver, the co-polarization will happen when the polarization will be the same for the emitting and the receiving part.

2.8.5 Cross polarization discrimination

In the radar systems, when the signal is backscattered by a target, the signal polarization can be affected depending on the target shape and orientation. If the

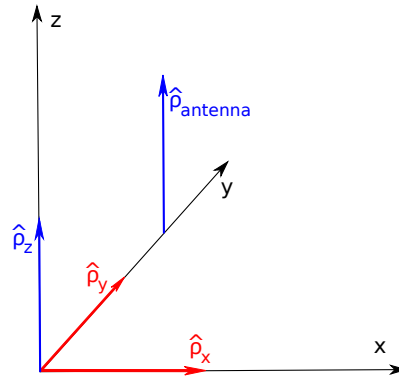


Figure 2.10: Co and cross polarization example

target has an “I-plate” shape oriented in the z -axis then the backscattered signals will mainly be linearly z -polarized. Depending on the width of the I-shape target (assumed in the y -axis direction), the cross sectional component will be the signals y -polarized. The variation of the receiving polarization can permit us thanks to the PLF to filter the received signals. To continue with the previous example, if the antenna is z -polarized in emission and reception (co-polarization) then the reception of the backscattered signals will be optimized and only the length of the I-shape will impact the reception quality. However if the antenna is z -polarized in emission and y -polarized in reception (cross-polarization) then the reception will mainly be due to the width of the I-shape: its cross-sectional part to the emitted polarization. Consequently the part of the target oriented in the emitted polarization direction will be the co-sectional part. The cross polarization discrimination (XPD) is then the loss or gain going from a co-polarization to a cross polarization.

Using the polarization we are able to detect the co-sectional part of an object or its cross-sectional part independently. It could be used to discriminate objects in an environment knowing its co and cross-sectional properties. It is obvious that we need to use multiple polarizations to exploit these properties.

2.8.6 Linear polarization modulation

The polarization of an antenna could be adapted to a given polarization by changing the amplitude of the signals which fed them. If the two components are respectively directed in the x and y axis with the same signals amplitude then the resulting unit polarization vector will be in the diagonal. If the amplitude of the signal feeding the x -axis component is twice the y -axis one, then the polarization unit vector will have a 22.5° angle with the x -axis. The two cases are illustrated in Figure 2.11.

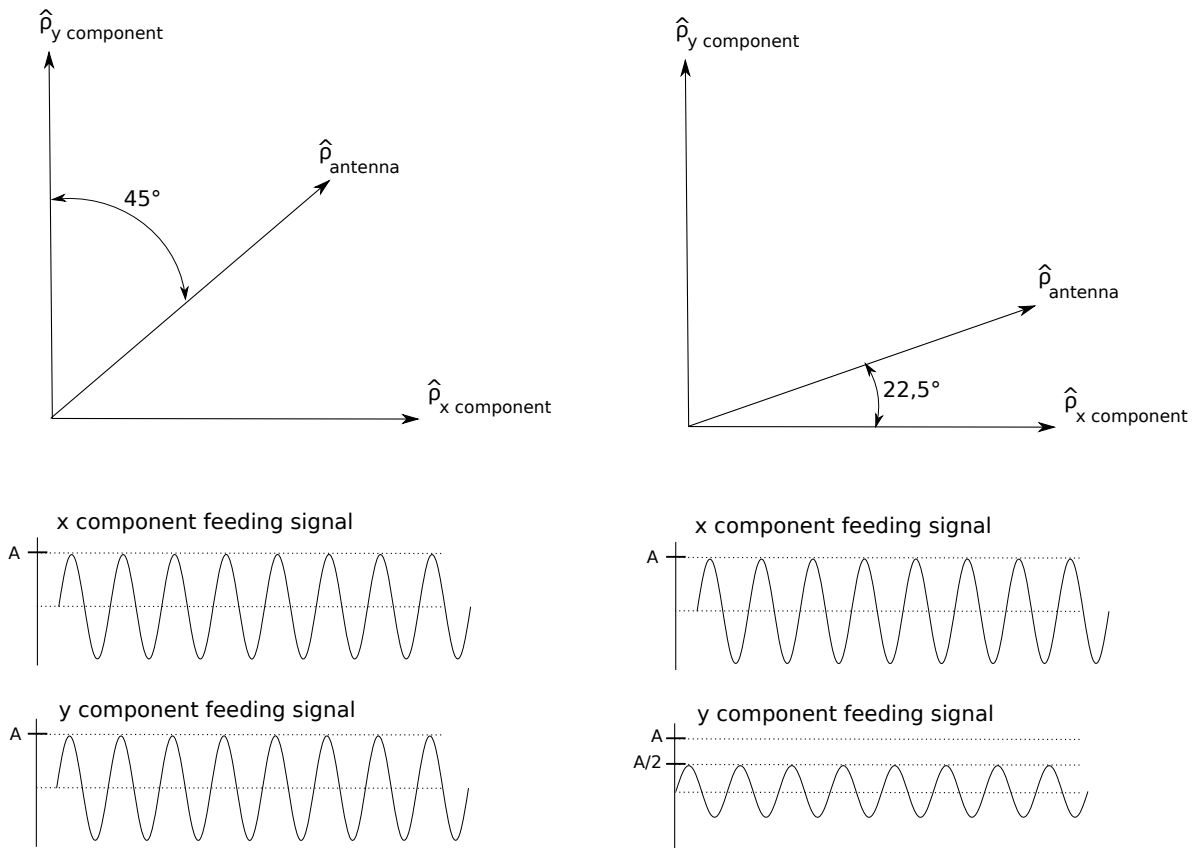


Figure 2.11: 2 components antenna polarization affected by a change in the feeding signals

Chapter 3

Model

This chapter introduces the model we use for the near-field MIMO radar. It is divided in two parts: the general description of the system that is modeled and the basic assumptions made for this project.

3.1 General overview

This first part defines a model representing the complete near-field MIMO system. Figure 3.1 shows the main features of the project model.

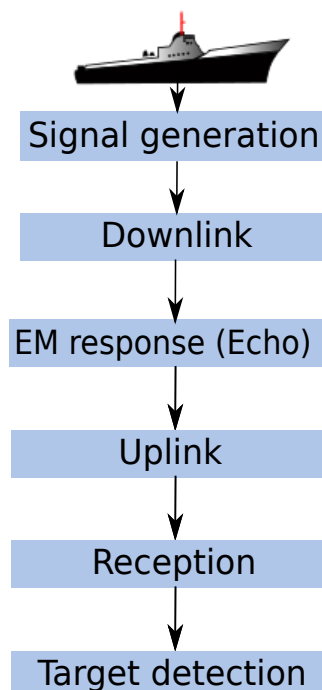


Figure 3.1: General process in the model

Some steps of the main process could be divided into several parts, such as the echo calculation. Figure 3.2 shows how to build the downlink calculation part.

The downlink consists in calculating the range attenuation depending on the sea-state. That range attenuation can use either the double path propagation model or the simple free space equation. The shadowing and angular correlation are calculated in the echo part described later.

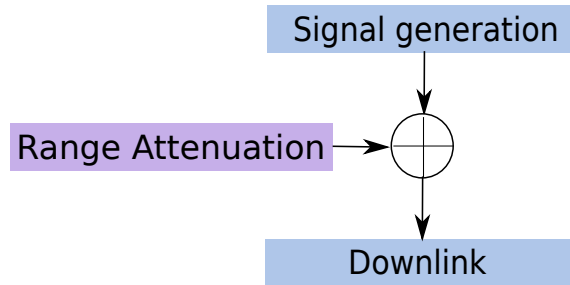


Figure 3.2: Calculation of the downlink signal

In the same fashion, figure 3.3 shows how to build the echo calculation part. This echo part consists in calculating the shadowing and sea effect on the EM response. Shadowing will affect the boat RCS but also the sea electromagnetic response. The angular correlation calculation will be described in *Appendix C. Signal correlation*.

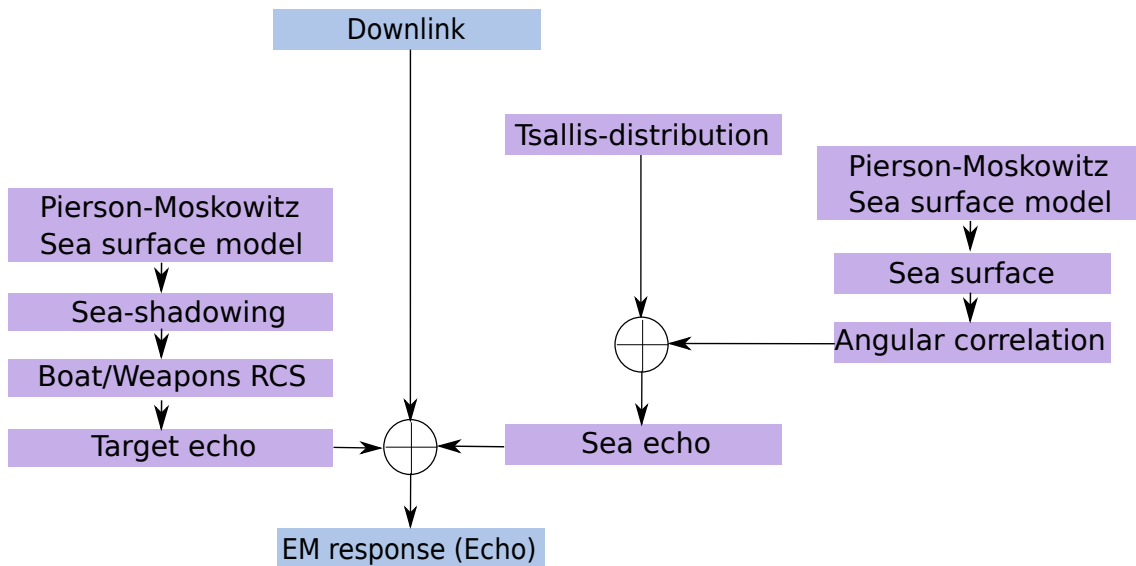


Figure 3.3: Calculation of the global EM response

Finally, the uplink part can be divided into subparts as shown by Figure 3.4.

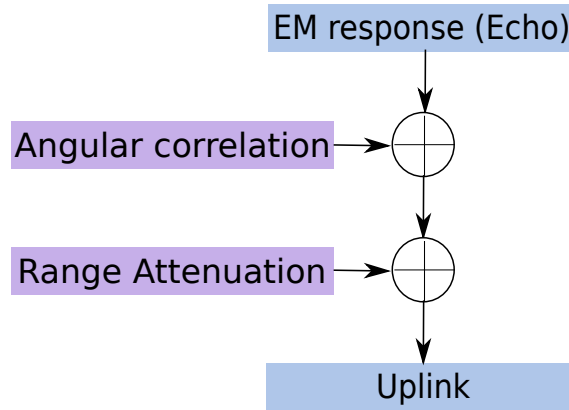


Figure 3.4: Uplink part in the model

In the following, a radar transmission description and definition will first be provided, looking at the transmitted signal and the number of antennas and their positions. Second, we want to characterize and simulate the sea-clutter environment. A physical description and model will be provided for that sea-clutter. The model of the sea clutter will cover the sea surface and the electromagnetic responses of that sea-clutter. (See Fig. 3.1). Finally, we will also define the processing applied to signals to detect and locate targets.

3.2 Radiating near-field

According to the Balanis book [11], the far field region for an antenna is considered to be any point further away than $D_{far-field}$ from this antenna defined by (3.1).

$$D_{far-field} = \frac{2D_a^2}{\lambda} \quad (3.1)$$

Where:

- D_a Largest size of the antenna array: almost the vessel dimensions
- λ Wavelength corresponding to the operating frequency.

According to this equation, the radar detection will happen in the near-field region. If we take the example of $f = 1 \text{ GHz}$ and a vessel with a length of $D_a = 300 \text{ m}$, we obtain

$$D_{far-field} \approx 600 \text{ km}$$

In the exact vessel axis, we obtain the following range for 1 m antennas:

$$D_{far-field} \approx 6.6 \text{ m}$$

The gain obtained by the boat large dimension diversity is lost when the antenna is trying to illuminate in front of the boat since all antennas are aligned and the information they will get could be really close with each other. The performance of the detection will be the same as with a single radar in the exact axis of the boat.

We can calculate the limit of the far-field for 10 km (see section 3.3.1). The limit angle is given by (3.2)

$$\alpha_{LIMIT} = \sin^{-1} \left(\frac{\sqrt{\frac{\lambda}{2}} D_{far-field}}{D_a} \right) \quad (3.2)$$

Where:

α_{LIMIT} Limit angle with the axis of the boat to be in the near-field up to $D_{far-field}$ m.

In the axis of the boat, we obtain $\alpha_{LIMIT} \approx 7^\circ$. Figure 3.5 shows that angle.

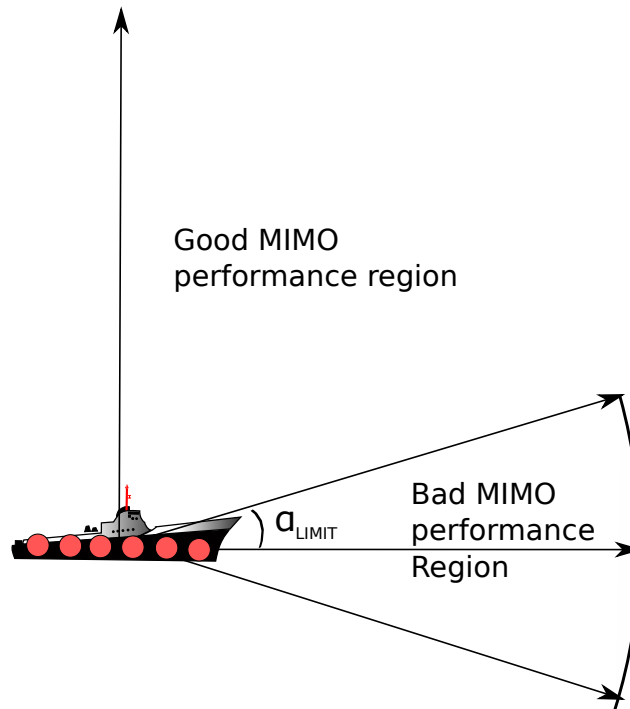


Figure 3.5: Bad MIMO performances region

3.3 Earth curvature

The earth curvature decreases the geometrical range of the vessel. We can calculate the geometrical horizon of the radar, it is given by (3.3)

$$D_{vessel} = \cos^{-1} \left(\frac{R_e}{R_e + h_{vessel}} \right) \cdot R_e \quad (3.3)$$

Where:

- R_e Earth radius.
- h_{vessel} Height of the vessel, waves included.

We can do the same calculation for the horizon seen from the pirate dinghy. Finally, the real horizon is given by (3.4)

$$D_{horizon} = D_{vessel} + D_{dinghy} = \left(\cos^{-1} \left(\frac{R_e}{R_e + h_{vessel}} \right) + \cos^{-1} \left(\frac{R_e}{R_e + h_{dinghy}} \right) \right) \cdot R_e \quad (3.4)$$

Where:

- R_e Earth radius.
- h_{vessel} Height of the vessel, waves included.
- h_{dinghy} Height of the dinghy, waves included.

We calculate that geometrical horizon for $h_{vessel} = 30 \text{ m}$ and $h_{dinghy} = 1.5 \text{ m}$, we obtain the following result:

$$D_{horizon} \approx 24 \text{ km}$$

From this statement, we can consider that the radar will operate in a smaller range to ensure the dinghy is visible.

3.3.1 Maximum range

Outboard motors can reach up to 300 *hp*. [14]. Tests made with different 300 *hp* motors reveal that they achieve satisfactory performances: they can reach 50 *knots* speed at maximum. The average speed of these motors is 30 *knots*. In our simulation, we consider pirates moving towards the vessel at a speed of 30 *knots*, which represents

15 m/s . Then, if the pirates are detected at a distance of 10 km , it leaves a bit more than 10 minutes to the vessel crew to get ready to counter an eventual attack.

If we consider the weapons range, (See section 4.3.1 for considered weapons) We should have the following effective ranges [15]:

- AK-47 : Around 400 m
- Rocket Launcher : Around 200 m

Several detections within a big enough time interval can allow to estimate the relative speed of the boat compared to the vessel. We can assume that if pirates want to attack a vessel, they are traveling towards the vessel.

We want the dinghy to be detected when it is in the 10 km . Therefore, the maximum detection range will be 10 km in our simulation, which represents less than half of the theoretical vessel effective range (24 km).

3.3.2 Flat earth model

We denote d_{curv} the distance along the earth taking into account the earth curvature. d_{flat} would represent the same distance, but considering the earth completely flat. An illustration is given in Figure 3.6

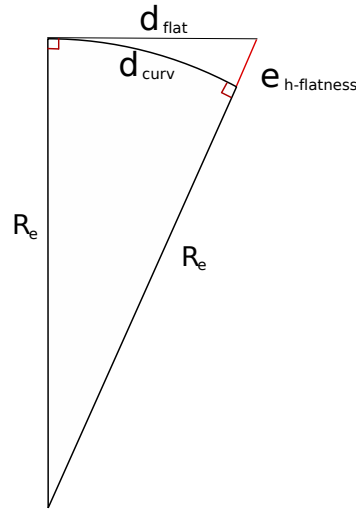


Figure 3.6: Earth curvature error representation

We can calculate the error percentage $e_{d-flatness}$ thanks to the formula given by (3.5).

$$e_{d-flatness} = \frac{|d_{curv} - d_{flat}|}{d_{curv}} = \frac{\left| d_{curv} - R_e \cdot \tan\left(\frac{d_{curv}}{R_e}\right) \right|}{d_{curv}} \quad (3.5)$$

Considering our maximum detection range, if we take $d_{curv} = 12 \text{ km}$, we obtain that d_{flat} is 14.2 cm longer than d_{curv} , whether $e_{d-flatness} \approx 10^{-4} \%$

Since the $e_{d-flatness}$ value is small, we can consider that distances given by d_{curv} or d_{flat} are the same in our model. The radar resolution will not be able to see the error induced by the earth curvature.

From this calculation, we can also calculate the height error denoted $e_{h-flatness}$ with equation (3.6)

$$e_{h-flatness} = \sqrt{R_e^2 + d_{flat}^2} - R_e = R_e \left[\sqrt{1 - \tan^2 \left(\frac{d_{curv}}{R_e} \right)} - 1 \right] \quad (3.6)$$

In our case, we obtain $e_{h-flatness} \approx 11 \text{ m}$ for $d_{curv} = 12 \text{ km}$. This value will be calculated and subtracted from the sea-height in the sea-surface model, because it is important compared to the dinghy and vessel heights.

3.4 System Grid

3.4.1 Symmetry axis

In our system, we will focus on a detection over a $10 \times 10 \text{ km}^2$ square. For the sake of simplicity and to save processing power and memory, we will only focus on one quarter of the available space for the vessel. Everything on the other side is completely symmetric. The region of interest is illustrated in Figure 3.7

Indeed, fig. 3.7 arrows show the symmetry axis with respect to the boat and the sea. The antenna elements are symmetric along the horizontal arrow. Then, every detection under and above the horizontal arrow will be considered as identical configuration.

The same things happen with the vertical arrow, that shows a symmetry axis between antennas as well. Then, everything that happens at the right and left side of that arrow is basically the same case.

Therefore, we can ignore the hatched region in fig. 3.7, since it does not bring anything new if the simulation is restricted to the region of interest. At the same time, memory and processing power will be saved for the simulation.

3.4.2 Resolution

In our model, we will consider antennas with a bandwidth $W_a = 60 \text{ MHz}$. The bandwidth is chosen in order to have a resolution that will match more or less the

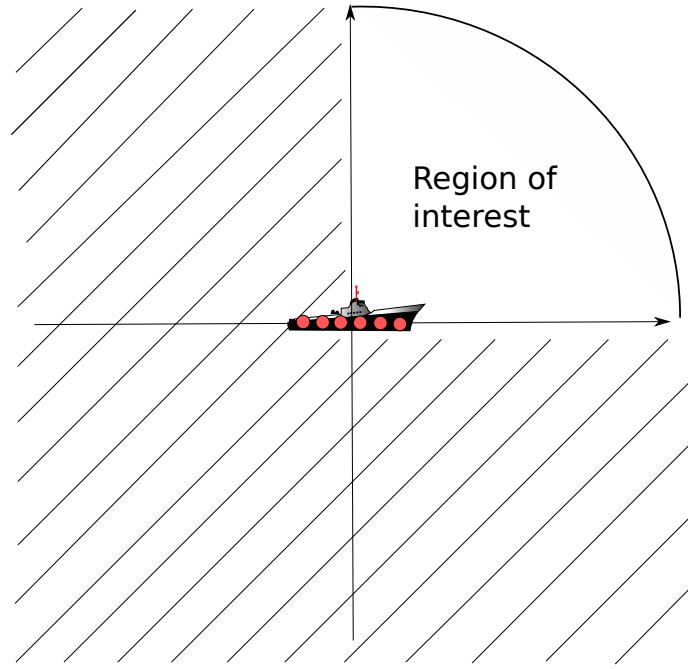


Figure 3.7: Region of interest for the analysis

target size [9]. With such a bandwidth, we can find our spatial resolution with the following equation (3.7).

$$S_{resolution} = \frac{c_0}{W_a} \approx 5m \quad (3.7)$$

Therefore, in our system, each grid pixel will represent a $5 \times 5 m^2$ square. This is the radar resolution.

3.4.3 Radar pulses

From the bandwidth, we can calculate the length of the signal in seconds, which is given by (3.8).

$$T_{pulse} = \frac{1}{W_a} = \frac{1}{60 \cdot 10^6} \approx 1.67 \cdot 10^{-8} s \approx 0.016 \mu s \quad (3.8)$$

With T_{pulse} , we can calculate the minimum range for the radar, given by (3.9).

$$R_{min} = \frac{c_0 \cdot T_{pulse}}{2} = 2.4 m \quad (3.9)$$

R_{min} is way sufficient for our application, due to the high bandwidth. To increase this value, we can raise the bandwidth. Then, for a given operating frequency, we can therefore find the number of pulse sent with equation (3.10).

$$n_p = \frac{1/W_a}{1/f_c} = \frac{f_c}{W_a} \quad (3.10)$$

Chapter 4

Radar Cross Section

In this section we will see what amount of energy is backscattered from an object depending on its material, its directivity and its area visible by the radar. All these parameters define the RCS (σ) of an object. It corresponds to a fictional area that intercepts the energy radiated by the radar and backscatters a part of it. The RCS can be defined by (4.1) [10]. It is fictional because the RCS does not represent the area that reflects energy but it also takes into account the material properties and the directivity of the reflected waves.

$$\sigma = \frac{\text{power reflected toward the source/unit solid angle}}{\text{incident power density}/4\pi} \quad [m^2] \quad (4.1)$$

According to [16] the RCS could also be defined by (4.2).

$$\sigma = A_p \cdot R_r \cdot D_r \quad [m^2] \quad (4.2)$$

Where:

- A_p is projected object surface [m^2]
- R_r is the reflectivity, re-radiated fraction of intercepted power
- D_r is the directivity, ratio of the maximum intensity of the radiator to the intensity of an isotropic source.

4.1 Sea-clutter radar cross section

4.1.1 Models

Two main models exist to model the sea-clutter RCS, the GIT and the TSC models [17]. In our simulation, we are working with low grazing angles ($\alpha < 2^\circ$, see section 5.1.5). In our case, the most fit model is the GIT sea clutter model [17]. Table 4.1 shows the model delimitations.

Parameter	GIT model	TSC model
Operating frequency [GHz]	1-100	0.5-35
Average wave [m]	0-4	1-2
Wind speed [$m \cdot s^{-1}$]	1.5-15.5	0-2.5
Grazing angle [$^{\circ}$]	0.1-10	0.1-90

Table 4.1: Sea-clutter radar cross section models [18] [6]

4.1.2 GIT model

We denote the RCS of the sea-clutter for an illuminated zone σ_{sea} . To calculate σ_{sea} , we first compute the multi-path factors which can be obtained with (4.3) and (4.4).

$$\sigma_{\phi} = \frac{(14.4\lambda + 5.5) \cdot \alpha(R) \cdot h_{avg}}{\lambda} \quad (4.3)$$

$$A_{\iota} = \frac{\sigma_{\phi}^4}{1 + \sigma_{\phi}^4} \quad (4.4)$$

Then, another factor called sea-direction factor is computed in equation (4.5)

$$A_u = \exp [0.2 \cdot \cos(\vartheta) \cdot (1 - 2.8\alpha(R)) \cdot (\lambda + 0.02)^{-0.4}] \quad (4.5)$$

ϑ is the angle between the wind direction and the radar measurement direction, in radian. Finally, we have the wind speed factors. They are computed in (4.6), (4.7) and (4.8)

$$qw = \frac{1.1}{(\lambda + 0.02)^{0.4}} \quad (4.6)$$

$$V_w = 8.67(h_{avg})^{0.4} \quad (4.7)$$

$$A_w = \frac{1.94V_w}{(1 + V_w/15.4)^{qw}} \quad (4.8)$$

When all of the above parameters A_{ι} , A_u and A_w have been calculated, we can compute the sea RCS which is given by either (4.9), (4.10) or (4.11)

$$\sigma_{sea-normalized}(HH) = 10 \cdot \log(3.9 \cdot 10^{-6} \lambda \alpha^{0.4} \cdot A_{\iota} \cdot A_u \cdot A_w) \quad (4.9)$$

$$\sigma_{sea-normalized}(VV) = \sigma_{sea-normalized}(HH) - 1.73 \ln(h_{avg} + 0.015) + 3.76 \ln(\lambda) + 2.46 \ln(\alpha(R) + 0.0001) + 22.2 \quad \text{when } f \in [0; 3] \text{ GHz} \quad (4.10)$$

$$\sigma_{sea-normalized}(VV) = \sigma_{sea-normalized}(HH) - 1.05 \ln(h_{avg} + 0.015) + 1.09 \ln(\lambda) + 1.27 \ln(\alpha(R) + 0.0001) + 9.70 \quad \text{when } f \in [3; 10] \text{ GHz} \quad (4.11)$$

To obtain the real RCS σ_{sea} , we need to take into account the surface of the illuminated area. σ_{sea} is obtained in (4.12).

$$\sigma_{sea} = \sigma_{sea-normalized} \cdot S_{area} \quad (4.12)$$

Where:

S_{area} Surface of the illuminated area [m^2]

4.2 Target fast fading : Swerling models

Targets are not perfect ideal shapes and their RCS experiences fast fading, often going from 5 to 20 dB [10]. We can explain the phenomenon by the following assumption: the complete RCS is the contribution of many little components of the target which contribute more or less to the backscattered signal. A target RCS is illustrated in figure 4.1.

From that statement, models have been implemented by Peter Swerling to compute the distribution of the target RCS fading. Depending on the target properties, it can be classified into five different categories which are listed below. All following equations are taken from [20].

4.2.1 Swerling I

The target RCS changes every scan and follows the probability density function given by (4.13)

$$p(RCS_{real}) = \frac{1}{RCS_{average}} e^{-\frac{RCS_{real}}{RCS_{average}}} \quad (4.13)$$

For example, if we take a target with a theoretical $RCS_{average} = 0.25 m^2$, then we have the probability of RCS for each scan showed in figure 4.2

Such a model suggests that an infinite value for the RCS can happen, which is not realistic. In the implementation, we cannot really pick up infinite value, we have

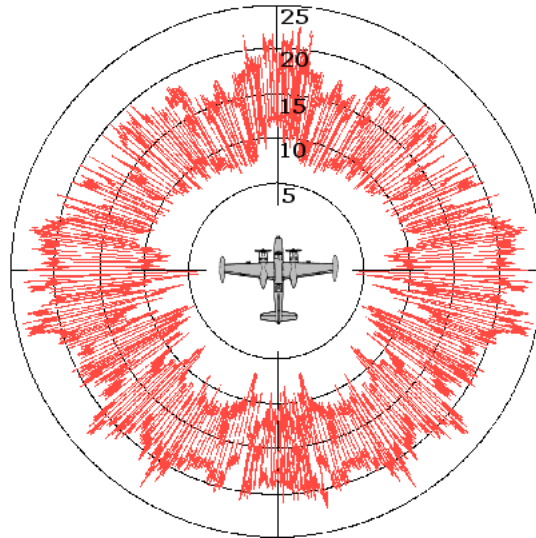
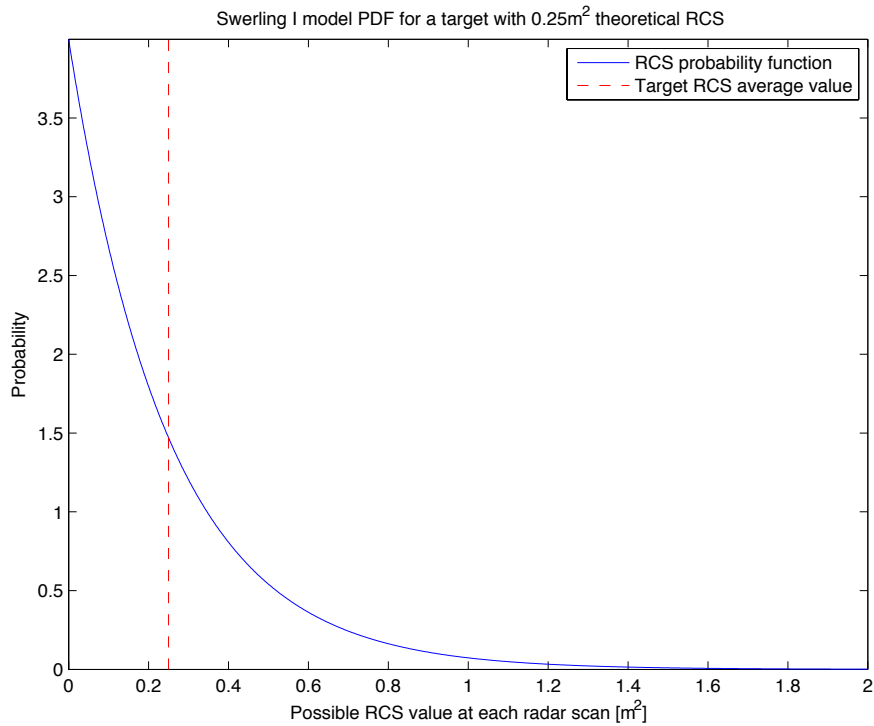


Figure 4.1: Target RCS fast fading [19]

Figure 4.2: Target RCS probability at each scan for a $RCS_{average} = 0.25 \text{ m}^2$ target following Swerling I model.

to choose a maximum possible one. In that case, we can look how important is the contribution of the tail for values higher than T_p . The probability that a higher value happen is given by (4.14)

$$p(x > T_p) = \int_{T_p}^{+\infty} \frac{1}{RCS_{average}} e^{-\frac{x}{RCS_{average}}} dx \quad (4.14)$$

From (4.14), we can derive the result given by (4.15)

$$p(x > T_p) = e^{-\frac{T_p}{RCS_{average}}} \quad (4.15)$$

If we take $T_p = 30 \cdot RCS_{average}$ we have $p(x > T_p) \approx 9.36 \cdot 10^{-14}$. This means that the probability for a $RCS_{average} = 0.25 \text{ m}^2$ target to have $RCS_{real} \geq 7.5 \text{ m}^2$ is less than 10^{-13} .

4.2.2 Swerling II

It is the same case as the Swerling I model, but the RCS value changes (new realization) every pulse, instead of every scan. Therefore, equation (4.13) is used for Swerling II model.

4.2.3 Swerling III

Based on the same principle as Swerling I, the equation of the probability density function changes and gives more freedom to the distribution. The target RCS for a Swerling III model follows the PDF given by (4.16). This PDF is plotted in figure 4.3 for a $RCS_{average} = 0.25 \text{ m}^2$ target [10].

$$p(RCS_{real}) = \frac{4 \cdot RCS_{real}}{RCS_{average}} e^{-\frac{2 \cdot RCS_{real}}{RCS_{average}}} \quad (4.16)$$

4.2.4 Swerling IV

Swerling IV is the same case as the Swerling III model, but the RCS value changes (new realization) every pulse, instead of every scan. Therefore, equation (4.16) is used for Swerling IV model.

4.2.5 Swerling V or Swerling 0

In this case, we consider the RCS to be constant. The RCS is always the same and do not experiences fast fading. Therefore the RCS is given by (4.17)

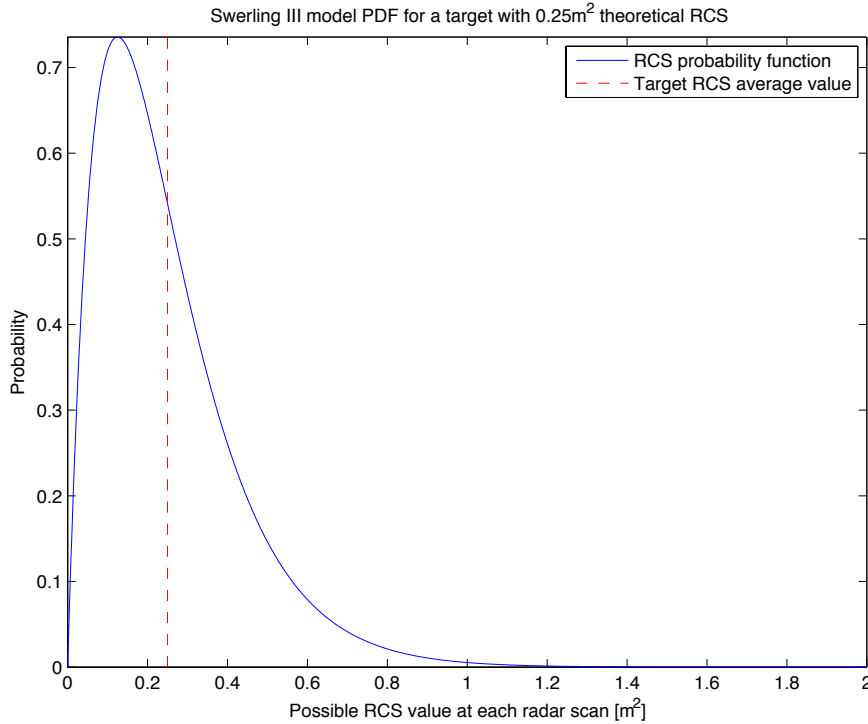


Figure 4.3: Target RCS probability at each scan for a $RCS_{average} = 0.25 \text{ m}^2$ target following Swerling I model.

$$RCS_{real} = RCS_{average} \quad (4.17)$$

We will pick up the Swerling V model for the sea RCS because the fast fading experienced is already modeled by the Tsallis distribution (see section 5.2 for further details).

If measurements with enough data are available, the computed PDF can ensure the corresponding Swerling model to apply.

4.3 Target radar cross section

4.3.1 Boat composition

In this report we will define the radar cross section of the target depending on its shape and properties. It is composed by the hull, the engine and weapons carried by humans. For the project we will study only the following:

- **The hull** needs to be the size of the pirate dinghies such as the boat studied

in [21].

- **The rifles.** We will consider the most used rifle for wars in the world according to the *United Nations Office on Drugs and Crimes*: the AK-47 [22]. In [18] Thayaparan described the AK-47 geometry as 50 cm length, 21 cm width and 3cm of thickness.
- **The human bodies** will not be considered due to their properties close to water ones.

The target components geometry can be seen in Figure 4.4 and their number aboard could be chosen as a parameter of the simulation. We are now going to study independently the RCS of each object on the target.

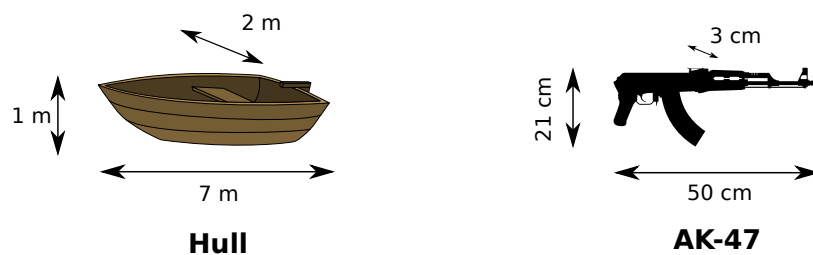


Figure 4.4: Target components geometry

4.3.2 Hull RCS

The pirate boat will be considered as a small dinghy made of wood. Its dimensions will be seven meters long, two meters large and one meter height. From [9], we defined the RCS of the boat to be 0.25 m^2 . According to [16], maritime targets RCS usually follows Swerling model I. Therefore, we are going to use it for the boat RCS.

4.3.3 Rifles RCS

AK-47 RCS measurements

The ak-47 is a weapon mainly made of steel with some wood parts, such as the handle [23]. We are going to study only the basic shape and composition as shown by Figure 4.5. A second handle could be added in half wood and steel part but for the sake of simplicity we are going to concentrate on the basic AK-47.

Measurement campaign has been done in [18] to find the RCS of an AK-47 rifle. The results are given for specific positions of the weapon compared to the antenna. Indeed the weapon has been ideally placed to optimize its response power as shown by Figure 4.6. The measurements take into account two different polarizations. First



Figure 4.5: AK-47 shape and composition

the antenna is co-polarized with the weapon echo and then the polarization is cross-polarized. E_{inc} is the incident E-field, E_{back} is the backscattered E-field and \hat{P} is the propagation vector. The results are shown respectively in Figure 4.7a and Figure 4.7b

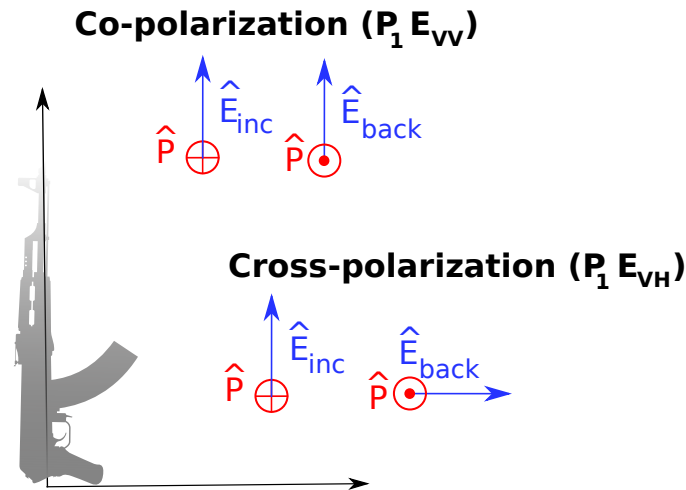


Figure 4.6: orientation of the weapons compared to polarization in [18].

In Figure 4.7a we can see the co-polarization AK-47 RCS behavior depending on the frequency. Higher we go in the frequencies, higher is the RCS going from 0.2 m^2 at 1 GHz to 1.41 m^2 at 2.7 GHz. However it is not true for the cross polarization case. The RCS of the AK-47 for the cross-polarization has a main peak of 0.061 m^2 for 0.4 GHz and a second one of 0.032 m^2 at 550 MHz. Apart from these two peaks the RCS is below 0.01 m^2 . There is also a specific co-polarization AK-47 RCS signature which is not visible on these curves. For the low frequencies, we can observe a really important peak of the RCS of 1.18 m^2 at 245 MHz. These peaks are specific to the AK-47 shape and EM properties, they are visible in Figure 4.8. They represent a resonance effect which is due to the wavelength compared to the size of the weapon. Based on *Appendix B. 3-planes study of weapon RCS* we also have the estimated 3-plans RCS of the AK-47.

In this project we will use linear polarization because the weapons have a shape

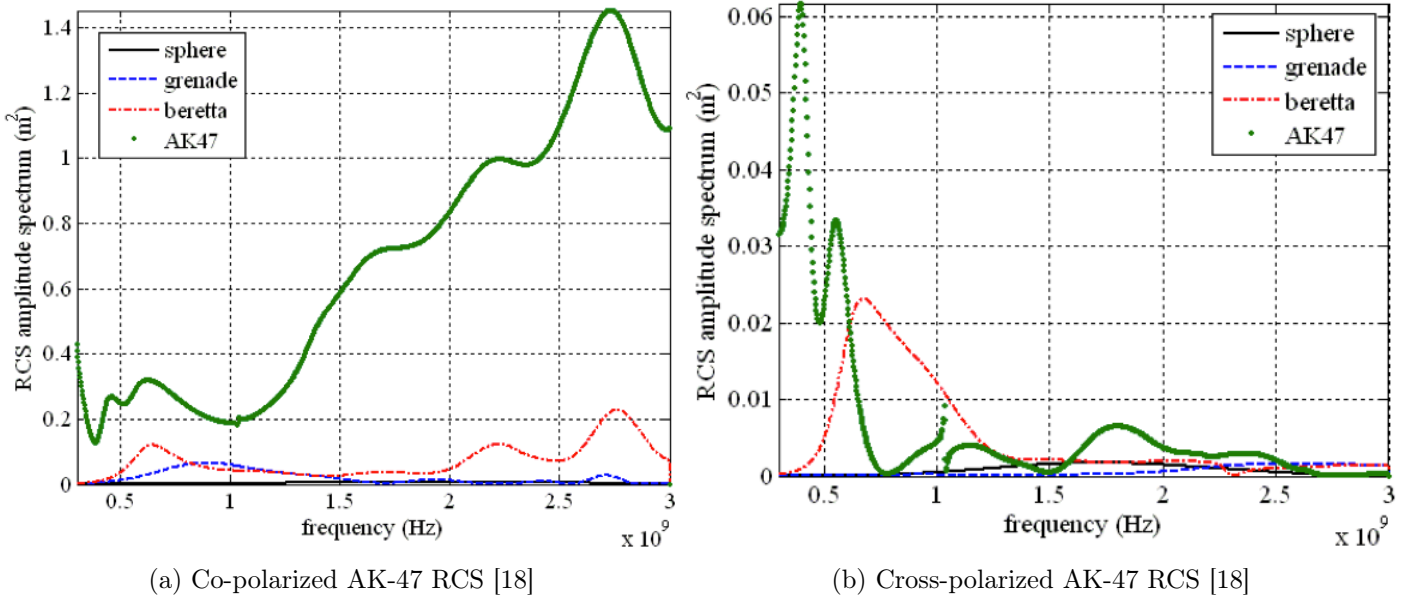


Figure 4.7: Co and Cross-polarization RCS signature of the AK-47.

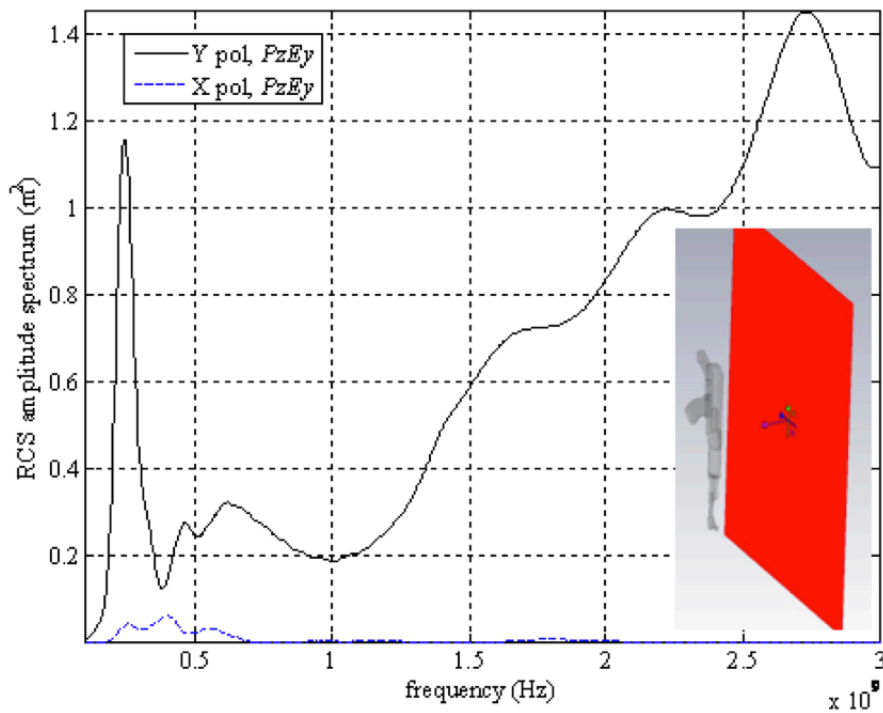


Figure 4.8: Comparison between co and cross-polarization looking at the AK-47 RCS [18].

of cylinders and so they react more in the way dipoles or tubes do. Also [18] did the experiment with linear polarization and it provides us the needed information on the weapon RCS behavior.

4.3.4 Environment polarimetric sensitivity

The entire environment has to be taken into account if we want to use the polarimetric properties of weapons with aim to maximize the RCS. For the backscattered signals we have to verify the polarimetric signature of:

- **The sea:**

According to [24], the sea RCS is around 20 dBm^2 less for a cross-polarization than a co-polarization. It comes from measurements that have been done with a bistatic radar. The incident angle of the measurements is 20° and we will assume it is true for the project parameters.

- **The boat:**

Boats properties are studied in [25] and it is shown that boats have a loss of 10 dBm^2 looking at the cross-polarization RCS compared to the co-polarization RCS. Even if the results are found for an incident angle between 41° and 67° we are going to assume that it is also the case in our experiment.

- **The weapons:**

As studied before the weapons shape is close to simple shape and their RCS have been found using this property (see *Appendix B. 3-planes study of weapon RCS*). It has been shown that weapons RCS is significantly higher for co-polarization than cross-polarization. For most of the cross-polarization cases the weapon RCS is even null.

We can say from the polarimetric sensitivity of the global environment that the use of co-polarization and cross-polarization discretization for the weapon detection could be helpful. Moreover we can notice that the use of cross-polarization could permit to increase the RCS by 10 dBm^2 .

4.4 Objects orientation

4.4.1 Studied planes

For the sake of understanding we are first going to define the studied planes of the antenna and the dinghy:

- **Antenna plane** The antenna will be the reference for the simulations and so its plane. We will consider the cartesian plan with x-axis being the axis where the antenna is placed (the vessel axis), the y-axis will define the sea plane (azimuthal plane) with the x-axis. The z-axis characterizes the elevation. From this we can define the polar plane where the angle φ is the angle between the dinghy direction and the antenna to dinghy straight line. It represents the rotational angle of the dinghy. θ is the elevation angle of the dinghy (Figure 4.9).

- **Dinghy plane** For the pirate dinghy, we will consider a polar plane that will have the same notation as the antenna polar plane but marked with primes (Figure 4.10).

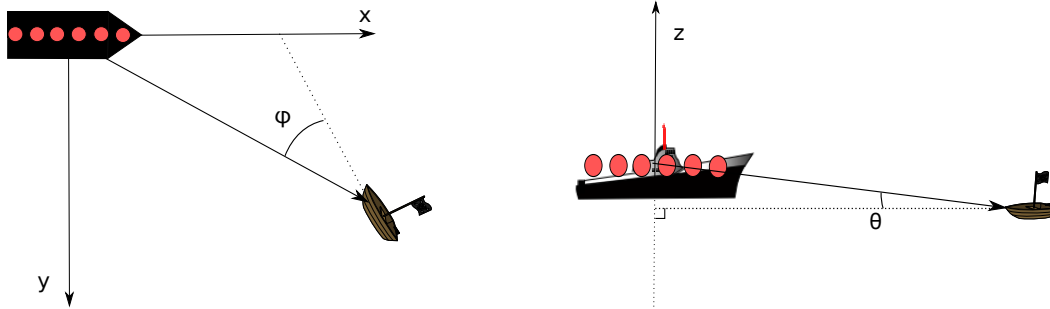


Figure 4.9: Antenna plane illustration

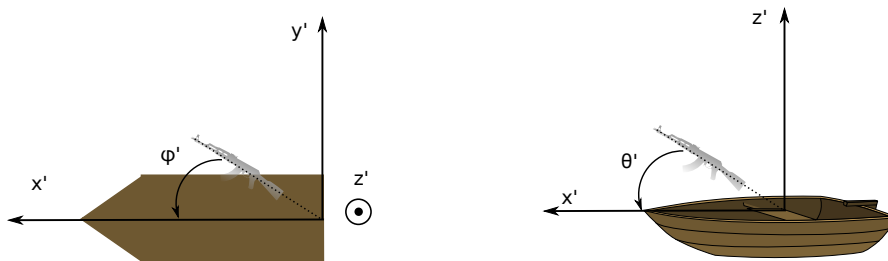


Figure 4.10: Dinghy plane illustration

We separate the two planes to be able to obtain first a weapon orientation depending on how the pirates hold it (dinghy plane). Secondly, we adapt this orientation depending on the dinghy orientation compared to the antenna (antenna plane).

4.4.2 Weapons orientation in the dinghy plane

As we said the weapons orientation is characterized in the dinghy plane. The pirates could stand facing the dinghy direction or by the side. We will consider different ways for the pirates to carry the rifles and the RPG. Six ways will be defined for each standing possibility which makes 12 combinations as shown by Figure 4.11. The figure also shows that the possibilities are canceled between turning the pirates position aboard and the position of the weapon. Finally only 6 possibilities remain.

4.4.3 Boat orientation

The boat is oriented depending on its way to go towards the vessel. For the simulation we are going to study only three positions of the dinghy:

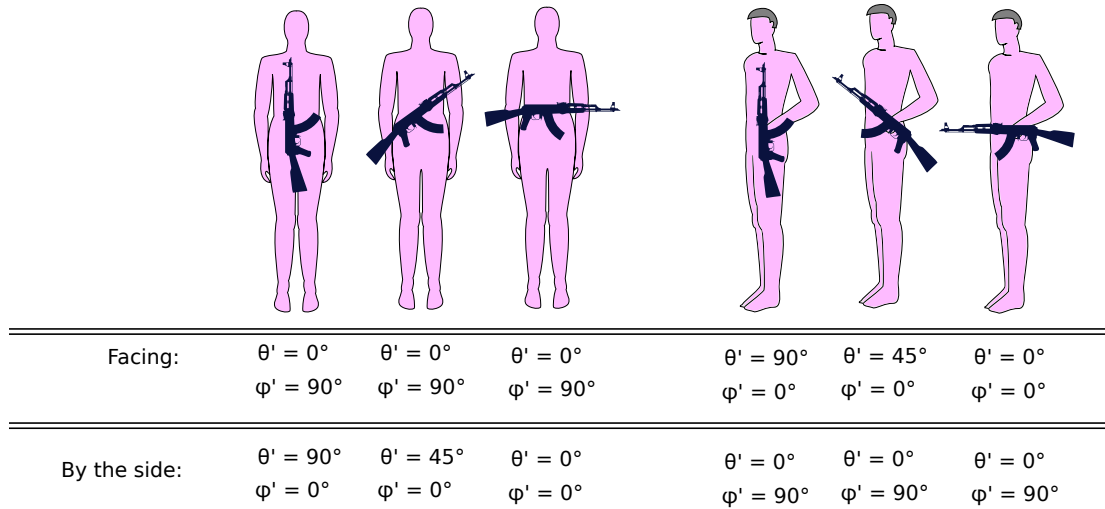


Figure 4.11: Possible ways for a weapon to be carried and the corresponding angles in the Dinghy plane.

- **Position A.**

The pirate dinghy is arriving from the side of the vessel. To compensate the vessel speed it has to navigate with an angle and straight away. For this position we will suppose the angle to be 45° .

- **Position B.**

The pirates planned the vessel trajectory and try to hit it as quick as possible. Depending on the dinghy speed different directions will be taken into account. If they are very fast they will go directly to the vessel and if they are not they will take a 45° angle to cross the vessel trajectory.

- **Position C.**

The pirates arrive directly from the front of the vessel.

These cases are illustrated in Figure 4.12. It shows well how much the target orientation could change depending on the trajectory taken. It will also impact the weapons orientation with respect to the antenna plane. It should be computed using all the parameters as we will do in the next section.

4.4.4 Weapons orientation in the antenna plane

Knowing the orientation of the weapon in the dinghy plane and knowing the orientation of the dinghy in the antenna plane we are now able to find the weapons orientation seen by the antenna. It means to find θ_{weapon} and φ_{weapon} :

- φ_{weapon} .

The weapon rotational angle φ_{weapon} can be found subtracting the boat angle φ_A , φ_{B1} , φ_{B2} or φ_C to φ' .

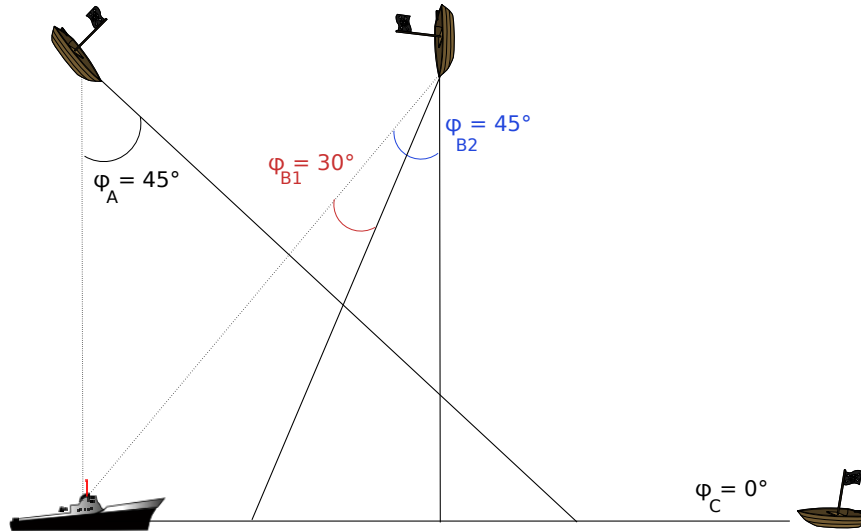


Figure 4.12: Possible configurations for pirates attack

- θ_{weapon} .

The weapon elevation angle θ_{weapon} depends on φ_{weapon} . If φ_{weapon} is null then it can be calculated by subtracting the angle of arrival α (see section 5.1.5) to θ' otherwise it will be α .

Finally, we can compute the weapon elevation and rotational angle using respectively (4.19) and (4.18) :

$$\varphi_{weapon} = \varphi_{A, B1, B2 \text{ or } C} - \varphi' \quad [^\circ] \quad (4.18)$$

$$\theta_{weapon} = \alpha \quad \text{or} \quad \theta_{weapon} = \alpha - \theta' \quad [^\circ] \quad (4.19)$$

The weapon angle for all studied positions can be found in Table 4.2.

$\varphi_{A, B1, B2 \text{ or } C} [^\circ]$	$\varphi' [^\circ]$	$\varphi_{weapon} [^\circ]$
0	0	0
	± 90	-90 / 90
30	0	30
	± 90	-60 / 120
45	0	45
	± 90	-45 / 135

Table 4.2: All possible angles of the weapon from the antenna point of view

Due to symmetry compare to 0° and 90° the possible angles remaining for φ_{weapon} are then 0, 30, 45, 60 and 90° . Concerning θ_{weapon} all values between 0 and

90° are possible and to define the RCS we will use a coefficient that depends on this orientation (see *Appendix B. 3-planes study of weapon RCS*).

4.5 AK-47 polarimetric detector

Looking at the information given by *Appendix A. Weapons length impact on RCS* and *Appendix B. 3-planes study of weapon RCS*, we can predict the behavior of the AK-47 RCS depending on the frequency and the polarization. We should be able to use this behavior to detect the weapon. By changing the polarization and looking at the reaction of the environment it should be possible to confirm the presence of an AK-47.

First it came with the definition of key point indicators (KPI) to define the polarimetric signature of the target. Second, ideal case study of the desired target has been done to define thresholds. These thresholds permit to insure the nature of the a detection to correspond to the signature of a known object.

Playing with the launched and received polarizations using antennas weight as explained in *Appendix D. Singular Value Decomposition technique* we can obtain the corresponding KPI to the simulated cases. These KPI are studied in *Appendix E. Weapon polarimetric signature*. This study shows well that the target identification using polarimetric properties of an object is something realistic. The only problem to that target classification is the environment.

Hence, the environment polarimetric sensitivity is also to be taken into account. If this technique is used, a too important environment or a sensitive environment to polarization could make the weapon signature invisible.

Chapter 5

Sea-clutter

5.1 Physical sea clutter

5.1.1 Physical description

In that first section, we first physically characterize the sea surface. This surface model is useful to compute the shadowing caused by the sea waves. We can distinguish two main types of sea waves:

- **Gravity waves**

These waves are the results of gravitational effects. They are macro-waves with amplitude and wavelength about meters.

- **Capillary waves**

These waves are the results of the sea-surface tensions. They have small amplitude and wavelength and they are superposed on the gravitational ones. They become dominant when the gravity waves are small or not present. This capillary waves will be called speckle.

5.1.2 Sea state

The sea can have different states. Mostly depending on the wind, the sea can be perfectly calm or very rough. Table 5.1 shows the different sea-states related to the wind speed [26].

We know that the echo produced by the sea will strongly depend on the sea-state. Including the sea-state knowledge in the signal processing of the echo permits to have a better clutter echo rejection and therefore to increase the *SCR*. To illustrate table 5.1, we can look at figures 5.1a and 5.1b, showing two different sea states.

The sea state is an information that we will take as a parameter. The problem now is to be able to model the sea surface and its EM responses.

Sea-state (Beaufort)	Description	Wind speed [$m \cdot s^{-1}$]	Wave height [m]
0	Calm	< 0.3	0
1	Light air	0.3 to 1.5	0 to 0.2
2	Light breeze	1.6 to 3.4	0.2 to 0.5
3	Gentle breeze	3.5 to 5.4	0.5 to 1
4	Moderate breeze	5.5 to 7.9	1 to 2
5	Fresh breeze	8 to 10.7	2 to 3
6	Strong breeze	10.8 to 13.8	3 to 4
7	Moderate gale	13.9 to 17.1	4 to 5.5
8	Gale	17.2 to 20.7	5.5 to 7.5
9	Strong gale	20.8 to 24.4	7 to 10
10	Storm	24.5 to 28.4	9 to 12.5
11	Violent storm	28.5 to 32.6	11.5 to 16
12	Hurricane	≥ 32.7	≥ 14

Table 5.1: Different sea-states associated with the wind speed. [26]



(a) Beaufort 4 - Moderate breeze [26]



(b) Beaufort 8 - Gale [26]

Figure 5.1: Beaufort scale examples

5.1.3 Pierson-Moskowitz model

One used algorithm to model sea surface is the Pierson-Moskowitz model. The goal is to model the sea surface frequency spectrum and then to deduce the sea surface. This model has been established using measurements made from a boat. In that model, the assumption is made that the wind blows over a large area in a homogeneous way. Then the waves would tend to reach an equilibrium point. This model is less precise in the case of a wind coming in blasts.

Pierson and Moskowitz established their first sea spectrum from measurements in 1964. The spectrum is given by (5.1).

$$S_{PM}(\omega) = \frac{\alpha g^2}{\omega^5} e^{-\beta \left(\frac{g}{\omega U_{19.4}}\right)^4} \quad (5.1)$$

Where:

$\omega = 2\pi f$	Where f is the wave frequency
α	Philips constant : 0.0081
β	Numerical constant : 0.74
g	Earth gravity : $9.81 [m \cdot s^{-2}]$
U_x	Speed of the wind at x meters above the sea surface. $[m \cdot s^{-1}]$

The given spectrum represents the distribution of the energy with the frequency of the sea waves within the ocean. Then, the operation consists in switching to the wavelength domain to be able to extract the sea surface from the spectrum. When the spectrum is switched to the wavenumber domain, white gaussian noise is added to the spectrum. Using Inverse Fast Fourier Transform (ifft) the spectrum goes from wavenumber domain to the space domain where the amplitude corresponds to the height of the waves.

A public available Matlab function will be used for the sea-surface generation: `sea_surface.m` which implements equation (5.1) and can be downloaded from the *MathWorks* website.

Earth curvature consideration

Once the sea-surface is modeled, we have to take into account the earth-curvature calculated in section 3.3.2. Therefore, we will apply the height shift calculated in equation (3.6). From the boat, the sea surface height will be given by (5.2).

$$h_{sea} = h_{PM-sea} - \sqrt{R_e^2 + d_{flat}^2} - R_e \quad (5.2)$$

Where:

h_{sea}	Sea height including the earth curvature $[m]$
h_{PM-sea}	Sea height computed with the Pierson-Moskowitz algorithm $[m]$
d_{flat}	Distance between the vessel and the sea considering flat earth $[m]$
R_e	Earth radius $[m]$

5.1.4 Flat see range attenuation

When the sea state is calm (0 or 1), the sea surface can be considered to be flat. In that case, the range attenuation will use the double path propagation model instead of the free space model. The decay exponent is found to be 4 instead of 2.

That model is valid for flat ground, i.e. when the root mean squared (RMS) roughness in z denoted δz_{RMS} is smaller than λ [27]. The two-ray model can also

be applied when application distance are short, therefore the earth curvature can be ignored. The double path model works for distance $d < 10\text{-}30\text{ km}$ and frequency $f < 30\text{ GHz}$. [27]

The sea-roughness can be computed at different states. The RMS sea-roughness is given by equation (5.3)

$$\delta z_{RMS} = \sqrt{\frac{1}{n} \cdot \sum_{i=1}^n z_i^2} \quad (5.3)$$

For different wind powers, the computed δz_{RMS} and threshold values for the double path model application are shown in figure 5.2

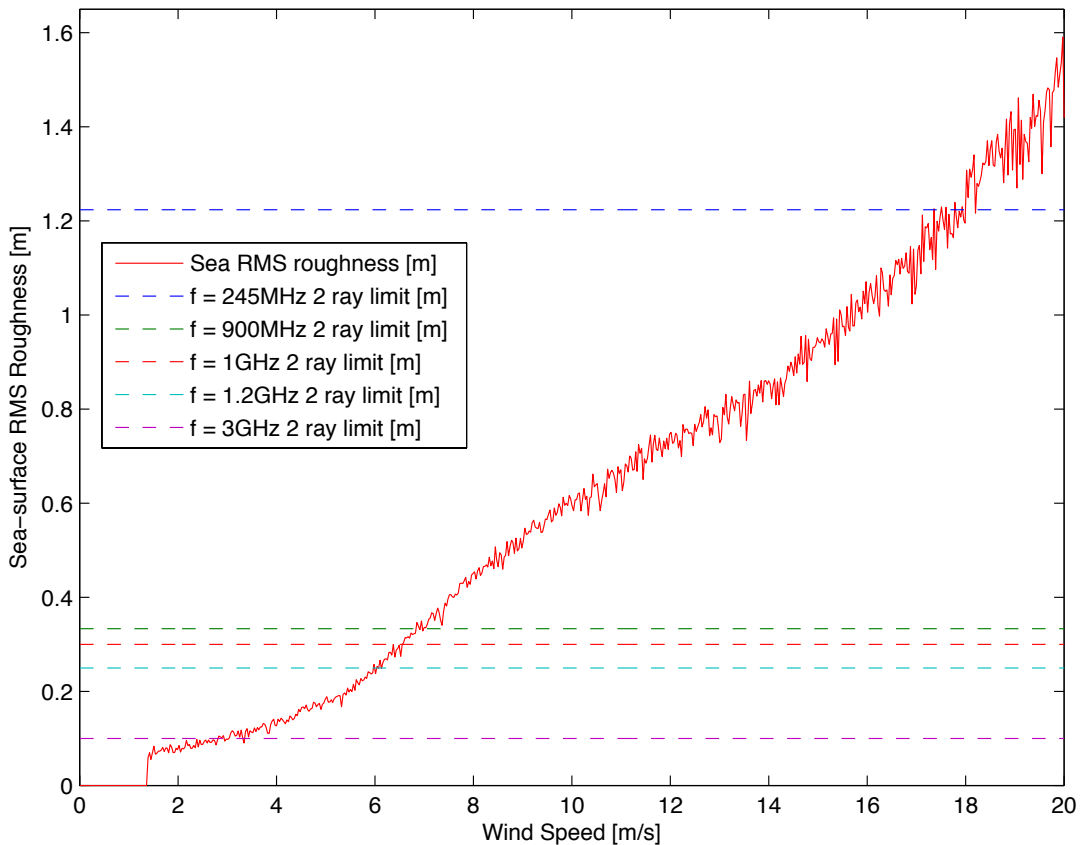


Figure 5.2: RMS roughness depending on the wind power with double-path model threshold for different candidate frequencies.

The double-path model application thresholds are summed up in table 5.2 for several candidates frequencies. In that table, we give the maximum wind speed where the double path model is valid depending on the frequency.

Frequency [GHz]	Wind speed [$m \cdot s^{-1}$]
0.245	17.5
0.900	6.8
1	6.3
1.2	5.9
3	2.8

Table 5.2: Thresholds for two ray model application

However, in real life application, the radar range equation with a 2 decay exponent models in a satisfactory way the wave propagation over the sea [9]. Most of the time, in our simulations, we will work with sea-states 6 and 9 (see section 1.5.2), where the average wind are respectively 12 m/s and 22 m/s , which are above most of the thresholds. Adding the 2-path model attenuation in the simulation will not create any benefit. The used range attenuation will therefore be given by the free space equation, and we will chose $\gamma = 2$ as a decay exponent.

5.1.5 Shadowing

The main issue with the sea-surface is that the small dinghy could be hidden by big waves. Then, there would be no target echo. Depending on the angle of arrival and the waves height, we can define what part of the boat is hidden. Even if effects such as diffraction could help the signal to reach a boat behind a wave, the power of that small amount of energy would not be significant compared to a single reflection echo.

We can calculate the effect of waves depending on their height and how far they are from the dinghy. Then, a proportional coefficient from 0 to 1 will be applied to the RCS of the dinghy.

We denote the shadowing coefficient $c_{shadow} \in [0; 1]$, which is applied on the dinghy RCS in (5.4). Note that shadowing coefficient is applied for both downlink and uplink processes.

$$RCS_{shadowed} = c_{shadow}^{DL} \cdot c_{shadow}^{UL} \cdot RCS_{dinghy} \quad (5.4)$$

There are two possible shadowing sources: earth curvature and sea-waves. The total coefficient c_{shadow} is then a function of c_{wave} and c_{earth} (see eq. (5.5)).

$$c_{shadow} = f(c_{earth}, c_{wave}) \quad (5.5)$$

Where:

c_{earth} Shadowing coefficient due to earth curvature

c_{wave} Shadowing coefficient due to sea waves

Earth curvature shadowing

First, we have to take a look at the earth curvature, which could be responsible for shadowing. Section 3.3 shows how to calculate D_{vessel} . As long as R is smaller than D_{vessel} , there is no shadowing due to the earth curvature. In the configuration $D_{vessel} < R < D_{vessel} + D_{dinghy}$, we have to apply a linear proportionality coefficient to c_{shadow} . This coefficient c_{earth} is given by (5.6)

$$\begin{aligned}
 c_{earth} &= 1 - \frac{R - D_{vessel}}{D_{dinghy}} && \text{when } D_{vessel} < R \leq D_{vessel} + D_{dinghy} \\
 c_{earth} &= 1 && \text{when } R \leq D_{vessel} \\
 c_{earth} &= 0 && \text{when } R > D_{vessel} + D_{dinghy}
 \end{aligned} \tag{5.6}$$

This means that if pirates are farther away from D_{vessel} , they start disappearing up to be completely invisible after $D_{vessel} + D_{dinghy}$. In our case, $D_{vessel} = 19 \text{ km}$, which means the earth curvature shadowing will always be $c_{earth} = 1$.

Under the $D_{vessel} = 19 \text{ km}$ threshold, the earth curvature is taken into account in the sea surface generation (see section 5.1.3). Therefore, the computation of c_{wave} takes into consideration the earth curvature shadowing.

Therefore, we can say that (5.5) becomes (5.7).

$$c_{shadow} = c_{wave} \tag{5.7}$$

Sea-waves shadowing

Waves are the main shadowing factor. A picture of the situation is provided in Figure 5.3.

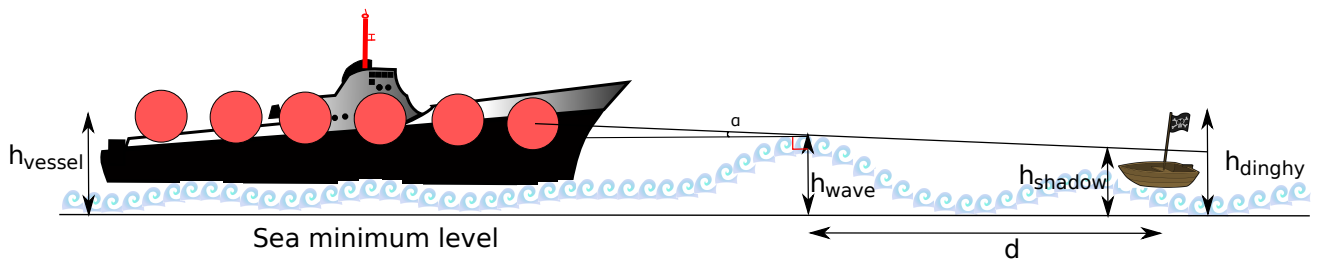


Figure 5.3: Shadowing created by waves

To get the wave coefficient, we need to compute the signal angle of arrival first. It can be found with equation (5.8).

$$\alpha(R) = \tan^{-1} \left(\frac{h_{vessel} - h_{wave}}{R} \right) \quad (5.8)$$

With a 30 m high vessel, the angle of arrival goes from $\alpha = 1.71^\circ$ to $\alpha = 0.14^\circ$ for respective range from $R = 1 \text{ km}$ to $R = 12 \text{ km}$.

From the small dinghy height and the angle of arrival, we can find how much the sea waves hide the dinghy. c_{wave} is calculated with simple geometrical relations. It represents the proportion of the dinghy height that is shadowed. First, we have to compute h_{shadow} which represents the shadowed height at the dinghy place by a wave. Equation (5.9) shows how to compute h_{shadow} .

$$h_{shadow} = \max(h_{sea} - d \cdot \tan(\alpha(R - d))) \quad \forall d \in]0; R[\quad (5.9)$$

Where:

h_{shadow}	Maximum shadow created by a sea wave
h_{sea}	Height of the sea calculated with eq. (5.2).
h_{vessel}	Height of the vessel, sea-waves included
d	Distance between the dinghy and the shadowing sea wave
α	Angle of arrival of the EM-wave at the sea wave.

In equation (5.9), we have to sweep d from 0 to R in order to find the maximum h_{shadow} value.

Equation (5.9) can be simplified in (5.10)

$$h_{shadow} = \max \left(h_{sea} - d \cdot \frac{h_{vessel} - h_{sea}}{R - d} \right) \quad \forall d \in]0; R[\quad (5.10)$$

h_{shadow} represents the height shadowed at the dinghy place. If h_{shadow} is found negative, then it means that the boat is not shadowed. Finally, we can calculate c_{wave} from h_{shadow} with (5.11)

$$\begin{aligned}
 c_{wave} &= \frac{h_{dinghy} - h_{shadow}}{h_{dinghy} - h_{wave-dinghy}}, & \text{when } h_{wave-dinghy} \leq h_{shadow} \leq h_{dinghy} \\
 c_{wave} &= 0, & \text{when } h_{shadow} > h_{dinghy} \\
 c_{wave} &= 1, & \text{when } h_{shadow} < h_{wave-dinghy}
 \end{aligned} \quad (5.11)$$

Where:

$h_{wave-dinghy}$	Height of the sea wave under the dinghy
-------------------	---

5.2 Electromagnetic sea responses

To model the sea electromagnetic response, we have several choices. This electromagnetic response is modeled by a distribution. The common used distribution to model the sea echo is the K-distribution.

5.2.1 K-distribution

This distribution has been created in order to model electromagnetic radar responses. It was considered as the most fit distribution for that kind of model because it has been created for that purpose. [6] uses the K-distribution to model the sea-clutter response for example.

K-distribution probability density function is given by (5.12)

$$p_K(x) = \frac{2}{x} \left(\frac{L\nu x}{\mu} \right)^{\frac{L+\nu}{2}} \frac{1}{\Gamma(L)\Gamma(\nu)} K_{\nu-L} \left(2\sqrt{\frac{L\nu x}{\mu}} \right), \quad x > 0 \quad (5.12)$$

Where:

K_x	Modified Bessel function of the second kind of x^{th} order
μ	Mean value for x .
$\Gamma(z)$	Gamma function with z parameter defined by (5.13)
ν	Shape parameter to be estimated.
L	Shape parameter to be estimated.

The Gamma function for $z \in \mathbb{R}$ is defined by (5.13).

$$\Gamma(z) = \int_0^{\infty} e^{-t} t^{z-1} dt \quad (5.13)$$

We have to estimate ν and L parameters. The distribution is composed by two independent distributions. One of those distributions represents the radar cross section and the other one the speckle component. The speckle component is the addition of randomly phased complex contributions [28].

5.2.2 Tsallis distribution

Recently, works have been done about another distribution called Tsallis-distribution. This distribution models sea-clutter response in a better way than K-

distribution, according to [8]. K-distribution results are not satisfactory enough because the sea-clutter electromagnetic response is a highly nonstationary process [8]. When differentiating sea-clutter data, it is shown that Tsallis distribution fits sea-clutter response much better than any other commonly used distributions such as K-distribution [8].

Therefore, it could be more appropriated to use the Tsallis distribution instead of K distribution. To better understand how does the Tsallis-distribution model work, we have to consider the electromagnetic response amplitude. We first discretize the response into bins which correspond to the distance between the radar and the backscattering point. Equation (5.14) represents that differentiation depending on n .

$$x(n) = y(n + 1) - y(n), \quad n = 1, 2, \dots \quad (5.14)$$

Where:

$y(n)$	Sea-clutter EM response for bin n
$x(n)$	Differential amplitude function for bin n .

The density probability $p_{Tsallis}(x)$ of the differentiated function $x(n)$ is then given by Tsallis-distribution (5.15)

$$p_{Tsallis}(x) = \frac{[1 + \beta \cdot (q - 1) \cdot q^2]^{\frac{1}{1-q}}}{Z_q} \quad (5.15)$$

Where:

β	is related to the variance of x
Z_q	is a normalization constant
q	is a normalization coefficient
	which quantifies the departure of $p_{Tsallis}(x)$ from a Gaussian distribution.
	if $q=1$, $p_{Tsallis}(x)$ is a Gaussian distribution
	if $q=2$, $p_{Tsallis}(x)$ is a Cauchy distribution
	if $\frac{5}{3} < q < 3$, $p_{Tsallis}(x)$ is heavy-tailed (not exponentially bounded)

To get an idea of the Tsallis distribution shape, Figure 5.4 shows different sketches of Tsallis distribution with different q and β parameters..

Z_q is a normalization constant in order to get the property given by equation (5.16). Z_q cannot be calculated without q and β given.

$$\int_{-\infty}^{+\infty} p(x)dx = 1 \quad (5.16)$$

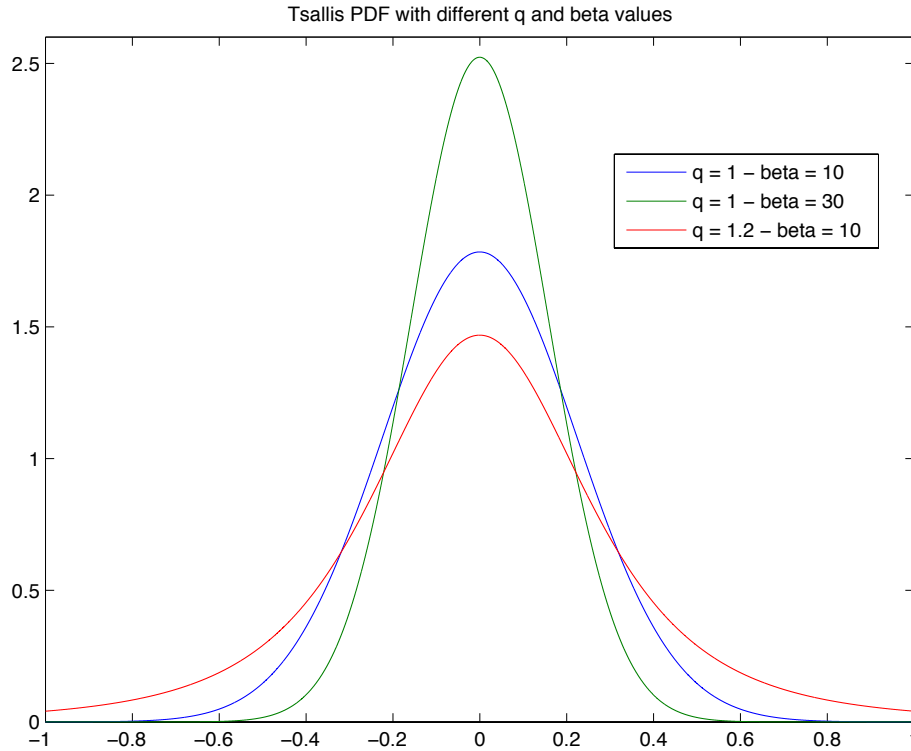


Figure 5.4: Tsallis probability distribution function

Therefore, we can calculate Z_q with (5.17).

$$Z_q = \int_{-\infty}^{+\infty} (1 + \beta \cdot (q - 1) \cdot x^2)^{\frac{1}{1-q}} dx \quad (5.17)$$

In our application, we can define q and β and then create a Tsallis distributed variable set. From this set, the main sea-clutter EM-response can be computed.

5.2.3 Distribution comparison

A complete analysis of the match of the distributions is made in *Appendix F. Tsallis and K-distributions*. From this analysis, we chose to model the sea-response with the Tsallis distribution.

Chapter 6

MIMO Radar

This project goal is to reveal potential MIMO radar benefits.

In our context, the main advantage we have is the near-field configuration (as we discussed in 3.2). Working in the near-field region allows to take advantage of special properties, especially at the radio propagation level such as the wavefront curvature for example.

The large dimension of the vessel and the absence of regulation constraints or shipping constraints do not impose any restrictions concerning the signal processing. We are therefore able to investigate any possibility to improve the MIMO system. The main aspects we can play with are:

- Near-field properties
- Space diversity
- Polarization diversity

Therefore, this chapter aims to look at the usual use of MIMO in radar systems first. Secondly, using the results of our study of the signal correlation to conclude on a way to place antennas on the vessel. Third, it defines a corresponding MIMO system to implement using the chosen antenna placement.

6.1 Usual MIMO radars

6.1.1 Basics

The use of MIMO system in radar has several motivations. First, it is interesting to note that 2×4 MIMO radar outperforms the 1×8 SIMO configuration in term of *SCR* in homogenous clutter [29]. The angular spread also helps to get diversity gain in target RCS, since most of the targets experience fading as mentioned in section 4.2.

The use of such MIMO configurations is particularly useful when we need to have different views of the same clutter and targets. MIMO systems can be used

to enhance localization by arranging emitting and receiving antennas around a given area. This kind of application is useful in airports for example, to watch the air-traffic. The space between antennas helps to localize aircrafts easier in 3 dimensions.

Usually in radar systems, MIMO radar consists to use several independent antennas to transmit waveforms and it could jointly process the received signals. It can be used with an omnidirectional beampattern or a chosen one defined by controlling the correlation among the transmitted waveforms [30]. In our case the MIMO radar would be a sparse array along the vessel for the transmitting and receiving parts.

The placement of the antennas also has to take into account the target beamwidth coverage [31]. It consists of an inter-elements spacing Δ_{IES} following equation (6.1).

$$\Delta_{IES} > \frac{\lambda R}{D_d} \quad [31] \quad (6.1)$$

MIMO configurations are based on the emission and reception of waveforms by several antennas. The emitted waveforms can be coherent or non-coherent. In the case of non-coherent waveforms, only the delay and the amplitude can be studied in reception.

On the other side the coherent waveforms also permit to study the phase of the received signals. Therefore, more information is carried by the coherent waveform model. Non-coherent waveforms are useful for target detection only. If we want to investigate the detected target informations such as its speed the coherent-waveform is needed [30].

6.1.2 Target detection and quality indicators

The processed echo of each Tx-Rx link is then investigated to proceed to a classical detection, explained in section 7.7. The classical reception process is therefore applied and a threshold for detection is set. The signal processing is mainly done here. Each detection at the receiver side is taken into account, even when only one antenna can see the target.

The ability to detect targets is found using the autocorrelation coefficient of the received waveforms s . The received waveforms are the amplitude of the received signals. For the non-coherent waveforms we have (6.2) whilst we have (6.3) for the coherent waveforms.

$$\sum_{k=1}^M \sum_l^N \left| \int s_k(t) \cdot s_k(t - \tau_{lk}(X)) dt \right|^2 \quad [30] \quad (6.2)$$

$$\left| \sum_{k=1}^M \sum_l^N \int e^{-j2\pi f_c \tau_{lk}(X)} \cdot s_k(t) \cdot s_k(t - \tau_{lk}(X)) dt \right|^2 \quad [30] \quad (6.3)$$

The further away the elements are placed, the more chance there is to work in the near-field region. Therefore the existing NF methods to find the DOA are based on the delay between the emissions and the receptions (see section 6.4.1). These delays are given by equation (6.4). As the time delay is nonlinear function of target location it is important to define a linear perturbation model of the delay and which is given by (6.5). It linearizes the perturbation around nominal target location (X_c, Y_c) [15]. Figure 6.1 illustrates the corresponding configuration [30].

$$\tau_{lk} = \frac{\sqrt{(X_{tk} - X)^2 + (Y_{tk} - Y)^2} + \sqrt{(X_{rl} - X)^2 + (Y_{rl} - Y)^2}}{c} \quad [30] \quad (6.4)$$

$$\tau_{lk} = -\frac{X}{c} \cdot (\cos(\phi_{tk}) + \cos(\phi_{rl})) - \frac{Y}{c} \cdot (\sin(\phi_{tk}) + \sin(\phi_{rl})) \quad [30] \quad (6.5)$$

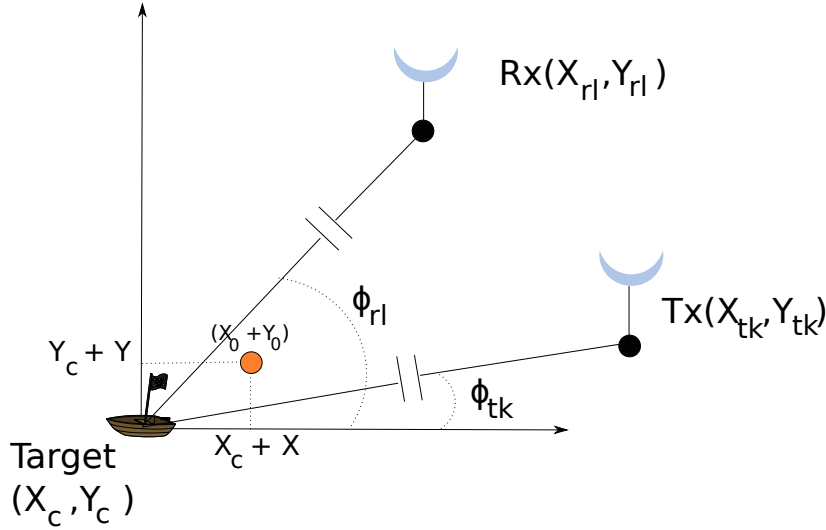


Figure 6.1: Illustration of the configuration for the linear perturbation model.

Algorithms then permit to find the DOA, they will be studied in 6.4. Two possible ways that we can use to classify the quality of the found DOA are The Cramér-Rao lower bound (CRLB) and the Geometric Dilution of Precision (GDOP) [30].

6.2 Antenna placement

6.2.1 Antenna spacing

Usual MIMO antenna spacing recommendations are from 0.5λ to 5λ [32]. 5λ value allows to achieve the best MIMO SNR gain [32]. For a carrier frequency $f_c =$

1 GHz, we have a 5λ spacing of 1.5 m. Therefore, to get this maximum potential MIMO SNR gain on the SCR, we have to place antennas at least 1.5 m apart from each other (for $f_c \geq 1$ GHz).

However, these antenna spacing recommendations are for short term process (mobile communications) whilst our case is more global. Signals at each transmitter/receiver are de-correlated by many factors such as Tsallis, fading phenomena or shadowing (see *Appendix C. Signal correlation*). The antenna placement should be done to get the maximum de-correlation between received signals.

We know that the lower is the correlation between two antennas, the higher is the potential SCR gain. Therefore, we want to optimize that potential gain placing antennas in a certain way. With the correlation results presented in *Appendix C. Signal correlation*, we have the following properties:

- Long range radar ($> 3km$): As seen in figure C.20 and C.21 the correlation tends to be flat even for the smallest antenna spacing (Δ_{IES}) whatever are the other parameters (antenna/wind angle, beam-width...). We can therefore place antennas close or not, the diversity benefit will tend to be the same.
- Short range radar : ($\leq 3km$)
The de-correlation is higher and signal is often de-correlated after 100 m ($r_{XY} \leq 0.5$) as shown in figure C.20, C.21 or C.22. The overall shape of the correlation function remains the same for any set of parameters. The slope and size change depending on the parameters, but these changes are small. In most cases, the signal is not correlated anymore ($r_{XY} \leq 0.5$) after 100 m. Therefore, we can assume that antennas should be placed at least 100 m apart for the combined process (Tsallis/shadowing/fading).

With these results, we know that the antenna placement for the long range echo has no significative impact since the correlation tends to be flat. Therefore, antennas could either be placed close ($5\lambda \leq 1.5$ m apart) or further away (100 m). For the short range and also middle range, we can see that the de-correlation is high at the beginning. Therefore, a good solution would be to place antennas as far as possible with each other.

However, for a Near-field long range ($> 5 - 6km$) operating distance, antennas can be placed every $\Delta_{IES} = 5$ m and get a good small scale/short term process de-correlation. Never the less, this close antenna placement setting affects the middle and short range radar performances ($< 4km$).

6.2.2 Single antennas or Cluster

We have several choices regarding the antenna array structure and configuration. Near-field properties can be used thanks to the huge vessel dimensions.

If we want to work in the near-field and use the near-field advantages such as the wavefront curvature information, we should place the antennas all along the boat to have a large antenna array. However if we want to use the far field techniques with phased array (e.g. DOA estimation) we will have to use the antenna cluster configuration, e.g. each antenna in the MIMO system could be a phased antenna array.

Then, the cluster would be phased array and the complete antenna set would be a sparse array. An illustration is given in figure 6.2 for a 2×2 system with each of the antennas being a $N_a = 2$ elements aperture array antenna. The use of clusters permits to obtain local FF for each of the antenna cluster. Then local far-field and global near-field could be exploited at the same time.

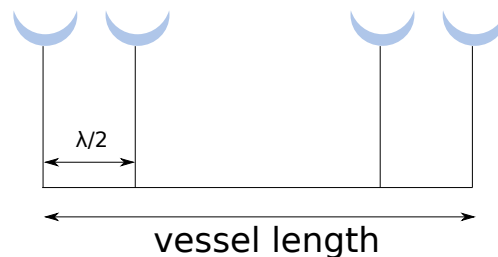


Figure 6.2: Possible antenna configuration : Phased clusters in sparse antenna array.

For example, the signal DOA is easier to find thanks to the far-field aspect of the clusters while the close range target localization and space de-correlation are more suitable in near-field region. The combination of global NF and local FF techniques could be useful, especially in the axis of the vessel, where the radar operates in the far-field after a short distance (as explained in section 3.2).

6.3 Target detection techniques

Playing with the space diversity (which includes phased and sparse antenna arrays) and polarimetric diversity, we want to enhance the following parameters:

- Detection probability P_D and Signal-to-Clutter Ratio SCR
- Illumination/Scanning time.
- Target discrimination.
- Localization.

6.3.1 Space diversity

The first obvious aspect of that MIMO radar along a 300 *m* vessel is the space diversity. As seen in *Appendix C. Signal correlation*, the vessel size helps us to get de-correlation between signals and also to minimize the shadowing effect.

The signal diversity will be achieved placing antennas all along the vessel and combining the detection at each receiver. Therefore the P_D is increased. For example, in a 2×2 system, if $P_D = 0.6$ (i.e. the probability of each scan to detect a target is 0.6), then the total probability that at least one of the antennas detects the target is calculated in (6.6)

$$P_{D|MIMO} = 1 - (1 - P_D)^{N \times M} = 1 - (1 - 0.6)^{2 \times 2} = 0.97 \quad (6.6)$$

This works in the post-detection combining, i.e. the detection is made before combining the different signals informations. For MRC, we first combine signals and then perform the detection procedure. The P_{fa} follows the same equation as the P_D , as shown in equation (6.7).

$$P_{fa|MIMO} = 1 - (1 - P_{fa})^{N \times M} \quad (6.7)$$

Since the P_{fa} is chosen small (less than 10^{-2}), then $(1 - P_{fa})$ is close to 1 and has less decay with a $M \times N$ exponent than a close to 0 value.

This little example illustrates figure 6.3, where the overall new detection probability is plotted for a MIMO 2×2 system versus a simple antenna. At the same time, we can see that the P_{fa} is less increased with a MIMO system in figure 6.4.

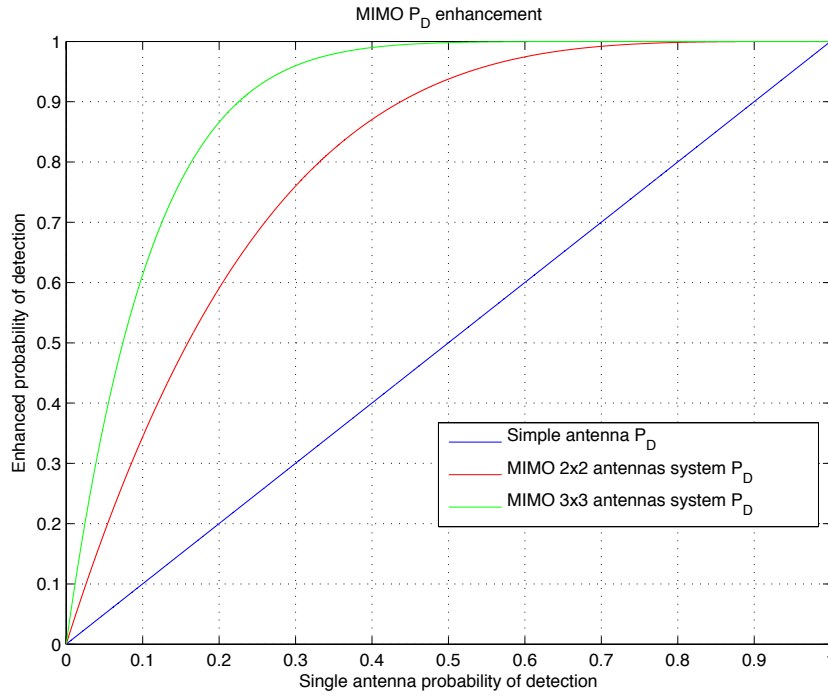


Figure 6.3: Detection probability for a $N \times N$ MIMO radar with equation (6.6) versus a single antenna probability of detection.

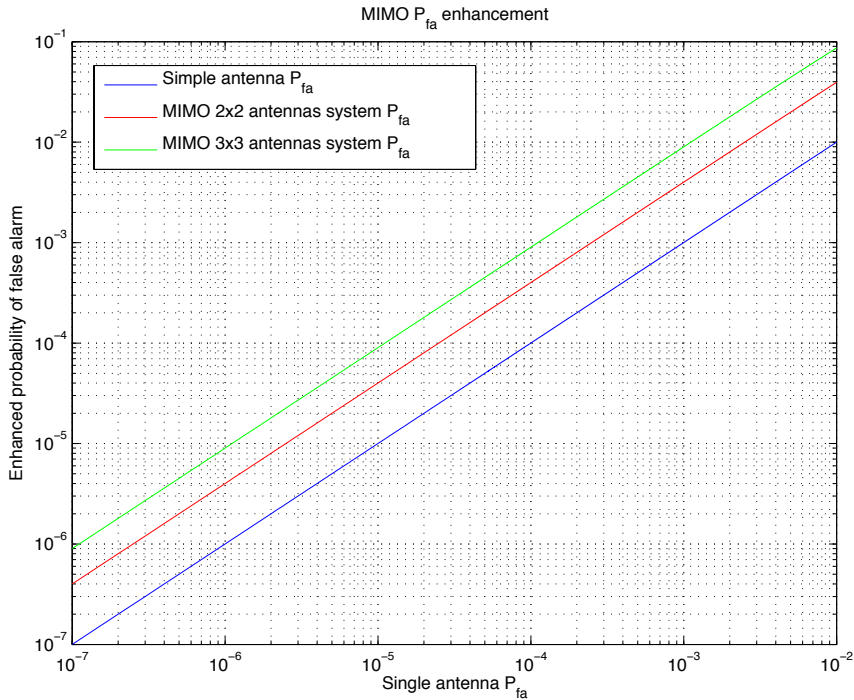


Figure 6.4: Probability of false alarm for a $N \times N$ MIMO radar with equation (7.24) versus a single antenna probability of false alarm.

We can illustrate figures 6.3 and 6.4 with an example. If all antennas have a defined $P_{fa} = 10^{-3}$ and a SCR such as $P_D = 0.2$, the following gain will apply:

SISO :	$P_D = 0.2$	$P_{fa} = 10^{-3}$
MIMO 2×2 :	$P_D = 0.59$	$P_{fa} = 4.10^{-3}$
MIMO 3×3 :	$P_D = 0.87$	$P_{fa} = 9.10^{-3}$

Therefore, the low-amplitude response targets will be found more systematically. With respect to shadowing, there also could be a better visibility of the target from one antenna to another. The SCR would therefore be increased and the P_D value as well.

6.3.2 Beam-less radar technique

An interesting technique is the beam-less radar scan or illumination. It can be applied with antenna cluster, i.e., phased arrays, but also with simple antennas when we are operating in the near-field. It is used to save time because the focus is created electronically or by processing rather than mechanically. Instead of using a narrow beam-width signal to scan each part of the azimuthal plane with a mechanical sweep, a large beam covering most of the azimuthal plans is sent. Then, at the reception, using localization techniques, studied in section 6.4, it is possible to know which part of the signal is coming from where, and therefore to find the range and the direction of a detection from a global scan.

The beam-less technique can be used with any multi-static radar configuration. This principle works as long as we are in the near-field region or able to find the DOA from antennas. An illustration is given in figure 6.5.

Figure 6.5 shows only the case where each antenna receives its own signal (multi-static SISO radar). In the case of the MIMO implementation, ellipses between the antennas will also help to triangulate targets. If too many targets are present, the system would not work anymore because of ambiguities (a third target would not be found in range 1 for antenna #2 in figure 6.5 unless antenna #2 can perform DOA detection).

This technique works when the emitted in waveforms are coherent or not. And even if the entire azimuthal plane is illuminated, it could be used to localized targets. It will be studied in section 6.4.1.

6.3.3 Space focusing

In the case of multiple scatterers, ambiguities can appear in the detection. For this reason space focusing is required. From the beam-less technique in the case of non

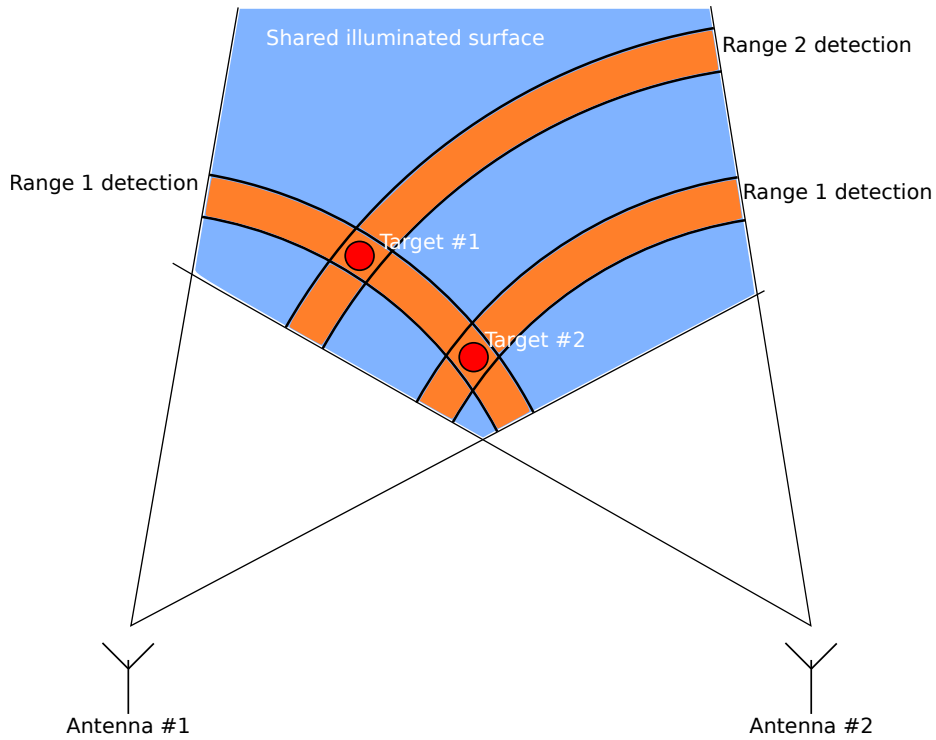


Figure 6.5: Beam-less multi-static radar illustration

coherent waveforms, the parameters which are known are the time delay between the antennas and the amplitude loss. These parameters can be used to focus on specific places even if the entire azimuthal plane is illuminated (dashed track in Figure 6.6).

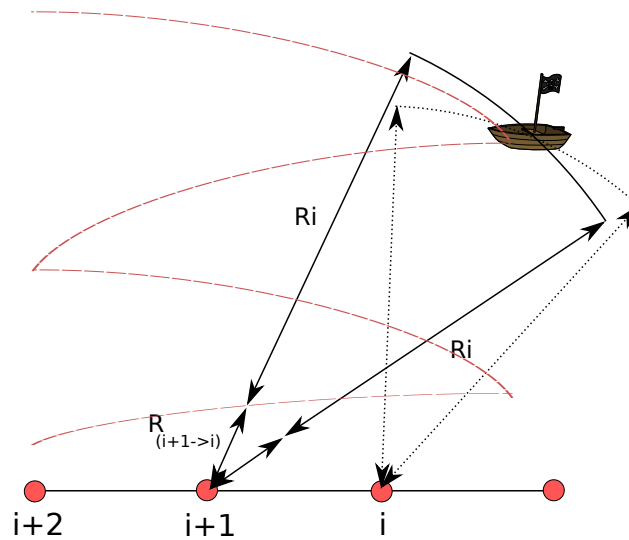


Figure 6.6: Post detection focus scan with knowledge of the ranges.

Time reversal

Time reversal is a candidate for creating a focus on the target. This method has several benefits, which are spatial focusing, temporal focusing and channel diversity.

In our radar system the main interest of the TR is the spatial focusing. This focusing is based on delay and amplitude adjustments between antennas. It could be used after a first entire illumination of the environment to concentrate on some points. The principle is to send a prop signal to obtain the channels impulse responses: $h(t, m)$ where m corresponds to the m^{th} antenna.

Afterwards, instead of the usual sent signal $x(t)$, the TR principle is, at the m^{th} antenna, to send: $h^*(-t, m) * s(t)$ where $*$ represents the conjugate. At the receiving side we obtain:

$$y(t) = R_{hh}(m) * s(t) \quad [33] \quad (6.8)$$

Where:

$R_{hh}(m)$ is the correlation function of the channel impulse response corresponding to the m^{th} antenna.

Experiment has been done in [34] and the results show that the time reversal permits to have a space focusing getting more compact with the increasing number of antennas. Indeed, it is on the focus point that the received signal is the higher one as shown by Figure 6.7 and even close to the focal point, the signal is weak which limits interference in the echo 6.8. The time reversal acts like a *matched filter* and hence it should suppress a major part of the sea response.

Even for non-coherent wavefronts, every signal amplitude with random phase would sum up at the focusing point and would also tend to create a sum on the focal point. Hence, this candidate works for both coherent and non-coherent cases, but it is more efficient in the coherent case.

This method implies that all transmitters send a same copy of the signal. Then, if one of the antennas is in a deep fade, it is not likely that another one is also in a deep fade.

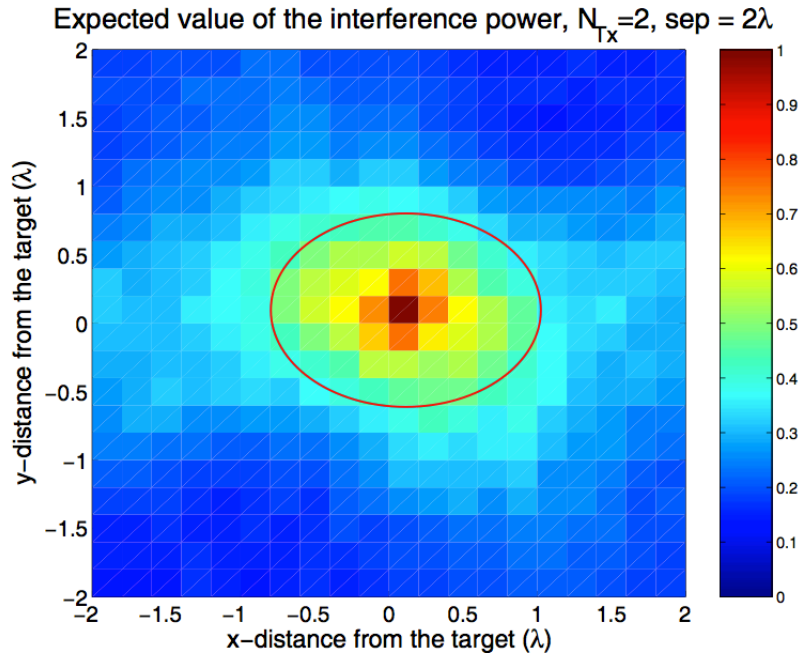


Figure 6.7: Expected value of the interference [33].

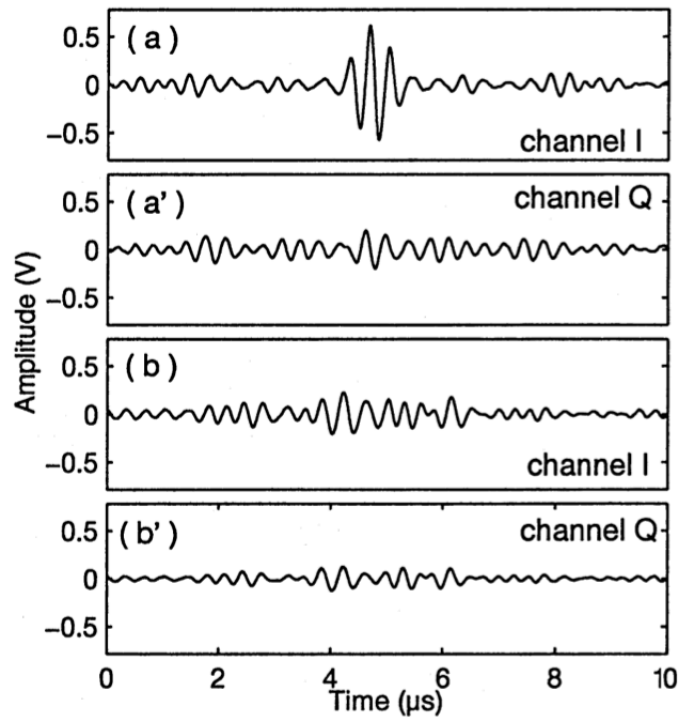


Figure 6.8: (a),(a') Baseband representation $[m_I(t)$ and $m_Q(t)]$ of the signal transmitted by antenna A. (b),(b') Baseband representation [i.e., $m'_I(t)$ and $m'_Q(t)$] of the signal reverberated inside the cavity and received by antenna B [34].

6.3.4 MIMO added-value for detection

The MIMO system helps to get several copies of the same sea-clutter or target signal. Classic wireless communication systems often use Maximal Ratio Combining (MRC) to improve the SNR and therefore the bit-rate.

MRC can be both used in SIMO or MIMO radar. It helps then to better discriminate targets from the sea-clutter.

We denote h_l the response of the radar for the m^{th} transmitting antenna and n^{th} receiving antenna. We have $L = M \times N$. We have the received signal given by (6.9)

$$S_l = x_l \cdot h_l + N_0 \quad (6.9)$$

Where:

x_m	Sent signal (radar pulse)
h_l	Target impulse response for transmitter m and receiver n
N_0	Noise

MRC consists in multiplying each received signal by the channel complex conjugate divided by the noise for this link: h_l^*/N_0^l . In our case, we assume that the noise level is the same for any link: $N_0^l = N_0, \forall l$. The MRC expression simplifies and consists in multiplying by the channel complex conjugate h_l^* only. The signal S_l becomes the expression given in equation (6.10)

$$S_l^{MRC} = (x_l \cdot h_l + N_0) \cdot h_l^* = x_l |h_l|^2 + N_0 h_l^* \quad (6.10)$$

Finally, for several transmitter/receiver links (multiple input or output), all received signals are summed together after being multiplied by the channel complex conjugate. The signal is therefore given by equation (6.11)

$$S_L^{MRC} = \sum_{l=1}^L x_l |h_l|^2 + N_0 \sum_{l=1}^L h_l^* \quad (6.11)$$

In the radar case, we consider the complete echo as being a possible target. Impulse responses are multiplied by their conjugates and added together. The radar MRC is given by equation (6.12).

$$S_L^{MRC} = \sum_{l=1}^L |S_l|^2 \quad (6.12)$$

In this case, we have a pre-detection combining, i.e the detection is made after the MRC.

6.4 Target Localization techniques

In this section, we will study several localization techniques. Using TR it would have been possible to locate the target as it is studied in [35]. However, due to the lack of time, it has not been investigated in this project.

6.4.1 Near-field localization

With the received signals time delays we can easily find the range of a target. Sometimes we also need the DOA of the received signal to be able to perform a better range estimation.

Regarding the near-field region, the interesting advantage to use propagation properties on the received signals. As the antennas are far away from each other compared to the target location and time resolution, an incoming signal will arrive with specific delay and free-space attenuation for each antenna (Figure 6.9).

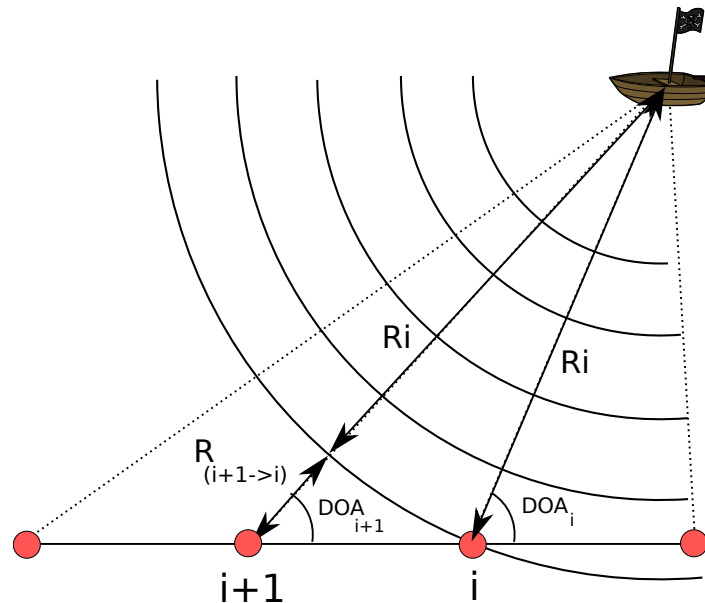


Figure 6.9: Near field delay and attenuation between antennas.

In the case of a detection with non coherent waveforms: studying only the amplitude loss and the delay, we are able to find the location of the target. This is possible in the near-field region.

Indeed, as shown by Figure 6.9, the backscattered signal wavefront from a target

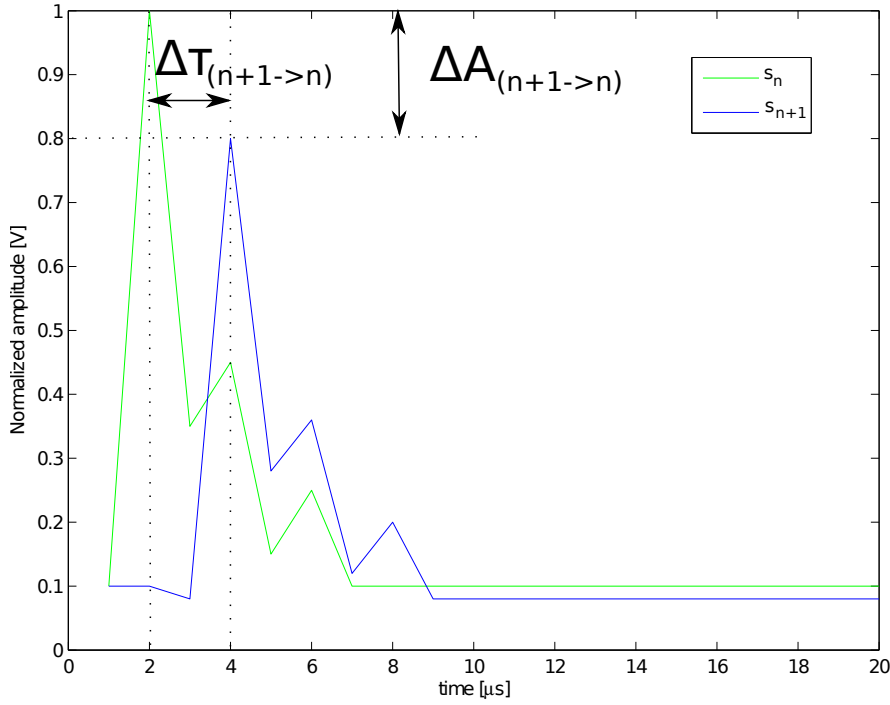


Figure 6.10: Example of near-field induced delay and amplitude loss between two receiving antennas.

will arrive to the antennas with a certain curvature that implies a specific delay and amplitude loss between the received signal of each antenna. Figure 6.10 illustrates possible received amplitude. As we use MIMO system we will have M transmitters of orthogonal waveforms which implies M distinct signals for each antenna at the receiver side. At the n^{th} antenna, the amplitude of the received signal corresponding to the m^{th} transmitter can be given by:

$$A_{m,n}(t) = A_{target} \cdot \frac{\lambda}{4\pi \cdot (R_m + R_n)} \quad (6.13)$$

The received amplitude difference between two antennas is then given by:

$$\Delta A_{(n+1->n)} = A_{m,n+1}(t - \tau_{(n+1->n)}) - A_{m,n}(t) = A_{m,n} \cdot \frac{\Delta R_{(n+1->n)}}{R_{n+1}} \quad (6.14)$$

Where $\tau_{(n+1->n)}$ is the delay between the received signal at the $n + 1^{\text{th}}$ antenna compared to the n^{th} antenna. These two equations work in theory and for the ideal cases but in practice the channel fast fading can impact these amplitudes. The use of several transmitters permits to avoid this fast fading effect. Using M transmitters, we have M times the values of $\Delta A_{(n+1->n)}$. The delay $\tau_{(n+1->n)}$ permits to calculate the target range difference between the two antennas using:

$$\Delta R_{(n+1->n)} = R_{n+1} - R_n = c_0 \cdot \tau_{(n+1->n)} \quad (6.15)$$

Combining (6.14) and (6.15) and then deriving the expression we can estimate the range R_{n+1} :

$$R_{n+1} = \frac{A_{m,n} \cdot c_0 \cdot \tau_{(n+1 \rightarrow n)}}{\Delta A_{m,(n+1 \rightarrow n)}} \quad (6.16)$$

Once one range is found we can also compute the others parameters such as DOA_n and R_n . However, this technique has a limit and requires a big enough number of transmitters to make the amplitude information reliable to use. Therefore the differential amplitude between two received signals cannot be used in an accurate way to locate a detection but as a secondary localization indicator.

An alternative to the use of the amplitude is to use the array geometry and the EM wave propagation properties to estimate the wavefront curvature and then the target relative coordinates. The defined configuration for relative coordinates can be seen in Figure 6.11. The difference in target range between the antennas are given by $\Delta R_{(n+i \rightarrow n)}$: [36]

$$\Delta R_{(n+i \rightarrow n)} = \sqrt{R_n^2 + (i \cdot d)^2 - 2 \cdot R_n \cdot i \cdot d \cdot \sin(DOA)} - R_n \quad (6.17)$$

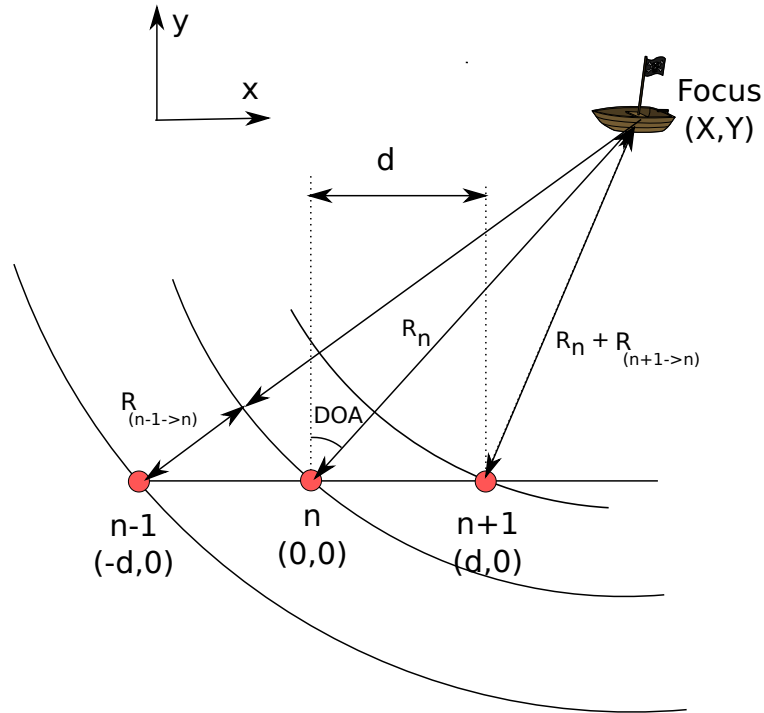


Figure 6.11: Define configuration for ranges estimation

Using the second-order derivative Taylor expansion we obtain: [36]

$$\Delta R_{(n+i \rightarrow n)} = (-d \cdot \sin(DOA)) \cdot i + \left(\frac{d^2}{2 \cdot R_n} \cdot \cos^2(DOA) \right) \cdot i^2 + o\left(\frac{d^2}{R_n^2}\right) \quad (6.18)$$

Where $o\left(\frac{d^2}{R_n^2}\right)$ denotes the accuracy of the estimation. To give an idea of the approximation, using a 3×3 MIMO system with a target localized at a range of 300

meters, the approximation is about 0.25 meters. Tolerating this approximation we can remove this term.

Using three antennas, one on each side of the n^{th} antenna we obtain:

$$\begin{cases} \Delta R_{(n+1 \rightarrow n)} = -d \cdot \sin(DOA) + \frac{d^2}{2 \cdot R_n} \cdot \cos^2(DOA) \\ \Delta R_{(n-1 \rightarrow n)} = +d \cdot \sin(DOA) + \frac{d^2}{2 \cdot R_n} \cdot \cos^2(DOA) \end{cases} \quad (6.19)$$

Deriving this system we obtain:

$$\begin{cases} DOA = \sin^{-1} \left(\frac{\Delta R_{(n-1 \rightarrow n)} - \Delta R_{(n+1 \rightarrow n)}}{2 \cdot d} \right) \\ R_n = \frac{d^2 - \Delta R_{(n+1 \rightarrow n)}}{2(\Delta R_{(n+1 \rightarrow n)} + d \cdot \sin(DOA))} \end{cases} \quad (6.20)$$

We have shown two techniques to localize a target. The most accurate is the technique based on the delays while the amplitude one is more sensitive to the environment fading. Combining these two localization methods would be an efficient way to optimize this localization. However proper weights have to be given depending on the methods accuracy.

6.4.2 MIMO value-added for NF localization

The section before described how to estimate a target position using the detected target echo delays and amplitudes at each receiver. These delays characterize the wavefront curvature. Figure 6.12 illustrates the possible delays of the received signals at each antenna. To see the wavefront curvature, the simulation has been run with eleven receiving antennas.

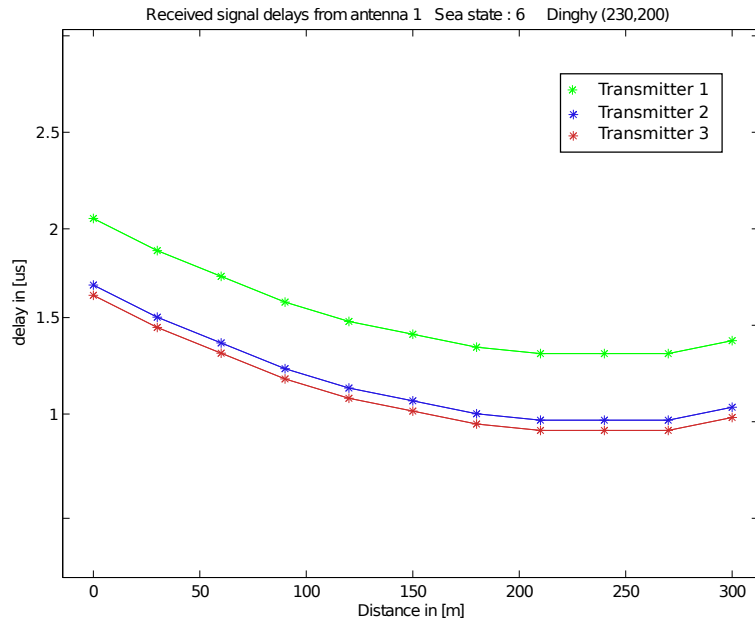


Figure 6.12: Possible received signals delays for 11 receivers on the boat with possible offsets depending on the transmitter position. Sea state 6 and the dinghy placed at (230,200).

Antennas used for the transmission radiate orthogonal waveforms which allows them to be differentiated the one from the other at the reception side. Each of them can be proceeded to estimate the target coordinates relatively to the antenna. M estimations can be done in order to increase the accuracy of the estimation but it requires a minimum of three receiving antennas.

Indeed, the environment and thermal noise impact the EM wave propagation and could induce jitter as shown in Figure 6.13.

At the receiver side we can obtain M delays curves with different offsets. However since the peak at each receiving antenna comes from the same place (target position), then the delays difference between the receivers should be the same. It characterizes the wavefront curvature. Using three transmitters the possible delays could be the ones given in Figure 6.12.

If the localization estimations of the orthogonal transmitted signals are not related or if they appear to be randomly varying then we can consider that we are not in presence of a real target but multiple scatterers. It could permit to conclude that the detection comes from sea-waves instead of a target.

In the case of coherent waveforms, there is a variable that can also be taken into account which is the phase of the received signal. Using small antenna spacing, the knowledge of the phase shift between the antennas permits to obtain the direction of arrival of the signal.

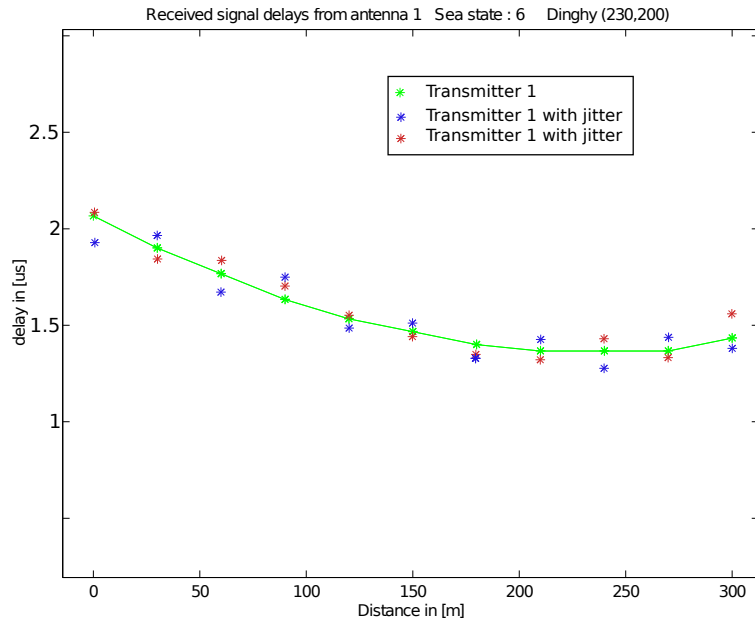


Figure 6.13: Illustration of the possible jitter induced by the environment, thermal noise and the wave propagation.

6.4.3 Far-field localization

If antennas are organized in clusters, which means operating in local far-field, it works in a complete different way. As the incoming EM wave is supposed to be planar, the range could be found using the delay between the transmission and reception. To obtain the precise localization of the detection we also need the direction-of-arrival (DOA) of the signals.

Several algorithms exist to localize passive sources such as the Wigner-Ville distribution-based method, the maximum likelihood method or the linear prediction methods [37]. However the two main algorithms are the Estimation of Signal Parameters via Rotational Invariance Techniques (ESPRIT) and the 2-Dimensional Multiple Signal Classification (2D-MUSIC). [37]

DOA

These two techniques work properly when the passives sources are in the far-field region which is the case when using local clusters organization for the antennas. However the principal disadvantage of the ESPRIT algorithm is that there is a limit to its functionality which is the number of passives sources compared to the number of antennas in a cluster. The ESPRIT algorithm fails when the number of passives sources is higher than the antenna element number [37].

Looking at our radar cases, we assume that the antenna organization in cluster is not a problem and the sea echos do not have more passive sources than antennas

by cluster. In this case, as the ESPRIT has a significantly less important processing complexity we will use it instead of the MUSIC algorithm even if the MUSIC algorithm is more stable. [37]

Moreover, [37] compared the accuracy of the two techniques which gave the results shown in table 6.1. When the SCR (or SNR) is 0, with a $P_{fa} = 10^{-3}$, we have a probability of detection $P_D < 0.1$. The detection for a single antenna will start to occur from $SCR > 5$ dB. Thus, depending on the found SCR , the error margin will be evaluated according to Table 6.1 results.

SNR/SCR (dB)	MUSIC (θ)	ESPRIT (θ)
-20	21.66	-39.08
-19	24.00	23.47
0	24.66	26.02
9	25.00	25.67
20	25.00	25.21
21	25.00	24.99

Table 6.1: DOA Estimation by MUSIC & ESPRIT for varying SNR. (Input $\theta = 25$ deg, $M=4$, $k=100$). [37]

With the D signals impinging on M elements array with different angles ($DOA_1, DOA_2, \dots, DOA_D$), the number of signal eigenvalues and eigenvectors is D and there are $M-D$ noise eigenvalues and eigenvectors. The antennas are organized in two clusters separated by d_c as shown by Figure 6.14. Therefore the signals received by the cluster are given by:

$$\begin{aligned} S_1 &= A \cdot s + n_1 \\ S_2 &= A \cdot \Lambda \cdot s + n_2 \end{aligned} \quad (6.21)$$

Where:

$$\begin{aligned} A &= [a(DOA_1), a(DOA_2), \dots, a(DOA_D)] \quad \text{is } M \times D \text{ steering matrix.} \\ \Lambda &= \text{diag}\{e^{jd_c \sin(DOA_1)}, e^{jd_c \sin(DOA_2)}, \dots, e^{jd_c \sin(DOA_D)}\} \\ &= D \times D \text{ diagonal unitary matrix with phase shifts between} \\ &\quad \text{doublets for each DOA.} \end{aligned}$$

The signal subspaces for the two arrays are characterized by two matrices Z_1 and Z_2 [37]. The arrays are translationally related so the subspaces of eigenvectors can be obtained from the other using a unique nonsingular transformation matrix Φ following:

$$Z_1 \cdot \Phi = Z_2 \quad (6.22)$$

This configuration implies that it exists an unique nonsingular transformation

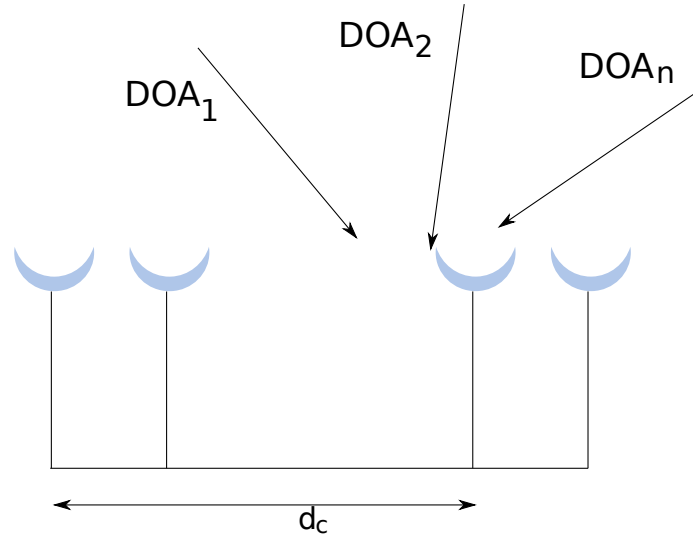


Figure 6.14: Antenna organization for ESPRIT algorithm

matrix T_{ns} with properties that gives:

$$\begin{aligned} Z_1 &= A \cdot T_{ns} \\ Z_2 &= A \cdot \Lambda \cdot T_{ns} \end{aligned} \quad (6.23)$$

Which leads to:

$$T_{ns} \cdot \Phi \cdot T_{ns}^{-1} = \Lambda \quad (6.24)$$

Obviously the eigenvalues of $\Phi (\lambda_1, \lambda_2, \dots, \lambda_D)$ should correspond to the elements in $\Lambda (e^{jd_c \sin(DOA_1)}, e^{jd_c \sin(DOA_2)}, \dots, e^{jd_c \sin(DOA_D)})$. Finally the DOA of the impinging signals are obtained using:

$$DOA_i = \sin^{-1} \left(\frac{\arg(\lambda_i)}{d_c} \right) \quad (6.25)$$

Assuming we use aperture antenna array [9], we can apply the ESPRIT algorithm on such an array.

Range localization

When the DOA is found, we can calculate the range and therefore know the coordinates of any target. Two cases are distinguished : Transmitter and receiver are the same or Transmitter and receiver are different.

- Same Tx/Rx :

In that case, we know that the EM wave has followed a round trip from the antenna to the same antenna. Each time delay corresponds therefore to a circle of R radius with R given by (6.26). An illustration is given in figure 6.15.

$$R_{tot} = c_0 \cdot t \quad (6.26)$$

According to figure 6.15, we can see that the distance from the antenna is the circle radius, which is given by (6.27)

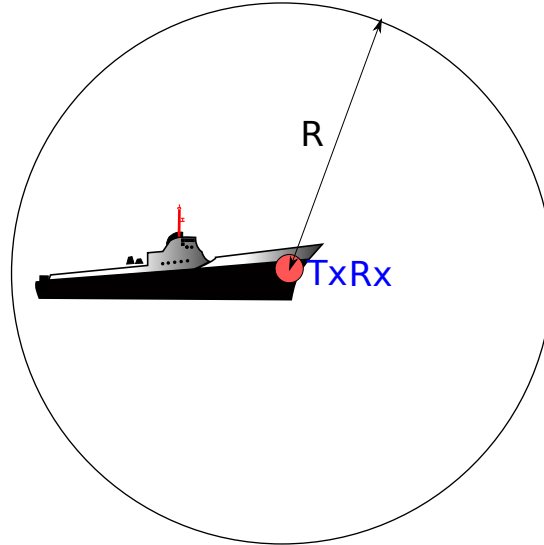


Figure 6.15: Wave possible path for same Tx/Rx

$$R = \frac{R_{tot}}{2} = \frac{c_0 \cdot t}{2} \quad (6.27)$$

- Different Tx/Rx :

In that case, we know that the total distance the EM-wave travelled with one reflection between the Tx and Rx antennas is R_{tot} , focal distance of an ellipse, where the two focus points are the Tx and Rx antennas. An illustration is given in figure 6.16.

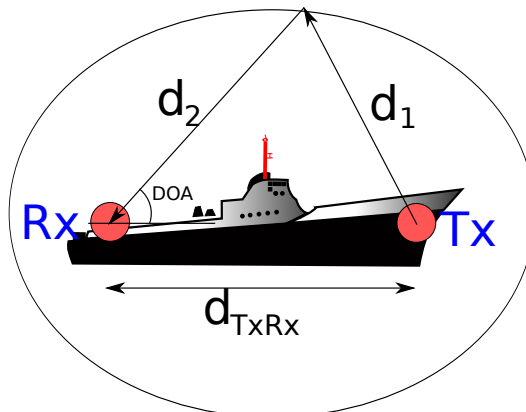


Figure 6.16: Wave possible path for different Tx/Rx

In that case, we want to find the d_2 distance. Thanks to the ellipse properties, we know that :

$$R_{tot} = c_0 \cdot t = d_1 + d_2 \quad (6.28)$$

With the law of cosines, we can find (6.29)

$$d_1^2 = d_2^2 + d_{TxRx}^2 - 2d_2d_{TxRx}\cos(DOA) \quad (6.29)$$

Using (6.28) in (6.29), we obtain :

$$(c_0 \cdot t - d_2)^2 = d_2^2 + d_{TxRx}^2 - 2d_2d_{TxRx}\cos(DOA) \quad (6.30)$$

Isolating d_2 in (6.30) gives:

$$d_2 = \frac{c_0^2 t^2 - d_{TxRx}^2}{2 \cdot [c_0 t - d_{TxRx} \cos(DOA)]} \quad (6.31)$$

Where:

t	Signal delay. [s]
c_0	Speed of light [$m \cdot s^{-1}$]
d_2	Range of the target from the Rx [m]
d_{TxRx}	Distance between Transmitter Tx and Receiver Rx [m]
DOA	Direction of Arrival of the signal [rad]

The range of the target from the receiving antenna is then given by d_2 from the time delay and the DOA in equation (6.31). Once all ranges from receivers and DOA for each signal is found, we can easily merge targets and create a map from the detections that occurred.

6.5 Target classification technique

6.5.1 Polarization discrimination

Independently to the antenna placement, to help the detections, it is possible to use the polarimetric sensitivity of the sea to be able to say if a detection comes from the sea echo. The sea as we discussed in 4.3.4 has a specific XPD and the boat also. It is then possible to use this XPD to be able to characterize the nature of the detection and to eliminate the largest sea echos leading to false detections. Thus the large waves detection should be avoided.

Once a detection occurred, the aim is to be able to confirm the nature of the target. Is it a wave, an emerging rock, a fish or a pirate dinghy? As we saw before in this project, the pirate dinghy is composed of weapons that have a specific polarimetric signature. The polarimetric discrimination would be to use these polarimetric properties to justify their presence using polarization diversity. There are two problems using this discrimination:

- The environment also has polarimetric sensitivity that can hide the weapon signature.
- In several positions the weapon RCS would be too small to be detected with respect to the polarization.

Their impact on an eventual way to use the polarimetric discrimination is discussed in *Appendix E. Weapon polarimetric signature*. Variables are defined to characterize the polarimetric signature of the target. Even if in the ideal case, the weapon discrimination is large, our environment has a too strong impact on the backscattered signal and completely hide the weapon signature.

This technique has also been studied, in a second time, for the boat polarimetric signature. Applying a Swerling model I on the dinghy RCS makes it uncorrelated from a scan to another and leads to an unpredictable RCS and therefore an unpredictable polarimetric signature.

Finally, the polarimetric discrimination of targets is a tool that is possible to be used for target classification in specific environments.

6.6 MIMO radar scenario

The candidates algorithms and signal processing techniques that we could use and combine are listed in the following subsections. They are also summed up in Figure 6.17.

6.6.1 Choice discussion

In our project, we have to choose between the use of the *full-NF* MIMO system where we only use the NF aspects to find the range and the DOA of targets, or the use of the *hybrid-NF-FF* MIMO system (cluster and sparse array), where only the DOA is found thanks to the clusters inside the sparse array.

Appendix C. Signal correlation shows that the de-correlation is stronger with a wide illumination beam. In that case, the use of cluster or sparse array would come to the same space diversity. In the case of a narrow beam, the *full-NF* system (no cluster) is more suited.

The performance would however tend to be better with fewer number of pulses. Therefore wider is the beam, faster could operate the radar if the post processing is efficient enough. (Less scans to retrieve as much information)

The chosen scenario for the use of our MIMO radar application is represented in figure 6.18. Each part is detailed in sections 6.6.2 to 6.6.3

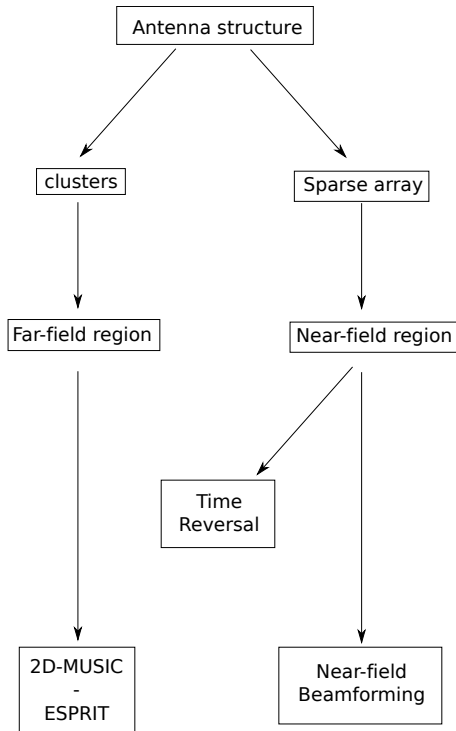


Figure 6.17: Different MIMO possibilities concerning space implementation.

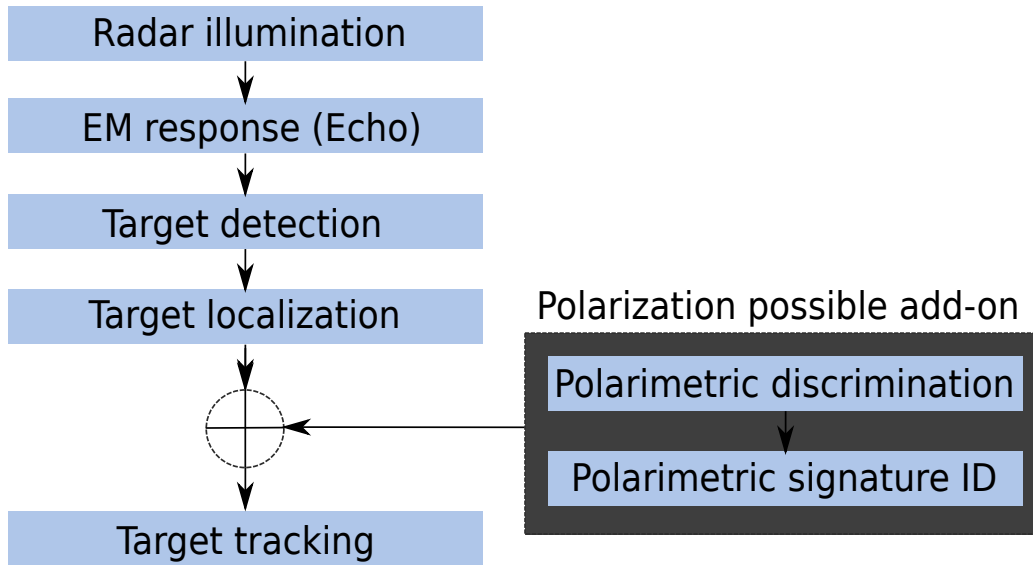


Figure 6.18: MIMO radar scenario

When applying MRC, the sum of the received signals leads to a loss of information necessary to compute the NF localization.

Two possibilities remain that could be chosen depending on the SCR:

- **High SCR.**

With a high SCR the probability of detection is high enough to use the post-detection combining between the transmitters and no MRC. Then the delays between the receivers signals are kept and the NF localization can still be applied.

- **Low SCR.**

With a low SCR the probability of detection is low and it is advantageous to apply the MRC (pre-detection combining) over all signals in order to maximize the chances of detection. Then the delays between the receivers signals are not kept and the NF localization cannot be applied anymore.

6.6.2 Radar illumination

Radar illumination and detection are made using beam-width that can be set for the illumination (6.3.2). It occurs every $\Delta t = 300 \text{ ms}$ (see 6.6.3) which gives the time for the radar to process the received signals.

6.6.3 Target tracking

This technique can also be applied with classic SISO radar. Target tracking has to be done and updated at every new scan. Then, the behavior of each target can be found, including their speed and acceleration.

When interesting targets are discriminated, relevant information can be retrieved with target tracking methods. Target tracking methods can go from the simple object range or angle tracking, to the multiple targets tracking with speed, direction and acceleration estimation.

Knowing the target position, its polarimetric signature, its speed, direction and acceleration are all factors that improve the probability to detect serious threats.

There are two main methods in target tracking [20]:

- Single target tracking.

This method is used in the case where we want to focus on only one target, such as missile detection. The principle is to use narrow beam pattern around the target to evaluate how it is moving or behaving around its position. Then, the result of the echo is used in a feedback closed loop to estimate the new target position and track it.

- Track-While-Scan (TWS).

This method is more adapted when we want to follow any detected target on a map. When a target is detected, a tracking file is created where the target data (position, estimated velocity and acceleration) are saved. They must decide for each detection whether it is a new target or an already detected one.

In our case, TWS seems more suited. The principle is explained in [20]. For each degree of freedom of the target (for us, it is a 2D detection, so only x and y axis), the current position, speed and acceleration is calculated from previous measurements. Then, if we know the radar sampling interval, we can estimate the future position of the target. With a residual error, it is then possible to steer the radar beam (in a narrow-beam case) to scan around the estimated new position of the target, to be sure not to lose track of it.

One of the most common used tracking procedure is the $\alpha\beta\gamma$ tracker [20]. This tracker is a filter which integrates the previous positions and allows to estimate the future ones. The filter just estimates the new position integrating the previous positions. To ensure that the target tracking gives satisfactory results, we must ensure that the sampling time is the best-suited. In our case, it can be chosen $\Delta t = 300 \text{ ms}$, which represents a $\Delta R \approx 5 \text{ m} = S_{\text{resolution}}$ for a 15 m/s moving target.

Obviously if the target is moving towards the vessel, we can deduce that it is a more serious threat than any other target.

Chapter 7

Radar signal simulation

This chapter introduces the implementation done for the simulations. It will be organized in blocks that are all linked following the overall organization plan shown in Figure 7.1.

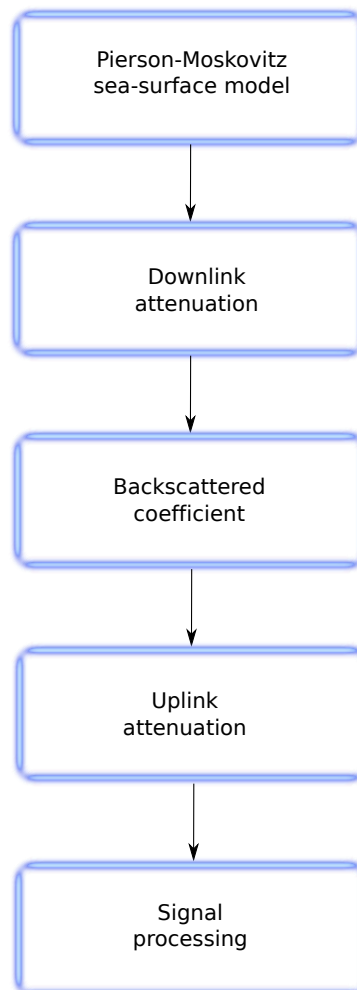


Figure 7.1: Overall implementation block diagram

7.1 Sea surface generation

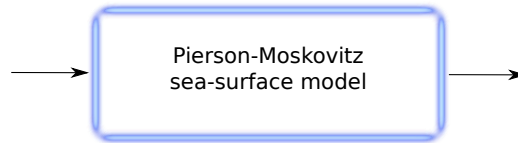


Figure 7.2: Pierson-Moskovitz sea-surface model block

The main parameter to take into account is the sea-state. From the sea-state, a wind power is randomly chosen, sea surface computed. Then the earth curvature is applied on the sea-height and that height is shifted down in order to work only with positive values.

Figures 7.4, 7.3 and 7.5 show the sea-surface after the earth curvature application. In figure 7.5, the chosen range is higher, and we can see the effect of the earth curvature on the right up corner. The curvature is applied from the vessel point of view which is in coordinates (0;0).

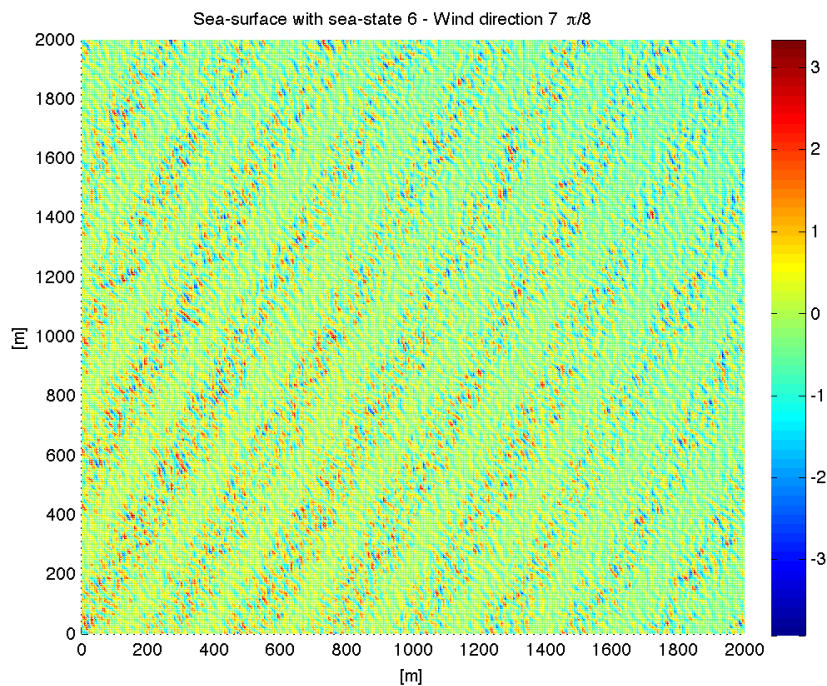


Figure 7.3: Sea-surface height model in meter with the Pierson-Moskovitz algorithm for sea-state 6 and wind direction $7\pi/8$ taking into consideration the earth curvature with 2km range

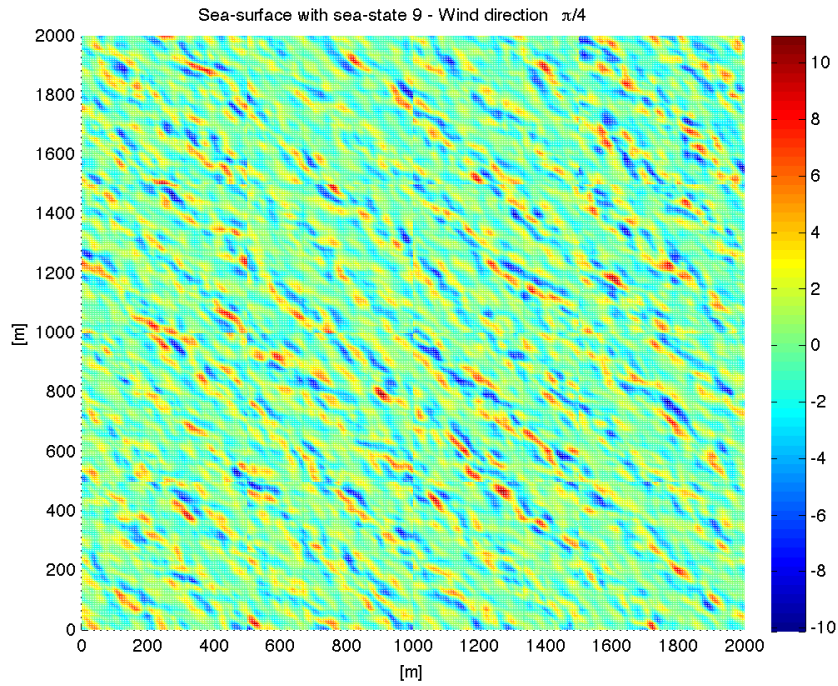


Figure 7.4: Sea-surface model with the Pierson-Moskovitz algorithm for sea-state 9 and wind direction $\pi/4$ taking into consideration the earth curvature with 2km range

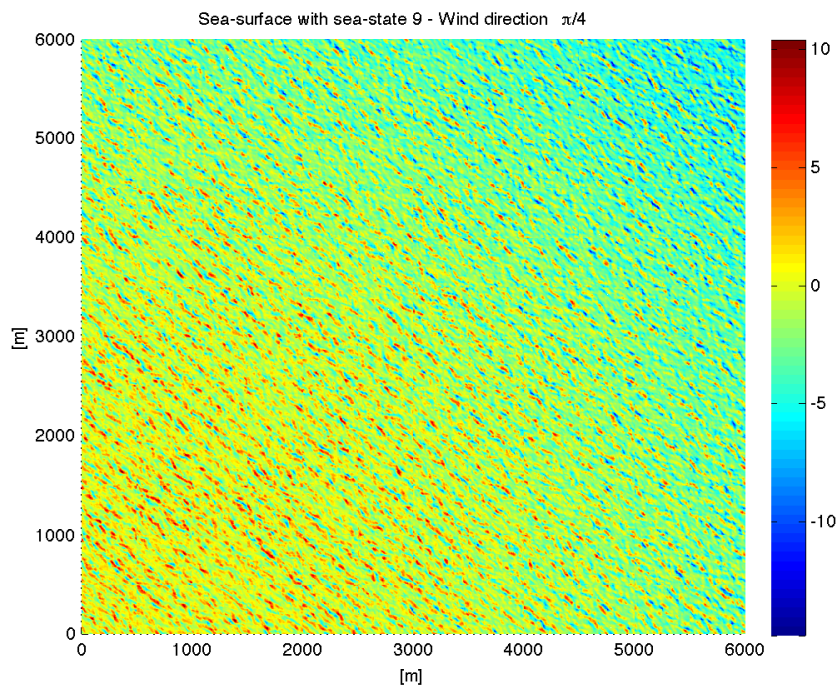


Figure 7.5: Sea-surface model with the Pierson-Moskovitz algorithm for sea-state 9 and wind direction $\pi/4$ taking into consideration the earth curvature with 6km range

7.2 Pre-processing

7.2.1 Signals properties

In radar systems, the detection part is based on the received signal amplitude [9]. Since we are in short range, we can however keep the phase information, which could be useful for the Doppler tracking or speed informations. Hence, each signal will carry those two informations:

- Amplitude
It will be denoted $A_R \geq 0$.
- Phase
It will be denoted $\zeta \in [0; 2\pi]$

Signal will be modeled with complex numbers. They will have the form given by equation (7.1)

$$S_{x,y}(t) = A_R(t) \cdot \exp [i\zeta(t)] \quad (7.1)$$

Signals will be stored in a $M \times N$ matrix, M being the number of transmitters and N the number of receivers. Each received signals will be stored in that matrix, depending on t. We finally have a 3D matrix. This matrix has to be built with the simulation, through the *Downlink*, *Reflection* and *Uplink* process which are explained above.

$$S_{m,n}(t) = \begin{pmatrix} S_{1,1}(t) & S_{1,2}(t) & \cdots & S_{1,N}(t) \\ S_{2,1}(t) & S_{2,2}(t) & \cdots & S_{2,N}(t) \\ \vdots & \vdots & \ddots & \vdots \\ S_{M,1}(t) & S_{M,2}(t) & \cdots & S_{N,M}(t) \end{pmatrix} \quad (7.2)$$

The initial phase will be denoted by ζ_{ini} and the initial signal power A_{ini} . We take in-phase signals for all antennas, i.e. $\zeta_{ini} = 0 \text{ rad}$. The initial amplitude A_{ini} is calculated with the total power shared among all antennas and the bandwidth. In the simulation, we use a pulse radar sending a rectangle at a carrier frequency f_c . We can calculate the power of this pulse signal from its amplitude with equation (7.3) over a period.

$$P_{\text{cosine}} = \frac{1}{1/f_c} \int_{t=0}^{t=1/f_c} |A \cos(2\pi f_c t)|^2 dt = \frac{A^2}{2} \quad (7.3)$$

For n_p periods, we have the relation given by (7.4)

$$P_{Tx} = n_p \frac{A^2}{2} \Rightarrow A = \sqrt{\frac{2P_{Tx}}{n_p}} \quad (7.4)$$

Finally, we share the total power P_{Tx} among all transmitting antennas (M antennas). Therefore, we have $P_{Tx} \rightarrow P_{Tx}/M$. We can calculate initial amplitude with (7.5).

$$A_{ini} = \sqrt{\frac{2P_{Tx}}{M \cdot n_p}} \quad (7.5)$$

With n_p the number of pulse (i.e. the number of signal periods) calculated with (3.10).

7.2.2 Illuminated path

After the sea-surface generation, we have to compute the illuminated path. This illuminated surface can be calculated from the antenna measurement angle and the angle beam width.

For the simulations, we assume that the minimum azimuthal beam-width permitted by the antenna is 1° . Then, we obtain the path taken by the EM wave to go to the target and the sea-height on these pixels. For a beam-less scan, the azimuthal beam-width is set to be 90° (Limited to the region of interest as discussed in section 3.4).

Two examples are given for a short range illumination and a long range illumination (Figure 7.6 and 7.7). They highlight that the multiple wave paths are not illuminating the same area when they are close to the vessel. However, when we get closer to the focused distance, the same areas are illuminated by the different antennas. Then we can observe the space diversity because the same part of the sea is illuminated from different paths. Else, the performance would tend to be the same as a SIMO radar.

For each illuminated surface, we have to compute the area between different ranges to get the cell-size, in order to be able to compute the sea RCS.

7.3 Downlink

The downlink process is composed of the propagation attenuation and the sea-waves shadowing as shown by Figure 7.8.

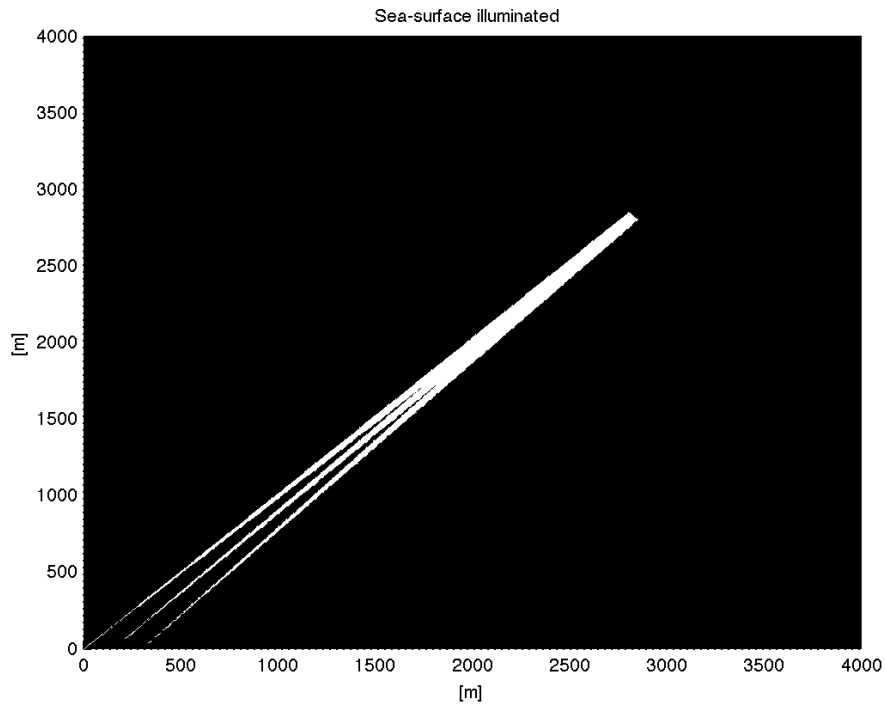


Figure 7.6: Total illuminated area for a maximum range of 4km and 3 transmitters.

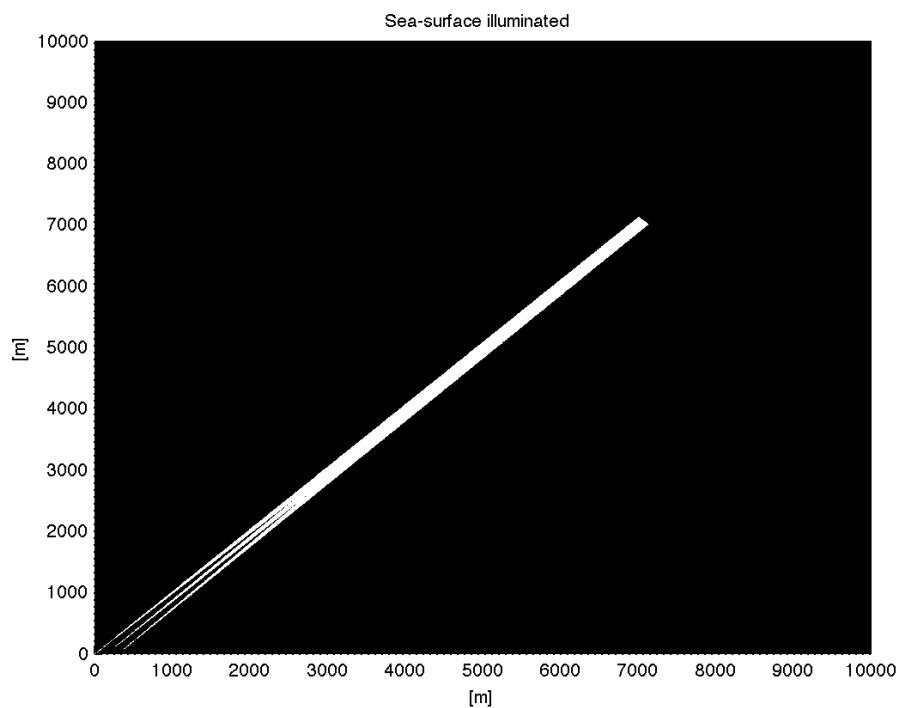


Figure 7.7: Total illuminated area for a maximum range of 10km and 3 transmitters.

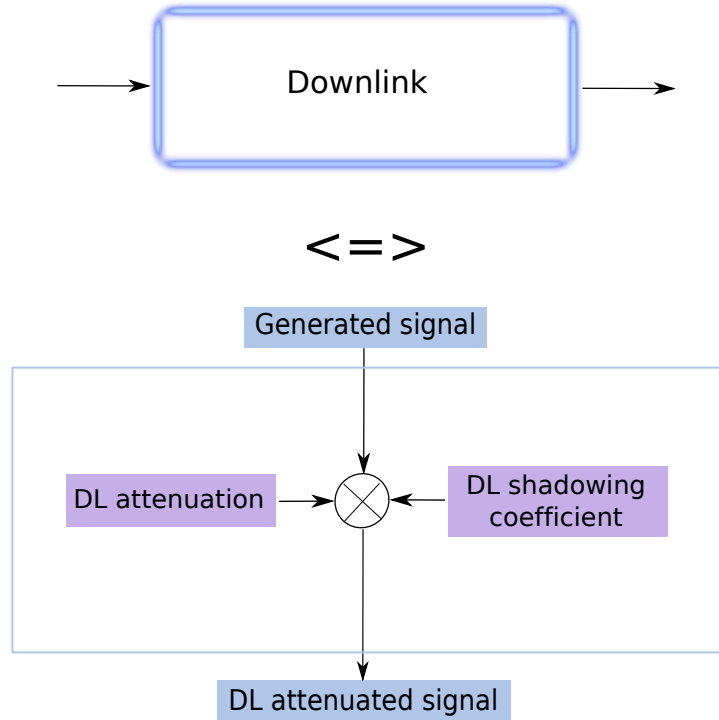


Figure 7.8: Downlink attenuation block

7.3.1 DL attenuation

For the downlink, we use the free-space propagation model (See section 5.1.4). Therefore, a signal matrix is built to know what will be the signal amplitude and phase at each illuminated area. The matrix is given by (7.6)

$$S_m^{DL}(t) = \begin{pmatrix} S_1(t) \\ S_2(t) \\ \vdots \\ S_M(t) \end{pmatrix} \quad (7.6)$$

In (7.6), the matrices $S_m(t)$ are the signals complex representation, composed by their phase and amplitude. The phase and amplitude for the downlink will depend on the initial parameters and the traveled distance. The new amplitude at the downlink is given by (7.15) and the new phase is calculated with (7.8)

$$A_R^{DL}(t) = A_{ini} \sqrt{G_{Tx}} \frac{\lambda}{4\pi c_0 t} \quad (7.7)$$

$$\zeta(t) = \zeta_{ini} + \frac{2\pi c_0 \cdot t}{\lambda} \mod 2\pi \quad (7.8)$$

7.3.2 DL shadowing

The computation of the illuminated area per transmitter allows to find the sea height on wave path. From these heights the shadowing coefficient for each path is given by the definition made in section 5.1.5.

We can therefore build the following matrix for the DL process:

$$c_{shadow|m}^{DL}(t) = \begin{pmatrix} c_{shadow|1}^{DL}(t) \\ c_{shadow|2}^{DL}(t) \\ \vdots \\ c_{shadow|M}^{DL}(t) \end{pmatrix} \tag{7.9}$$

7.4 Backscattered coefficient

For each illuminated area, we compute the echo of that area. This response is the one of the sea-clutter plus eventual dinghy or weapon on the sea including the shadowing of the downlink and uplink paths. It is organized as shown in Figure 7.9.

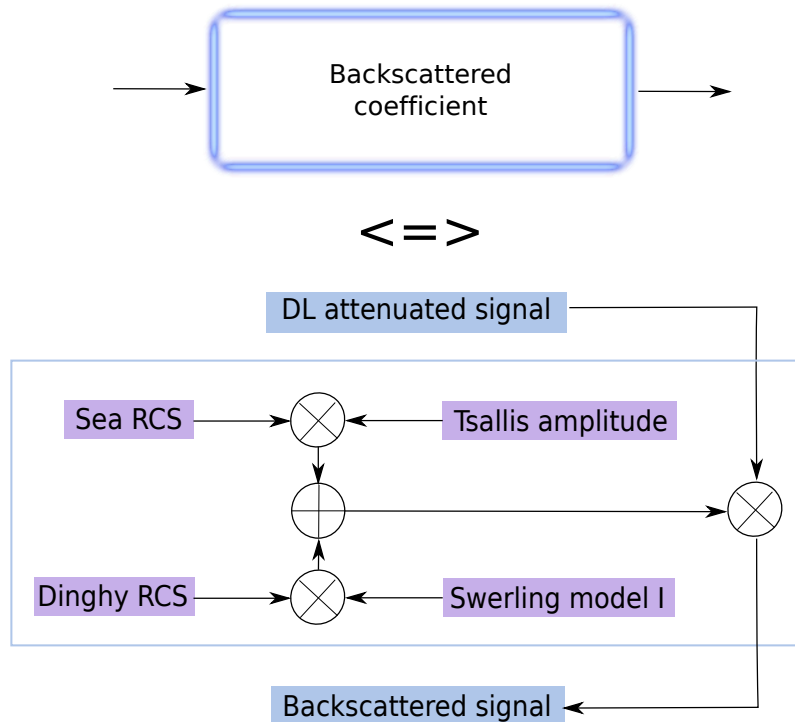


Figure 7.9: Backscattered coefficient block.

7.4.1 RCS

The RCS for each cell needs to be computed as well.

- **Sea RCS**

The RCS calculation is explained in section 4.1.2. We have :

$$RCS_{sea} = \sigma_{sea} = \sigma_{sea-normalized} \cdot S_{area} \quad (7.10)$$

Where $\sigma_{sea-normalized}$ is calculated with (4.9), (4.10) or (4.11) and S_{area} is calculated with the illuminated area surface. The sea RCS for a HH polarization and sea-state 4 versus the range is sketched in Figure 7.10.

- **Dinghy RCS**

The hull RCS is defined to be 0.25 m^2 in section 4.3.2 and to have a loss of 10 dBm^2 going from co-polarization to cross-polarization (section 4.3.4). As discussed in section 4.3.2, we use an exponential distribution for the RCS using the Swerling models. The boat being of Swerling model 1 [16], the corresponding probability density function is given by (7.11). The Swerling models are described in section 4.2.

$$P(RCS_{hull}) = \frac{1}{RCS_{average}} \cdot \exp\left(-\frac{RCS_{hull}}{RCS_{average}}\right) \quad (7.11)$$

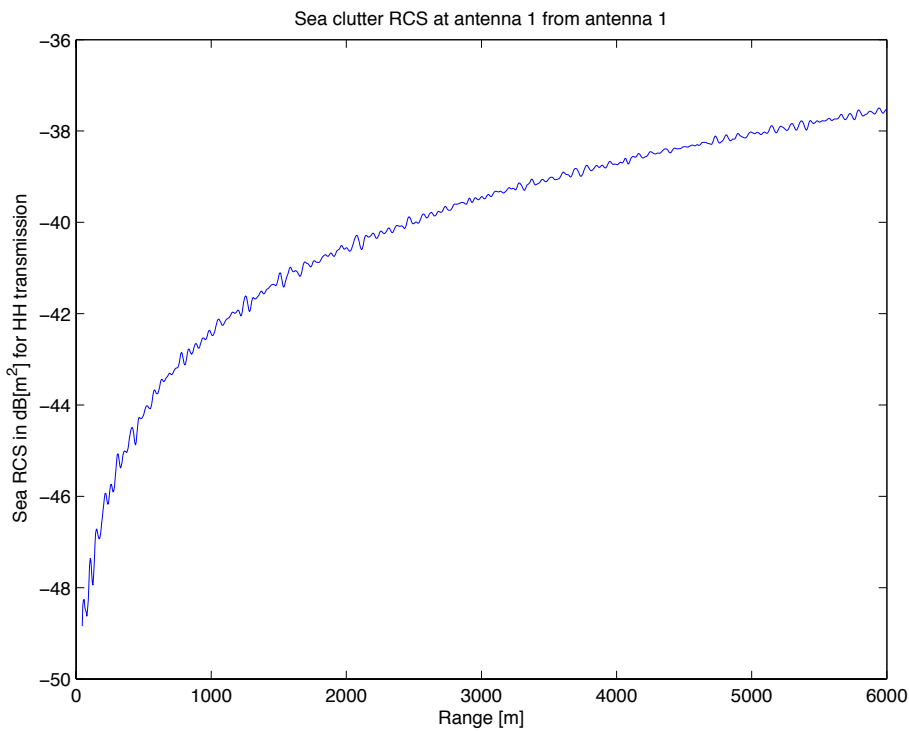
As explained in section, 4.2 we can cut the tail of this PDF and ignore the RCS_{hull} values above $30 \times RCS_{hull}$.

- **Weapons RCS**

First step is to define the values of the RCS for the three different points of view depending on the polarization. The second step is to compute φ_{weapon} and θ_{weapon} using (4.18) and (4.19). Then depending on these values we can predict the RCS. The equations used for the different possible positions are given in Table 7.1.

The number of weapons and their orientation are settings that can be defined manually. Once we have the RCS of all the weapons, we sum them to obtain the total RCS of the weapons.

$\varphi_{\text{weapon}} [^\circ]$	$\theta_{\text{weapon}} [^\circ]$	RCS in m^2
0	0	$\cos(\alpha) \cdot P3$
	45	$\cos(\alpha - \frac{\pi}{4}) \cdot (P3) + \sin(\alpha - \frac{\pi}{4}) \cdot (P2)$
	90	$\sin(\alpha - \pi) \cdot P2$
30	0	$\cos(\alpha) \cdot \cos(30) \cdot P3$
	45	$\cos(30) \cdot \cos(\alpha) \cdot \cos(\frac{\pi}{4}) \cdot (P3 + P2)$
	90	$\cos(\alpha) \cdot P2$
45	0	$\cos(\alpha) \cdot (P1 + P3) \cdot \cos(\frac{\pi}{4})$
	45	$\cos(\alpha) \cdot (P1 + P2 + P3) \cdot \cos(\frac{\pi}{4})$
	90	$\cos(\alpha) \cdot (P1 + P2) \cdot \cos(\frac{\pi}{4})$
60	0	$\cos(\alpha) \cdot \sin(60) \cdot P1$
	45	$\cos(\alpha) \cdot \cos(\frac{\pi}{4}) \cdot \sin(60) \cdot 2 \cdot P1$
	90	$\cos(\alpha) \cdot \sin(60) \cdot P1$
90	0	$\cos(\alpha) \cdot P1$
	45	$\cos(\alpha) \cdot \cos(\frac{\pi}{4}) \cdot 2 \cdot P1$
	90	$\cos(\alpha) \cdot P1$

Table 7.1: Possible RCS of the weapon depending on φ and θ .Figure 7.10: Sea RCS versus the distance in $dB[m^2]$ for a 1° beamwidth.

7.4.2 Tsallis amplitude

To calculate the backscattered signal, we have to compute a Tsallis realization, to apply it to the sea-pixels. This amplitude represents the amount of energy which is scattered back by each cell. Then, coefficients are multiplied together and a matrix can be build depending on the illuminated pixels per Tx/Rx links. Therefore, we will have the matrix for the $A_{m,n}^{Tsallis}$ given by (7.12).

$$A_{m,n}^{Tsallis}(t) = \begin{pmatrix} A_{1,1}^{Tsallis}(t) & A_{1,2}^{Tsallis}(t) & \dots & A_{1,N}^{Tsallis}(t) \\ A_{2,1}^{Tsallis}(t) & A_{2,2}^{Tsallis}(t) & \dots & A_{2,N}^{Tsallis}(t) \\ \vdots & \vdots & \ddots & \vdots \\ A_{M,1}^{Tsallis}(t) & A_{M,2}^{Tsallis}(t) & \dots & A_{M,N}^{Tsallis}(t) \end{pmatrix} \quad (7.12)$$

7.4.3 Operation on signals

If the illuminated area is composed of sea only, the RCS of the dinghy will be defined to be zero. The backscattered signal amplitude and phase will be given:

- Amplitude (A_R)

Will be calculated with a Tsallis realization. Parameters will be estimated depending on the wind speed and direction. Then, the amplitude is given with (7.13)

$$A_{R|m,n}^{reflected} = A_m^{DL} \cdot \sqrt{c_{shadow|m}^{DL} (A_m^{Tsallis} \cdot RCS_{sea} + RCS_{target}) \cdot c_{shadow|n,m}^{UL}} \quad (7.13)$$

- Phase (ζ)

Will follow a π reflection + the addition of speckle components, modeled by uniform random distribution in $[-\pi; \pi]$. Also, we will have $\zeta_{reflected} \in [0; 2\pi]$, since it is a phase.

7.5 Uplink

7.5.1 UL attenuation

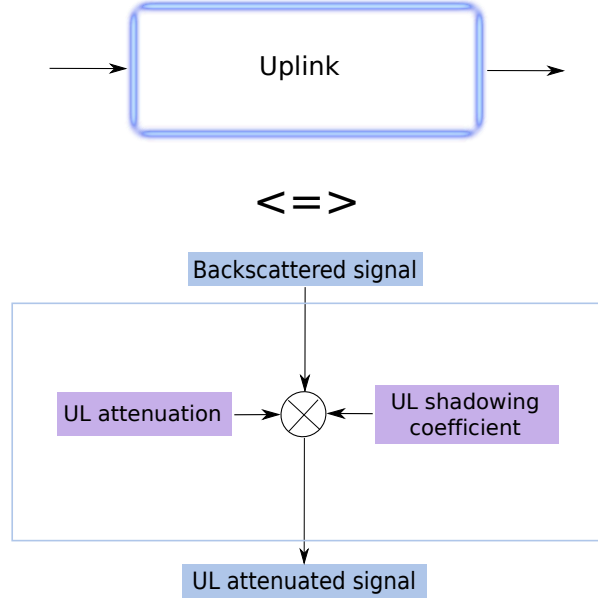


Figure 7.11: Uplink attenuation block

The uplink process is the same as the downlink one. The new phase at the receiver will be given by equation (7.14).

$$\zeta(t) = \zeta_{ini} + \zeta_{reflected} + \frac{2\pi c_0 \cdot t}{\lambda} \pmod{2\pi} \quad (7.14)$$

$$A_{R|m,n}^{UL}(t) = A_{R|m,n}^{reflected} \sqrt{G_{Tx} \cdot A_e} \frac{\lambda}{4\pi c_0 t} \quad (7.15)$$

7.5.2 UL shadowing

Using the same process as for the DL shadowing we obtain:

$$c_{shadow|n,m}^{UL}(t) = \begin{pmatrix} c_{shadow|1,1}^{UL}(t) & c_{shadow|1,2}^{UL}(t) & \cdots & c_{shadow|1,N}^{UL}(t) \\ c_{shadow|2,1}^{UL}(t) & c_{shadow|2,2}^{UL}(t) & \cdots & c_{shadow|2,N}^{UL}(t) \\ \vdots & \vdots & \ddots & \vdots \\ c_{shadow|M,1}^{UL}(t) & c_{shadow|M,2}^{UL}(t) & \cdots & c_{shadow|M,N}^{UL}(t) \end{pmatrix} \quad (7.16)$$

In equation (7.16), we have $c_{shadow|i,i}^{UL}(t) = c_{shadow|i}^{DL}(t)$, $\forall i \leq \min(M, N)$.

7.6 Signal processing: MIMO reception

The multiple copies of the same signal in $S_{m,n}(t)$ should help us to improve the SCR and therefore the detection reliability. To enhance the SCR , we decided to use Maximal Ratio Combining (MRC) described in section 6.3.4.

The received signals have to be synchronized/matched before an actual MRC process can be applied. Several options are possible.

- **First round detection**

We can proceed to a first detection round (post-detection combining) as shown on figure 7.12 and 7.13. Then, the targets are clearly detected and can easily be matched. We can expect to have a smaller SCR than after combining, therefore a higher P_{fa} can be used to ensure detection. In that case, some gain is lost, especially if for one link the SCR is low (shadowed target) and the detection cannot be properly performed. This approach permits to find more hidden targets when there are several of them.

- **Highest tap and delay curvature**

In the case where no detection is performed, the impulses responses can be matched taking the highest signal tap compared to the mean level. Then with the delay curvature properties explained in section 6.4.1 and the radar information, (illumination angle, antenna spacing...) a match can be done.

However, in our implementation, the matching is perfect. No synchronization or jitter issue is taken into consideration. A more complete model could take into consideration these issues. This perfect case is both applied to SIMO and MIMO configurations in our results.

Therefore, since we know that $S_{m,n}(t) \cdot S_{m,n}(t)^* = |S_{m,n}(t)|^2$, $\forall S_{m,n}(t) \in \mathbb{C}$, the final signal will be given by (7.17)

$$S_{MRC}(t) = \sum_{m=1}^M \sum_{n=1}^N |S_{m,n}(t)|^2 \quad (7.17)$$

This combined signal $S_{MRC}(t)$ will finally be the signal on which the detection can be performed. In the case of the SIMO radar, we would have $S_{MRC}(t)$ given by (7.18)

$$S_{MRC}(t) = \sum_{n=1}^N |S_{1,n}(t)|^2 \quad (7.18)$$

An example of MRC on a 1×2 SIMO system is given with figures 7.12 and 7.13 show the received signals and figure 7.14 shows their MRC combination. The detection

(mean-level and detection threshold) for figures 7.12, 7.13 and 7.14 is detailed in section 7.7.

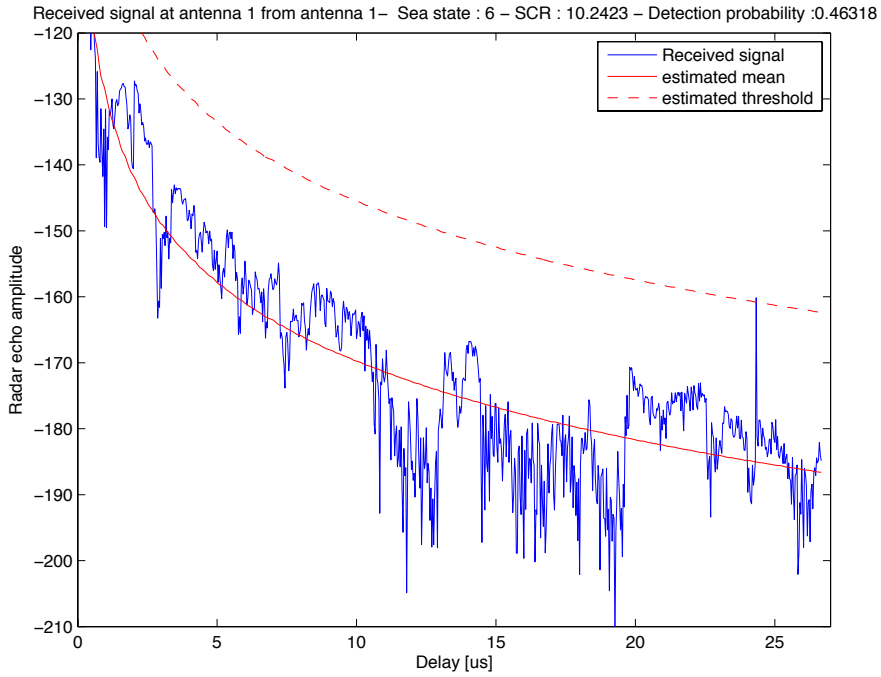


Figure 7.12: Received signal from antenna #1 to antenna #1 before MRC.

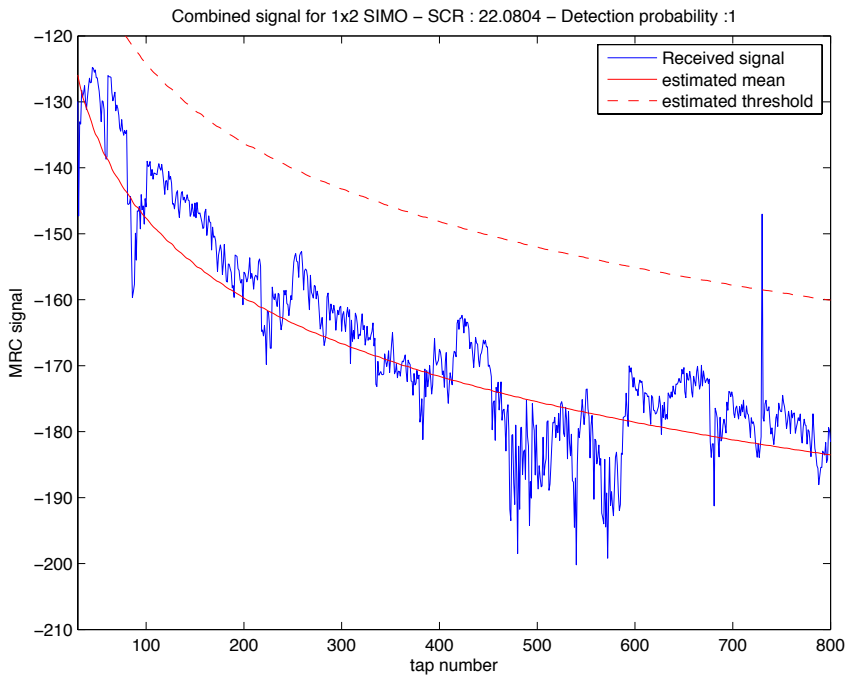


Figure 7.14: MRC of signals from fig. 7.12 and 7.13.

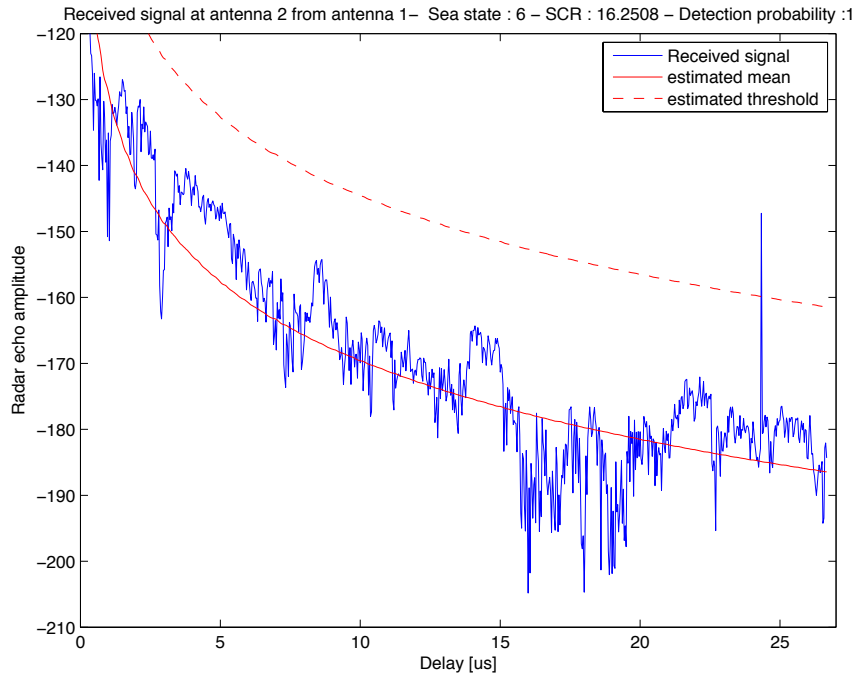


Figure 7.13: Received signal from antenna #1 to antenna #2 before MRC.

7.7 Signal processing: Detection

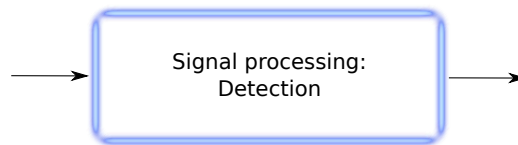


Figure 7.15: Signal processing block for target detection

With all of the processes above, we can then build the MIMO matrix $S_{m,n}(t)$. We keep the time as a parameter, but it is directly linked with the range. To get the range from the time delay, we can use equation (7.19).

$$R = \frac{c_0 \cdot t}{2} \quad (7.19)$$

The overall goal of the MIMO system is to enhance the SCR in order to improve the detection probability with a low P_{fa} . In the project, the SCR calculation is given in (7.20).

$$SCR = \frac{A_R^2}{2 \cdot \sigma_N^2} \quad (7.20)$$

Where:

A_R	Received amplitude
σ_N	noise standard deviation

We can perform a single detection for each Tx/Rx link. In the classic approach, a threshold value is defined depending on the P_{fa} . Then, the radar echo is compared with the threshold which decides to detect an object or not. P_{fa} is calculated with equation (7.21). All equations from (7.21) to (7.24) are taken or derived from [10]. They apply for a single link or for pre-detection combining.

$$P_{fa} = \int_{V_T}^{\infty} \frac{x}{\sigma_N} e^{(-x^2/2\sigma_N^2)} dx = \exp \left[\frac{-V_T^2}{2\sigma_N^2} \right] \quad (7.21)$$

Where:

P_{fa}	Probability of false alarm
σ_N	Noise standard deviation
V_T	Detection threshold [V].

Equation (7.21) also works for pre-detection combined signals (MRC) if we update the new noise standard deviation σ_N . The threshold value can therefore be calculated with equation (7.22)

$$V_T = \sqrt{2\sigma_N^2 \ln\left(\frac{1}{P_{fa}}\right)} \quad (7.22)$$

From the P_{fa} value, the probability of detection P_D can also be calculated. The used equation is (7.23)

$$P_D = \int_{V_T}^{\infty} \frac{x}{\sigma_N} I_0 \left(\frac{rA}{\sigma_N^2} \right) e^{(-x^2/2\sigma_N^2)} dx \quad (7.23)$$

Where:

P_D	Probability of detection
I_0	modified Bessel function of zero order

In [20], it is shown that (7.23) can be approximated with (7.24)

$$P_D \approx 0.5 \times \operatorname{erfc} \left(\sqrt{-\ln(P_{fa})} - \sqrt{SCR + 0.5} \right) \quad (7.24)$$

Where:

$erfc$ Error function given by (7.25)
 SCR Signal to clutter ratio

$$erfc(x) = \frac{2}{\sqrt{\pi}} \int_x^{+\infty} e^{-t^2} dt \quad (7.25)$$

An example is given in Figure 7.16 where the P_{fa} is set to be 10^{-5} on a sea at state 6. The target is easily detected in that case, with a $SCR = 30.8$ dB.

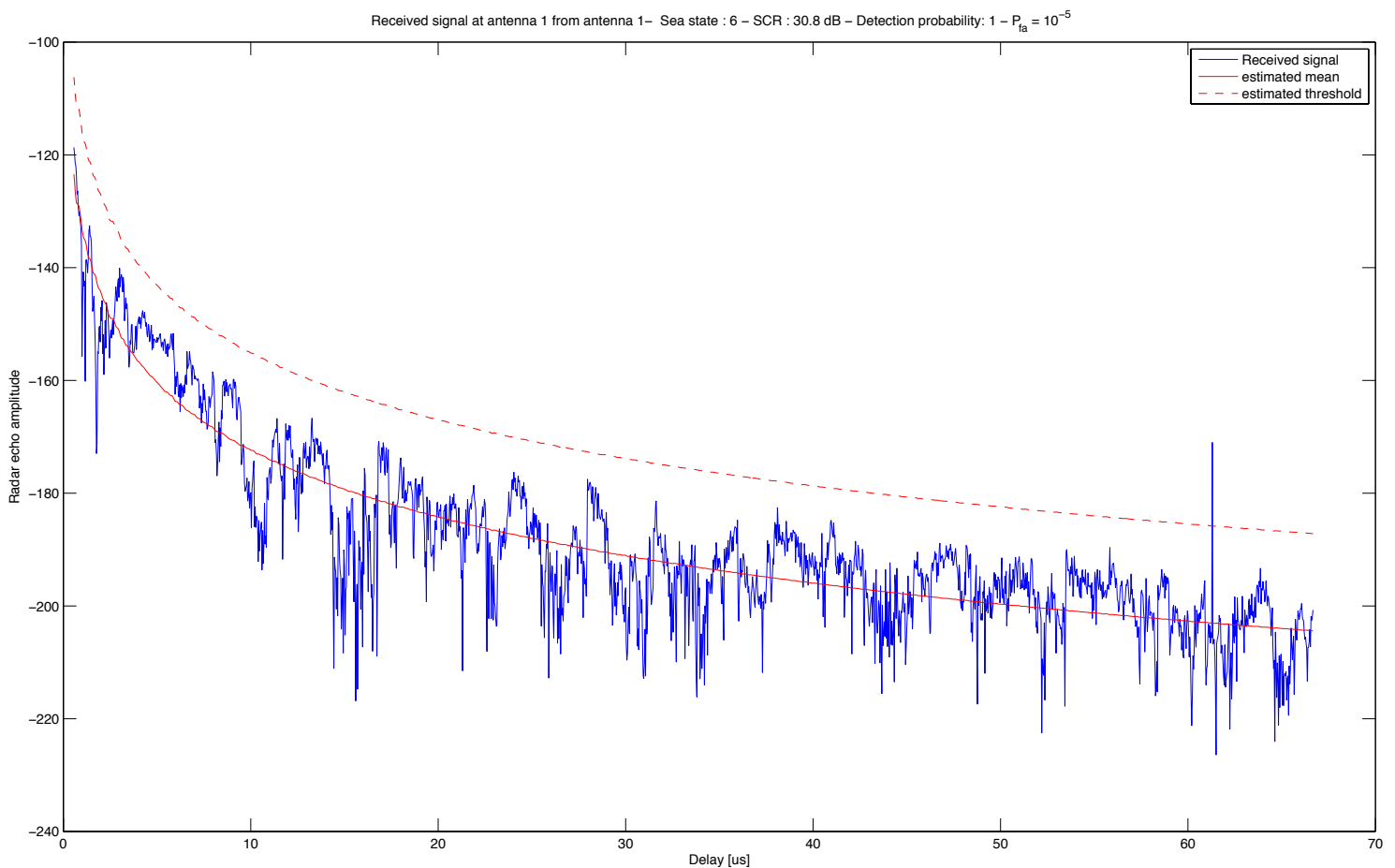


Figure 7.16: Received signal and the estimated mean and detection threshold

7.8 Signal processing: Localization

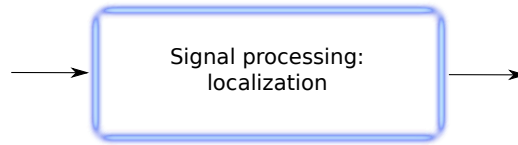


Figure 7.17: Signal processing block for target localization

We have to separate this part for each transmitter. When the signal from a transmitter is received by the receiving antennas, we look at the delays between them. From these delays, we can use the techniques described in section 6.4.1 and 6.4.3 to be able to assign relative coordinates to the detected object.

As explained for the NF localization, it requires that at least three antennas detect the target for the NF. From the delays between them we can compute the range and the DOA using:

$$\begin{cases} DOA = \sin^{-1} \left(\frac{\Delta R_{(n-1 \rightarrow n)} - \Delta R_{(n+1 \rightarrow n)}}{2 \cdot d} \right) \\ R_n = \frac{d^2 - \Delta R_{(n+1 \rightarrow n)}}{2(\Delta R_{(n+1 \rightarrow n)} + d \cdot \sin(DOA))} \end{cases} \quad (7.26)$$

Chapter 8

Radar operation results

This chapter introduces a comparison of SIMO and MIMO systems in order to highlight the improvement for a small target detection. We will compare systems where $M \times N$ is constant.

8.1 Metrics and simulation parameters

8.1.1 Metrics

The metric we will look at is the *SCR*. This metric shows how good and reliable is the response from the target. We also associate the detection probability P_D to the *SCR*, with equation (7.23).

We did not take into consideration the thermal noise impact in the model, and therefore the *SCNR* is not analyzed. The noise could play an important role for long range ($> 6 \text{ km}$) when the signal attenuation is high. However, we want to discriminate the clutter signal in our project, this is why we show how the *SCR* is improved with a MIMO system compared to the SIMO system.

The following parameters have been used for the simulation.

P_{fa} :	10^{-5}	Probability of false alarm.
f_c :	2.7 GHz	Carrier frequency.
W_a :	60 MHz	Bandwidth.
E_{xx} :	'VV'	Polarization for any antenna.
R_a :	$\pi/6$	Angle of illumination of the radar.
P_{Tx} :	25 kW	Total transmitted power by the input antennas.
R :	4000 m	Range at which the radar operates.

The transmitted power P_{Tx} is in our case equally shared among input antennas. The calculation of the power amplitude for each antenna is described in subsection 7.2.1.

8.1.2 Antenna placement

In a real-case radar on a vessel, the radar is often placed at the highest point possible on the boat: the bridge. Antenna placed on the hull would not be as high as the radar placed on the bridge.

For this simulations, we will define two placement scenarios (see figure 8.1):

- *hull.*

A system denoted 2×2 *MIMO hull* means that all antennas (transmitters and receivers) are placed along the hull. (30 m above the sea for the hull)

- *bridge.*

In a system denoted 2×2 *MIMO bridge*, the first antenna is placed on the bridge, higher than the rest of them on the hull. Then this antenna is less affected by shadowing, which allows a better target visibility. (50 m above the sea for the bridge)

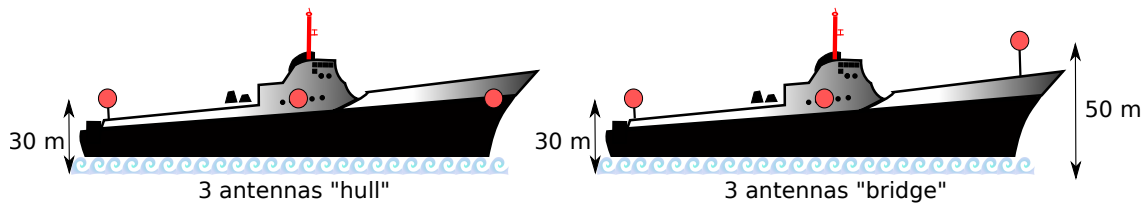


Figure 8.1: Hull and bridge antenna configurations.

The overall dimension of the antenna array remains the same in any configuration, which is the vessel length ($L_a = D_a$). All Tx/Rx are linearly spaced on the vessel, i.e. for 3 transmitters, we consider there are placed every 100 m on the 300 m vessel. The transmitter power P_{Tx} is equally shared among the transmitting antennas.

8.1.3 Scenario

In our case, we will compare the SCR improvement between systems listed in table 8.1

$M \times N$	Systems	
	SIMO bridge	MIMO hull
4	1×4	2×2
6	1×6	2×3
9	1×9	3×3
12	1×12	3×4

Table 8.1: Compared MIMO and SIMO systems.

Each of our simulation will occur with the set of parameters defined in table 1.2. We consider 12 receiving antennas as a maximum, which represents one antenna every $\Delta_{IES} = 25 \text{ m}$ on a $D_a = 300 \text{ m}$ vessel.

8.2 Simulations results

For a radar illumination angle of $\pi/6$ (with the x axis), we can see with figures 7.4, 7.3 and 7.5 that the wind direction is more likely to create shadow zones for $\pi/4$ than for $7\pi/8$. Then, in the following simulation, it is therefore more likely that the *SCR* is higher for $7\pi/8$ than for $\pi/4$ wind direction.

The results given in table 8.2 are averaged *SCR* over 60 scans per parameter set. The configuration are grouped by equivalent system ($N \times M = \text{constant}$) in the table.

		Sea state				
		6		9		
		Wind direction	$\pi/4$	$7\pi/8$	$\pi/4$	$7\pi/8$
1×4 SIMO bridge	SCR [dB]		20	25.1	4.8	3.6
	P_D with (7.23)		1	1	0	0
2×2 MIMO hull	SCR [dB]		21.4	28.9	4.9	16.5
	P_D with (7.23)		1	1	0	1
1×6 SIMO bridge	SCR [dB]		22.7	26.1	6	4.1
	P_D with (7.23)		1	1	0	0
2×3 MIMO hull	SCR [dB]		23.2	30	6.8	17.4
	P_D with (7.23)		1	1	0.1	1
1×9 SIMO bridge	SCR [dB]		22.9	26.5	7.5	4.4
	P_D with (7.23)		1	1	0.1	0
3×3 MIMO hull	SCR [dB]		27.2	32.8	12.3	22.3
	P_D with (7.23)		1	1	0.9	1
1×12 SIMO bridge	SCR [dB]		23.8	26.6	7.7	4.7
	P_D with (7.23)		1	1	0.1	0
3×4 MIMO hull	SCR [dB]		27.6	33.5	12.1	23.6
	P_D with (7.23)		1	1	0.8	1

Table 8.2: Results table for SIMO and MIMO radars SCR improvement for dinghy range 4000 m.

The overall trends of table 8.2 is also displayed on figure 8.2 (*SCR*) and figure 8.3 (P_D) depending on the number of links ($M \times N$). On these figures, we can also see the *MIMO bridge* and *SIMO hull* configurations. We can see the system averages in table 8.3.

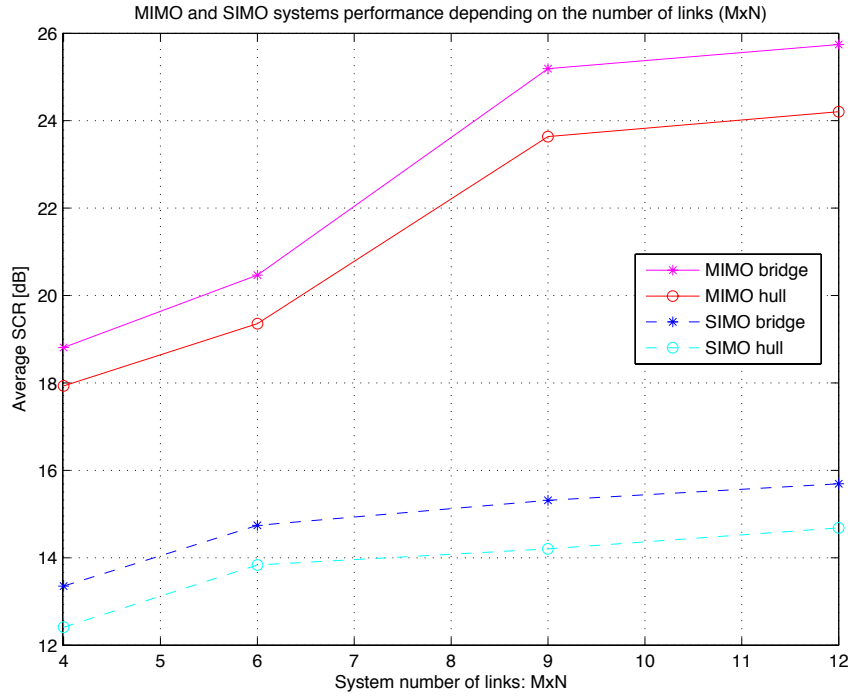


Figure 8.2: SCR for MIMO and SIMO systems.

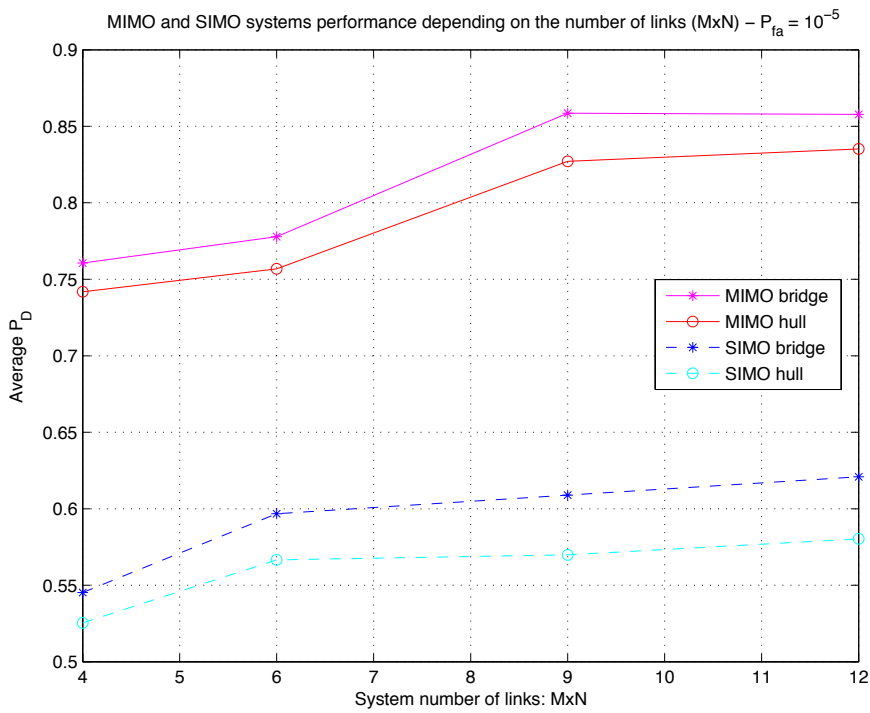


Figure 8.3: P_D for MIMO and SIMO systems.

8.2.1 Detailed results

In this section, results for each set of parameter are displayed and also the total 240 scans over plots to see the complete details of radar systems behavior.

Partial results per parameter set for table 8.2 are displayed with figures 8.4 to 8.7.

Detailed simulation results are displayed in figures 8.8 and 8.9. We can see that when the target is detected, the MIMO and SIMO systems have close values of SCR for calm sea-state.

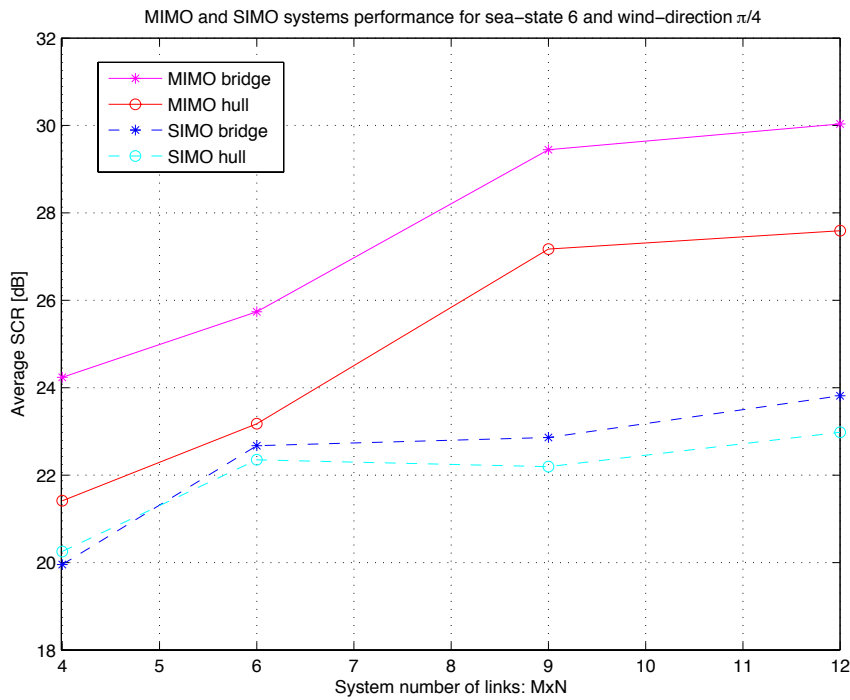


Figure 8.4: SCR for MIMO and SIMO systems - sea state: 6 - wind direction: $\pi/4$.

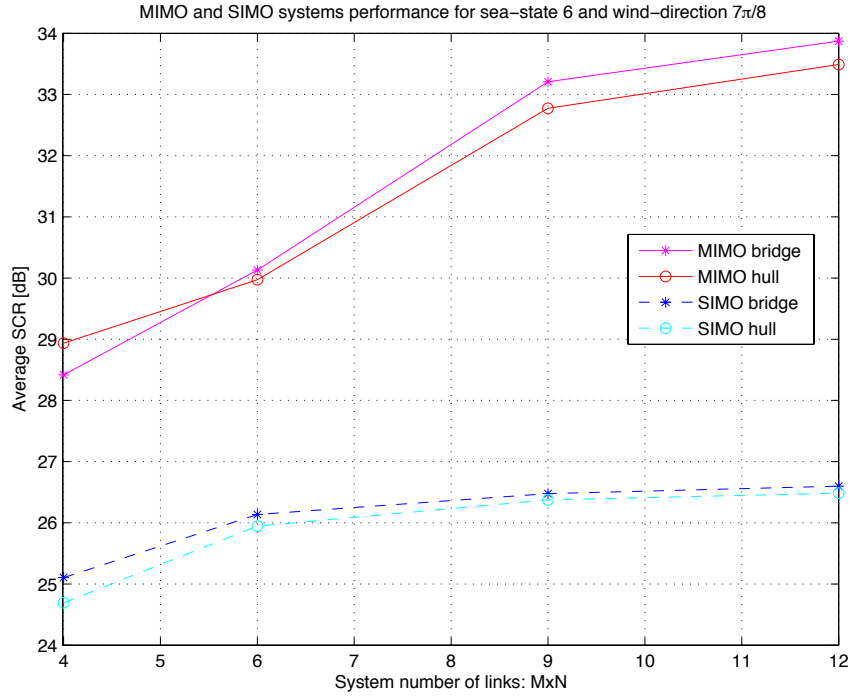


Figure 8.5: *SCR* for MIMO and SIMO systems - sea state: 6 - wind direction: $7\pi/8$.

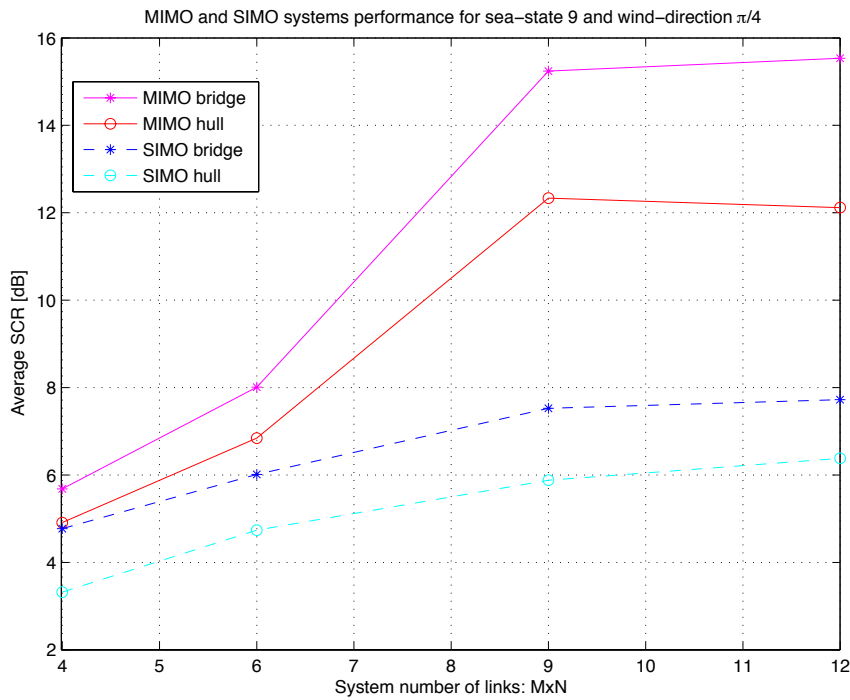


Figure 8.6: *SCR* for MIMO and SIMO systems - sea state: 9 - wind direction: $\pi/4$.

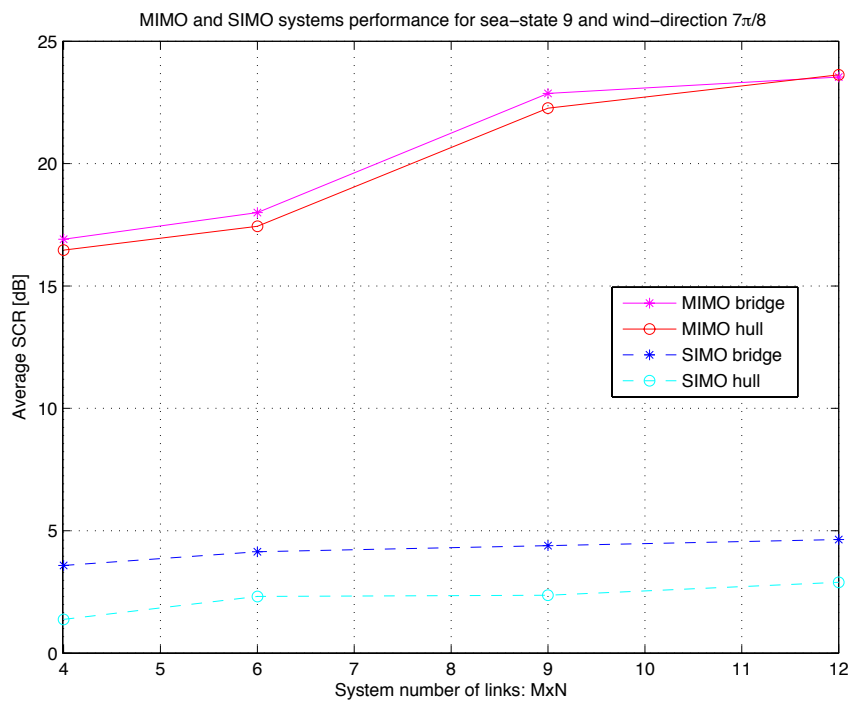


Figure 8.7: SCR for MIMO and SIMO systems - sea state: 9 - wind direction: $7\pi/8$.

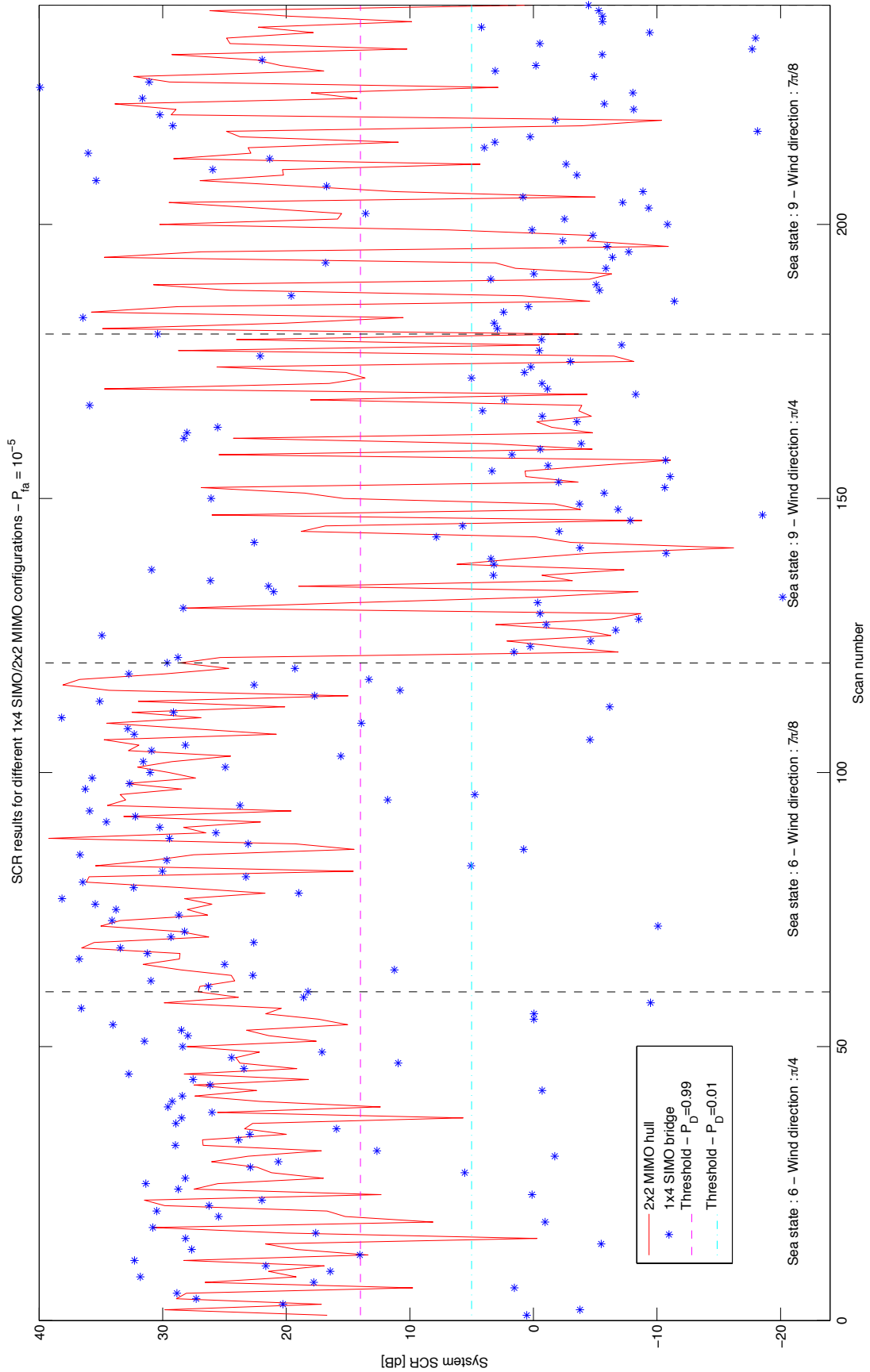


Figure 8.8: SCR results for the 240 scans with 1×4 SIMO and 2×2 MIMO systems.

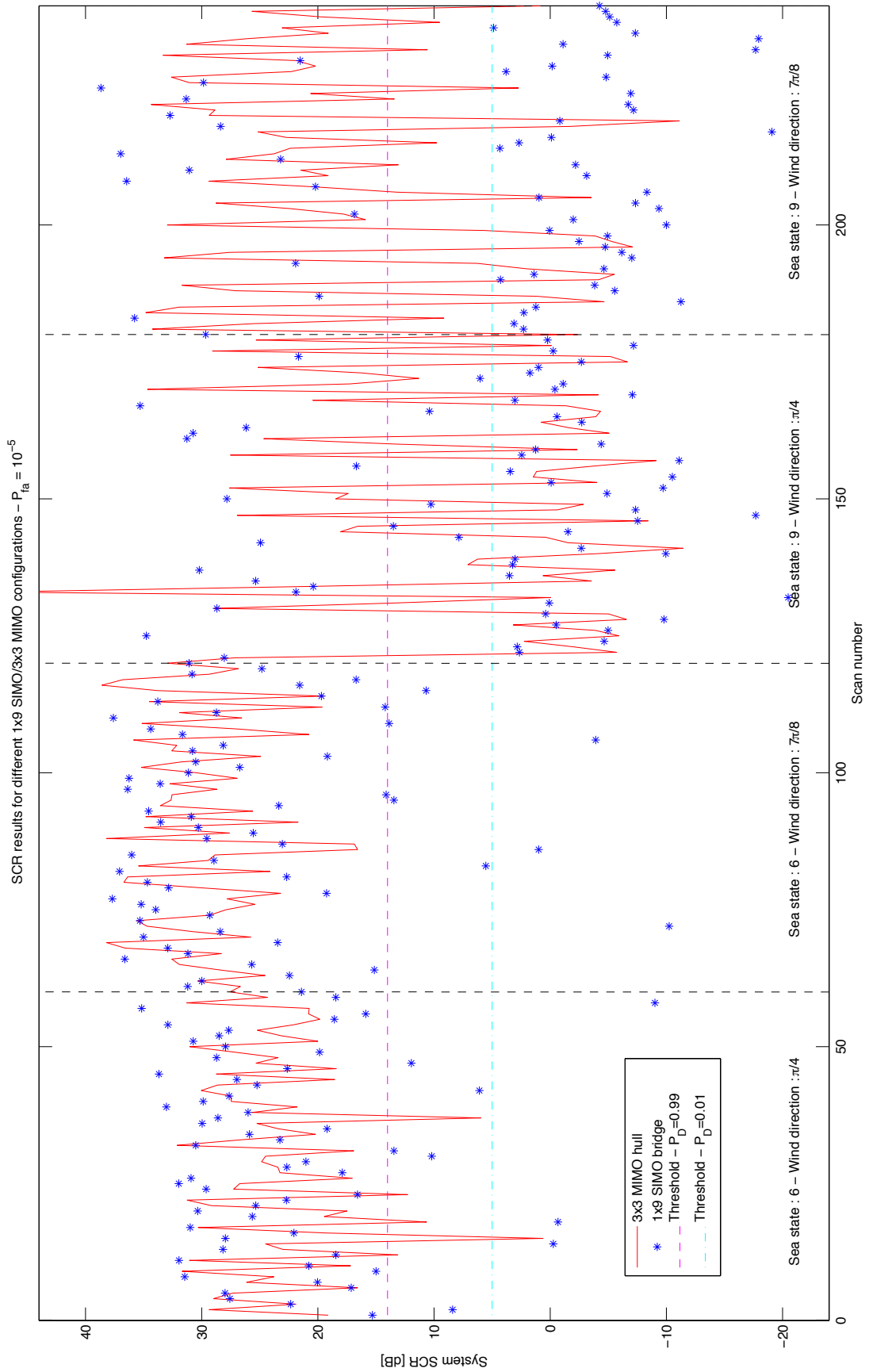


Figure 8.9: SCR results for the 240 scans with 1×9 SIMO and 3×3 MIMO systems.

8.2.2 Performance ranking

Table 8.3 shows the performance ranking of each system averaging their performance for any sea-state and wind-direction.

Rank	System	Avg SCR [dB]	$N \times M$
#1	3×4 MIMO hull	24.2	12
#2	3×3 MIMO hull	23.6	9
#3	2×3 MIMO hull	19.4	6
#4	2×2 MIMO hull	17.9	4
#5	1×12 SIMO bridge	15.7	12
#6	1×9 SIMO bridge	15.3	9
#7	1×6 SIMO bridge	14.7	6
#8	1×4 SIMO bridge	13.4	4

Table 8.3: Ranking for the MIMO and SIMO systems.

8.3 Discussions

The study made in [6] suggests that there is no significant improvement from a single SISO radar placed on the bridge of the vessel or a SIMO radar placed along the hull. In this project we compared the performance of a SIMO against a MIMO radar. The SIMO configuration is similar to the one defined in by [6].

MIMO radars usually offer a good clutter reduction capacity compared to SIMO radar [39]. We can therefore expect that the MIMO radar increases more efficiently the *SCR* than SIMO radar. The downlink path diversity also brings more stability to the MIMO radar than the SIMO with rapport to the sea-wave shadowing.

We analyze the results provided in table 8.2 separating the simulation conditions.

8.3.1 Calm sea

In that case, most of the time the target is illuminated and the space diversity does not really act against shadowing since the boat is completely visible. We can therefore see that from the 1×4 SIMO to the 3×4 MIMO, there is only **7.6 dB** improvement in average.

1×4 SIMO and 2×2 MIMO achieve a comparable result in that configuration (**1.4 dB** difference). The gap between more complex systems tends to grow to up **6 dB** for the 1×12 SIMO and 3×4 MIMO

It is interesting to note that SIMO system improves less with a higher link number than the MIMO system: 1×4 , 1×6 , 1×9 and 1×12 are all understood in a **4 dB** interval against **6.5 dB** for the MIMO systems.

8.3.2 Strong sea

With a high sea-state, the shadowing process gets more important and the target is often hidden by the waves. The MIMO radar here plays an essential role. Indeed, when the only downlink path of the SIMO radar is shadowed, there is no chance for the vessel to detect the dinghy. With the MIMO multiple downlink signals, this weak part is improved and the performance is better. The advantage of the 20 m more for the bridge height is not significative, especially at a 4 km range.

This is the point in the simulation where the MIMO system makes all the difference and improve the *SCR* dramatically more than the SIMO system.

8.3.3 Shadowing

Results show in our implementation that the sea-wavefront angle with the radar illumination angle plays an important role. When the sea-waves tend to be perpendicular to the illumination (wind direction : $\pi/4$), the SIMO and MIMO systems tend to achieve a closer performance, because the multiple downlink along this $D_a = 300\text{ m}$ do not really help to skirt around the sea-wavefront.

This phenomenon is visible in between figure 8.4 and 8.6. In figure 8.6, 1×4 SIMO bridge and 2×2 MIMO hull achieve the same performance.

The gap between MIMO and SIMO performances grows when the sea-wavefront is more parallel to the illumination angle (wind direction : $7\pi/8$). In that case, the multiple inputs offer more illumination diversity around sea-waves and fight more efficiently against shadowing. This is visible in figures 8.5 and 8.7. This multiple inputs gain is strong and make the bridge gain negligible. Indeed, *MIMO hull* and *MIMO bridge* system achieve a close performance in figures 8.5 and 8.7.

8.3.4 MIMO/SIMO comparison

The result is quite straightforward, a 2×2 MIMO system achieves a better *SCR* in average than a 1×12 SIMO system. MIMO systems completely outperform SIMO systems. For equivalent system (equal number of links) MIMO offers in average **6.5 dB** more than SIMO.

We can conclude stating that SIMO system offers a weak downlink part and therefore is less efficient in the target detection since shadowing and target RCS can

be strongly affected on this single downlink. This weak downlink on the SIMO configuration is reinforced with the bridge configuration, but it is not always significant compared to the operating range and sea-state.

MIMO system achieves a better performance than SIMO in any configuration, and sometimes with an significant difference.

Another interesting result is the comparison of 2×2 and 1×4 system. One of the main advantages of the 1×4 SIMO system compared to the 2×2 MIMO is that from 3 receivers, we can use the near-field target localization detailed in section 6.4.1. However, we can see that the 2×2 system offers a better *SCR*, which is **4.5 dB** more in average. In any system, we can therefore choose in between a better *SCR* or a better localization reliability thanks to near-fields properties. We also have to take into consideration that the *SCR* improvement is less in average for calm sea, approximately **2.6 dB**.

However, these results are taken for ideal cases and such *SCR* values will not happen in real-life radar applications because of noise (*SCNR*) and synchronization lack for example. The noise is also important for MIMO system, sometimes more than for SIMO configuration [39]. Never the less, the MIMO system shows a straight superiority to clutter reduction.

Conclusion

Pirates attacks raised the last decade and they could be avoided by more efficient detection systems.

To improve actual radar performances, we investigated the benefit of the use of MIMO technology in radar systems. Main approaches are to use space and polarization diversity, but we also investigated the fundamentals like RCS models or distributions.

Regarding the sea-clutter model, Tsallis distribution appears more suited to model the measured data than the usual K-distribution. It confirms what is reported in [8]. The Tsallis distribution has shown more robust modeling of the sea-amplitude response, especially for the distribution tails. Radar algorithms could use the Tsallis distribution to help to discriminate the sea-clutter response from the target echo since it better models the sea-clutter EM-response than the usual K-distribution. Detection threshold can then be derived from that model and provide a better threshold setting.

The study of the polarimetric properties of weapon RCS permitted us to predict the RCS behavior depending on the weapon orientation and the polarization. We found that weapons have a defined polarimetric signature which is different from the sea-clutter or classic boat target. However, this signature is often hidden in real-life scenario due to the sea-clutter and boat superposed responses and therefore make the prediction of weapons presence hard.

Finally, it has been shown that a MIMO radar configuration achieve better *SCR* than any SIMO radar. Even a 2×2 MIMO system performs better than a 1×12 SIMO. The main weakness of SIMO system is the unique downlink, which could be shadowed. The diversity brought by the multiple input ensure a better target visibility. With high sea-state, the MIMO radar outperforms the equivalent SIMO configuration. In the case of low sea-state, equivalent MIMO and SIMO systems tend to achieve comparable performance.

Another step for this project could be the investigation of the frequency diversity among the transmitters and receivers. It should permit to resolve the target discrimination from the sea but not from the sea-waves shadowing.

References

- [1] M. S. McDaniel.
http://www.cargolaw.com/presentations_pirates.html [Assessed in February 2012]
- [2] ICC International Maritime Bureau.
Piracy and Armed Robbery Against Ships, Annual Report, 1 January - 31 December 2008
- [3] UQAM - Institut d'études internationales de Montreal.
La piraterie maritime contemporaine - pp 2. Bulletin n°72 - December 2004
- [4] Web article: *<http://www.smart-http.com/negotiations-avec-les-pirates-somaliens>*
[Assessed in February 2012]
- [5] S. Kingsley and S. Quegan.
Understanding radar systems. McGraw Hill, first edition, 1992.
- [6] G. Casellas, L. S. Do, S. Hermoso, J. A. Mendez, I. Rodriguez and A. Tatomirescu.
Near Field Macro Array Reception for Small Radar Targets in Sea-clutter Aalborg University 8th semester Mobile Communication Report - February-June 2010.
- [7] One Earth Future Foundation.
<http://oceansbeyondpiracy.org/cost-of-piracy/human-cost-somali-piracy> [Assessed February 2012]
- [8] J. Hu, W. Tung and J. Gao.
A New Way to Model Nonstationary Sea Clutter IEEE SIGNAL PROCESSING LETTERS, VOL. 16, NO. 2, FEBRUARY 2009 - pp 129-132.
- [9] A. Thomsen, M. O. Pedersen
Private conversation with Terma A/S Visit in Terma A/S, Lystrup on 22/03/2012
- [10] M. I. Skolnik,
Introduction to radar systems McGraw-Hill - Third edition - 2002
- [11] C. A. Balanis.
Antenna Theory: Analysis and Design. (Third edition) - 2005
- [12] Web article:
<http://www.radartutorial.eu/06.antennas/an11.en.html>. [Assessed in February 2012]
- [13] D. K. Barton.
Radar System Analysis and Modeling. Artech House Radar Library, 2005

- [14] Web article:
<http://www.mercurymarine.com/engines/engine-tests/boat-house-bulletin/?ID=607> [Assessed in March 2012]
- [15] Web articles:
<http://en.wikipedia.org/wiki/AK-47> - <http://en.wikipedia.org/wiki/RPG-2> [Assessed in March 2012]
- [16] I. Harre.
RCS in Radar Range Calculations for Maritime Targets
http://www.mar-it.de/Radar/RCS/RCS_xx.pdf. [Assessed in February 2012]
- [17] I. Antipov.
Simulation of Sea Clutter Returns
- [18] T. Thayaparan.
Ultra-wideband (UWB) high-resolution noise radar for concealed weapon detection: electromagnetic simulation - phase 1
- [19] Web article:
http://en.wikipedia.org/wiki/Radar_cross-section [Assessed in May 2012]
- [20] B. R. Mahaza.
Radar Systems Analysis and Design Using MATLAB COLSA Corporation
- [21] G. Brooker, C. Lobsey and R. Hennessy.
RADAR CROSS SECTIONS OF SMALL BOATS AT 94 GHZ.
- [22] Web article:
<http://www.unodc.org> [Assessed in March 2012]
- [23] Web article:
http://en.wikipedia.org/wiki/Comparison_of_the_AK-47_and_M16 [Assessed in March 2012]
- [24] L. Wei, G. Li-Xin, and W. Zhen-Sen.
Polarimetric scattering from a two-dimensional improved sea fractal surface
School of Science, Xidian University, Xi'an 710071, China
- [25] P. W. Vachon, M. Dragosevic, N. Kashyap, C. Liu, D. Schlingmeier, A. Meek, T. Potter, B. Yue and J. Kraft.
Processing and Analysis of Polarimetric Ship Signatures from MARSIE Defence R&D Canada - Ottawa
- [26] Web article:
http://en.wikipedia.org/wiki/Beaufort_scale [Assessed in February 2012]
- [27] Dr C. Constantinou.
Introduction to Radiowave Propagation School of Electronic, Electrical and Computer Engineering - University of Birmingham.

- [28] J. W. Goodman.
Speckle phenomena in optics - Theory and application
- [29] N. Lehmann, A. Haimovich, R. Blum, L. Cimini and R. Valenzuela.
MIMO Radar Application to Moving Target Detection in Homogenous Clutter Adaptive Sensor Array Processing (ASAP), Workshop. June 2008
- [30] A. Haimovich.
Coherent MIMO Radar: High Resolution Applications New Jersey Institute of Technology
- [31] E. Fishler, A. Haimovich, R. Blum, D. Chiznick, L. Cimini and R. Valenzuela.
MIMO radar: an idea whose time has come.
- [32] J. Lv, Y. Lu, Y. Wang, H. Zhao and C. Han.
Antenna Spacing Effect on Indoor MIMO Channel Capacity IEEE Conference Publishing 2005 - Beijing University of Posts and Telecommunications
- [33] P. C. F. Eggers.
P3-2 Special topics in antenna systems Aalborg University
- [34] G. Lerosey, J. de Rosny, A. Tourin, A. Derode, G. Montaldo, and M. Fink, *Time Reversal of Electromagnetic Waves*
- [35] F. Yongqing, J. Yulei and L. Zhanya.
NEAR-FIELD SOURCE LOCALIZATION METHOD AND APPLICATION USING THE TIME REVERSAL MIRROR TECHNIQUE
- [36] W. Zhi and M. Yan-Wah Chia.
Near-Field Source Localization via Symmetric Subarrays
- [37] T.B. Lavate, V. K. Kokate and A.M. Sapkal *Performance Analysis of MUSIC and ESPRIT DOA Estimation Algorithms for Adaptive Array Smart Antenna in Mobile Communication* International Journal of Computer Networks (IJCN)
- [38] Web article:
http://tosa.mri.co.jp/sounddb/2dmusic/2D-music_e.htm [Assessed in March 2012]
- [39] P. P. Vaidyanathan and P. Pal
MIMO radar, SIMO radar, and IFIR radar: a comparison. California Institute of Technology - Nov. 2009.
- [40] R. Iqbal, T. D. Abhayapala and T. A. Lamahewa.
Generalized Clarke Model for Mobile Radio Reception IET Commun., 2009, Vol. 3, Iss. 4, pp. 644-654
- [41] J. H. Winters *Effect of Fading Correlation on Adaptive Arrays in Digital Wireless Communications* 1993 IEEE.

- [42] F. Khalid, J. Speidel.
Advances in MIMO Techniques for Mobile Communications
- [43] Public available radar measurements:
http://www.csir.co.za/small_boat_detection/datasets.html [Assessed in March 2012]
- [44] T. M. Cover, J. A. Thomas *Elements of Information Theory*. Second Edition, July 2006

Appendix A

Weapons length impact on RCS

In this appendix we are going to study the way weapons length impact their RCS. The arguments shown in this appendix mainly come from [18]. Indeed, they measured the RCS of handguns, rifles, I-shape cylinders, Γ -shape cylinders and Γ -shape plates. Studying the results, they went to the fact that the RCS of the AK-47 has two resonant peaks (Figure A.1).

In the figure, the weapon is placed with the barrel along the y-axis and the handle along the x-axis. The RCS of several sizes of I-plates from Table A.1 are visible in Figure A.2. The resonant wavelength is biased in the experiment by a coefficient λ_{bias} . This bias could come from parameters such as the material. Since all the plates and the weapons are taken with the same materials and environment, therefore we have the same coefficient for all the results. From Table A.2 we can say that $\lambda_{bias} = 5$.

I-plate	Length (cm)	Width (cm)	Thickness (cm)
1.	10	1	3
2.	20	2	3
3.	30	3	3
4.	40	4	3

Table A.1: Cylinders size corresponding to [18] experiment.

I-plate	Theoretical resonant frequency (m)	Observed resonant frequency (m)
1.	0.05	$0.24/\lambda_{bias}$
2.	0.1	$0.5/\lambda_{bias}$
3.	0.15	$0.75/\lambda_{bias}$
4.	0.2	$1/\lambda_{bias}$

Table A.2: Cylinders theoretical and observed reasoning wavelength corresponding to [18] experiment.

If we take into account the fact that the AK-47 is 50 cm long then its barrel resonant frequency would be 240 MHz. The observed AK-resonance peak in the

low frequencies is said to be 245 MHz. The length is confirmed to be the dominant parameter of the resonance. However where does the 2,7 GHz peak come from?

If the plate shape representing the AK-47 barrel does not explain the second peak we should look at the plate that approximates the handle. The AK-47 is now approximated by a Γ -plate shape. The Γ -plate shapes studied are shown in Table A.3. The results are shown by Figure A.3. The curve goes really high for high frequencies due to the presence of the handle: the cross-sectional part of the weapon [18]. It is then obvious that the handle is the reason of the 2.7 GHz peak in the RCS of the AK-47.

[18] did the measurements for several weapons and especially for a handgun which has the same shape as the AK-47. It is found that the handgun also have two resonant peaks in the RCS at 700 MHz and 2.7 GHz. 700 MHz corresponds to a 17 cm long barrel resonant frequency and the barrel of the experiment is 16,6 cm long. And the second peak is the same as the AK-47 one with less amplitude. Looking at the geometry of the weapon (cartridge clip similar to handle) we can say that the second peak comes from the handle which is approximately 4-5 cm width and corresponds to a resonant frequency going from 2.4 GHz to 3 GHz.

Γ -plate	Length (cm)	Width (cm)	Thickness (cm)
1.	10	5	3
2.	20	10	3
3.	30	15	3
4.	40	20	3

Table A.3: Γ -plates size corresponding to [18] experiment.

Conclusion

The Γ -plate shape could approximate the AK-47 and the handgun. When looking at the RCS of these objects we can observe similarities that allow us to predict the RCS behavior of these weapons depending on their barrel length and handle.

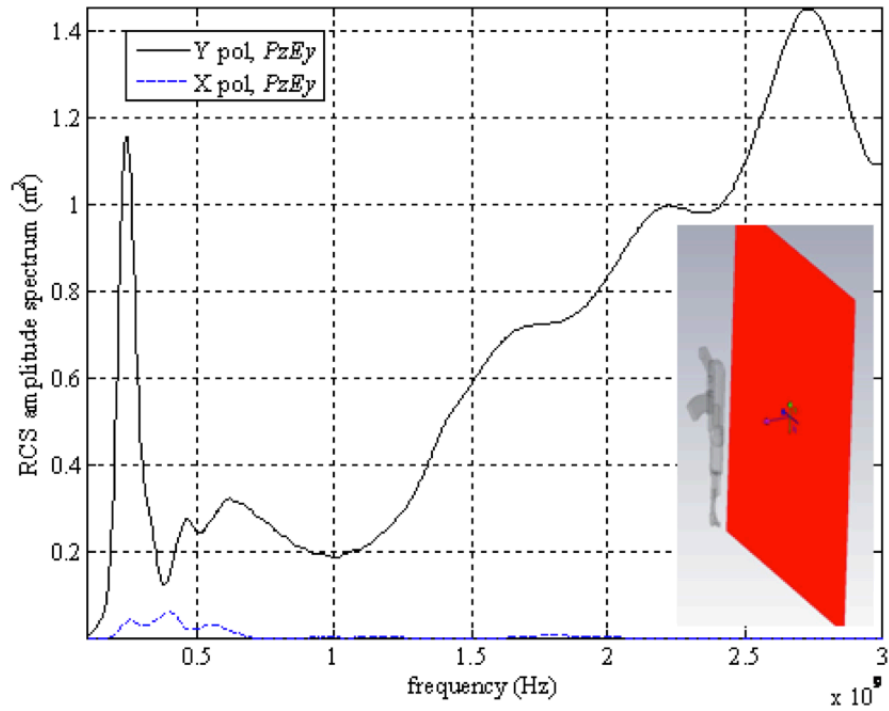


Figure A.1: Comparison between co (Y pol) and cross-polarization (X pol) AK-47 RCS [18].

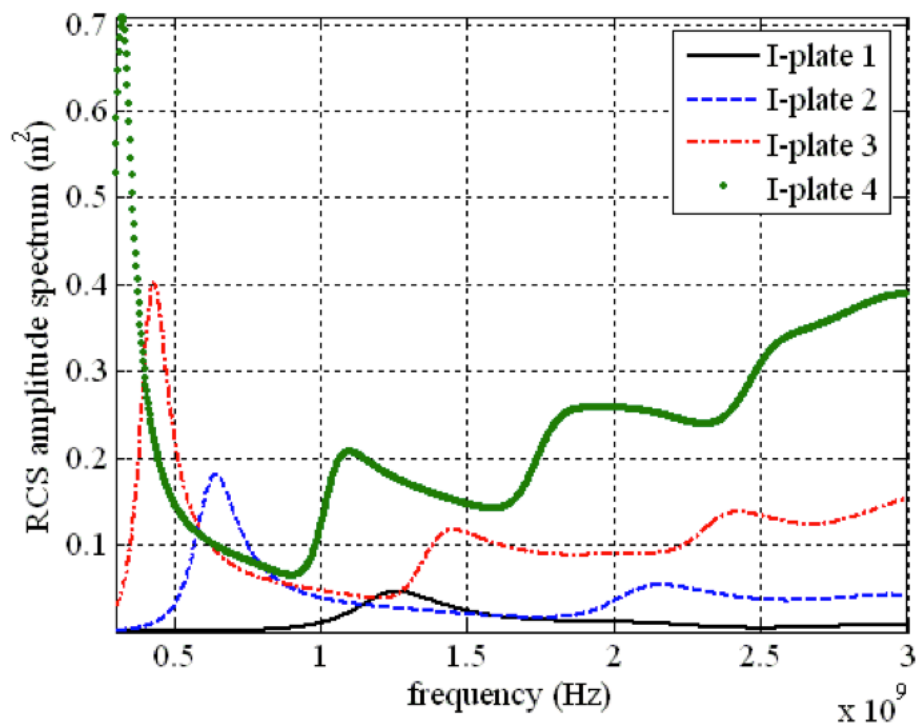


Figure A.2: I-plates co-polarisation RCS [18].

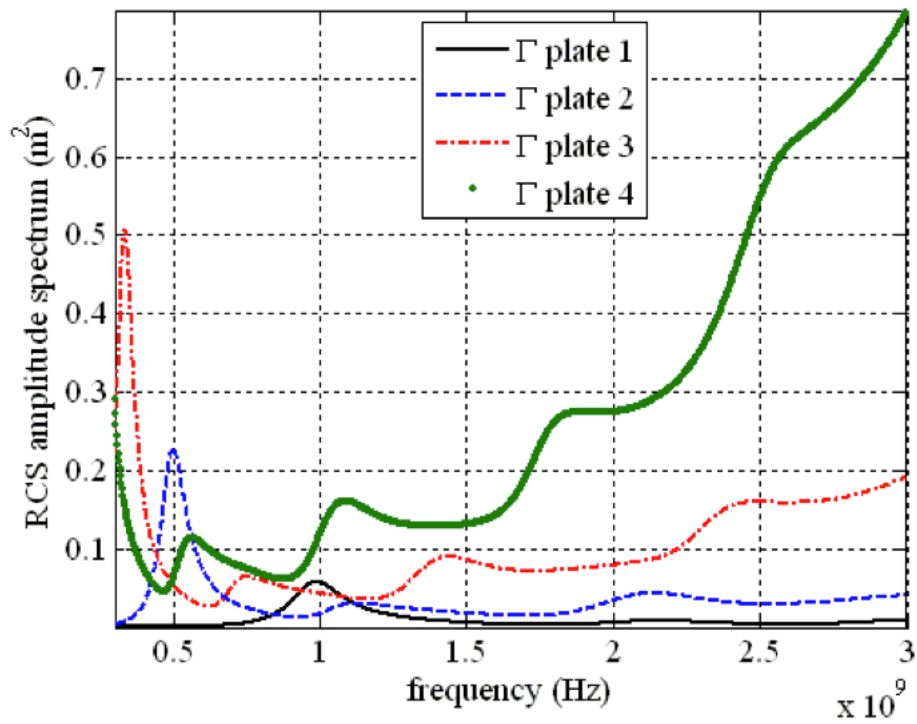


Figure A.3: T-plates co-polarisation RCS [18].

Appendix B

3-planes study of weapon RCS

[18] did RCS measurements looking at three planes of a handgun (Figure B.1). The handgun is said to be 16.6 cm long, 10.6 cm width and 4cm of thickness. The 3-planes study of the handgun is useful for us because guns and rifles can be approximated by I-plate and Γ -plate shapes (as detailed in *Appendix A. Weapons length impact on RCS*). The three planes are denoted by:

- P_1 : which corresponds to a side point of view (barrel and handle are seen). The E-field will be able to take two directions: either it will be oriented horizontally H in the handle direction or it will be vertically oriented V , corresponding to the barrel direction.
- P_2 : which corresponds to a top point of view (only the barrel is seen). The E-field will be able to take two directions: either it will be oriented horizontally H : orthogonal to the handle direction or it will be vertically oriented V , corresponding to the barrel direction.
- P_3 : which corresponds to a front point of view (only the handle is seen). The E-field will be able to take two directions: either it will be oriented vertically V in the handle direction or it will be horizontally oriented H , orthogonal to the barrel direction.

When we use the polarization notation we define for example $P_1 E_{HV}$ which corresponds to the antenna polarized in H for transmission and V for reception. Depending on the position where the antenna is placed compared to the weapon P_1 , P_2 or P_3 the wave orientation changes. The wave propagates in P_1 , P_2 or P_3 respectively in the orthogonal direction to handle and barrel plane, the handle direction and the barrel direction.

The results from P_1 to P_3 are given respectively in Table B.1 and B.2.

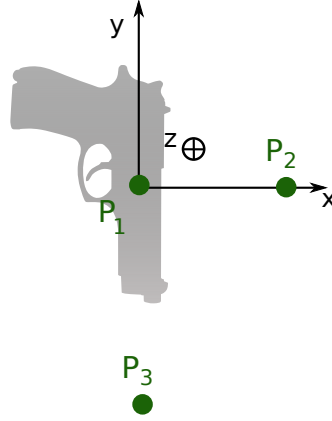


Figure B.1: 3-planes looking to find gun RCS

		RCS (m^2)			
		Polarization (E)			
		HH	HV	VH	VV
Place	P_1	0.025	0.025	0.025	0.12
	P_2	-	-	-	0.095
	P_3	-	-	-	0.025

Table B.1: 3-planes RCS values for a handgun at 700 MHz [18].

		RCS (m^2)			
		Polarization (E)			
		HH	HV	VH	VV
Place	P_1	0.24	0.0025	0	0.24
	P_2	-	-	-	0.025
	P_3	-	-	-	0.05

Table B.2: 3-planes RCS values for a handgun at 2.7 GHz [18].

Using the handgun measurements and *Appendix A. Weapons length impact on RCS* study we can estimate the RCS values of the AK-47 at 245 MHz and 2.7 GHz. (Respectively Table B.3 and Table B.4). We also based our estimations on the fact that the RCS is proportional to the projected area of the target for a fixed frequency (4.2). Concerning the AK-47 barrel viewed from the top, its projected area is 2.3 times the one of the handgun. From the side point of view (P_1), the AK-47 barrel area is at least 4 times bigger than the handgun one.

Concerning the handle and the cartridge clip viewed from the side (P_1), we will use a coefficient given by the ratio between the co-polarizations ($P_1 E_{VV}$) at P_1 of the two objects at 2.7 GHz. As the measurements give us these data the coefficient is

given to be $1.44/0.24 = 6$. For the front point of view we will consider them as the same for the worst case of the AK-47. The cross sectional part of the AK-47 is then 5.85 the one of the handgun from a side point of view and the same for the front one.

We are going to neglect the radial polarization because we do not have the data to have it and it should be insignificant compared to the others. The unknown values noted with a - in the table will be defined as $1e^{-6} m^2$, a largely low value to match reality.

		AK-47 RCS (m^2)			
		Polarization (E)			
		HH	HV	VH	VV
Place	P_1	0.146	-	0.146	1.15
	P_2	-	-	-	0.215
	P_3	-	-	-	0.025

Table B.3: 3-planes RCS estimation for the AK-47 at 245 MHz [18].

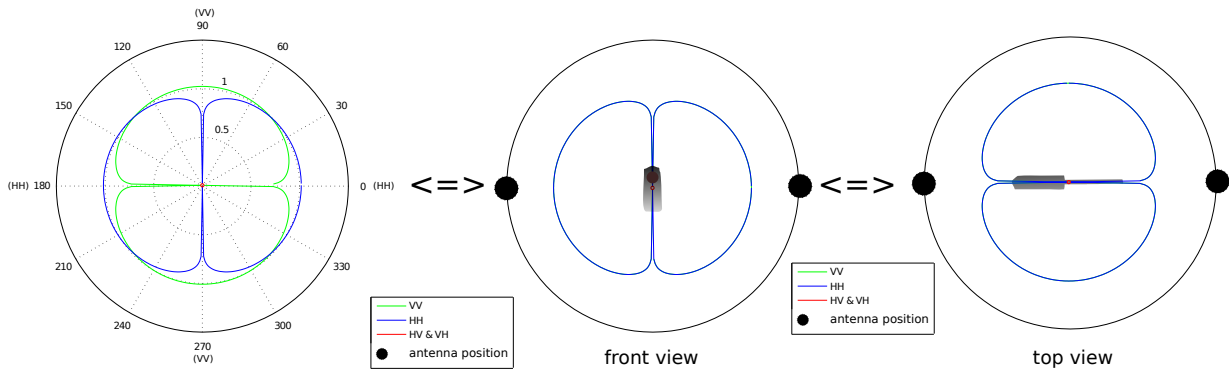
		AK-47 RCS (m^2)			
		Polarization (E)			
		HH	HV	VH	VV
Place	P_1	1.44	-	0.001	1.44
	P_2	-	-	-	0.056
	P_3	-	-	-	0.05

Table B.4: 3-planes RCS estimation for the AK-47 at 2.7 GHz [18].

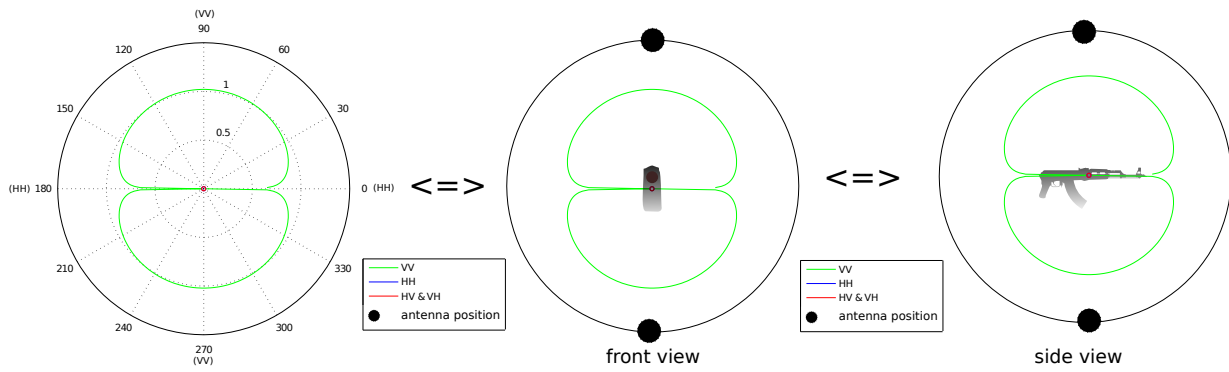
From these tables we are able to define the backscattering pattern of the weapons. To obtain them we will have to define a behavior of the RCS depending on the weapon orientation. When the weapon rotates of a certain angle from the perfect case of the experiment, there will be a polarization mismatch.

This is the reason why we have to defined a coefficient that will adapt the RCS. As we can interpret the shape of the weapon by cylinders, the backscattering pattern should look like a cylinder (or dipole) one. To construct such a pattern, we use a sine function. As weapons have not really a dipole shape, its pattern can not be exactly the same as the dipole's pattern with a null in the 0 direction. Therefore we are using the RCS data to fill the nulls of the sine function.

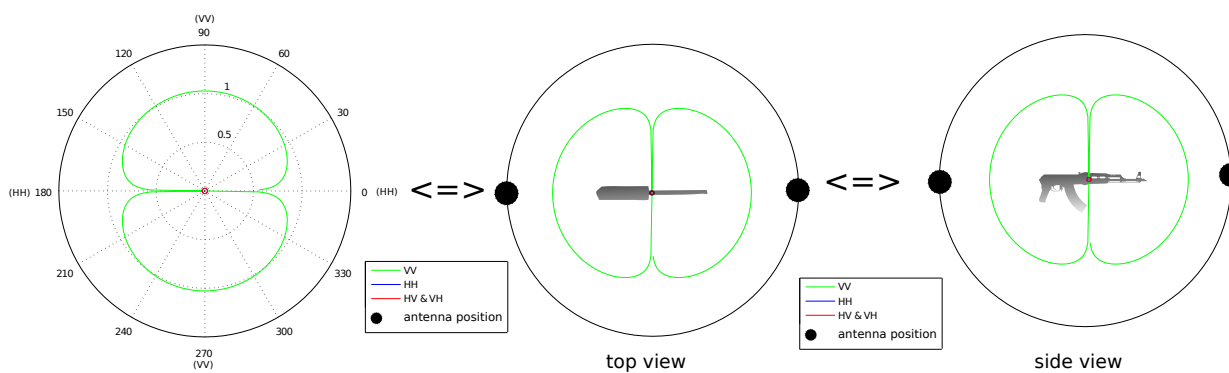
The normalized backscattering patterns in dBm^2 of the co-polarization (HH and VV) and the cross-polarization (VH and HV) are visible in Figure B.2.



P1: side illumination



P2: Top illumination



P3: Front illumination

Figure B.2: Normalized backscattering patterns of the weapon RCS for a co and cross polarizations in the three possible illumination.

Appendix C

Signal correlation

C.1 Correlation definition

In the following, we want to assess the signals correlation properties. We will work with normalized coefficients, showing how much from 0 to 1 the signal is correlated. The correlation coefficient will be denoted by r_{XY} . We can define several thresholds.

- $0.9 \leq r_{XY}$
In that case, we can say that the signals or compared distributions are highly correlated.
- $0.7 \leq r_{XY} \leq 0.9$
The two realizations are correlated.
- $0.3 \leq r_{XY} \leq 0.7$
The two realizations are neither correlated, nor completely uncorrelated nor independent.
- $r_{XY} \leq 0.3$
The two realizations are completely uncorrelated.

The correlation coefficient r_{XY} can be found with statistical tools. The expected value will be denoted $E[\cdot]$. First, the expectation of a realization will be given by (C.1).

$$\mu_X = E[X] \tag{C.1}$$

To compute r_{XY} , we also need the variance definition, which is given by equation (C.2)

$$\sigma_X^2 = E[(X - E[X])^2] = E[X^2] - E[X]^2 \tag{C.2}$$

Then, we can introduce the covariance coefficient C_{XY} , given by (C.3)

$$C_{XY} = E[XY] - E[X]E[Y] \tag{C.3}$$

One can notice that $C_{XX} = \sigma_X^2$. Finally, the correlation coefficient between X and Y distribution is given by (C.4)

$$r_{XY} = \frac{C_{XY}}{\sqrt{C_{XX}C_{YY}}} = \frac{E[XY] - E[X]E[Y]}{\sqrt{\sigma_X^2\sigma_Y^2}} \quad (\text{C.4})$$

For discrete processes, the mean μ_X and the variance σ_X^2 can be found with statistic estimators. The mean μ_X is given in equation (C.5)

$$\mu_X = E[X] = \frac{1}{n} \cdot \sum_{t=1}^n X(t) \quad (\text{C.5})$$

In the same way, σ_X^2 is given with equation (C.6).

$$\sigma_X^2 = \frac{1}{n-1} \cdot \sum_{t=1}^n (X(t) - \mu_X)^2 \quad (\text{C.6})$$

All along the correlation chapter, we placed receiving antennas every $\Delta_{IES} = 5 \text{ m}$. With a $D_a = 300 \text{ m}$ vessel, we have $N = 60$ antennas. Only one transmitter is taken for the computations.

C.2 Shadowing coefficients correlation (UL and DL)

This section will investigate the correlation between shadowing paths, i.e. how likely one antenna could see something that the other antenna does not see. This shadowing correlation we are investigating is the correlation between different shadowing paths for different emitting or receiving antennas when they illuminate or receive the same part of the sea. Figure C.1 shows that case.

The correlation between shadowing coefficients in the uplink process helps us to see how de-correlated will be signals between antennas, when we try to match the targets. From (C.4), we can find the correlation for uplink or downlink shadowing. We are mainly going to study the uplink case. $X(t)$ and $Y(t)$ are replaced by the shadowing coefficients $c_x(t)$ and $c_y(t)$ for antennas x and y . Then, the coefficient is associated to the distance between receivers d_{xy} . The correlation coefficient is given by (C.7)

$$r_{XY}^{\text{Shadowing}}(d_{xy}) = \frac{E[c_x c_y] - E[c_x]E[c_y]}{\sqrt{\sigma_{c_x}^2 \sigma_{c_y}^2}} = \frac{1}{\sqrt{\sigma_{c_x}^2 \sigma_{c_y}^2}} \cdot \left(\frac{\sum_{t=1}^n c_x(t)c_y(t)}{n} - \mu_{c_x}\mu_{c_y} \right) \quad (\text{C.7})$$

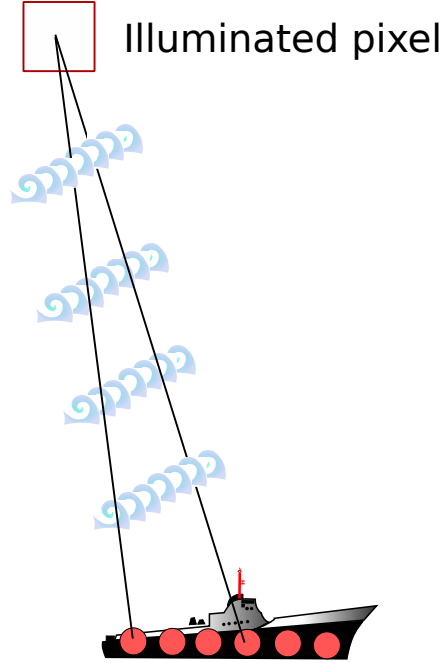


Figure C.1: Representation of angular correlation.

Where:

$r_{XY}^{Shadowing}$	Correlation between different shadowing paths
d_{xy}	Distance between antennas x and y [m]
n	Total number of cells for shadowing coefficient $c_x(t)$
c_x	Uplink (or downlink) shadowing coefficient, $c_{shadow m,n}^{UL}(t)$ with $n = x$ described in section 7.4.
μ_{c_x}	Mean of shadowing coefficient $c_x(t)$
$\sigma_{c_x}^2$	Variance of shadowing coefficient $c_x(t)$

Once again, we can find the mean μ_{c_x} and the variance $\sigma_{c_x}^2$ with non-biased estimators given in equations (C.5) and (C.6). The computation of this correlation in the uplink process gives the results displayed in figures C.2, C.3, C.4, and C.5.

The correlation sometimes follows a wave pattern, just like the sea-waves, depending on the chosen parameters. This effect can be really strong with specific parameters. We notice that higher is the sea state less correlated is the response. This is due to the fact the sea-waves do not follow a well defined wavefront when the sea-state gets higher (See figures 7.3 and 7.4 for illustration). An example is given with sea state 9 in figure C.5. As expected, the correlation is lower when the sea-state is higher. It means that there are more chances that one antenna *sees* something hidden by another antenna with a higher sea-state.

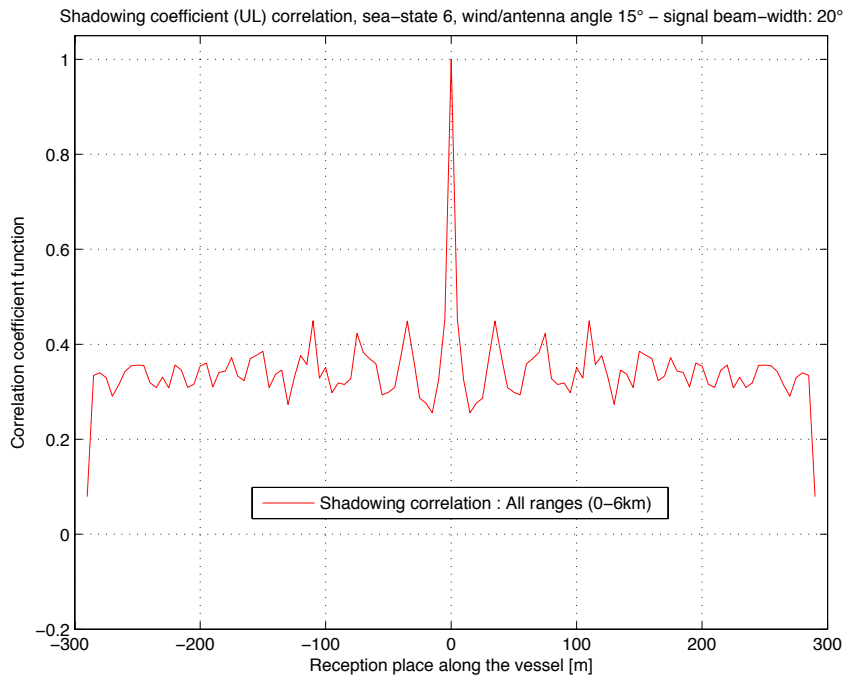


Figure C.2: Angular shadowing correlation. Sea state 6 - antenna/wind angle 15° - Beam-width : 20°

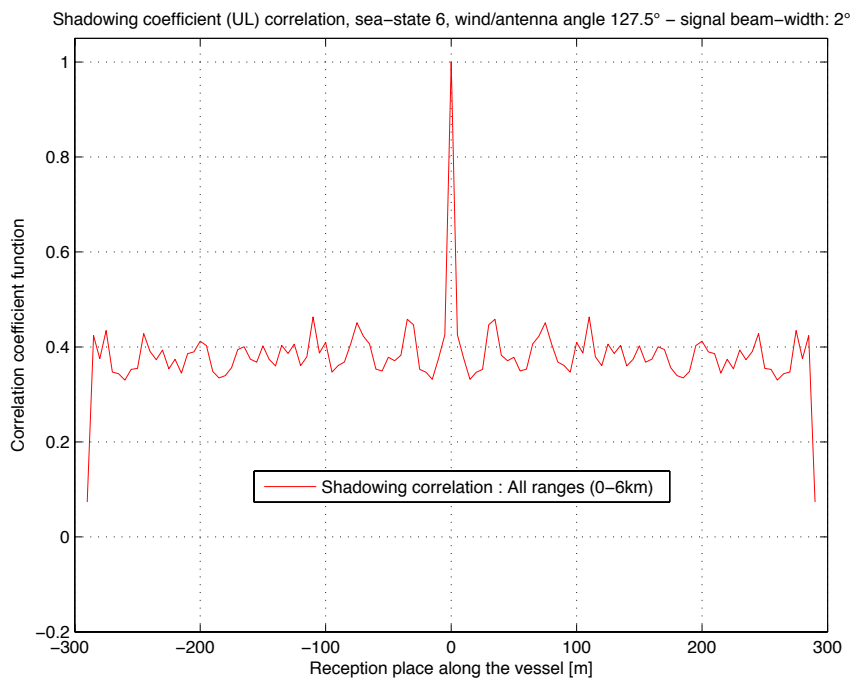


Figure C.5: Angular shadowing correlation. Sea state 6 - antenna/wind angle 127.5° - Beam-width : 2°

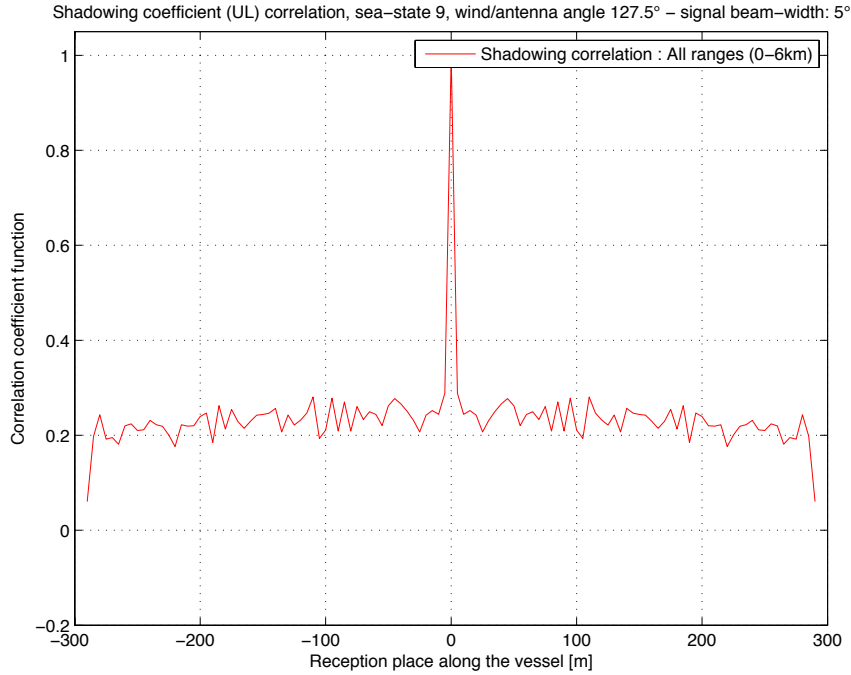


Figure C.3: Angular shadowing correlation. Sea state 9 - antenna/wind angle 127.5° - Beam-width : 5°

We can note that the shadowing process is symmetric in our simulation, (we assume the environment does not move during the wave travel, i.e. $c_{shadow|m,n}^{UL}(t)$ is calculated the same way as $c_{shadow|m,n}^{DL}(t)$). (See section 5.1.5)). For the correlation, the space shift in downlink will have the same effect as a shift along the vessel. This is due to the parallel sea-waves fronts. An illustration is given in figure C.6. In that figure, we see that the uplink and downlink shift will just create a mirror image around the sea-waves, which are parallels.

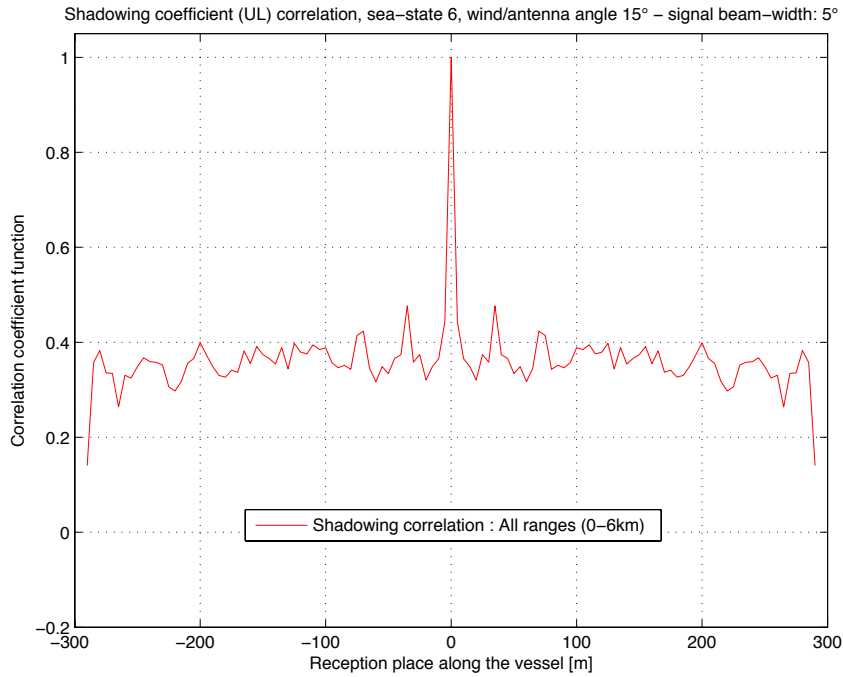


Figure C.4: Angular shadowing correlation. Sea state 6 - antenna/wind angle 15° - Beam-width : 5°

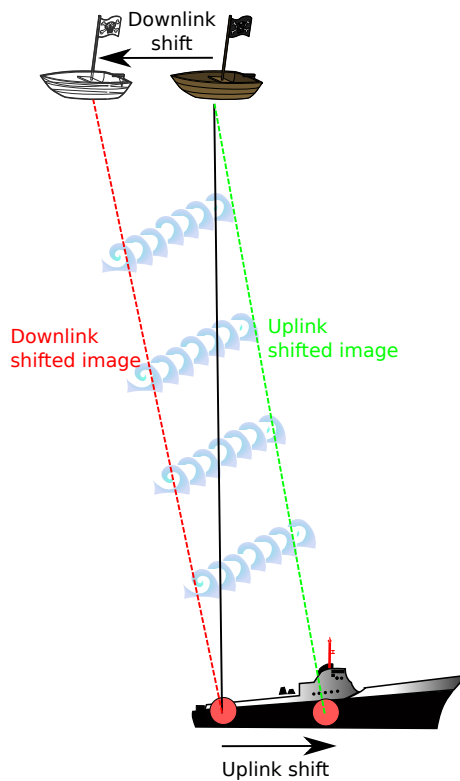


Figure C.6: Shadowing correlation for downlink and uplink case

Therefore, for given parameters, the shadowing correlation tends to be the same between uplink and downlink (C.8).

$$r_{XY}^{Shadowing}|_{Downlink} \approx r_{XY}^{Shadowing}|_{Uplink} \quad (C.8)$$

The case where the antenna illumination exactly follows the sea wave crests and peaks happens seldom, since the illumination beam and the waves have to be perfectly parallel. In that case, the wave effect on the correlation function is higher than the one with the perpendicular configuration.

The highest is the sea-state, the less correlated are the paths from the target to antennas on the vessel. We can see the presence of peaks on path correlation, certainly due to sea-wave front effect. With higher sea-state, the de-correlation tends to be stronger all along the vessel, the difference is visible between figure C.3 and C.4.

C.3 Tsallis distribution : Neighbors cells amplitude correlation (DL)

The neighbors cells amplitude is found with the Tsallis realization from one sea-pixel to another. The correlation between each cell should be present due to that differential Tsallis realization. We can compute the correlation between adjacent sea-clutter pixels from the estimated parameters q and β .

To illustrate this correlation property, we are going to compute the correlation coefficient of a Tsallis realization with some given parameters. The correlation coefficient given by (C.4) will be computed between the Tsallis realization $X(t) = A_R(t)$ and a shifted version of that realization $X(t+\tau) = A_R(t+\tau)$ to see how the realization is correlated few cells apart. The realizations $X(t)$ and $X(t+\tau)$ have the same mean μ_X and variance σ_X^2 . The correlation coefficient formula is then given by (C.9).

$$r_{XY}^{Tsallis}(\tau) = \frac{E[X(t)X(t+\tau)] - \mu_X^2}{\sigma_X^2} \quad (C.9)$$

We can study the correlation for that case, illustrated in figure C.7. In our case, we only consider the correlation between adjacent cells with the Tsallis distribution, and we ignore the shadowing effects. Therefore, we can calculate the Tsallis realization correlation coefficient with equation (C.10)

reflecting cells

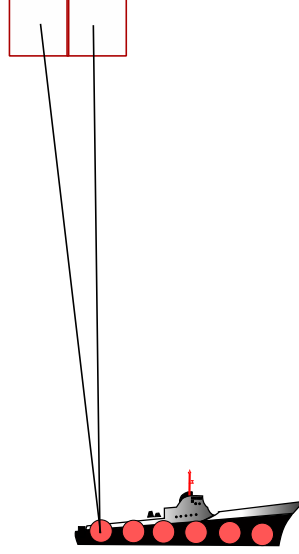


Figure C.7: Correlation response from adjacent cells.

$$r_{XY}^{Tsallis}(\tau) = \frac{1}{\sigma_X^2} \cdot \left(\frac{\sum_{t=1}^{n-\tau} A_R^{Tsallis}(t) A_R^{Tsallis}(t + \tau)}{n - \tau} - \mu_X^2 \right) \quad (C.10)$$

Where:

$A_R^{Tsallis}(\tau)$	Tsallis realization with τ representing the number of the cell.
τ	Number of cells apart from the first cell.
n	Total number of cells in the Tsallis realization.
μ_X	Tsallis realization mean value.
σ_X^2	Tsallis realization variance.

Figure C.8 shows the correlation coefficient function $r_{XY}^{Tsallis}(\tau)$ with (C.10) of a given Tsallis realization with sea state 6. The Tsallis correlation coefficient functions are all close to the others, even when using different sea states.

The correlation with another set of parameters (wind direction and speed, which basically modify the q and β parameters from the Tsallis distribution) have an overall similar shape. The sea amplitude response should not be highly correlated, especially with $5 \times 5 \text{ m}^2$ pixels.

In fig. C.8, we see that the correlation between two adjacent cells is good (≈ 0.75), but drops rapidly. After 5 sea-cells apart, i.e. 25m of sea clutter, the amplitude response is totally uncorrelated since the correlation is below 0.25. Therefore, we can conclude that the sea-clutter amplitude response is correlated from one cell to another, but not at all after several cells.

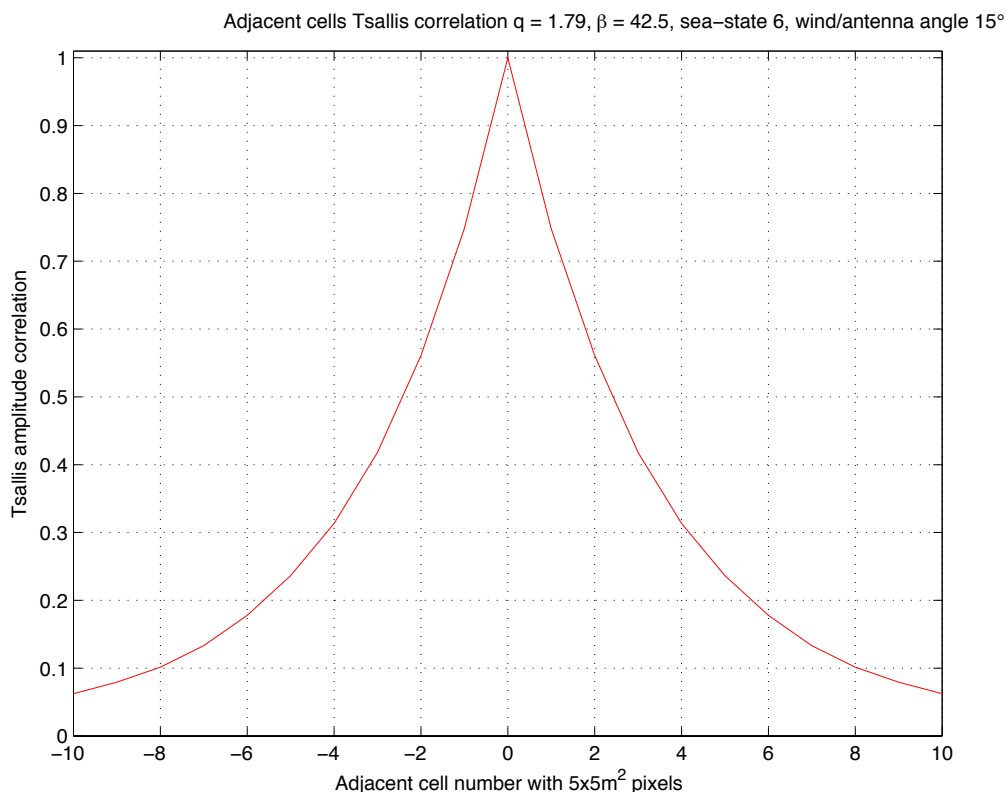


Figure C.8: Tsallis amplitude correlation coefficient of adjacent cells, with sea state 6 and antenna/wind angle 15°

We have to notice that the correlation would look the same, with any radar spatial resolution because q and β parameters do not depend on the spatial resolution in our implementation. From this statement, we know that the correlation would be the same every m^2 if the spatial resolution was $1 \times 1 m^2$ pixels. That correlation could also depend on the Tsallis distribution parameters, which themselves could change from a resolution to another.

C.4 Tsallis : Backscattered signal and pixel mismatch

We assumed that the sea reflection is isotropic, for each pixel in our simulation. We ignore the little contributions due to extra reflections/diffractions over the sea surface. Then, the addition of the pixels echo along the illuminated pixels give an angular spread of the signal contributions, analog to multiple scatterers scenario in mobile communication.

In classic mobile communication, Clarke's model applies over the correlation between antenna elements when the multiple placed sources follow an angular spread in a stationary situation. That situation happens often in mobile communication when there are several back-scatterers. This angular spread creates a doppler spectrum at the receiver side [40]. In our case, the angular spread is linked with the beam-width, transmitter and receiver positions. This angular spread is illustrated in fig. C.12. A plot of the doppler spectrum depending on the angular spread is given in figure C.9

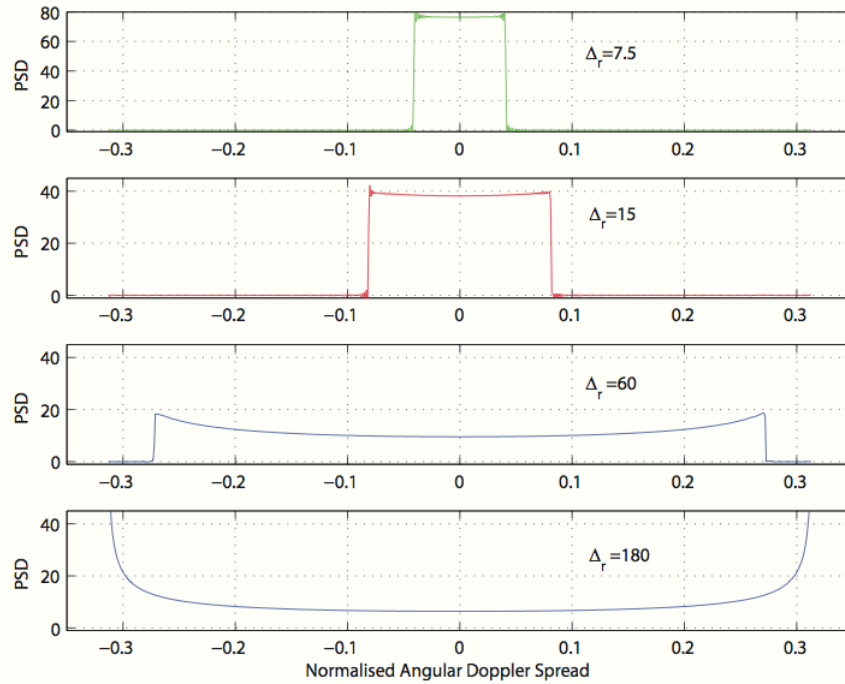


Figure C.9: Doppler shift for 7.5°, 15°, 60° and 180° angular spread from [40]

From that doppler spectrum, the signal correlation can be found with a Fourier Transform. The signal power correlation corresponding to the Doppler spectrum in fig. C.9 is shown in figure C.10

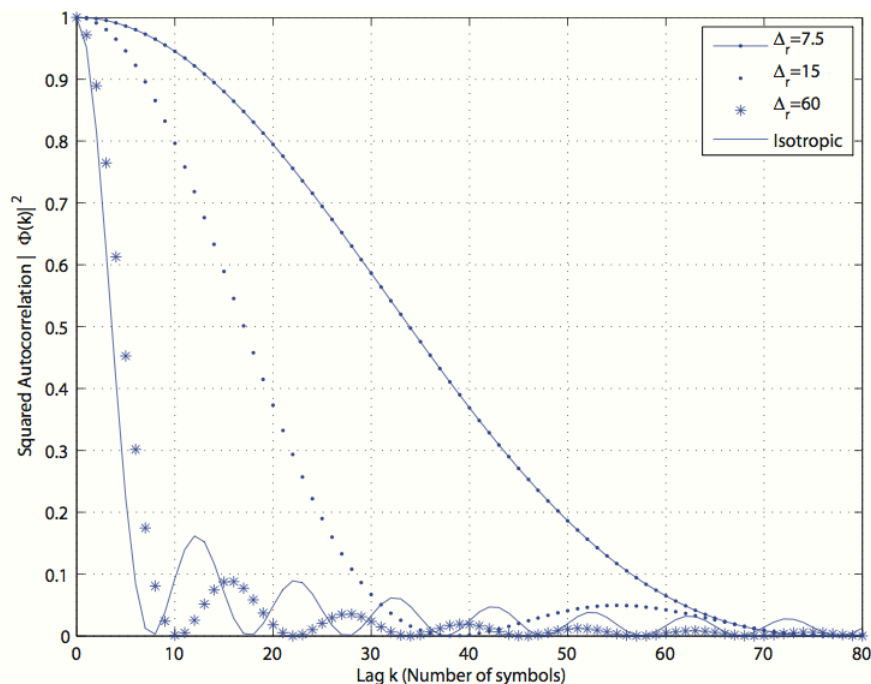


Figure C.10: Signal power correlation for 7.5°, 15°, 60° and 180° angular spread from [40]

However, in our implementation, the Clarke's model hardly ever applies. Indeed, we can introduce a pixel mismatch (detailed later in the section, in particular with fig. C.13) in the backscattering zone, which is due to the radar properties (different illuminated zones depending on the delay and transmitter/receiver) and also due to the Near-field aspect. This effect would not happen if the radar was working in the far-field. The Tsallis backscattered signal correlation is computed in order to show this de-correlation due to the pixel mismatch. There is also an impact due to the sea-pixels size. Depending on the size and shared part of the illuminated areas, the correlation could be either high or low between antennas. The beam-width, range and the bandwidth will also influence the results since they define how many pixels are illuminated. We have first defined 3 different cases:

- Short range :
It will be all range under 400 m from the vessel. For that range, 1 to 6 pixels are illuminated with a 10° beam-width. With a comparable range to the vessel size (300 m), we can guess that the correlation will be sensitive to antenna displacement.
- Middle range :
This range is in between the short and long ones. It is picked up to show the transition between the large range and the short one. This middle range will be 1500 m , approximately 5 times the vessel length.

- Long range :

After 5 – 6 km, the vessel tends to look like a point from the target, even though antennas can be placed up to 300 m apart. One can note that we are still in the near-field. Nevertheless, the correlation would be less sensitive to the antenna displacement. The correlation between 5 m apart antennas is then higher.

For a specific focal distance, a specific size of the area is illuminated by the radar depending on the beam-width. To get an idea of it, the illuminated surfaces are computed and summarized in table C.1. This table shows the number of pixels and the surface in m^2 , but it does not tell the shape, which follows either a circle or an ellipse and which is most of the time no more than 1 pixel thick.

Examples of illuminated areas are given in figure C.11 and C.12. The shared illuminated pixels depend on the range illumination, the beam-width. The bigger is the shared surface, the best would be the correlation. The pixel-mismatch is illustrated in figure C.13

		Illuminated surface [pixels(m^2)]			
		Beam width (°)			
		2°	10°	45°	90°
Range (m)	200	1 (25)	6 (150)	29 (725)	58 (1450)
	400	3 (75)	13 (325)	62 (1550)	124 (3100)
	1000	7 (175)	34 (850)	155 (3875)	310 (7750)
	4000	28 (700)	138 (3450)	636 (15900)	1272 (31800)
	6000	42 (1050)	208 (5200)	713 (17825)	1426 (35650)

Table C.1: Surface of $5 \times 5 m^2$ pixels illuminated depending on the range and beam-width.

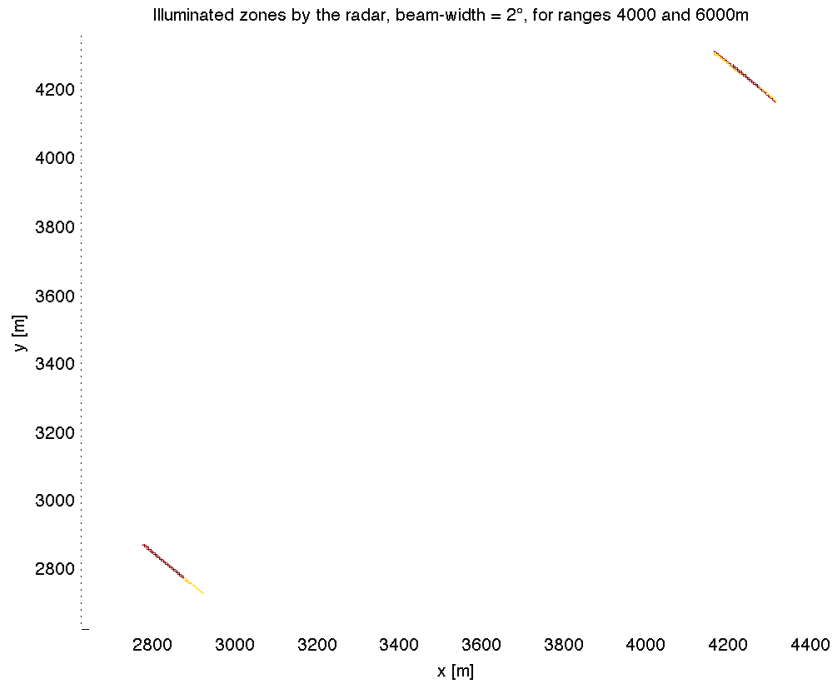


Figure C.11: Illuminated areas by transmitters 1 (brown) and 2 (yellow) (300 m apart) for ranges 4000 m and 6000 m - Beam-width : 2°

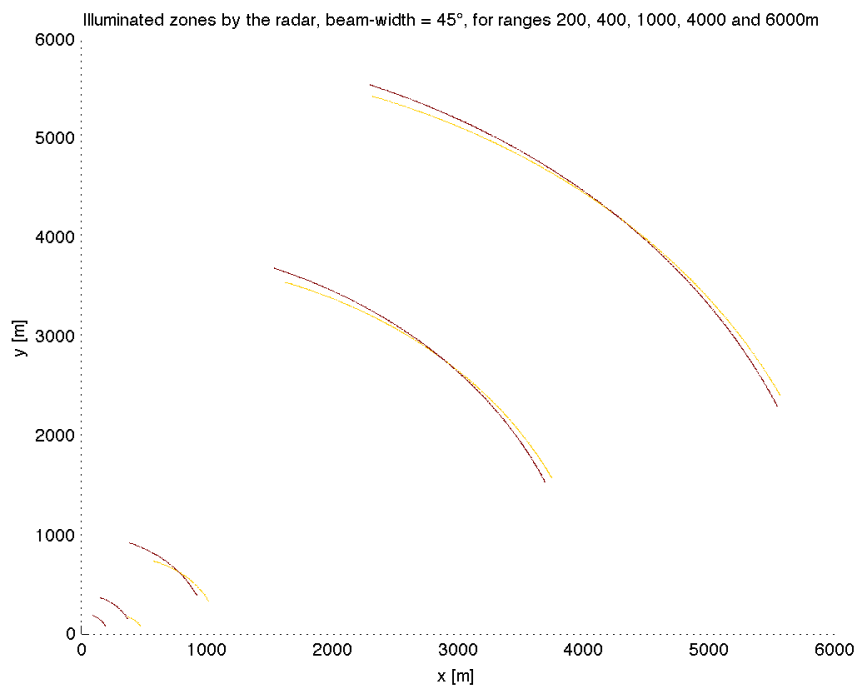


Figure C.12: Illuminated areas by transmitters 1 (brown) and 2 (yellow) (300 m apart) for ranges 200 m, 400 m, 1000 m, 4000 m and 6000 m - Beam-width : 45°

In our implementation, the sea has been discretized into 25 m^2 pixels. It is the same value with the radar spatial resolution. However, there is no link between those resolutions. The sea-pixel resolution is chosen the smallest as possible keeping at the same time a reasonable script execution time. The illumination for a 2° beam-width at 200 m range is only one pixel. This is an approximation and if the sea-grid was composed of 1 m^2 pixels, there would be several pixels inside that illuminated area. From pixel to pixel, the Tsallis correlation would stretch to get wider and keep the same shape as shown in section C.3. We can therefore say that these correlation coefficients are approximated due to the implementation limits. To fight this effect, a smaller sea-grid than the radar resolution could be picked up.

However, that pixel mismatch phenomenon would also happen in real-life since the illuminated zone and therefore the sea-source would not be the same, even if the resolution tends to be infinitely small. With a wide beam, this approximation becomes less important because of the higher number of illuminated pixels.

In figure C.13, the example of 3 illuminated pixels in a short range and their mismatch is shown. Antenna 1 will receive the backscattered signal from the 3 red pixels, whilst antenna 2 will receive the backscattered amplitude of the 3 blue pixels. According to fig. C.8, the correlation of adjacent pixels is approximately 0.75. Then, we can deduce that the backscattered signal for antenna 1 and 2 will be around 0.92 if each pixel has an equal contribution.

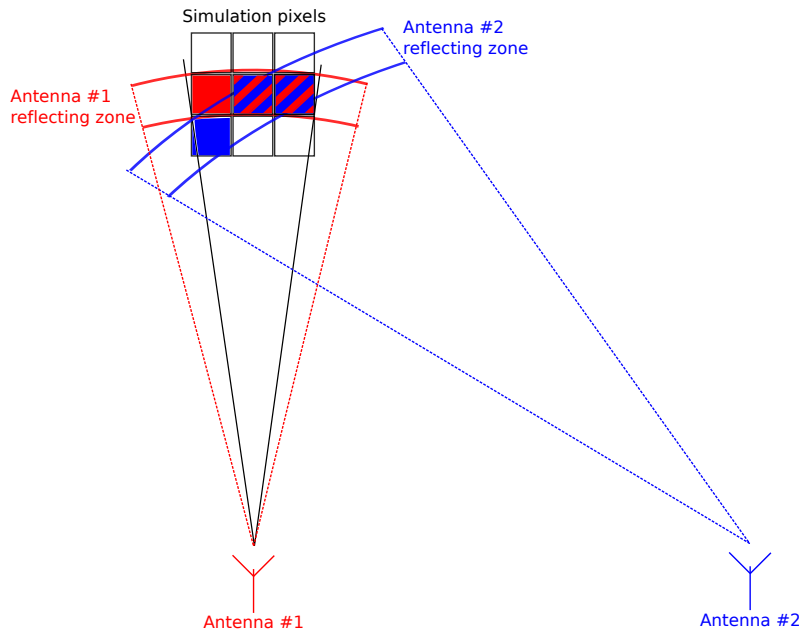


Figure C.13: Pixel mismatch illustration between receivers 1 and 2 for 3 pixels illuminated (short range and narrow beam-width case)

In this section, we want to calculate the correlation between backscattered signals for different receivers. Then, we will know that the classic mobile scenario will be scaled down by a de-correlation due to the pixel-mismatch and Tsallis de-correlation

between pixels.

It is straightforward that higher is the pixel mismatch, lower will be the correlation. By intuition, we can also guess the higher is the beam-width, the less correlated will be the signals between antennas, because the shared part of the illuminated area will be decreased, as shown in figures C.11 and C.12 for 300 m apart antennas. In the same way, smaller is the operating range and more correlated will be backscattered amplitudes, because that pixel mismatch will be less important.

In that section, we therefore compute the total Tsallis backscattered signal amplitude correlation for a given time delay, which represents the Tsallis amplitude response of the sea-clutter for a given receiving antenna and fixed emitting antenna. This correlation tells how correlated are the backscattered signals from the sea for a matched time delay.

The Tsallis correlation results are given in figures C.14, C.15, C.16 and C.17. One can note the presence of peaks in the correlation coefficient functions. This is mainly due to the two following factors:

- Pixel discretized system. Transitions are rough since we "jump" from one pixel to another, sometimes including and excluding new pixels at the same time, which leads to peaks in the computations. A higher sea-grid definition would allow smoother transitions.
- Few samples to work with for statistics: 65, 220 and 200 samples for respectively short, middle and long range. This makes the results sometimes unstable, especially for the short range.

In fig. C.17, we can see the simulation where only few pixels are illuminated (3), the correlation is high in average (≈ 0.9) for the short range placed within 100 m around the reference antenna. This 0.9 value has been previously explained and is the value for 2 pixels in common over 3 and 1 adjacent pixel to the other antenna.

An artifact appears when only 1 pixel is illuminated, i.e. the correlation is then always 1 all along the vessel. When the beam gets wider, the correlation drops (the difference is visible between fig. C.14 and C.15). Even for the short range, the correlation in the Tsallis backscattered signal drops fast when the beam-width is 20° . It is the main result of our simulations, the wider the beam, the less correlated are the backscattered amplitudes from the sea-clutter. The sea-state plays a role in the Tsallis q and β parameters and therefore has a little impact on the correlation coefficient, which is basically a higher standard deviation in the correlation coefficients, as we can see between figures C.15 and C.16 (More peaks when the sea-state is higher).

These values will have an effect on the overall signal. In the main process, the Tsallis amplitude and signal amplitude are multiplied. Then, it makes their PDF convolved. The correlation of backscattered signals at the antennas is multiplied with these correlation coefficients because the PDF are convolved. It will scale down the

maximum correlation properties, e.g. if Tsallis backscattered signals are less correlated than 0.5, then the overall received signals will be less correlated than this 0.5 value (because correlation values are never higher than 1). For example, the long range correlation with a 20° beam-width plotted in fig. C.14 is limited by 0.4 value. Therefore, in the final correlation plotted in section C.5 will not be better than 0.4.

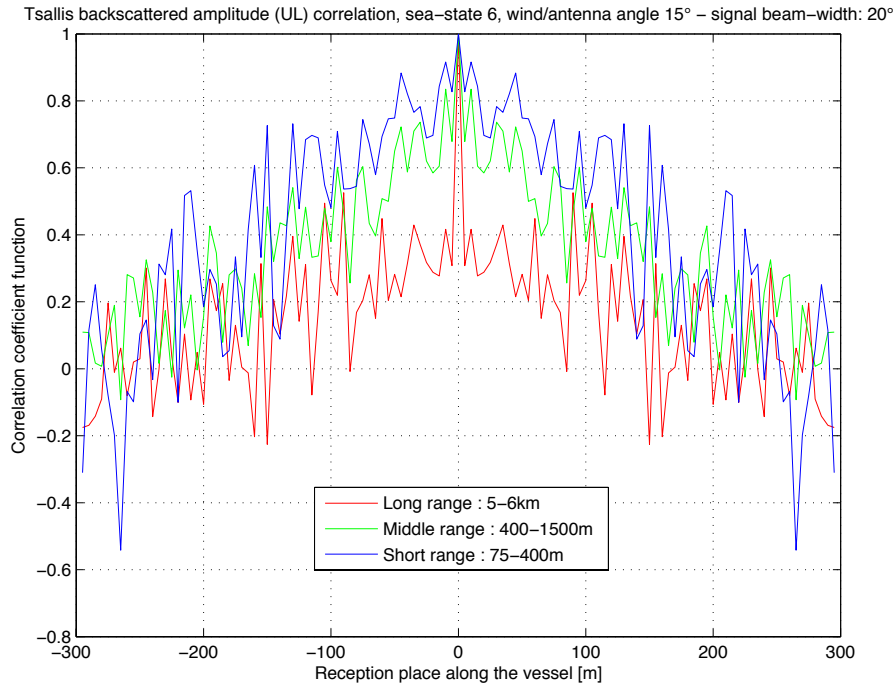


Figure C.14: Tsallis correlation in uplink. Sea state 6 - antenna/wind angle 15° - Beam-width : 20°

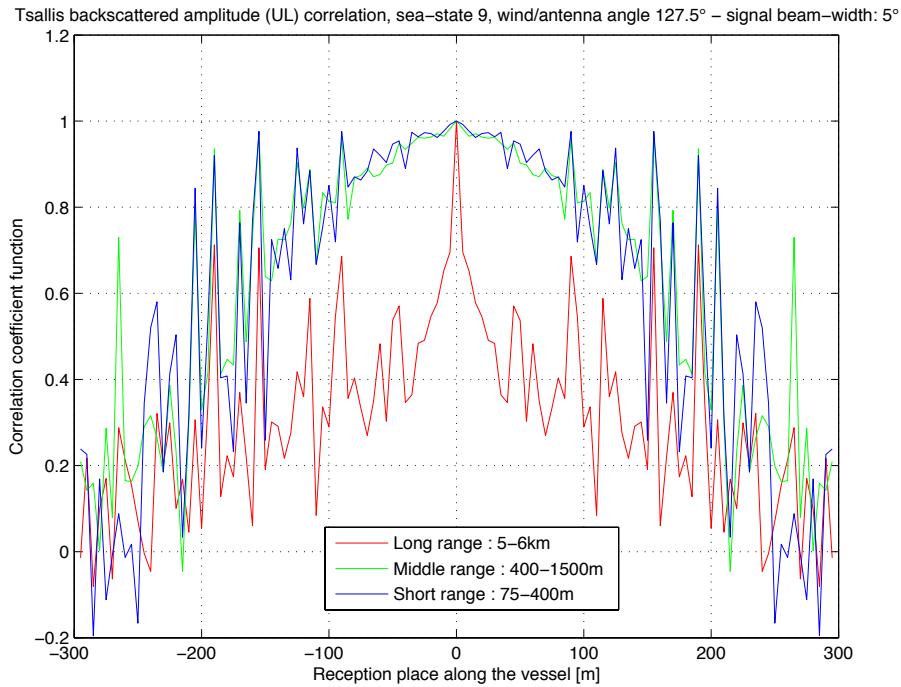


Figure C.15: Tsallis correlation in uplink. Sea state 9 - antenna/wind angle 127.5° - Beam-width : 5°

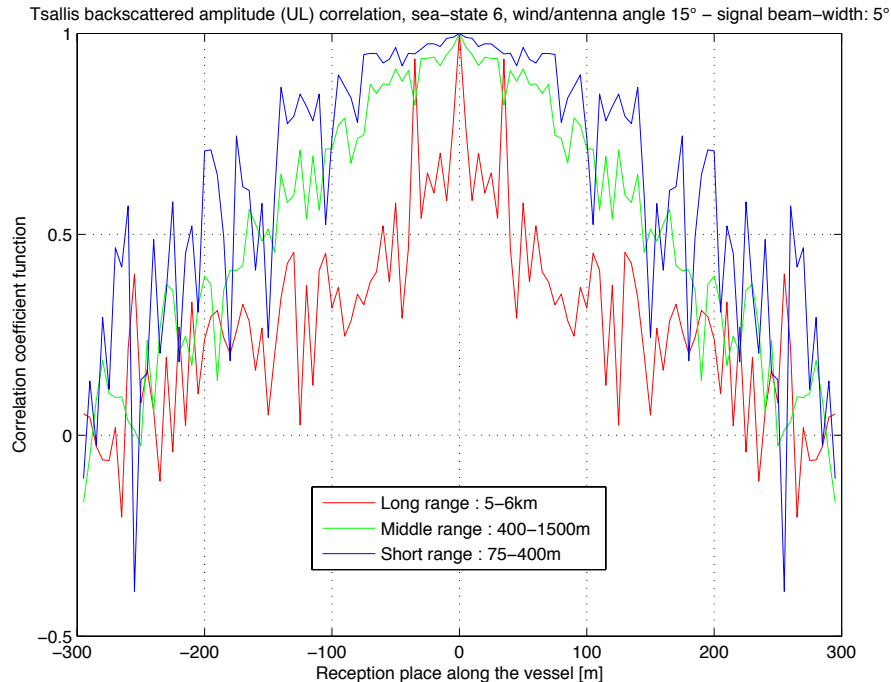


Figure C.16: Tsallis correlation in uplink. Sea state 6 - antenna/wind angle 15° - Beam-width : 5°

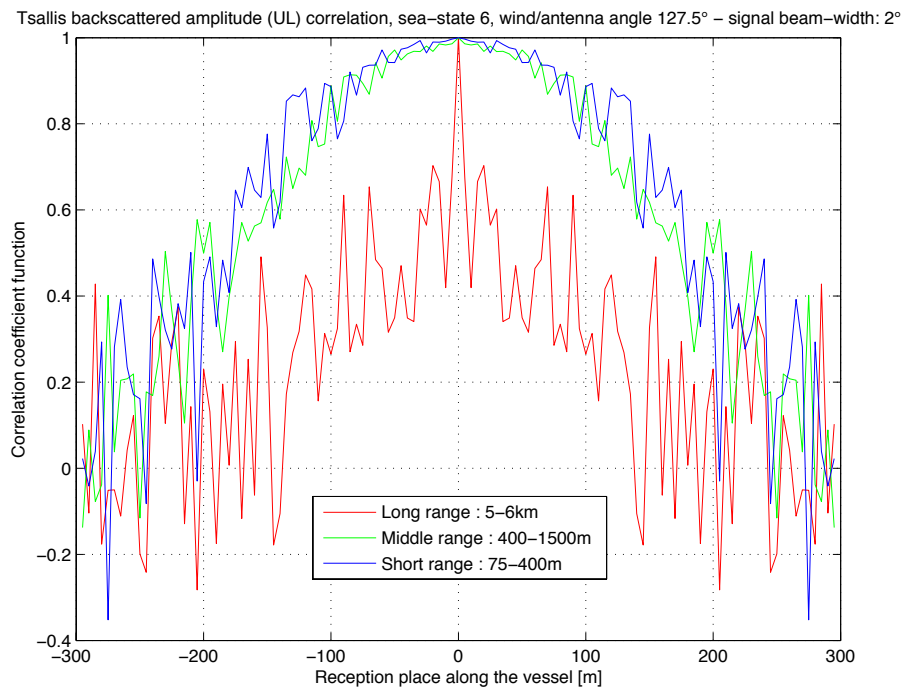


Figure C.17: Tsallis correlation in uplink. Sea state 6 - antenna/wind angle 127.5° - Beam-width : 2°

C.5 Overall signal amplitude correlation along the vessel (UL)

The most interesting result is the overall signal envelope correlation. It will be calculated with equation C.11, replacing $X(t)$ by the signal amplitude $A_x(t)$.

$$r_{XY}^{Amplitude}(d_{xy}) = \frac{E[A_x A_y] - E[A_x] E[A_y]}{\sqrt{\sigma_{A_x}^2 \sigma_{A_y}^2}} = \frac{1}{\sqrt{\sigma_{A_x}^2 \sigma_{A_y}^2}} \cdot \left(\frac{\sum_{t=1}^n A_x(t) A_y(t)}{n} - \mu_{A_x} \mu_{A_y} \right) \quad (C.11)$$

Where:

$r_{XY}^{Amplitude}$	Correlation between signal amplitude at different receivers.
d_{xy}	Distance between antennas x and y [m]
n	Total number of samples in $A_x(t)$
A_x	Signal amplitude for antenna x at the receiver side.
μ_{A_x}	Mean of $A_x(t)$
$\sigma_{A_x}^2$	Variance of $A_x(t)$

According to works made on usual wireless communication transmissions, we know that a single source signal correlation across an antenna array should also follow a Bessel function shape [41], even with no angular spread (see fig. C.18). This perfect case happens only if the same illuminated area reflects the signal (No pixel mismatch). In the biased case of only one pixel illuminated zone (See table C.1), a J_m Bessel function should appear since the source is a single pixel. In the case of several pixels, there is a implied de-correlation included in the reflecting area since the sources are multiple (Tsallis de-correlation between sources seen in section C.4) and the illuminated area is not the same.

Then, we can deduce that when illuminated pixels are few, the correlation will get closer to the a Bessel function shape. Else, de-correlation effect will scale down the function and kill the Bessel shape of the antenna array and also of the possible angular spread.

According to [41] and [40], the Bessel function flattens when the moving target angle gets low. See figure C.18. In our case, with the equivalent system as [41], the angles Δ_i would respectively be $\Delta_i = [0.36^\circ, 0.09^\circ, 0.02^\circ]$ for short, middle and long ranges defined in section C.4. Compared to figure C.18, in our case, $D/\lambda = 45 m$ because we operate at $f_c = 2.7 GHz$ in our simulation. Therefore, we can guess that with those really low angles, the Bessel function will not be visible, unless the correlation is computed for really close range. To get $\Delta_i = 3^\circ$, we have to operate at a $52 m$ range, which is close. For the short range correlation, the Bessel function appears since we take signals from 75 to 400 m for the computation. Else, for middle

and long ranges, the correlation function will tend to be extremely flat, with no visible Bessel function. To sum up, we are either in one of these cases:

- Short range:
Only few pixels are illuminated. In that case, the pixel mismatch is poor and the correlation is high between the backscattered signals from the illuminated areas. This low number of pixels includes a small angular spread (in most cases no more than 2°) and therefore a flattened correlation.
- Long range:
In that case, the angular spread starts to be important for large beam-width, but the pixel mismatch also gets important (illustrated in fig. C.12). The de-correlation between adjacent pixels is quite important, as shown in fig. C.8. In this case, the Bessel function should appear but it is actually hidden by a de-correlation due to the high pixel-mismatch.

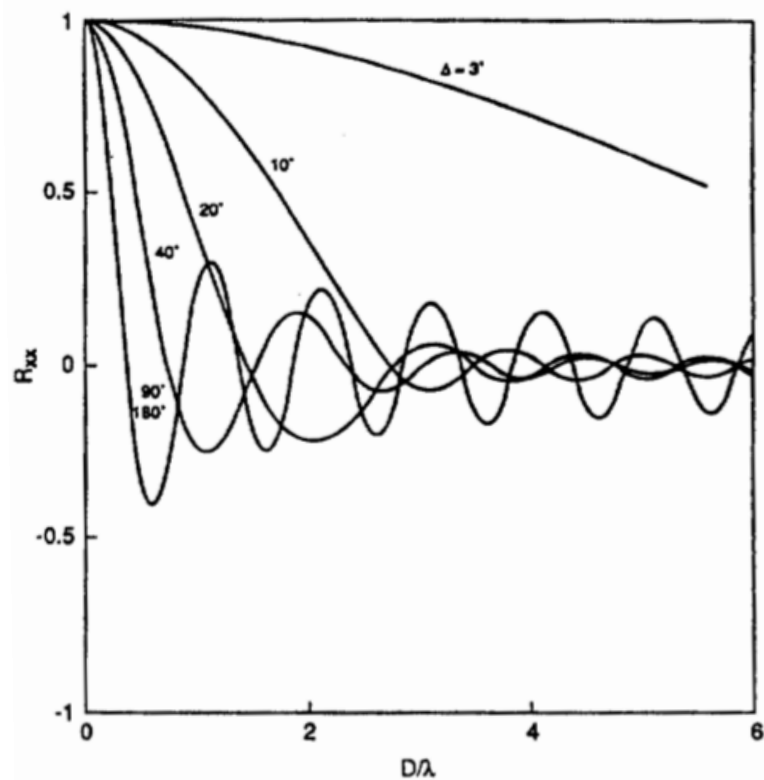


Figure C.18: Signal power correlation of a single source (MS) versus the place on the antenna array from mobile communication system. [41]

Overall signal correlation is given in figures C.19, C.20, C.21 and C.22. One can note that there are many peaks in the correlation coefficient functions, due to the

same causes as mentioned in section C.4, i.e. sea-grid discretization and few pixels to work with statistics.

In those plots, the 3 scenarios are present, the short range signal (75 to 400 m) in blue color, the middle range (400 to 1500 m) and the long range (5 to 6 km) in red color. For small range, one can notice that the pseudo-period of the correlation function is approximately $6 \times D/\lambda = 270 m$. Between figures C.19 and C.20, we can see that the large beam-width enhances the high de-correlation between signal, as seen for the Tsallis UL correlation (section C.4). On the other hand, the correlation is better with a narrower beam-width (2°) on fig. C.22 compared to fig. C.21 for the short range.

The middle range behavior is visible in fig. C.21, where the Tsallis UL de-correlation is not high and the angle Δ_i is low enough to behave like in fig. C.18 for the smallest Δ_i . For long range, the Δ_i angle is so small that the correlation is always the same, and scaled down by the Tsallis UL de-correlation. Figures C.20 and C.21 long range correlation are de-correlated by figures C.15 and C.16, which explain why the average correlation value is around 0.4.

In fig. C.21, the long range correlation is strongly affected by the correlation of the Tsallis backscattered signal shown in fig. C.16. The shape of the long range correlation is the same. This means that the correlation for close elements would tend to behave like the short range correlation, but the pixel-mismatch scales down this value.

High sea-state tends to reduce the correlation and to flatten its shape (see fig.C.20). Among all simulations we ran, the antenna/wind angle had no specific impact on the correlation values.

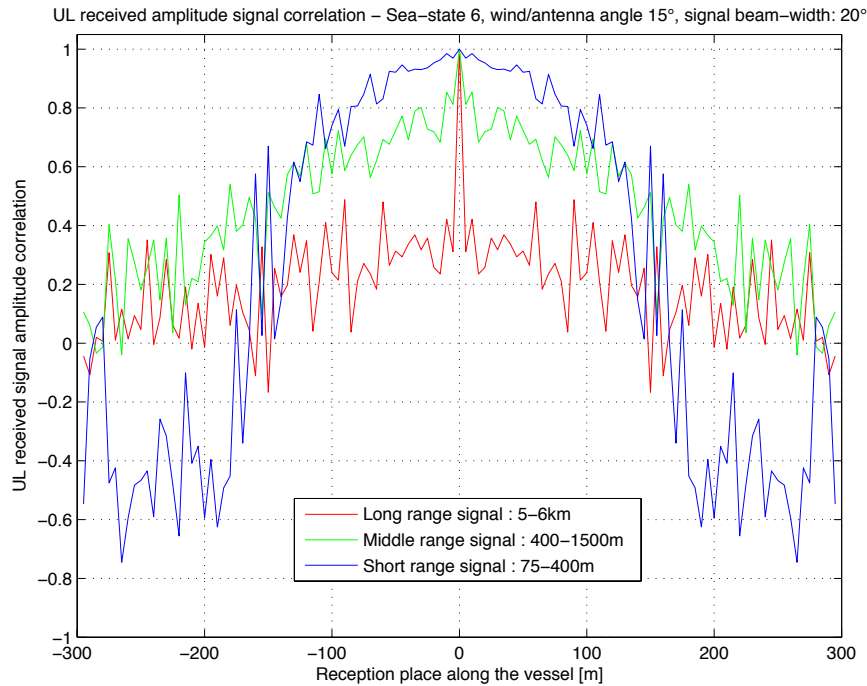


Figure C.19: Signal correlation along the vessel for short and long range echo. Sea state 6 - antenna/wind angle 15° - Beam-width : 20°

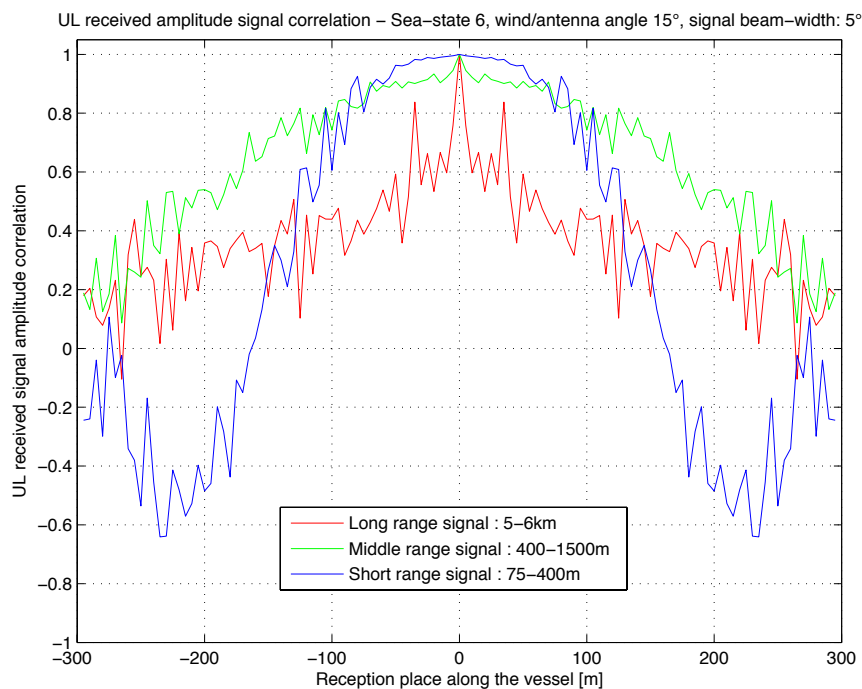


Figure C.21: Signal correlation along the vessel for short and long range echo. Sea state 6 - antenna/wind angle 15° - Beam-width : 5°

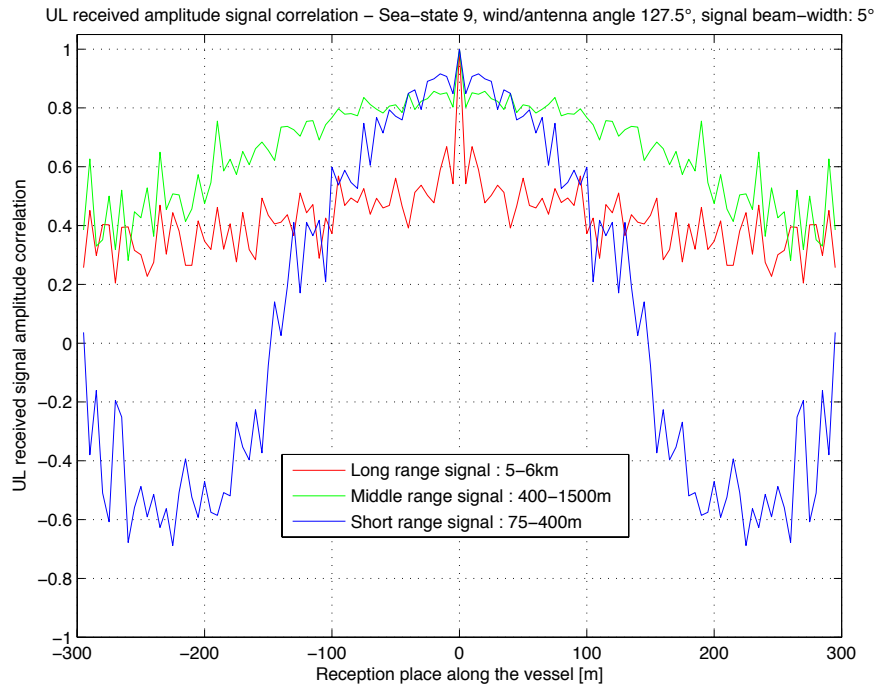


Figure C.20: Signal correlation along the vessel for short and long range echo. Sea state 9 - antenna/wind angle 127.5° - Beam-width : 5°

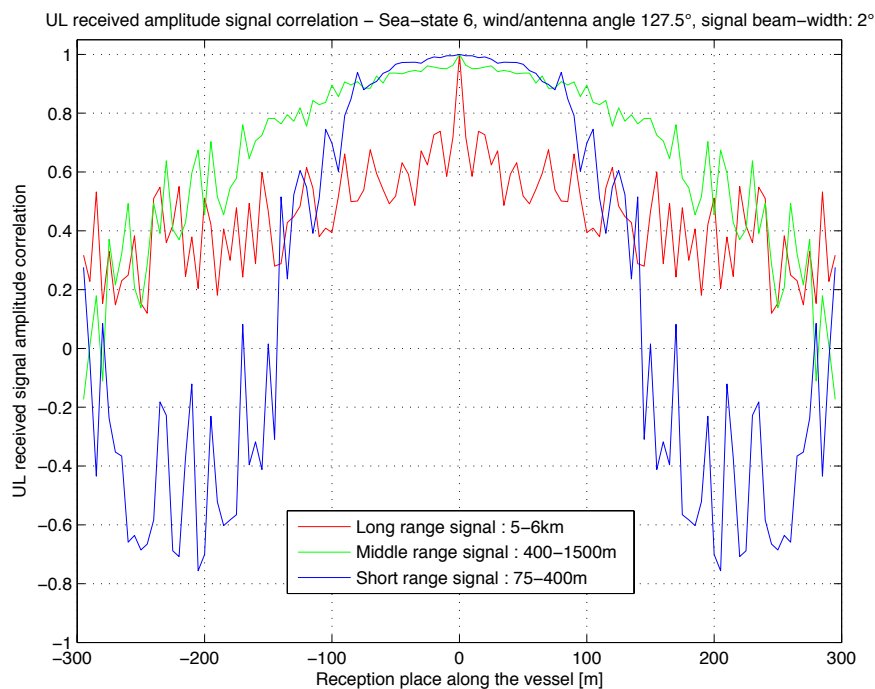


Figure C.22: Signal correlation along the vessel for short and long range echo. Sea state 6 - antenna/wind angle 127.5° - Beam-width : 2°

C.6 Correlation conclusion and discussions

From that study, we have seen that wider is the beam, less correlated is the received signal at each antenna. For narrow beams, there should be a bit of de-correlation but it is not visible due to the simulation limits and especially the pixel size.

The shadowing correlation is the same in any part of the boat, which means that the chances to see something hidden by a wave at a transmitter are the same whatever the position on the boat. This shadowing coefficient drops when the sea-state is higher, which means there is more chance to see around the sea-waves from different transmitters.

Appendix D

Singular Value Decomposition technique

D.1 Definition

In the MIMO radar case, we are going to use the received matrix $S_{m,n}(t)$ the same way as in wireless communications. $S_{m,n}(t)$ will be considered as $m \times n$ impulse responses from the sea-clutter. Therefore, the received signal can be interpreted as: $S_{m,n} = Hs + n$ where H is the channels gain, s the signal and n the additive noise. To achieve the best performance out of MIMO system, water-filling principle is applied using weights on antennas. These weights are found from the Singular Value Decomposition (SVD) of the H or in our case, $S_{m,n}$ matrix.

We can first compute the Singular Value Decomposition (SVD) of the received matrix, which is given in equation (D.1)

$$S_{m,n}(t) = U \cdot \Sigma \cdot V^* \quad (\text{D.1})$$

Where:

U	$m \times m$ Unitary matrix: Left singular values of S
Σ	$m \times n$ Diagonal matrix: eigen-values of S
V^*	$n \times n$ Unitary matrix, conjugate transpose of V : Right singular values of S

Classical MIMO systems use (D.1) for precoding at the transmitters [42]. Before to send the signal if we multiply it by V then at the receiver side the signal will be given by:

$$S_{m,n} = HVs + n \quad (\text{D.2})$$

Multiplying S by U^H we obtain:

$$\begin{aligned} U^H S &= U^H HVs + U^H n \\ &= U^H U \Sigma V^H V s + U^H n \\ &= \Sigma s + U^H n \end{aligned} \quad (\text{D.3})$$

The transmission represented by equation (D.3) is illustrated with Figure D.1. As the matrix Σ represents the MIMO processing gain, it is then obvious that this precoding scheme permits to increase the signal level compared to the noise level which is the sea one in our case.

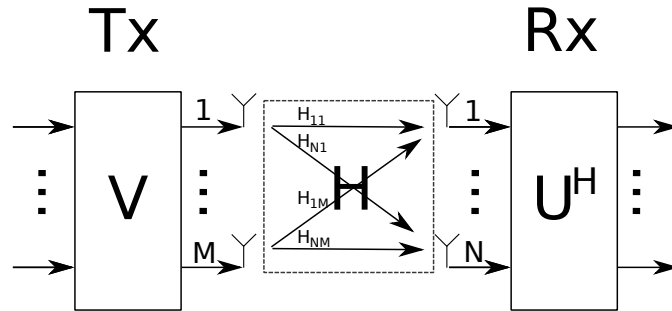


Figure D.1: Transmission using SVD of the channel

D.2 SVD interpretation

The SVD permits to obtain three matrices that define this operator. \mathbf{U} and \mathbf{V} are respectively the singular vectors of $\mathbf{S}\mathbf{S}^*$ and $\mathbf{S}^*\mathbf{S}$. They represent the rotational part of the operator \mathbf{S} . Σ is composed of the singular values of both $\mathbf{S}\mathbf{S}^*$ and $\mathbf{S}^*\mathbf{S}$ which define the amplitude of the variation of the two vectors that qualify \mathbf{S} , one for each vector. The SVD operator illustration is visible in Figure D.2

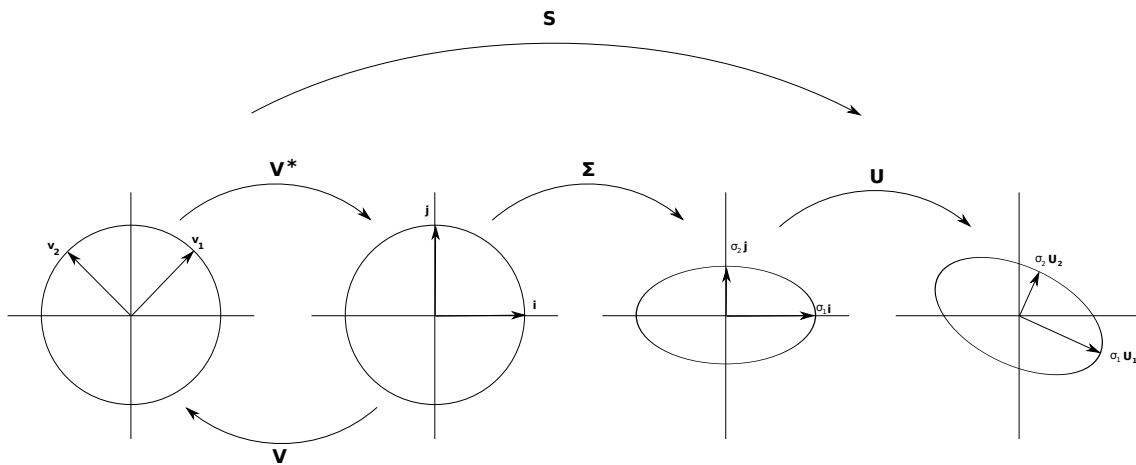


Figure D.2: SVD operator illustration on a simple circle

D.3 2×2 MIMO system

We first define a $M = 2$ transmitters and $N = 2$ receivers case. We finally have a 2×2 system. MIMO system diversity and de-correlation (see section C.3) increase the detection probability without impacting the false detection probability. Then, we can play on several aspects of the diversity which mainly are space and polarization.

Considering the SVD interpretation in the 2×2 MIMO system, we can take the case where:

$$\mathbf{S}_{m,n}(t = \tau) = \begin{pmatrix} 0.0717 + 0.0000i & -0.6846 + 0.2044i \\ 0.4659 + 0.2844i & 13.9092 - 0.0000i \end{pmatrix}$$

From the SVD we obtain:

$$\mathbf{\Sigma}_{m,n}(t = \tau) = \begin{pmatrix} 14 & 0 \\ 0 & 0.1 \end{pmatrix}$$

It means that one of the two vectors gives a higher echo and leads to more power received, here 140 times more power is received using the weights corresponding to the first element of $\mathbf{\Sigma}$ than using the second. Therefore $\mathbf{\Sigma}$ represents the repartition of the power of the echo for different rotations of the operator. The rotation is given in U and V which are in this case equal to

$$\mathbf{U}_{m,n}^H(t = \tau) = \begin{pmatrix} 0.0493 + 0.0132i & 0.9961 + 0.0721i \\ -0.8515 - 0.5219i & 0.0477 + 0.0180i \end{pmatrix}$$

$$\mathbf{V}_{m,n}(t = \tau) = \begin{pmatrix} -0.0389 & 0.9992 \\ -0.8520 - 0.5222i & -0.0331 - 0.0203i \end{pmatrix}$$

From the values of $\mathbf{\Sigma}$ two different modes can be distinguished. Each mode leads to a certain amount of received signal power defined by the values into $\mathbf{\Sigma}$. The first and bigger one is called the dominant mode. To apply the dominant mode of the SVD on the system we should apply the first row of \mathbf{V} as the weights of the antennas at the transmitter side and the first row of \mathbf{U}^H as the weights at the receiver side.

The previous 2x2 case shows well that the second antenna receives the most of the power and the weights of the dominant mode give almost the entire part of the reception power to the first antenna (i.e absolute value of the weights). The SVD permits to use water-filling which optimizes the transmitted and received power.

D.4 Weapon orientation estimation and polarization ellipticity

The shape of the weapon makes its backscattered pattern looking like the one of an imperfect dipole in most of the cases. From this property, the weapon orientation

compared to the antenna polarization gives us an idea of the received power. If it matches then the received power will be optimized, and it is what the SVD do.

Therefore, using the resulting polarization of the SVD we can observe the matching one corresponding to the weapon orientation. If the weapon is placed in the x-z plane then the polarization should be linear and directed in the orientation of the weapons in this plane. However if the weapon is also tilted in the y-z axis, then the polarization should turn to be an ellipse. Higher will be the ellipticity more tilted will be the weapon.

Taking the previous example, we can find the transmitted and received polarizations using the weights. To find the weapon orientation in the x-z axis we look at the middle polarization between the emission and reception polarizations while the tilt will be given by the ellipticity of the reception polarization.

As the second antenna is given to be the one polarized in VV therefore it represents the ordinates on the graphic and the first antenna polarization is HH so it represents the abscises. The weapon orientation $W_{\theta DM}$ for the dominant mode will then be defined by:

$$W_{\theta DM} = 0.5 \times \left(\frac{\frac{\pi}{2} \cdot |V(1,2)| + |V(1,1)|}{2} + \frac{\frac{\pi}{2} \cdot |U^H(1,2)| + |U^H(1,1)|}{2} \right) \quad (D.4)$$

The polarization comes from a change in the feeding signals amplitude. To obtain them we apply the weights of each antenna on the corresponding feeding signal which will be a cosine function by default. The resulting feeding signal absolute value for the HH polarized antenna will represent the abscises of the polarization and the resulting feeding signal absolute value for the VV polarization its ordinates. For the previous case we obtained the polarizations and W_{θ} shown in Figure D.3:

The ellipticity of the antenna polarization P_e is centered in zero and could be given by:

$$P_e = \frac{a_e}{b_e} = \frac{\max \left(\sqrt{F_{HH}^2 + F_{VV}^2} \right)}{\min \left(\sqrt{F_{HH}^2 + F_{VV}^2} \right)} \quad (D.5)$$

Where a_e is the semi-major axis of the ellipse and b_e semi minor axis of the ellipse. The more flat is the ellipse, the higher will be P_e value. If $P_e = 1$, the polarization is a circle. In (D.5), F_{HH} and F_{VV} are the HH and VV polarized antenna feeding signals.

In the previous case the receiving polarization of the dominant mode is characterized by $P_e = 99.7$.

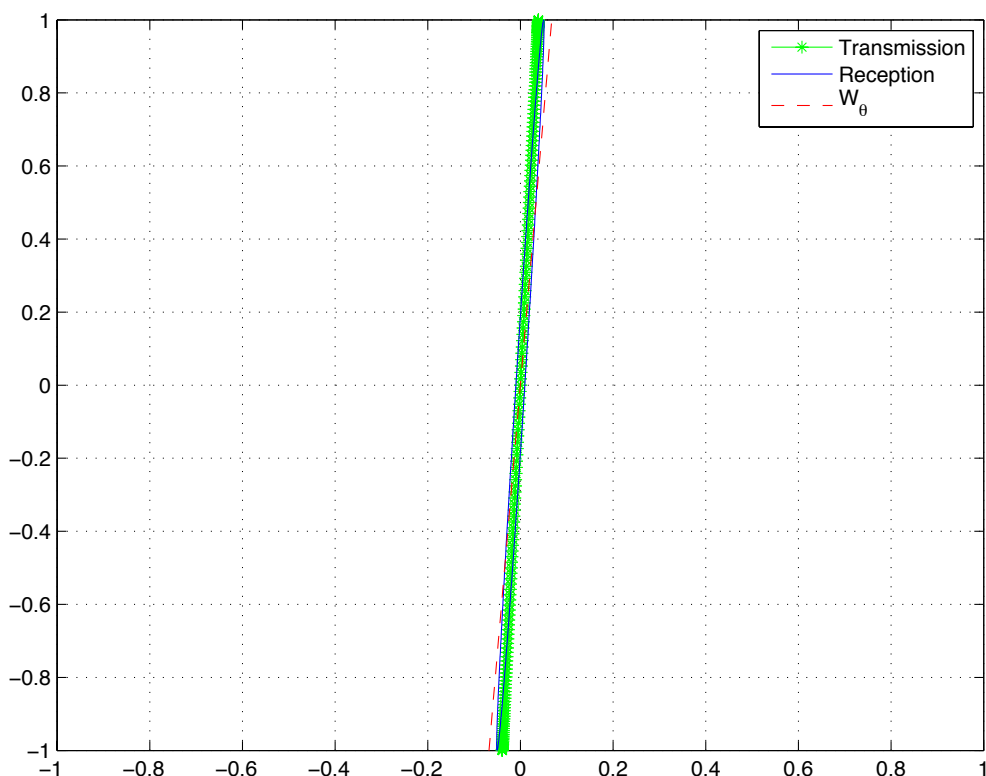


Figure D.3: Dominant mode transmission and reception polarizations corresponding to SVD example.

D.5 Polarimetric discrimination

D.5.1 Principle

The first idea is to use one antenna polarized HH and one VV . We then obtain polarimetric discrimination. We have seen in section 4.4 that weapons RCS are really sensitive to orientation and therefore provides a polarimetric diversity. With both launched polarizations, we might be able to discriminate the weapons and their orientation.

As the weights define the repartition of the power between the two antennas, it also defines a polarization since one component is polarized in HH and the other in VV . With respect to section 2.8.6, the coefficient given to an antenna compared to the other is traduced by a change in the feeding signals amplitude which carries favor to the preferred polarization of the weapons.

In the example we can note that the \mathbf{U} and \mathbf{V} weights give all the power to the

second antenna in the dominant mode and to the first antenna for the second mode. Therefore, the dominant mode would be a VV polarized antenna and the second mode a HH polarized antenna. The dominant mode corresponds to a polarization which is optimized compared to the weapon one. The second mode is an orthogonal polarization to the dominant mode.

We can then define three variables that can be found from this diversity which are the leakage, the XPD and the polarimetric discrimination (PD):

- **The XPD** is calculated making the ratio between the received power for the first mode co-polarization case and the cross-polarization (D.6). The cross-polarization is achieved using the second mode weights for the receivers instead of the first mode weights.
- **The leakage** is the same ratio as the XPD but the cross-polarization is achieved using the second mode weights for the transmitters instead of the receivers (D.7).
- **The PD** comes from the ratio between the received power for the dominant mode in co-polarization case and the second mode co-polarization case (D.8).

The notation is defined following the transmitter with first mode weights applied: Tx_{FM} and receiver second mode weights applied: Tx_{SM} . Apply to the weapon, they characterize its signature.

$$\begin{aligned}
 XPD_{weapon} &= \frac{\text{Power received from the weapon in co-polarization}}{\text{Power received from the weapon in cross-polarization}} \\
 &= \frac{[Tx_{FM}, Rx_{FM}]}{[Tx_{FM}, Rx_{SM}]} = \frac{[V(1, m), U^H(1, n)]}{[V(1, m), U^H(2, n)]} \quad (D.6)
 \end{aligned}$$

$$\begin{aligned}
 Leakage_{weapon} &= \frac{\text{Power received from the weapon in co-polarization}}{\text{Power received from the weapon in cross-polarization}} \\
 &= \frac{[Tx_{FM}, Rx_{FM}]}{[Tx_{SM}, Rx_{FM}]} = \frac{[V(1, m), U^H(1, n)]}{[V(2, m), U^H(1, n)]} \quad (D.7)
 \end{aligned}$$

$$\begin{aligned}
 PD_{weapon} &= \frac{\text{Power received from the weapon in dominant mode co-polarization}}{\text{Power received from the weapon in second mode co-polarization}} \\
 &= \frac{[Tx_{FM}, Rx_{FM}]}{[Tx_{SM}, Rx_{SM}]} = \frac{[V(1, m), U^H(1, n)]}{[V(2, m), U^H(2, n)]} \quad (D.8)
 \end{aligned}$$

Where:

- m is the m^{th} transmitter
- n is the n^{th} receiver

In the previous example case, as the weights give almost all the power in the VV polarized antenna then we can say that the weapon is oriented vertically and is seen from the top point of view P_2 (only the barrel is seen). If we were placed in the side point of view P_1 , the weapon would have had a vertical and horizontal backscattered coefficients of the same order. Therefore the Σ coefficients would be close one to each other. The dominant mode and the second mode would received almost the same amount of power.

The weights phase is also to take into account. As we studied in section 2.8.6, the phase of the weights define the phase difference between the two components. From the phase of the weights we can be able to know the shape of the polarization (linear, circular or elliptical).

D.5.2 Application

The SVD should permit to optimize the polarization to the weapon orientation by changing the weights of the antenna. The goal here will be to verify if it is possible using SVD to detected the weapon orientation looking at the dominant mode polarization. The experiment is done using the previously described 2×2 MIMO system. Three cases are studied to compare how reacts the SVD with three different weapon orientations. They are described in Table D.1.

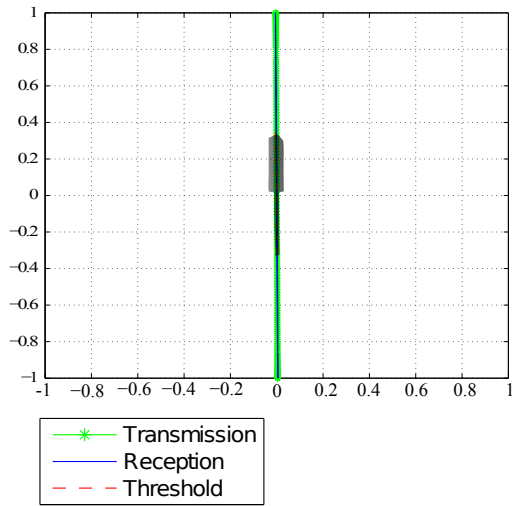
	Weapon orientation
Case I	$\phi_{weapon} = 0$ $\theta_{weapon} = 90$
Case II	$\phi_{weapon} = 30$ $\theta_{weapon} = 45$
Case III	$\phi_{weapon} = 90$ $\theta_{weapon} = 45$

Table D.1: Simple cases for 2x2 MIMO system study.

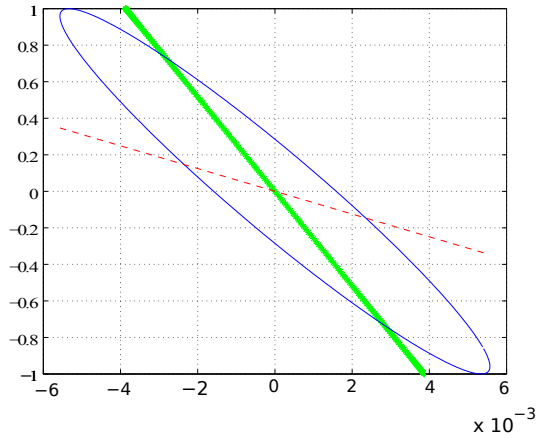
From these cases we want to find the orientation of the weapon. After using SVD we can note that it permits to adjust the polarization with the weapon orientation. Figure D.4 shows the radar dominant mode polarization in transmission and reception after the SVD weighting for each studied case while D.5 shows the study of the transmission polarization of the dominant and second mode after the SVD weighting. The two figures also show a threshold between the modes depending on the values of Σ which adjusts the polarization. This threshold should be oriented with the same angle as the weapon. The weapons are placed on the graphics with the same orientation that in the corresponding studied case.

In Figure D.4 and D.5, the polarizations have been drawn using two components represented by the antennas of the 2×2 system. The first antenna polarized

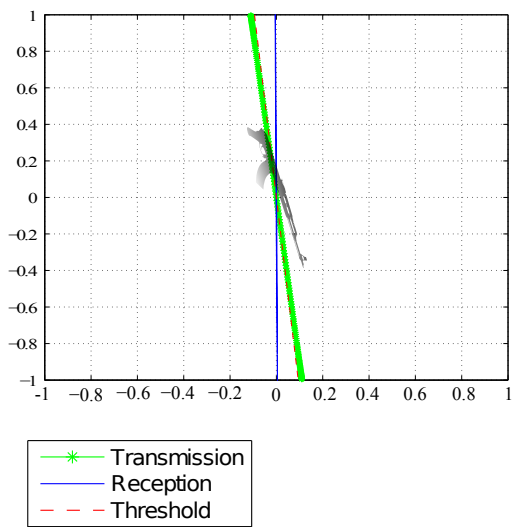
HH represents the horizontal component while the second antenna polarized in VV represents the vertical one. The amplitudes have been scaled using the absolute value of the weights and the corresponding coefficient in Σ . To implement this we created a cosine feeding function for each antenna and we used the amplitude and phase of the weights scaled with the Σ value corresponding to the studied mode. The horizontal and vertical feeding functions are then applied respectively to the horizontal and vertical axis. They permit to define the final polarization as explained in 2.8.6. Therefore the axis represents the normalized voltage of the feeding signals.



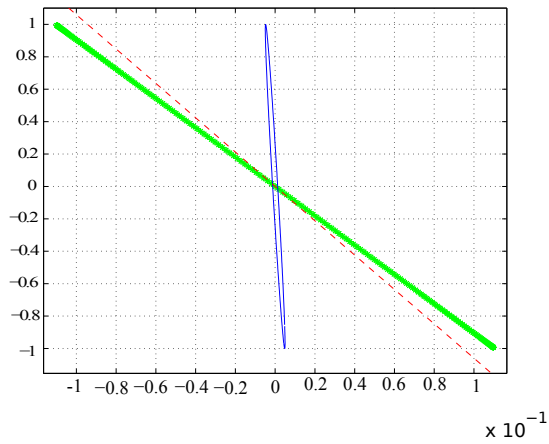
zoom
=>



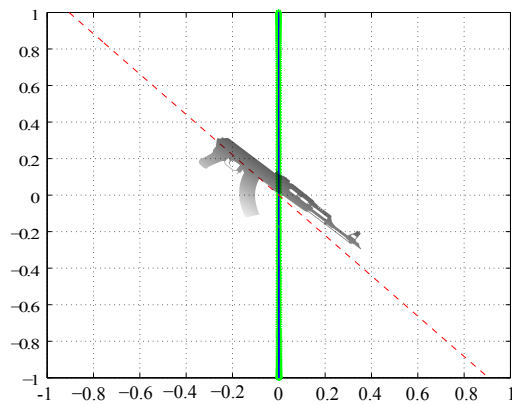
Case I



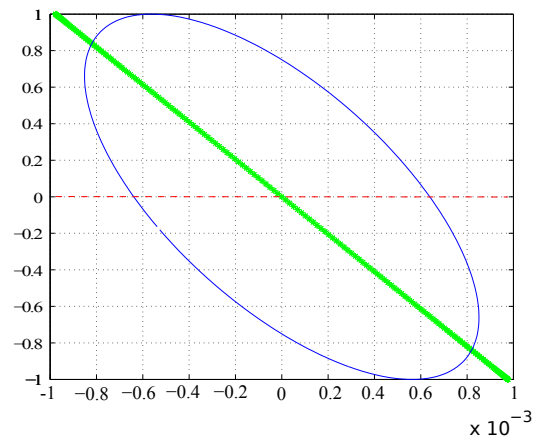
zoom
=>



Case II

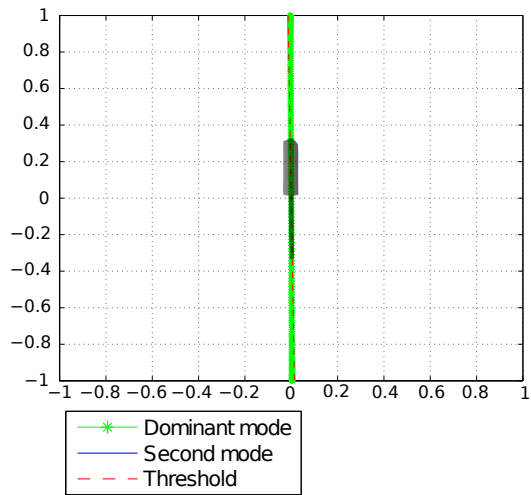


zoom
=>

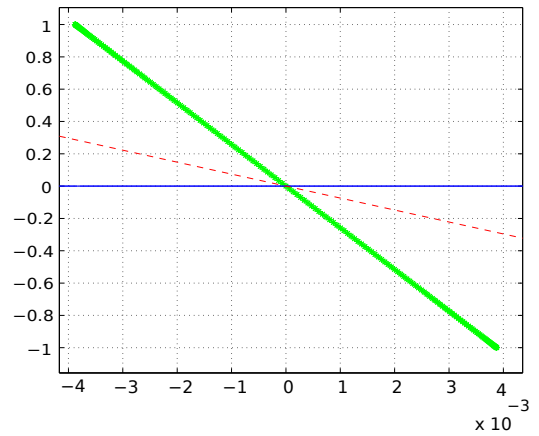


Case III

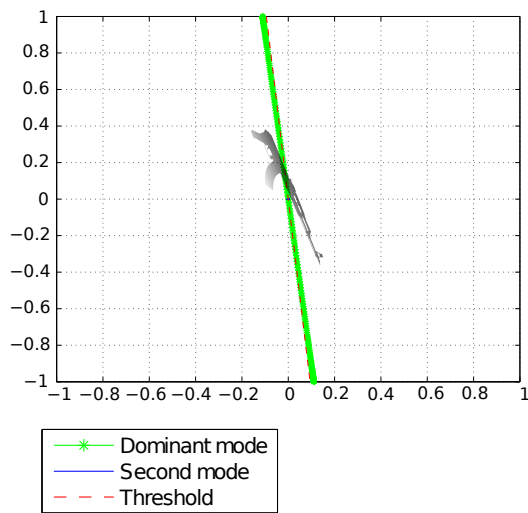
Figure D.4: Study of the dominant mode polarization in transmission and reception after the SVD weighting, the estimated weapon position (threshold) and the real weapon position in three basic MIMO cases.



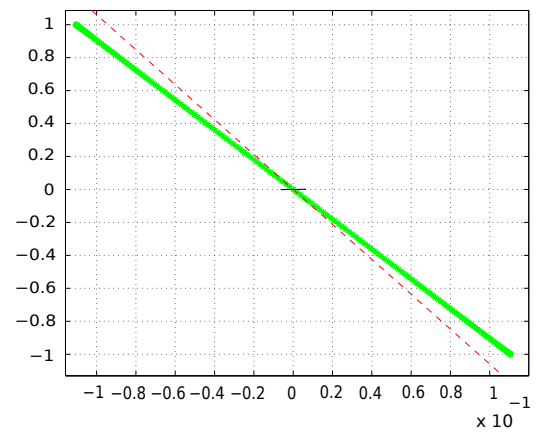
zoom
=>



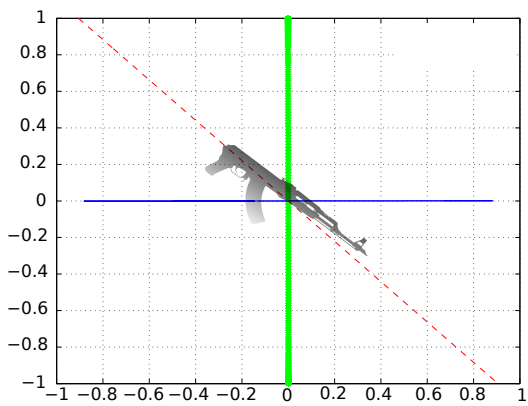
Case I



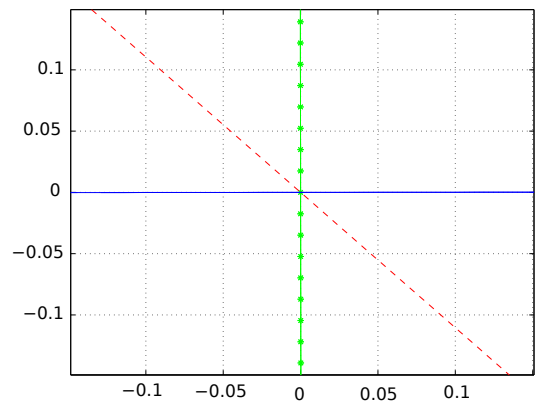
zoom
=>



Case II



zoom
=>



Case III

Figure D.5: Study of the transmission polarization of the dominant and second mode after the SVD weighting, the estimated weapon position (threshold) and the real weapon position in three basics MIMO cases.

Looking at the results we found that using SVD we can determine the weapon orientation in case of a unique weapon at least. Every iteration the SVD could give a good estimation of it and also concentrates the power to the more efficient antenna depending on the antenna polarization and the weapon orientation.

The resulting polarization is most of the time linear or elliptical with a very small ellipticity (high value for P_e). Fact explained by the defined backscattering pattern of the weapons. The kind of polarization obtained and its orientation plays a major role in the weapon classification because it is part of its signature.

To confirm that the oriented linear or with small ellipticity polarization obtained is specific to the weapons, we will plot the obtained polarization of the sea only, the boat only and boat and sea together as backscatterers (see Figure D.6). It results in a elliptical polarization oriented randomly around the vertical axis.

We can conclude that in presence of a weapon the SVD should be linear and oriented in the weapon's orientation. If there is no weapon then the polarization will neither be linear nor oriented in a specific orientation. This parameter can increase the weapon detection efficiency but it has limits because the boat could also be made of metallic pieces that could biased the polarization.

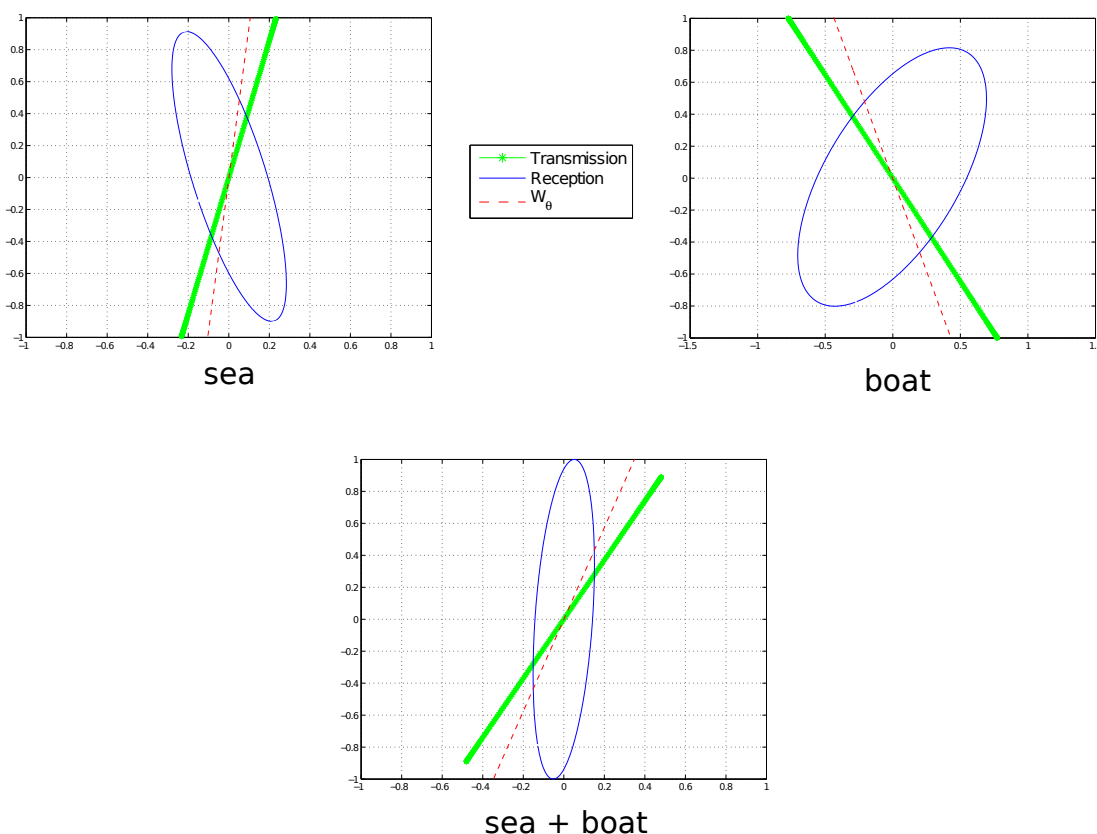


Figure D.6: Obtained normalized polarization for sea only, boat only and sea plus boat as backscatterer.

As expected, SVD in the 2×2 MIMO system gives two modes and the transmitted polarization of the dominant mode is near to the weapon orientation. Moreover, the second mode transmitted polarization corresponds to the orthogonal polarization to the weapon orientation. It also confirms then that the use of SVD in our radar system could permit to optimize the polarimetric discrimination of the weapons compared to the sea.

Appendix E

Weapon polarimetric signature

The aim of this appendix is to see if the polarimetric signature of a detection can be used to classify its nature to be a weapon. It follows the *Appendix D. Singular Value Decomposition technique* study and uses the same 2×2 MIMO system configuration for the simulations.

In this previous appendix we defined five variables that are to take into account if we want to classify a detection to be a weapon. These five variables are the ellipticity of the polarization, the orientation of the polarization, the *XPD*, the *leakage* and the *PD*.

From these properties we can define thresholds that will help us to classify the detection to be a weapon. Table E.1 shows the expected values of these variables and the corresponding thresholds.

	XPD			Leakage			PD			Polarisation orientation			Polarization ellipticity		
	I	II	III	I	II	III	I	II	III	I	II	III	I	II	III
Sea	4			-8			2			random V			7		
Dinghy	0			4			0			random			10		
Weapon	42	18	46	42	18	46	46	34	0	V	20° to V	mid(V-H)	28	20	32
Thresholds	15			15			15			fixed			17		

Table E.1: Expected values of the defined variables for target classification in dB with a sea-state 6.

These expected values are the values of the sea or the boat or the weapon alone with no external interactions such as shadowing effects. To see if it is possible in a real situation to use these properties to classify the nature of a detection we are going to simulate the average value of 30 realizations of each case including the external factors. Results are shown in Table E.2 and have also been done for the boat alone.

	XPD	Leakage	PD	Polarisation orientation	Polarization ellipticity
Case I	5	2	2.2	random	17
Case II	5	2.3	3.7	random	15
Case III	14	2.1	4.3	random	22
Boat only	4	1.15	1.5	random	8*

Table E.2: Simulated average values over 30 realizations of the defined variables for target classification in dB with sea-state 6.

* Shadowing can cause infinite ellipticity then the taken value is the median of the realizations value

The obtained values are below the thresholds in most of the configurations. The polarimetric properties of the weapon is masked in the simulations. Apparently, the interaction of the boat and the sea are too high compared to the weapon one. To verify this fact, we will study some *SCR*. We will first see the dinghy to clutter ratio (*DCR*), then the weapon to dinghy ratio (*WDR*) and we will also look at a weapon to clutter ratio (*WCR*) where the dinghy will be considered as a part of the clutter. We obtained Table E.3 for *HH* polarization and Table E.4 for *VV* polarization.

	DCR	WDR	WCR
Case I	82	-100	-100
Case II	82	-100	-100
Case III	82	24	24

Table E.3: SCR, WDR and WCR study for *HH* polarization in dB.

	DCR	WDR	WCR
Case I	68	-7	-7
Case II	68	-7	-7
Case III	68	24	24

Table E.4: SCR, WDR and WCR study for *VV* polarization in dB.

In one of the three positions only the weapon is detectable compared to the boat. As the *DCR* is important, we can detect it with no ambiguity. This will be the only case where the weapon polarimetric signature will be visible. Therefore it will not be possible to use the *XPD*, the *leakage* or the *PD* to classify the weapon since its orientation is random. The polarization does not fit with the weapon orientation and the properties corresponding to the *XPD*, *leakage* and *PD* of the weapon is are not kept.

The point of interest of that study is to open the theoretical possibility of the use of polarimetric properties to detect weapons. It would be efficient in the case of

an environment less dominant than the boat compared to the weapon. Typically in a house it may be possible to detect weapons through the walls.

An other point of interest would be to see if it is possible to use polarimetric discrimination only to classify the detection to be a boat or a sea wave. The *RCS* of the dinghy has been defined to be the same for *HH* or *VV* but to have a 10dB for the cross polarization *VH* or *HV*. Therefore the principle would be to use only the following polarizations: *HH*, *VV*, *HV* and *VH*. In this case the SVD resulting polarization will not match the wanted polarizations and therefore will not be used. With these polarizations, it is possible to obtain specific *XPD*, *leakage* and *PD* of a detection. The simulations have been done including the shadowing effects and the boat RCS fast fading to see if the boat keeps its polarimetric properties and the results are stored in Table E.5.

	XPD	Leakage	PD
Boat	10	10	0
Sea	25 (± 30)	21 (± 3)	2
Boat & sea	44 (± 30)	13 (± 25)	3

Table E.5: Simulations of the *XPD*, the *leakage* and the *PD* in *dB* for sea-state 6 and default polarization *VV*. Notation is: mean (\pm approximate range of values)

This experiment shows well the sea polarimetric behavior looking at these specific variables. The *PD* and *leakage* does not vary much and are respectively around 3dB and 21dB while the *XPD* varies randomly inside a large range of values. It comes from the part of random in the sea EM response defined in our implementation by the Tsallis distribution (section 5.2.2).

The dinghy *RCS* varies following a Swerling model I as described in section 4.2. It makes the results varying significantly and the polarimetric signature not predictable as well. The only possibility we have to argue on the dinghy presence is then to have a non-varying *leakage*. It would mean that the detected object is not a dinghy. But even in this case the polarimetric response is close to the sea one and this argument is too weak to be used.

The polarimetric signature is then a technique that can be used with specific environments compared to the signature of the target we want to identify. For our project the environment does not fit with the polarimetric signature of the weapon neither with the boat one. For this reason, it will not be used. However we also saw that in the corresponding environment, this technique can be largely precise enough to characterize the nature of a detection.

Appendix F

Tsallis and K-distributions

In this appendix, we estimate the best suited distribution between Tsallis and K-distribution to model the electromagnetic sea-response.

To compare these distributions and their accuracy, we are going to use public available radar measurements [43]. From these data, we compute the PDF and try to fit the theoretical distributions with them.

F.1 Parameters estimation

In K-distribution, we have to find values for ν and L . In Tsallis distribution, we have to estimate q and β parameters. In both cases, we use a brute force algorithm to determine these parameters. The accuracy of the fit depends on possible parameters sets. We took the following:

- Tsallis distribution
 - $q \in]1; 3]$ with $\Delta q = 0.01$
 - $\beta \in]0; 300]$ with $\Delta\beta = 0.01$
 - Total number of parameter sets : 6.000.000.
- K-distribution
 - $\nu \in]0; 40]$ with $\Delta\nu = 0.016$
 - $L \in]0; 40]$ with $\Delta L = 0.016$
 - Total number of parameter sets : 6.250.000.

Some extra brute force detection has been ran when any of the optimized chosen parameters (q , β , ν or L) were one of their upper or lower bounds.

When we have a fit, we want to estimate how good it sticks to the data distribution. For each couple of value L and ν or q and β , the match is to try to reduce the Relative Entropy (RE) between the theoretical PDF and the measurements PDF. The minimum found value for RE will be denoted Minimum Relative Entropy (MRE).

For that purpose, we need to introduce the Relative Entropy calculation, also called Kullback-Leibler divergence denoted by D_{KL} , given by (F.1) [44]:

$$D_{KL}(p_{dist}||p_{data}) = \int_{x=-\infty}^{x=\infty} p_{dist}(x) \cdot \log_2 \left(\frac{p_{dist}(x)}{p_{data}(x)} \right) dx \quad (\text{F.1})$$

Where:

$p_{dist}(x)$ K-PDF or Tsallis-PDF
 $p_{data}(x)$ Measurement PDF

This D_{KL} or RE value is more appropriated than usual standard deviation or first order moment calculation because it takes into account distribution tails, thanks to the logarithm. Table F.1 shows several measurements with their respective estimated K and Tsallis distributions.

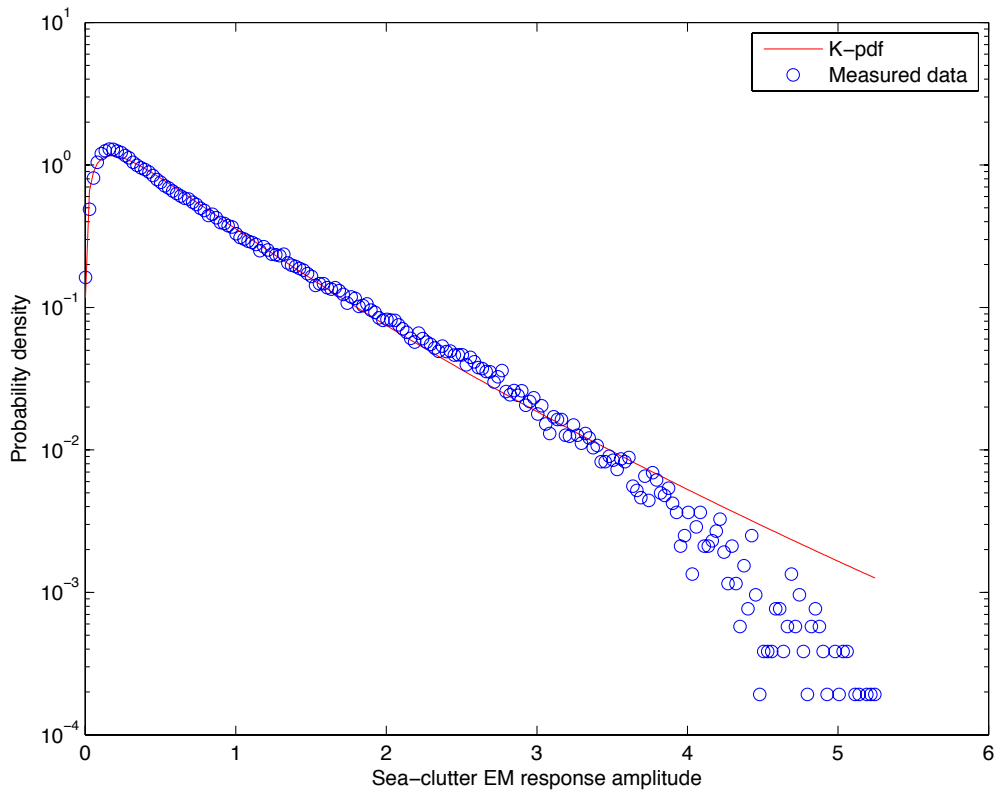
F.2 Simulation results

From these first statement, we computed the minimum D_{KL} for each couple of parameters for the two distribution over 245 radars measurements. It is first interesting to see plots of the pdf and the measured data

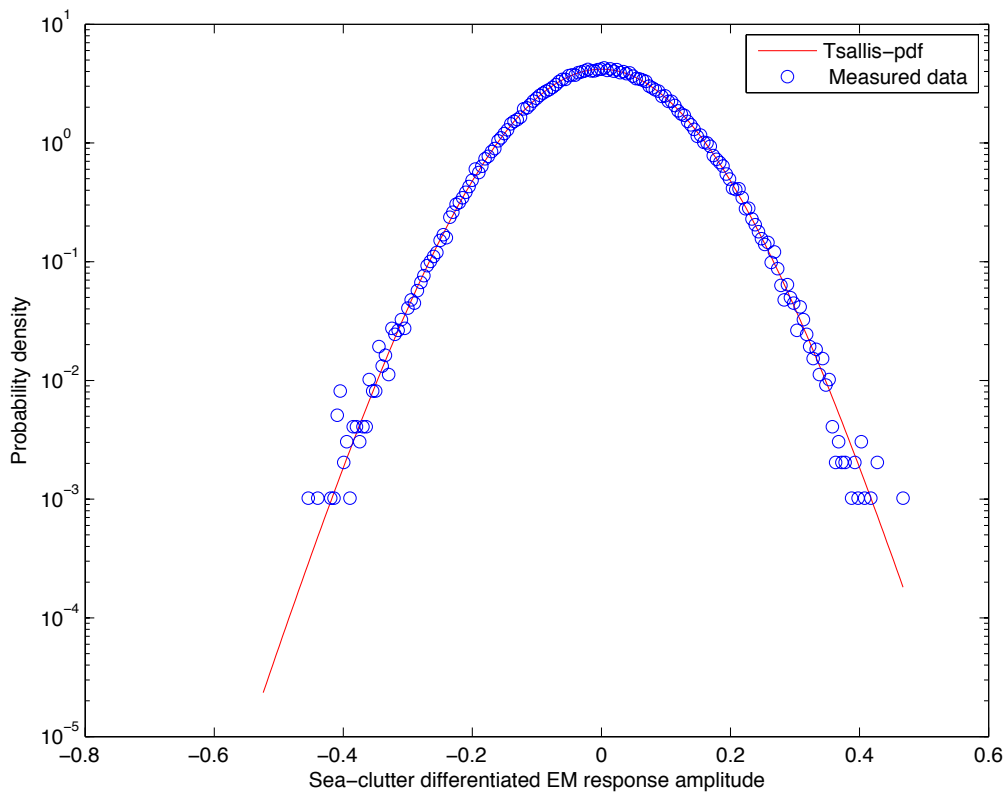
Tsallis parameters			K parameters			Measurements conditions	
q	β	$D_{KL-Tsallis}$	ν	L	D_{KL-K}	Wind speed [$m.s^{-1}$]	Antenna/Wind angle [$^{\circ}$]
1.20	39.6	0.0002	1.6	1.6	0.0703	8.11	-1
1.50	80.0	0.0017	2.0	4.8	0.0089	7.39	14
1.40	250.0	0.0117	1.4	1.6	0.0230	9.11	26
1.07	19.2	0.0003	2.7	11.1	0.0141	7.90	27
1.07	9.0	0.0009	2.8	20.0	0.0102	5.22	32
1.08	4.7	0.0004	2.6	15.6	0.0077	4.94	34
1.13	87.7	0.0003	1.8	1.8	0.0103	9.15	66
1.30	1.0	0.0207	3.0	20.0	0.0199	9.16	101

Table F.1: Tsallis and K distributions efficiency comparison

To illustrate the fit, we can look at Figures F.1a, F.1b, F.2a and F.2b representing the distributions and the measured data, associated with their MRE in the caption. The logarithm axis is used to show the importance of tail fitting.

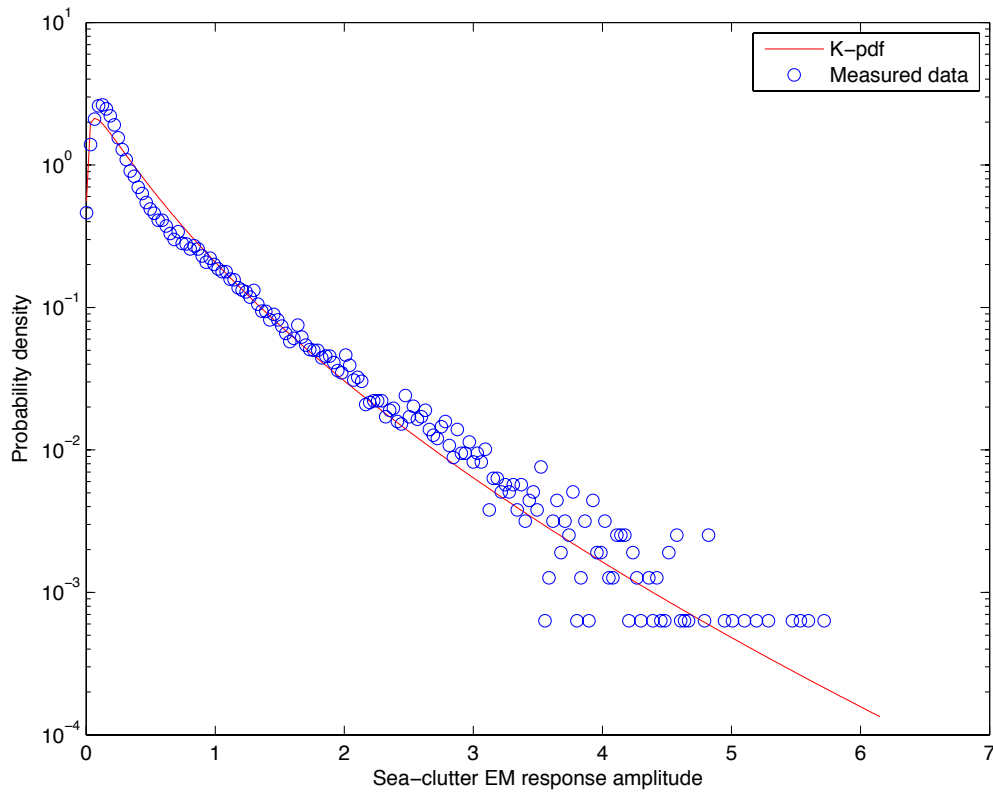


(a) K-distribution fit - MRE = 0.0077

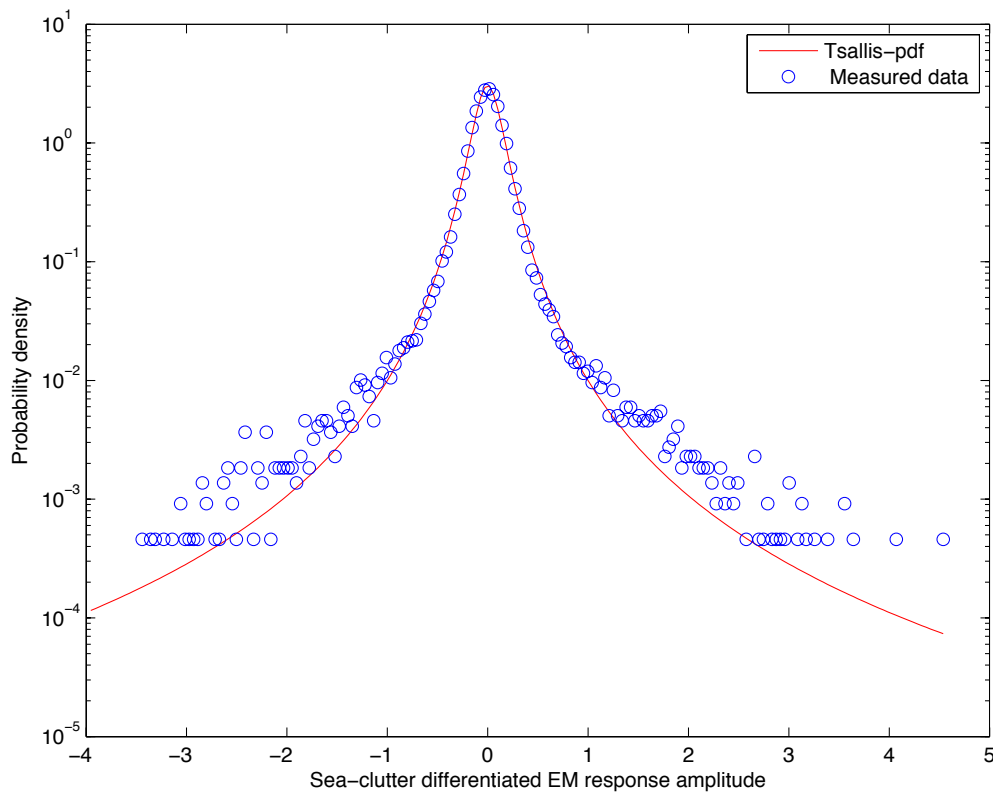


(b) Tsallis-distribution fit - MRE = 0.0007

Figure F.1: K and Tsallis distributions fit compared to a given dataset



(a) K-distribution fit - MRE = 0.0400



(b) Tsallis-distribution fit - MRE = 0.0062

Figure F.2: K and Tsallis distributions fit compared to a given dataset

Figure F.3 shows the computed D_{KL} for both Tsallis and K distributions over 245 data sets. The statistics are summed up in Table F.2.

Statistics over D_{KL}	Tsallis	K
Mean	0.0166	0.0242
Geometrical mean	0.0008	0.0142
Standard Deviation	0.1064	0.0380
Minimum value	$8.3278 \cdot 10^{-9}$	$5.6803 \cdot 10^{-5}$
Maximum value	0.9849	0.4002
Better than other D_{KL}	95.92%	4.08%

Table F.2: Tsallis and K distributions D_{KL} comparison

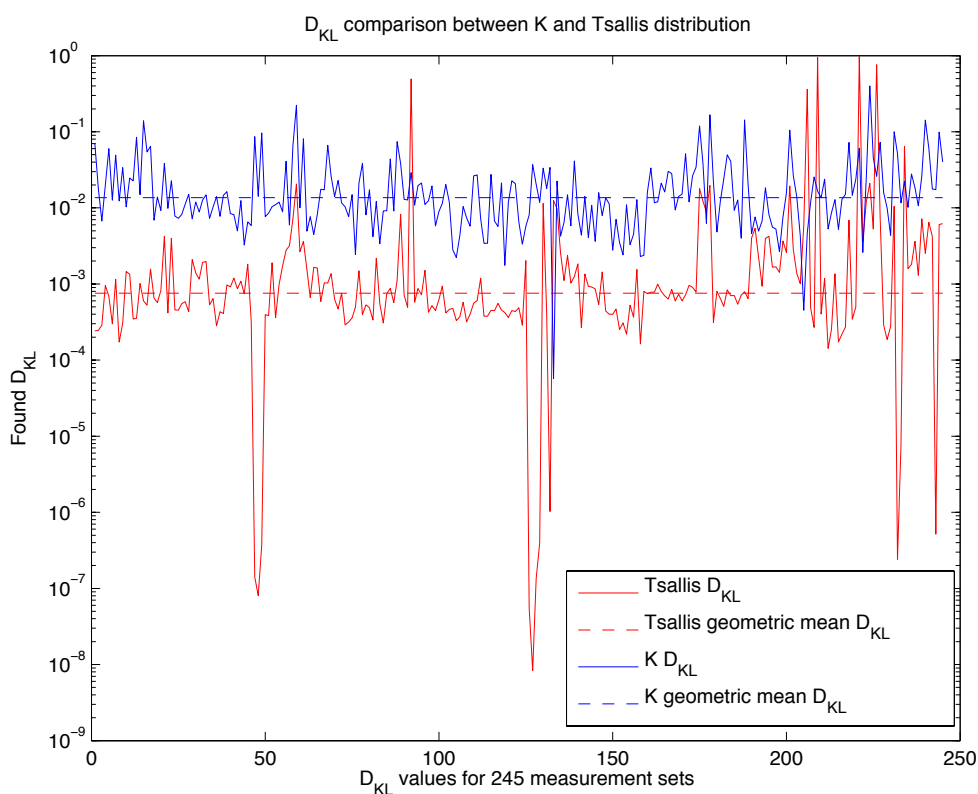


Figure F.3: D_{KL} comparison for K and Tsallis distributions over 245 radar measurements.

F.3 Metrics

It is important to note that the Tsallis distribution suits more the data, but both distributions do not estimate the same parameter. Indeed, K-distribution tries

to estimate A_R and Tsallis distribution estimates ΔA_R . Since the amplitude response is a high non-stationary process [8], it might be easier to estimate ΔA_R than A_R .

In order to compare on the same metrics for the two distributions, we are going to try to build ΔA_R from A_R with the K-fit and then find the A_R from ΔA_R and μ_{A_R} with the Tsallis-fit. We use the μ_{A_R} value for the reverse $\Delta A_R \rightarrow A_R$ operation. None of the distributions is favored with μ_{A_R} because the K-distribution also uses this parameter to build the theoretical fit.

This reversal should help us to see how each distribution fits the measured data with the other parameter. The operation would be to make a realization of the theoretical first fit with the measured data, and then to make either $A_R \rightarrow \Delta A_R$ for K-realization or $\Delta A_R \rightarrow A_R$ for Tsallis-realization. This operation will be called "cross-fit". The D_{KL} calculated with the measured data from a cross-fit will be denoted Cross- D_{KL} .

F.4 K-distribution cross-fit : $A_R \rightarrow \Delta A_R$

When we look for the best suited parameters, the K-distribution takes as a parameter the mean value of sea clutter response. It will be denoted μ_{A_R} .

We start from the K-fit, and compute a realization of the PDF with the estimated ν and L parameters. Once this realization has been done, we compute the ΔA_R by using equation (5.14) presented in section 5.2.2 for the EM-amplitude differentiation. Then, we merge the corresponding Tsallis-fit and ΔA_R K-fit and compare the D_{KL} .

Examples plots are shown with fig. F.4 and F.5

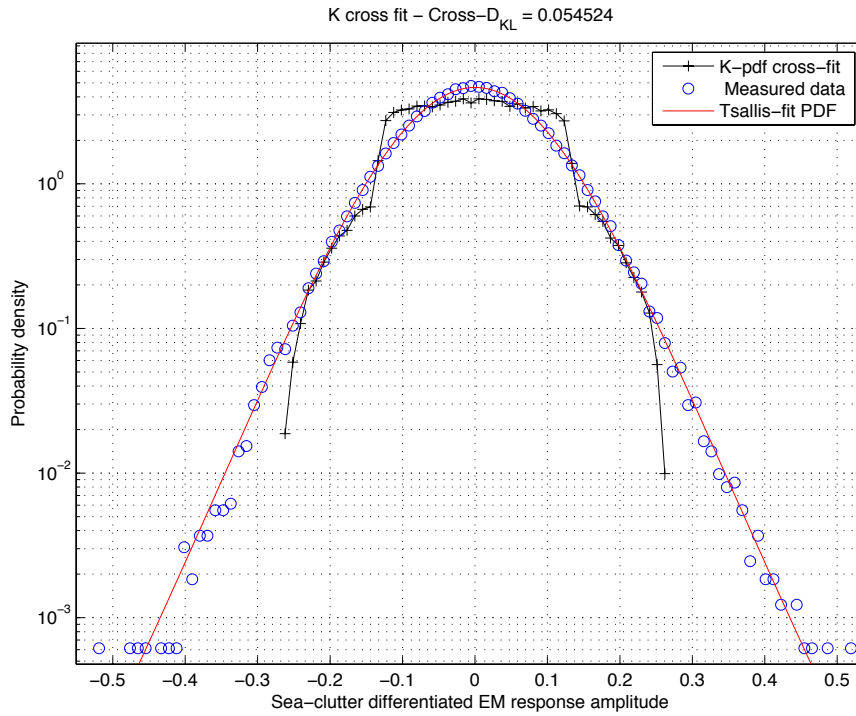


Figure F.4: Cross- D_{KL} of K-distribution over differentiated data (ΔA_R).

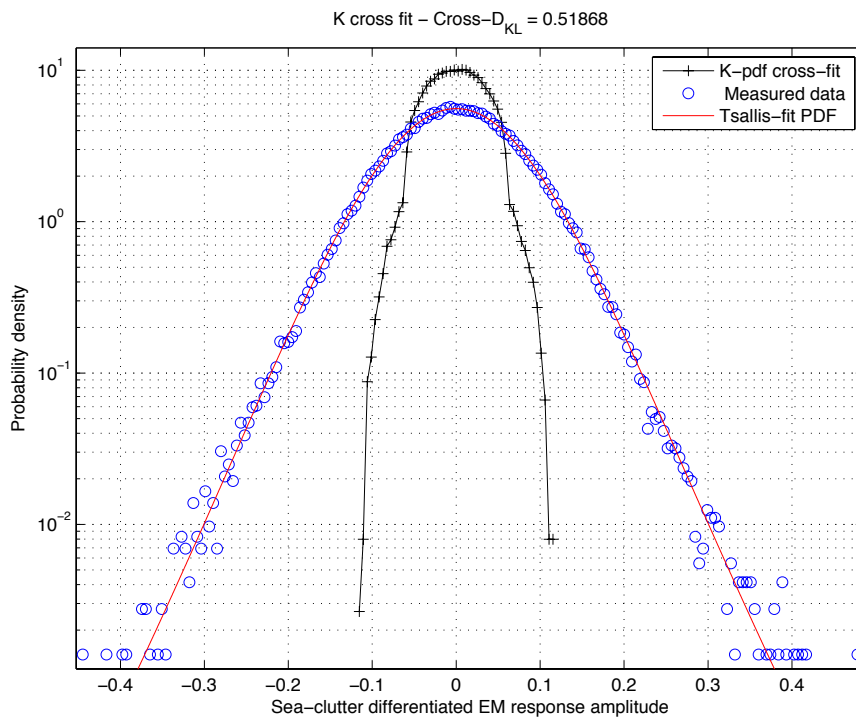


Figure F.5: Cross- D_{KL} of K-distribution over differentiated data (ΔA_R).

These results are based on a distribution realization and change for every simulation. Therefore, the given results are just shown to give an idea of the overall tendency. The K-cross-fit sometimes well matches the ΔA_R measured data (fig. F.4) but most of the time it is far from the data and theoretical fit. The K-distribution does not take into account the dynamics, and fig. F.5 shows that the differentiated data are too compact.

K-realization apparently does not model efficiently the dynamics of the distribution.

F.5 Tsallis-distribution cross-fit : $\Delta A_R \rightarrow A_R$

On the other hand, we apply the same process to the Tsallis-fit in order to compare it to the K-fit. After the q and β parameters estimation, we make a realization of the tsallis distribution. To compute A_R from ΔA_R , we use the equation (F.2) derived from (5.14)

$$y(n+1) = x(n) + y(n), \quad n = 1, 2, \dots \quad (\text{F.2})$$

Where:

$y(n)$	Sea-clutter EM response for bin n
$x(n)$	Tsallis Differential amplitude realization for bin n.

The mean value for a Tsallis distribution is 0, therefore, we know that the distribution will stay around that value. therefore, we take $y(0) = \mu_{A_R}$ for the first value. When the Tsallis realization makes the next amplitude going under 0, we "jump" that Tsallis value up to find a valid value. When the sea-amplitude gets higher, the jumped value is then used.

Examples plots are shown with fig. F.6 and F.7. In these figures, one can notice that the tail of the measured data is better modeled with the Tsallis cross-fit than the K theoretical fit. K-distribution is rough because it forces a straight slope in the log domain. However, Tsallis realization sometimes do not match the beginning of the distribution and the fit is not completely perfect.

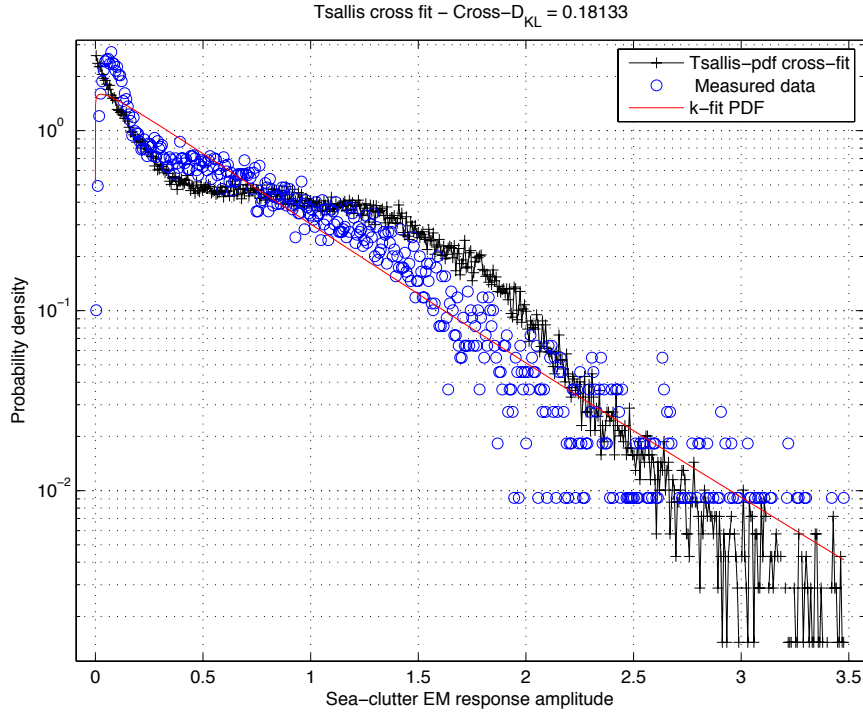


Figure F.6: Cross- D_{KL} of Tsallis-distribution over non-differentiated data (A_R).

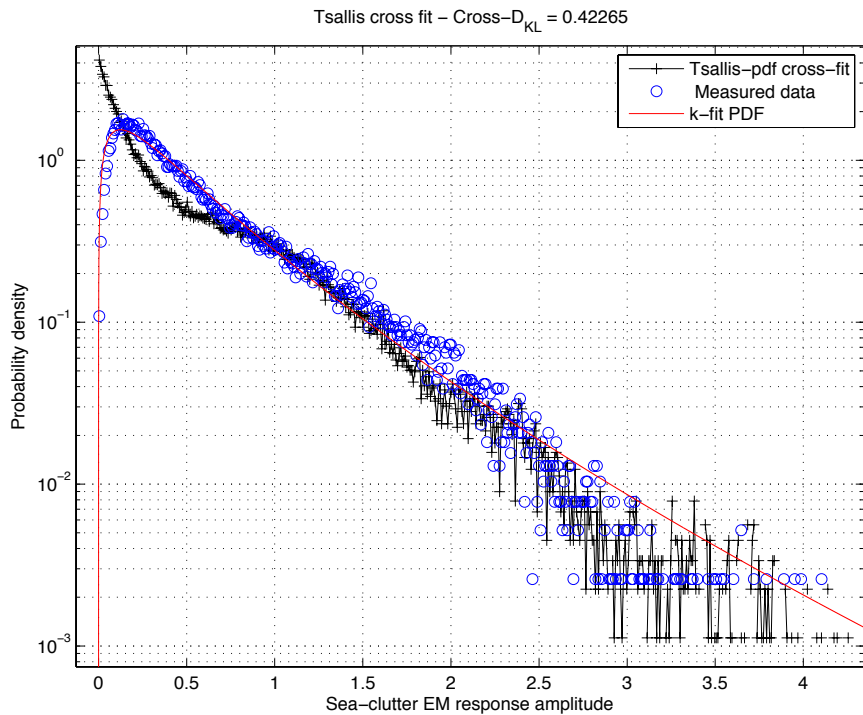


Figure F.7: Cross- D_{KL} of Tsallis-distribution over non-differentiated data (A_R).

F.6 Overall Cross- D_{KL} comparison

We have seen that the realizations are not matching the data as well as the theoretical fits. Therefore, we can introduce that we would call a Cross- D_{KL} . That Cross- D_{KL} value would represent the D_{KL} for the Tsallis realization over A_R and the D_{KL} value for the K-realization over ΔA_R . We can expect the Cross- D_{KL} is largely higher than the D_{KL} because of the following :

- D_{KL} encapsulation :
The realization is made over a Tsallis or K- fit which already has a $D_{KL} > 0$ and therefore this bias is added to the next fit.
- Pseudo-random computer :
Realizations are made with pseudo-random generator (matlab *rand()* function), there could be some bias due to small realizations because the mean of the realization is not exactly 0.5 and the equiprobability property is not perfect.
- Limited samples in the realization:
Realizations are made with 100.000 samples for all data sets. Some data sets are made from 30.000 to 800.000 samples. The PDF are then sometimes different when the samples number does not match, especially for the PDF-tails (values which occur few times overs 100.000 samples.)

The simulation we ran over 245 measurements gave the results shown in table F.3. Detailed results are visible on fig. F.8.

Statistics over Cross- D_{KL}	Tsallis	K
Mean	0.77	1.46
Geometrical mean	0.66	0.85
Standard Deviation	0.37	1.40
Minimum value	0.03	0.05
Maximum value	2.16	5.97
Better than other Cross- D_{KL}	62.45%	37.55%

Table F.3: Tsallis and K distributions Cross- D_{KL} comparison

For the theoretical fit, we can consider that the match is poor when $D_{KL} > 0.1$. When Cross- $D_{KL} > 1$, the fit hardly matches the data. We can have an idea with the example given in fig. F.9 for a Cross- $D_{KL} = 1.2$.

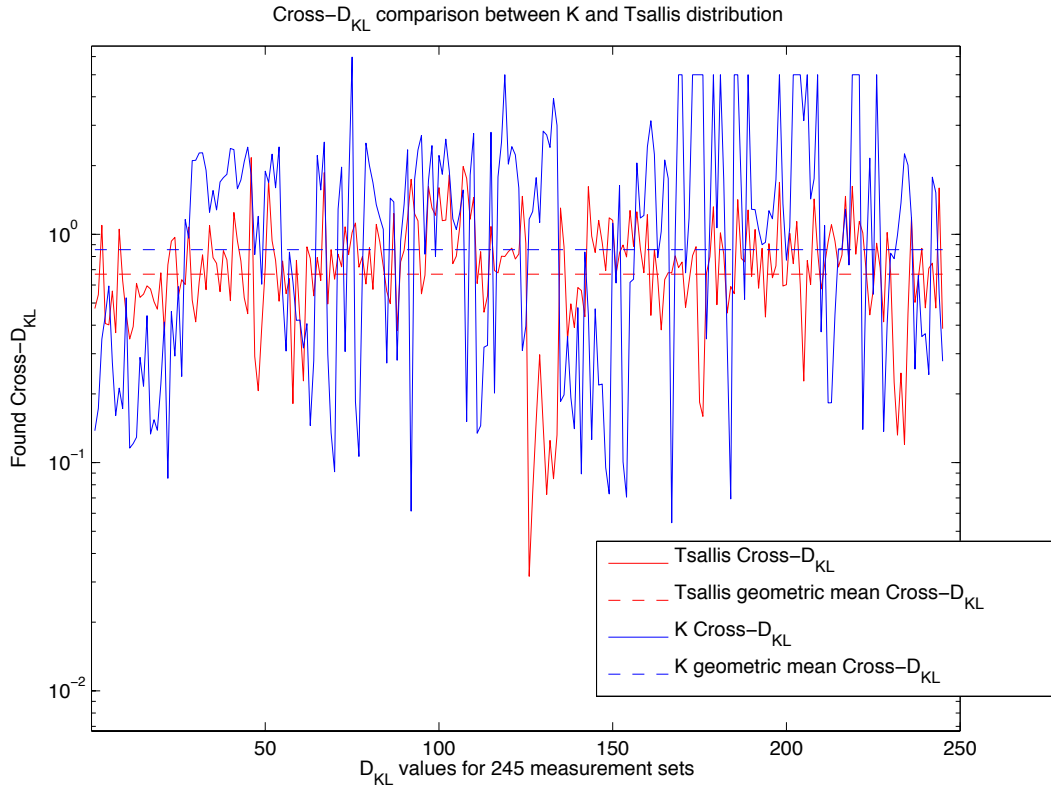


Figure F.8: D_{KL} comparison for K and Tsallis distributions over 245 radar measurements.

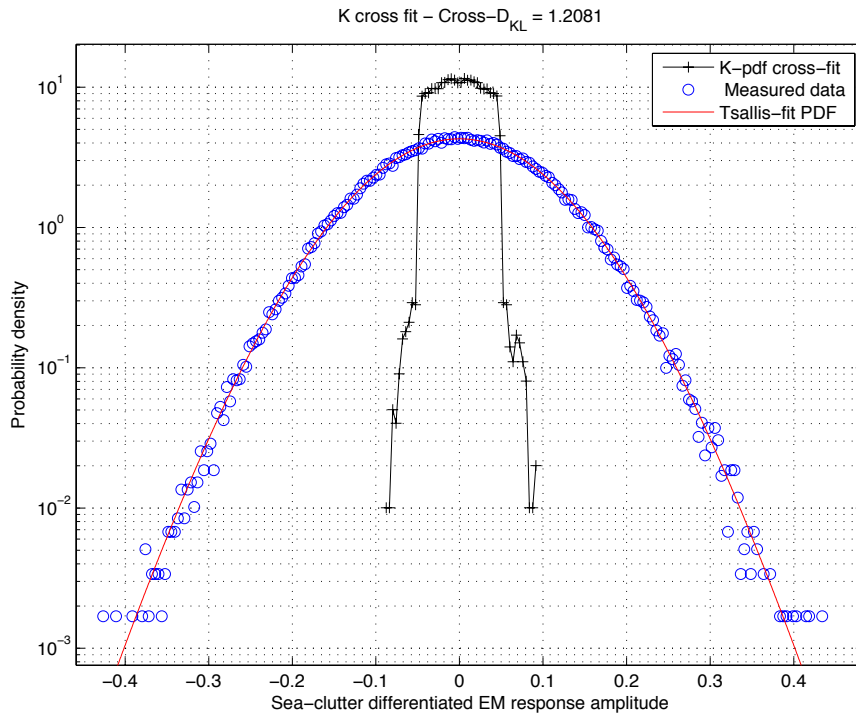


Figure F.9: Cross- D_{KL} of K-distributions over differentiated data (ΔA_R).

Of course, these measurements would change a bit if we ran further simulations because they are based on a given realization. However, they represent the overall behavior of each distribution and help to have an idea how it fits to the real measurements.

F.7 Distribution correlation

The correlation between adjacent cells in the amplitude is provided by the differentiation method of the Tsallis distribution. K-distribution does not handle the correlation between adjacent sea-clutter cells. Figure F.10

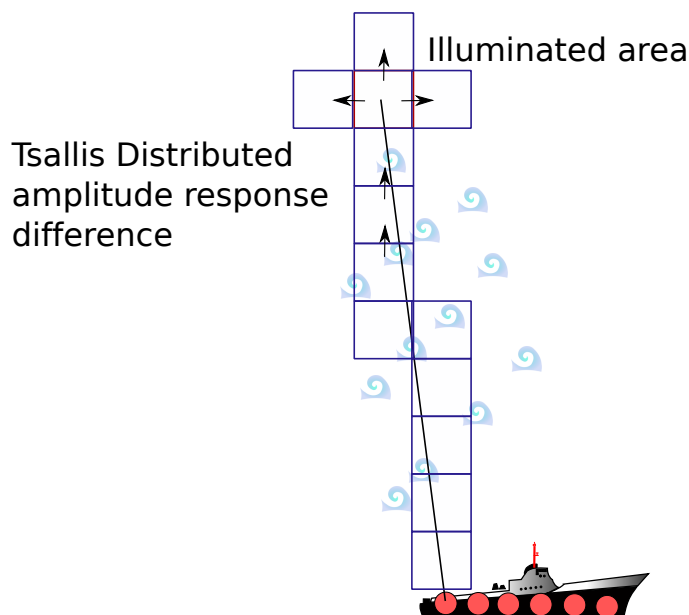


Figure F.10: Tsallis realization computed cell after cell

When we model the sea-response with the K-distribution, we have to take into account the correlation between cells. In [6] the author uses a correlated Gamma generator for their K-distribution, which needs more computation.

Tsallis realization has a memory because a sample is found from the previous one. The correlation between adjacent cells is therefore achieved with no more calculation (see *Appendix C. Signal correlation* for further details). The used q and β parameters of the Tsallis distribution will change depending on the direction we are applying the distribution.

The inconvenient with Tsallis is that we need an extra parameter, which is the mean of the clutter amplitude. From that mean value, we can compute a realization.

F.8 Conclusions

In that appendix, we have compared the following points in between the Tsallis and K distributions :

- D_{KL} :
As shown in fig. F.3 and table F.2, Tsallis distribution is better in average than the K distribution, and sometimes its RE is even close to 0.
- Cross- D_{KL} :
According to section F.6, Tsallis Cross- D_{KL} is equivalent in average than the K Cross- D_{KL} . The important metric for the Cross- D_{KL} is the standard deviation, which shows that the Cross- D_{KL} for the K-distribution is largely unstable, compared to the Tsallis one which is therefore more robust. Cross-fit shows that the Tsallis-distribution most of the time models the tails more accurately than the K-distribution.
- Correlation:
There is no correlation in between adjacent cells with a simple realization of K-distribution while Tsallis distribution has a no need for extra correlation implementation.

With results presented in this appendix, we are able to conclude that Tsallis distribution is the best suited distribution to model a sea-clutter EM response. In [8], this statement is made too. This is the reason why the Tsallis distribution will be used in this project.

Appendix G

Matlab scripts

In this appendix, we present all the developed Matlab scripts and their features. All the scripts are given in the CD which is provided with the report. They are organized in folders following their use in the report: Main scripts (common scripts for all), Tsallis/K-distribution comparisons, polarization diversity study and results plot.

G.1 Main scripts

There is a main process in our implementation which is developed in **main.m**. It follows the *chapter 7. Radar signal simulation* chapter. In this script the following structures have been defined:

- **Tx**
It is a array representing all transmitters, (Tx(1), Tx(2) \cdots Tx(M)). Each element contains all informations about the corresponding transmitting antenna (coordinates, frequency, polarization, etc.).
- **Rx**
It works the same way with Tx, but these represent the receiving antennas.
- **vessel**
Structure representing the vessel, with its dimensions and coordinates.
- **dinghy**
Same thing for the dinghy. Structure with size and coordinates, and also parameters for the weapons onboard.
- **sea**
Structure representing the sea, where the sea grid is generated, containing the illuminated area and any other information belonging to the simulation grid.
- **wind**
wind is a simple structure which contains basically the wind speed and direction.

After the main execution, we can look into the content of the structures typing their name in the main console. The name of the variable is often significative. Then, there are no many structures to work with, and each function takes few parameters because most of needed informations often belongs to 2 or 3 structures. The function taking all parameters is for example `plot_results.m` which is called the following way: `plot_results(sea, Tx, Rx, wind, vessel, dinghy, max_range);`

The main function is designed not to calculate or process anything by itself, but to delegate everything to the following functions:

- **get_transmitter_data**
This script assigns the basic parameters for Tx and Rx structures.
- **get_sea_parameters**
This is the initializing script for the sea structure.
- **get_wind_parameters**
It sets the first instance of the wind structure.
- **get_signal_data**
Signal is a structure inside the Tx(m) structure element. It stores every information and state about the launched and received signal.
- **generate_sea_surface**
Function that generates the sea-surface in the sea structure. This function uses the Pierson-Moskovitz algorithm described in 5.1.3 and implements equation (5.1).
- **tsallis_realization**
This function is called to compute a Tsallis realization, as defined in section 5.2.2. A first sub-function estimates the q and β parameters depending on the radar and sea conditions. Then, a realization of the sea-amplitude response is returned. This script implements equations (5.14), (5.15) and (5.17).
- **apply_earth_curvature_to_sea**
So far, the sea-surface is flat, i.e. the earth curvature is not taken into consideration. This script computes the distance from the vessel and apply a earth curvature to the sea-grid using equation (5.2). Example of sea-grid with earth curvature included are given in fig. 7.4 and 7.3.
- **remove_sea_grid_useless_values**
In the simulation, we define a maximum range. Then, the sea-grid is a square of $maximum_range \times maximum_range$. Every value in the sea-grid which are further away from $maximum_range$ are not taking into account and defined to be 0 for a faster Matlab computation.
- **get_illuminated_cells**
This function is used to know which cells are illuminated by an antenna or not. It returns a grid with either 0 or 1 for illuminated or not for each pixel. The output of this function is shown in fig. 7.6 and 7.7

- **get_illuminated_cells_in_range**
This function is used in many cases, it returns the same grid as *get_illuminated_cells.m* but for a given range ($x \times \text{spatial_resolution}$). Then it returns the illuminated cells corresponding to a given range. This function is used to plot fig. C.11 and C.12 for example. This function is also called many times in the main script.
- **get_distance_grid_from_transmitter**
This function returns a grid of the same size as the sea-grid, with zeros, but also with distance from the center of the cell from the Tx(m) only for the illuminated cells.
- **get_DL_signal**
This function applies the downlink effects (antenna gain + attenuation) to the signal initially sent by a transmitter.
- **get_sea_height_on_DL_path**
This function computes several parameters which are: the sea-height on downlink, the angle of arrival on the EM-wave path, the illuminated sea area for a given range, and the range of the dinghy from the area if the dinghy is illuminated. This script implements equation (5.8). The equivalent function to get the sea-height on the EM-wave path for the uplink is included into *get_UL_shadowing.m*
- **get_sea_RCS**
This function returns the sea-RCS following the GIT model described in section 4.1.2. It returns the sea-RCS depending on the range, beam-width and polarization. It implements equations (4.3), (4.4), (4.5), (4.6), (4.7), (4.8), (4.9), (4.10), (4.11) and (4.12).
- **get_weapons_RCS**
This script returns the weapons RCS according to the weapons parameters in the dinghy, and the polarization. It is based on the studies made in *Appendix A. Weapons length impact on RCS* and *Appendix B. 3-planes study of weapon RCS*. It also uses the equations given in Table 7.1.
- **get_boat_RCS**
This script returns the dinghy RCS, implementing the Swerling I model described in section 4.2 and implements equation (4.13).
- **get_DL_shadowing**
This function computes the DL shadowing coefficient, as explained in section 5.1.5. It implements equations (5.4).
- **get_UL_shadowing**
This function computes the UL shadowing coefficient in the same way as *get_DL_shadowing.m*.

- **get_backscattered_coefficient**
This function computes the backscattered signal, following section 7.4. It implements equations (7.13).
- **get_UL_signal**
In the same way as *get_DL_signal.m*, it computes the uplink attenuation as described in 7.5. It implements equations (7.14) and (7.15).
- **estimate_mean_signal_level**
This script estimates the mean signal level taking into consideration the mean path loss effects. This mean level is visible on figure 7.16.
- **exclude_range_attenuation_from_signal**
This script amplifies the received signal with the mean-estimated signal, in order to give the received amplitude without any path attenuation.
- **compute_clutter_noise_variance**
This script computes the noise variance (sea-echo variance) compared to the mean level found by *estimate_mean_signal_level.m*. It allows then to find the *SCR* with equation (7.20).
- **estimate_threshold**
This script uses the noise variance and the P_{fa} to estimate the detection threshold, which is defined by equation (7.22).
- **get_delayed_signals**
It delays the received signal depending on the distance traveled by the wave.
- **get_estimated_NF_localization**
It estimates the pirate dinghy relative coordinates using (6.20).
- **match_impulse_responses**
This function matches the impulse response in order to apply MRC afterwards.
- **get_mrc_result**
This function applies MRC on the matched signals and determine the *SCR* and P_D for a given MIMO or SIMO configuration.
- **plot_results**
This function takes all structures as parameters and displays the different interesting results of the main process.

One can note that a description of how to use the functions is available typing *help get_transmitter_data* for example. The output of the previous command is displayed in fig. G.1. All functions description follows the same format.

```
>> help get_transmitter_data
function get_transmitter_data

Assign all parameters of the transmitting antennas in the Tx structure,
either calculated or defined.

INPUTS :
- M : number of transmitting antennas along the vessel.
- vessel : structure containing the length of the vessel.
- max_range : maximum radar range in the simulation [m].

OUTPUTS :
- Tx = Structure with transmitting antenna parameters
  - x : x coordinate of the antenna [m]
  - y : y coordinate of the antenna [m]
  - z : z coordinate of the antenna [m]
  - direction : Direction of illumination of the antenna [rad]
  - f : Operating frequency of the radar [Hz]
  - lambda : Wavelength of the operating frequency [m]
  - azimuth : azimuth beamwidth [rad]
  - bandwidth : Antenna bandwidth [Hz]
  - time_resolution : time resolution [s]
  - spatial_resolution : spatial resolution [m]
  - gain : Antenna gain [Unitless]
  - polarization : either of 'VV', 'VH', 'HV' or 'HH'
  - effective_aperture : Effective antenna aperture [m^2]
```

Figure G.1: Matlab console - *help get_transmitter_data* output

Finally, the process through all sub-functions is visible in the main output, displayed in fig. G.2

```

MIMO Radar simulation
1.BASIC PARAMETERS:
  - Constants ... OK - 0.000 s
  - Vessel structure... OK - 0.000 s
  - Dinghy structure... OK - 0.000 s
  - Radar characteristics... OK - 0.060 s
  - Sea-grid parameters... OK - 0.002 s
  - Sea-state generation... OK - 0.004 s
2.SIGNAL GENERATION: OK - 0.002 s
3.SEA-CLUTTER:
  - Sea-surface ... OK - 86.645 s
  - Tsallis realizations for the 2 transmitters...
  - Applying earth curvature ... OK - 0.402 s
  - Remove useless values ... OK - 0.103 s
  - Update the transmitter height ... OK - 0.002 s
4.DOWNLINK:
  - Find illuminated zones ... OK - 0.248 s
  - Compute distances between sea cells and transmitters ... OK - 0.038 s
  - Apply DL effects on signal ... OK - 0.002 s
  - Compute transmitting DL information ... OK - 503.408 s
  - Compute Sea-RCS for transmitters ... OK - 0.361 s
  - Compute Weapon RCS estimation ... OK - 0.008 s
  - Compute Boat RCS ... OK - 0.009 s
  - Compute shadowing coefficient for DL ... OK - 0.082 s
5.UPLINK:
  - Compute shadowing coefficient for UL ... OK - 37.579 s
  - Compute entire backscattered coefficient ... OK - 0.005 s
  - Compute UL signal ... OK - 0.263 s
5.RECEPTION:
  - Estimation mean signal levels ... OK - 0.005 s
  - Apply mean level processing... OK - 0.001 s
  - Compute the clutter noise variance... OK - 0.007 s
  - Threshold selection ... OK - 0.032 s
  - Including threshold with the range attenuation... OK - 0.001 s
  - Extract detections from received signals... OK - 0.001 s
  - Estimate target coordinates... OK - 0.000 s
6.RESULTS:
  - Plot all the figures...
    - Displaying reception results:
Transmitter/Receiver : 1/1 - SCR : 30.80 dB - Pd : 1.00
Transmitter/Receiver : 1/2 - SCR : -3.12 dB - Pd : 0.00
Transmitter/Receiver : 2/1 - SCR : -5.56 dB - Pd : 0.00
Transmitter/Receiver : 2/2 - SCR : 2.04 dB - Pd : 0.00
Overall MIMO Pd : 1.00
fx OK - 4.544 s

```

Figure G.2: Matlab console - *main.m* output

The main results displayed in Table 8.2 of the *chapter 8. Radar operation results* chapter are computed with `compute_mrc_results.m`. This function executes several times the main in order to create several scan for given conditions.

G.2 Polarization

The polarization study is based on *Appendix D. Singular Value Decomposition technique* and *Appendix E. Weapon polarimetric signature*. To be able to argue on polarimetric properties variables and a system 2×2 MIMO system have been defined.

These variables are the XPD , the $leakage$ and the PD . They can be obtained using `compute_2_2_system.m`. To launch this script several times in order to get a large number of these values we use `calculate_polarimetry.m`. The third script is used to plot the polarization given by the SVD.

- **compute_2_2_system**

It returns the XPD , the $leakage$ or the PD value of a configuration defined in `calculate_polarimetry.m`.

- **calculate_polarimetry**

It permits to define values to create a configuration in order to obtain the XPD , the $leakage$ or the PD from `compute_2_2_system.m`.

- **plot_polarization**

It is used in `compute_2_2_system.m` to plot the first or second mode polarization depending on the weights given to the antennas by the SVD. We obtained the graphics in Figure D.6 for example.

G.3 Tsallis/K-distribution comparisons

The following scripts are present in the folder : *datasets*.

The following scripts have been written mainly for the *Appendix F. Tsallis and K-distributions* study. These scripts only works with public available data provided by [43].

Every scripts then work with a particular structure of folder, which is the following:

- date_folder (i.e. 01Aug2006)
 - disc_folder (i.e. Disc1o3)
 - * measurement_folder (i.e. TFC15_001)

This measurements folder must contains a file ending with : ".summary.mat"

This means that the radar measurements must be into the 3rd folder level. This structure can be modified with the *for* loops at the beginning of the scripts. Also, all scripts need **ExtrCData.m** provided by [43] in the same folder to work properly.

The two main scripts used for *Appendix F. Tsallis and K-distributions* are described below:

G.3.1 estimate_k_and_tsallis_parameters.m

This script estimates the K and Tsallis parameters for a best match with the dataset. For each folder, it load the data and calculate the D_{KL} (equation (F.1)).

Then, for any set of $(q;\beta)$ and $(\nu;L)$ parameter, the found D_{KL} is compared and the best parameters and their associated D_{KL} is saved in *results.mat* file. The Tsallis and K fits are also saved into figures, under the names *k_fit.fig* and *tsallis_fit.fig*.

Figures F.1 and F.2 are taken from the saved figures by this script.

G.3.2 compute_mre_results.m

This script makes a cross-fit from the best-estimated parameters saved with *estimate_k_and_tsallis_parameters.m*. It loads the measurements and compute the cross-fit with the cross- D_{KL} associated. All results are then saved in the *cross_MRE.mat* file. If the file already exists, the results are then just loaded and not computed. Cross-fit figures are also saved under the names *cross_k_fit.fig* and *cross_tsallis_fit.fig*.

At the end, the script sums up all results from *estimate_k_and_tsallis_parameters.m* and itself, and display the statistics shown in Tables F.2 and F.3 and plot figures F.3 and F.8.

All figures F.4, F.5, F.6, F.7 and F.9 are taken from the saved figures by this script.

G.4 figures

Few scripts that were used to make figures for the report are available in the *figures* folder. There are 5 of them listed below :

G.4.1 piracy_plot.m

This script is used to plot the fig. 1.1, showing the piracy acts all over the world each year. The data has been found with [2, 3]

G.4.2 sea_roughness.m

This script generates the sea for any wind condition and compute its RMS roughness with equation (5.3). This script needs the *sea_surface.m* in the same or

parent folder to execute properly. The script finally displays the figure 5.2

G.4.3 `tsallis_sketch.m`

This script is used to show several PDF of a Tsallis distribution with different parameters q and β . It implements equations (5.15), (5.17) and it is used to display figure 5.4

G.4.4 `plot_illuminated_range.m`

This script is used to illustrate the pixel mismatch. To work properly, it must be executed after the `main.m` with at least $M = 2$ transmitters. Then, the beam-width is updated in the script and it displays the illuminated pixels This scripts then displays the illuminated pixels for several ranges, and displays fig. C.11 and C.12 used for the pixel mismatch explanation in *Appendix C. Signal correlation*

G.4.5 `detection_probability.m`

This script is used to sketch examples of equation (6.6) to plot figure 6.3. It also uses equation (7.24) to plot 6.4.

G.4.6 `swerling_pdf.m`

This script is used to sketch the Swerling I and Swerling III pdf in fig. 4.2 and 4.3.

G.4.7 `plot_mrc_results.m`

This script is used to plot the results computed by `compute_mrc_results.m`. It displays figures 8.8, 8.9, 8.2 and 8.3.